The Dissertation Committee for Jessica O. Winter certifies that this is the approved version of the following dissertation:

Development and Optimization of Quantum Dot–Neuron Interfaces

Committee:

Christine Schmidt, Supervisor

Brian Korgel

John Ekerdt

Jason Shear

Dean Neikirk

Development and Optimization of Quantum Dot–Neuron Interfaces

by

Jessica O. Winter, M.S., B.S.

Dissertation

Presented to the Faculty of the Graduate School of

The University of Texas at Austin

in Partial Fulfillment

of the Requirements

for the Degree of

Doctor of Philosophy

The University of Texas at Austin

August 2004

Dedication

To my husband and children, without family all else is meaningless.

Acknowledgements

I would like to acknowledge all of the people who have aided me in completing my research. From the Schmidt group, Terry Hudson for getting me started, Beth Furnish and Jennie Baier for their career advice, and especially Natalia Gomez for serving as my sounding board. From the Korgel group, Lindsay Pell for her assistance with TEM, Fred Mikeluc for his technical advice, April Schricker for struggling through e-beam with me and Felice Shieh for showing me how to make particles. Also, special thanks to Adam Hendricson and Matt Sullivan from the Morrisett group for teaching my how to culture primary neurons and operate the patch-clamp rig.

Most importantly, I would like to acknowledge the faculty members that have opened my mind to new ideas and new questions: Jason Shear, Robert Martinez, and Josef Käs for asking tough questions about quantum dot physics, Dean Neikirk for his advice on microfabrication, Richard Morrisett for allowing me to use his whole-cell clamping rig and for answering my neuroscience questions, Rebecca Richards-Kortum for providing moral support and career advice, Brian Korgel who was virtually a second advisor, and my advisor, Christine Schmidt. I look forward to interacting with all of you as a colleague in the future.

Development and Optimization of Quantum Dot–Neuron Interfaces

Publication No._____

Jessica O. Winter, Ph.D.

The University of Texas at Austin, 2004

Supervisor: Christine Schmidt

Micron-scale neuroelectronic interfaces have been used as laboratory models in neuroscience, prosthetic devices, and components of computational systems. However, these devices interact with cells at the whole cell level, and cell signaling occurs through interactions with cell surface proteins that average 10 nm in size. To take advantage of these receptor-scale interactions additional systems are needed. We have designed and optimized one possible system, using semiconductor quantum dots.

Quantum dots are crystalline particles, typically less than 10 nm in diameter, that display many unique optical and electronic properties because of quantum confinement of the exciton. As a result, they have been used in a number of optoelectronic and biological applications. Our research attempts to combine these functionalities to create an optically excited interface capable of electrically communicating with nerve cells.

To achieve this goal, we manufactured CdS quantum dots using an aqueous synthesis. We characterized the effects of altered synthesis conditions on the size and quantum yield of the particles, indicators of their electrical properties. We then demonstrated three separate methods to produce quantum dot-neuron interfaces. The first

of these utilizes biorecognition molecules, including antibodies and peptides, to create controlled interfaces with cell membrane receptors. The second method uses non-specific interactions between the particle core and cell membrane surfaces to create diffuse binding, and the third technique provides interfacing through direct culture of cells on tethered films. Additionally, we present our initial attempts to incorporate these interfaces with existing micron-scale measurement technologies, which could be used to confirm quantum dot-neuron electrical connectivity. Our results, demonstrate one possible path to receptor-scale neuroelectronic interfacing. Ultimately, these devices could be incorporated into existing micron-scale systems to provide new classes of prosthetics and computational devices.

Table of Contents

List of Tables

List of Figures

Chapter 1: Introduction[1]

Nerve cells, or neurons, form the basis of thought and control in the body. Additionally, neurons compose a plastic system, capable of processing large amounts of information and learning from those results. While signal transmission among these cells is generally well understood, their ability to regenerate and form new connections is not. These properties have motivated the study of neurons by two diverse communities: the medical community and the computational community.

Neurons have provided fertile ground for study in the medical community because deficits in the nervous system are among the most challenging to treat. Damage to these cells can result from a variety of congenital conditions (e.g., retinosis pigmentosa, epilepsy), neurological diseases (e.g., stroke, Alzheimer's, Parkinson's) or mechanical injury (e.g., car accidents, gun shot wounds, etc.), leaving the patient with a potentially profound loss of function. While peripheral nerves, those located outside the brain and spinal cord, have the potential to regenerate, this process can take several months and the rate of recovery averages ~ 80%. [1] In the central nervous system (e.g., the brain), unaided regeneration does not occur. [2] Thus, there is a need for prosthetic devices that can repair or replace nerve function.

Additionally, neuroscience continues to search for an understanding of the physiological mechanism for learning and thought. Neurons process information by integrating the response of multiple inputs that differ in location and strength. It is believed that learning is mediated by the alteration of these connections, which occurs in

[1] Portions of this material have been previously published in the following reference: J.O. Winter and C.E. Schmidt. "Biomimetic Strategies and Applications in the Nervous System," in Biomimetic Materials and Design, A.K. Dillow and A.M. Lowman, Eds., Marcel-Dekker, New York: 2002.

reaction to repeated electrical or chemical stimuli from neighboring neurons. [3] This ability of neurons to process massive amounts of information in parallel, while constantly adjusting the strength of their connections, has made the nervous system an attractive model for computational devices. [2] These concepts form the basis of neural network software programs, which emulate neurons. However, the ability to harness the computational power of groups of living neurons is in nascent stages. Systems that allow for external, non-invasive stimulation of neurons will form a crucial component of neuro-computational devices.

1.1 THE ELECTRICAL BASIS FOR NERVE SIGNAL PROPAGATION

While neuron cell bodies and their extensions (neurites) are capable of interacting with standard electronic devices, neuronal signal propagation is actually ionic in nature. [4] Charge is carried by individual metal ions, and not migrating electrons. The nerve cell has an exterior membrane, composed of lipids, which serves as an insulator and separates these ions. The membrane is permeated with transmembrane proteins, known as ion channels, which allow ions to pass under certain conditions (Figure 1). Channels may be open constantly, passing ions based on their concentration gradient; or they may open in response to a stimulus, such as a voltage change or chemical binding event.

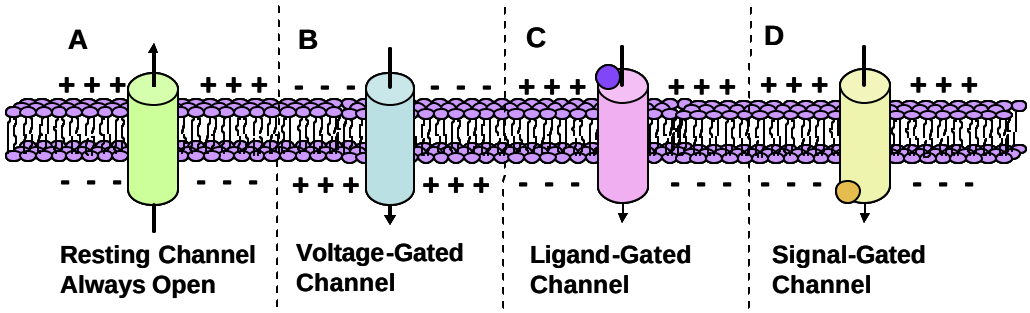

Figure 1: Transmembrane Channel Proteins in Neurons.

(A) Resting channel proteins are always open; these channels most commonly pass K^+ ions. (B) Voltage-gated channels open in response to a membrane potential change. (C) Ligand-gated channels open following external neurotransmitter binding. (D) Signal-gated channels open upon internal signal binding. [Adapted from Figure 21.2, H. Lodish, A. Berk, S.L. Zipursky, P. Matsudaira, D. Baltimore, and J.E. Darnell. Molecular Cell Biology, 4th ed., W. H. Freeman & Co, New York: 2000.]

These ion channels render the membrane permeable to the sodium (Na^+), potassium (K^+), calcium (Ca^{2+}) and chloride ions (Cl^-) that form the basis of signal transmission. At rest, the interior of the cell contains an abundance of K^+ ions, whereas the concentration of Na^+ ions greater externally. [5] These concentration gradients

establish a voltage difference, known as a resting membrane potential, across the cell membrane (Figure 2).

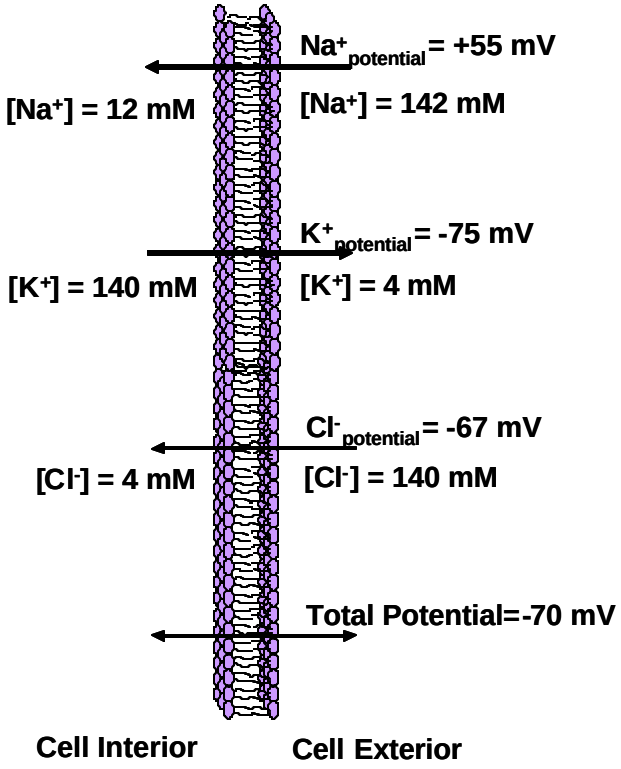

Figure 2: Origin of the Resting Membrane Potential.

Ions are segregated as a result of the cell membrane and ion channels, which selectively transport certain molecules. This creates a voltage potential across the membrane. The total potential is a combination of the values for the three most common ions transported by cells: Na^+, K^+, and Cl^-. Na^+ and Cl^- are more prevalent outside the cell, while K^+ is more common inside the cell. The total membrane potential is ~ -70 mV. [5]

In the standard model of neuronal signaling, propagation begins with the binding of a neurotransmitter to a ligand-gated channel (Figure 1c). These channels are primarily found on the extracellular surfaces of synaptic neuron extensions, known as dendrites, and also on the cell body. Binding produces a conformational change in the channel that allows ions to pass. These ions rush into the cell, altering the local membrane potential. These synaptic potentials can be either excitatory or inhibitory and decay in intensity with increasing distance from the synapse site. The signal is sensed at the cell body and its neurite extensions where it is integrated with other inputs. The decision to initiate an action potential is made in the axon hillock, which contains a high density of voltage-

sensitive channels that have a lower threshold than those in other parts of the neuron. If properly stimulated, these voltage-sensitive channels will open (Figures 1b, 3), causing the cell to fire a potential. The potential is carried away from the cell body by a nerve extension, known as an axon. [6]

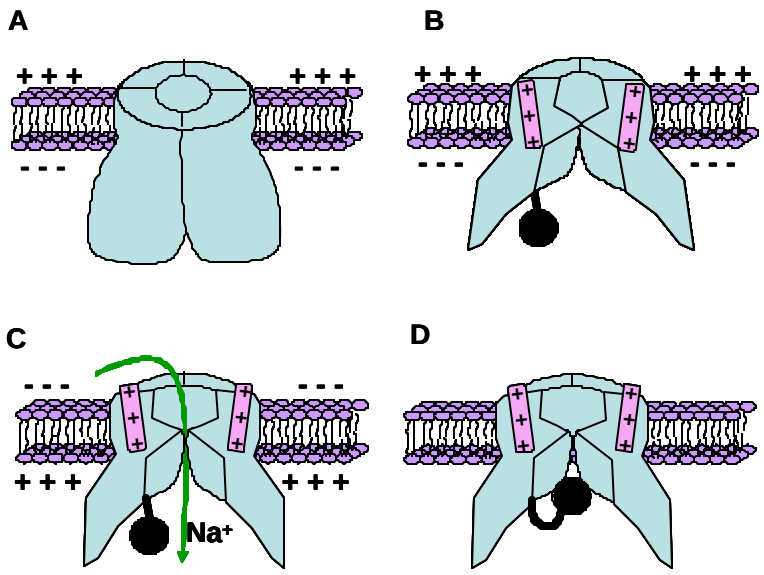

Figure 3: Voltage-Gated Ion Channel Structure and Signal Propagation.

(A) Ion channel at rest. The cell exterior is positively charged, while the interior is negatively charged. The ion channel consists of four repeated units containing six transmembrane spanning segments. (B) Ion channel at rest, cut-away view. Positively-charged alpha helices (pink) in the channel subunits are attracted to the negatively-charged cell interior. The channel deactivating segment (black) is not bound. (C) Ion channel after depolarization, cut-away view. After depolarization, the membrane charges are inverted. The positively charged alpha helices move toward the exterior of the cell, producing a conformational change in the ion channel. This change opens the channel pore allowing ions, typically Na^+, to pass. (D) Ion channel during the refractory period, cut-away view. To prevent continuous ion flow, the channel deactivating segment binds to the interior of the pore. [Adapted from Figure 21.13, H. Lodish, A. Berk, S.L. Zipursky, P. Matsudaira, D. Baltimore, and J.E. Darnell. Molecular Cell Biology, 4th ed., W. H. Freeman & Co, New York: 2000.]

Voltage-sensitive channels produce an influx of Na^+ ions, which alter the local membrane potential, opening yet more channels along the length of the axon. The signal

normally travels unidirectionally from the cell body to the axon terminal. This occurs because ion channels upstream from the signal are temporarily blocked by a globular protein shortly after the initial firing event (Figure 3d). At the axon terminal, voltage-gated Ca^{2+} channels open in response to the membrane potential change. This influx of Ca^{2+} ions initiates the release of neurotransmitters contained in synaptic vesicles, allowing the signal to pass into the synaptic cleft and to a neighboring cell. Thus, nerve signals are propagated by a combination of chemical neurotransmitters and electrical signals carried by metal ions. [6]

1.2 INTERFACING NEURONS AND ELECTRONICS

Since the late 1700's when Luigi Galvani discovered that electricity can cause nerves to fire, there has been a desire to manipulate nerves externally. [7] However, it was not until the next century that neurons were identified as the individual units of charge transmission, and the mechanism of signaling was explored until the 1950's. [8] Stimulation and measurement from individual neurons has proved more difficult than that of nerve cables (as per Galvani) because of their small size (e.g., 10 microns in diameter versus 1-10 millimeters for a nerve cable). [7]

The first significant manipulation of individual neurons occurred with the use of microelectrodes, which measured intracellular potentials in the giant squid axon. [8, 9] This was followed by the development of the patch-clamp technique by Sakmann and Neher in 1976 (Figure 4). [10] This method uses micron-sized (or smaller) capillary pipettes filled with electrolytic solution. Pipettes are placed in direct contact with the membrane; and, using suction, the membrane is torn away from cell. The membrane section is then held at a constant voltage, and the current required for maintaining that

voltage is measured. This current corresponds to the flux of ions that travel through the cell membrane in response to external stimuli.

There are multiple variations of this technique (Figure 4), which have proven quite useful for discrete investigations. [11] For example, the whole-cell configuration (Figure 4B) allows recordings to be collected from intact cell bodies. However, there are several limitations to the application of patch-clamp techniques in either a computational or clinical setting. For example, patch-clamp techniques cannot be used to stimulate a particular class of ion channels unless a broad-spectrum pharmacological "cocktail" is applied to limit electrical signaling to the ion channel of interest. [12] This restriction requires exposure to a variety of neurotoxins, thus this approach is unlikely to be implemented for any commercial computational device. Furthermore, patch-clamp is by nature an invasive technique. The requirement of direct physical contact between the cell and the recording electrode excludes the use of this technique in long-term studies of cell-ion channel interactions, or in a therapeutic intervention such as a self-contained neural prosthesis.

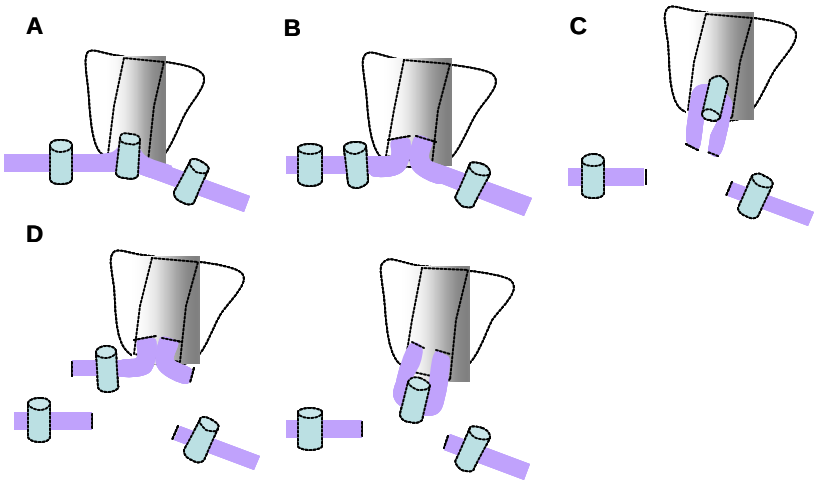

Figure 4: The Patch-Clamp Technique.

A micropipette (white) makes contact with ion channels (blue) in the cell membrane (purple). (A) Cell-attached configuration. The micropipette contacts ion channels in an intact membrane. (B) Whole-cell configuration. The membrane is broken inside the pipette allowing measurement of the entire cell through its intracellular fluid. (C) Inside-out configuration. A portion of the membrane is torn from the cell surface, allowing measurement of a single ion channel from the external side. (D) Outside-out configuration. Initially the membrane is torn from the cell surface in the whole cell configuration (left). Then, the membrane ends anneal to produce a continuous unit (right). This allows measurement of ion channels from the intracellular side. [Adapted from Figure I.4.Box A, D. Purves, G.J. Augustine, D. Fitzpatrick, L.C. Katz, A.-S. LaMantia, J.O. McNamara, S.M. Williams. Neuroscience, 2nd Ed., Sinauer Associates, Sunderland, MA: 2001.]

Thus, the development of neuron-based prosthetic and computational devices did not occur until micron-scale, non-invasive components could be manufactured by the microprocessor industry. The prototype prosthetic/computational device is based on a platform developed in 1979, known as the microelectrode array. [13] The device consists of gold conductors photolithographically patterned onto an insulating substrate connected to insulated wires that terminate at a bond pad. [13] Electrical signals are isolated by measuring the voltage difference between the cell culture medium (a conductor) and the

bond pad (Figure 5a). The electrode interacts with the cell through induction (Figure 5b) and can be used for either measurement or stimulation. [14]

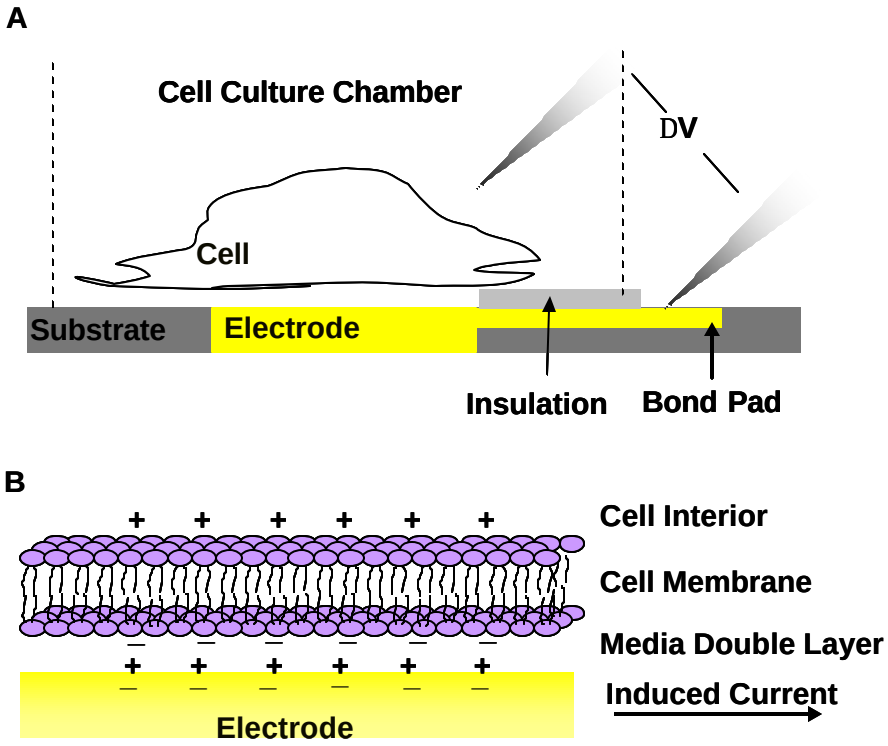

Figure 5: Microelectrode Arrays and Cells.

A) Microelectrode Schematic. A microelectrode interacts with a cell at a de-insulated electrode site. The signal is then carried through an insulted wire to a de-insulated bond pad. A two-point probe monitors the voltage difference between the medium and the de-insulated bond pad to determine the voltage change in the cell. A culture chamber isolates cell culture medium from the bond pads and external electrical components. B) Cell Interactions with the Electrode Surface. Upon firing, the cell experiences a voltage change that produces a charge at the membrane surface. The membrane acts as a capacitor, and can induce a charge in the electrode, which is then detected at the bond pad of the device.

The microelectrode array platform has served as the basis for two clinical devices: cochlear and retinal implants. The cochlear implant, which has been in use for over

twenty years, [15] restores sound perception to profoundly deaf patients by interacting directly with existing neural circuitry in the cochlea. The retinal implant, while more recent (~ 10 years), restores vision to patients with damaged photoreceptors (i.e., those with macular degeneration or retinosis pigmentosa), interfacing instead with bipolar, horizontal, amacrine and ganglion cells in the retina. [15] Both devices operate by turning an external signal (e.g., sound waves or light) into an electrical signal [16] that is transmitted to the remaining functional neurons through the microelectrode array. Other types of microelectrode prosthetic devices are being developed to replace spinal cord and peripheral nerve function. [17] These devices include perforations that allow the electrode array to interface directly with damaged or regenerating fibers.

Neuron-microelectrode arrays have also been of great interest to the electrical device community as a result of the unique way that signals are processed. Calculations in traditional digital computing occur in serial, one before the other, while nerves process signals in parallel, multiple calculations occurring simultaneously. [18] For example, in digital computing, calculation occurs by adding number A to number B to get number C, then adding number C to number D to get E and so on. Using this paradigm, internal circuit noise is eliminated at each calculation step by conversion of data into a single number (i.e. 1 or 0) which is passed to the next stage. However, the decision of a nerve to fire is not based on a sequential combination of two numbers, but comes from the simultaneous integration of multiple inputs that are either inhibitory or excitatory and which vary in magnitude. [18] There is no requirement for noise reduction between stages, because there are no stages. Instead, fidelity of the signal is ensured by providing a sufficient number of inputs to outnumber the sources of noise. [19] The result is the ability to perform multiple calculations simultaneously with a high signal to noise ratio and a dramatically increased speed compared to traditional digital systems.

While the promise of neuron-based computational systems is evident, development has been slow. Microelectrode arrays can measure and stimulate individual neurons, and can even be multiplexed to interact with multiple neurons simultaneously. [2] However, systems that allow multiple neurons to interact with the device *and each other* have not proven easy to develop. One of the only examples of this kind of system, developed by Peter Fromherz et al. [20], uses a capacitor for stimulation and the gate of a field effect transistor for measurement.

Fromherz employs neurons from the snail, *Lymnaea stagnalis*, which have the atypical ability to form synapses at their cell bodies instead of using axons and dendrites. This avoids the potential difficulties of guiding individual neurite extensions to form synapses. Additionally, synapsing cells may be hand picked from the culture dish and placed directly over the electrical components, eliminating cell adhesion and positioning concerns. While this system utilizes an ingenious juxtaposition of biology and microelectronic components, it represents a very unique application, one that is not likely to achieve commercial success and is not representative of the conditions found in mammalian cells. Additionally, it lacks the complexity that derives from large numbers of cells. Thus, the majority of computational systems are confined to the investigation of single neurons.

1.3 Limitations of Microelectrode Array Systems

The greatest challenge for both prosthetic and computational neuron-based devices has been the formation of an interface between the cell and electronic features. [7] To make contact with an array, cells must be carefully positioned on electrodes. Typically, this is accomplished by direct placement of hand-selected cells using micropositioners or random cell culture on device surfaces. If the cell migrates away

from the contact, the recording or stimulating interface is lost. One method to alleviate this difficulty is the incorporation of biorecognition molecules onto the array surface. [21] When peptides, such as the laminin fragment YIGSR, are added, cell adhesion is greatly enhanced. This technique has been used previously to modify implantable devices (i.e., neural probes, electrodes that are inserted directly into the cortex) [22]; however, this technology cannot be applied in every case. For example, in the retinal implant, the target cells (e.g., bipolar cells) are separated from the electrode surface by layers of additional cells and fibrous tissue [15]. Simply coating the electrode with peptides will not create interfaces with cells that may be up to 50 μm away. Additional steps must be taken to encourage cell growth to the device or bring electrode surfaces into greater proximity to the cell. Consequently, cell adhesion and migration remain significant issues in the development of neuroelectronic technologies.

Further, microelectrode arrays present one critical limitation to forming fully functional interfaces with neurons. Most microelectrode arrays stimulate neurons at the cell body [7], not cell extensions; providing a single, time-dependant signal. However, true nerve signals are integrated from multiple dendritic inputs that can vary in strength and frequency. At a more detailed level, the propagation of each signal is managed through the opening and closing of ion channels embedded in the cell membrane surface. It is the manipulation of these channels that would provide a complete ability to interface with the cell. Ion channels average 10 nm in diameter [23], an impossible feature size for even the most advanced photolithography facility. [24] Although excitation could occur through larger interfaces, electrode separation must ideally be sufficient to excite individual channels. The spacing between ion channels is approximately 200 nm [25], a more manageable size. However, it is unlikely that a patterned system would produce exact alignment between electrodes and ion channels using direct cell placement or

random cell culture. Therefore, microelectrode arrays currently can provide only a coarse approximation of true neural interfaces.

To address these limitations, we have developed novel methods for interfacing neurons and optically-activated *nano-scale* electrical components (i.e., quantum dots or nanoparticles). The advantage of employing nano-scale components is two-fold. First, cell adhesion and migration concerns are eliminated. Particles may be bound to the cell itself using biorecognition molecules (e.g., antibodies or peptides) ensuring continuous contact. Additionally, cells can be cultured directly on tethered nanocomponents to create a useful interface. Optical excitation of the particles removes the need for connections to large external electrical components (i.e., bond pads). Thus, cells may be plated randomly on a thin layer of particles and a stable interface will still be achieved. The second advantage of a nano-scale system is that the electrical components have sizes comparable to the ion channels that propagate neuronal signals. Using biorecognition molecules, it may be possible to couple these components directly to ion channels, providing unprecedented fine control in a neuroelectronic system. We are utilizing nanocomponents, known as quantum dots, to create these novel interfaces with neurons.

1.4 DISSERTATION OVERVIEW

This dissertation is divided into seven chapters. In **Chapter 2**, the nanocomponents utilized in this work (i.e., semiconductor quantum dots) are described. Quantum dots are crystalline solids averaging 1-10 nm in diameter. [26] Because of their small size, they follow the laws of quantum mechanics (i.e., they exhibit quantum confinement) producing several unique optical and electrical properties. These properties have generated a great deal of interest in the optics community, and quantum dots have been employed in a variety of optoelectronic applications, most notably light emitting

diodes and solar cells. [27] Additionally, their unique features have been exploited in a limited number of biological applications. Resistance to photobleaching, high quantum yields, and narrow bandwidths have made quantum dots ideal fluorescent labels for histology and cell staining. [28] Because of their ability to convert optical inputs to heat or Raman signals, they have been used in several biosensors platforms [29] and therapeutic treatments [30]. This chapter reviews the properties of quantum dots, their use in electrical devices, and existing biological applications. Finally, we present our proposed interface, which combines electrical and biological functionalities.

Chapter 3 discusses two basic methods of nanoparticle synthesis: arrested precipitation in aqueous solution [31] and precursor decomposition in organic solution [32]. Additionally, our characterization of the aqueous method is given in detail. Synthesis conditions are critical to the development of a neuron-quantum dot interface because they determine nanoparticle size, which has been linked directly to the optical and electrical properties of the crystals. [26] For the aqueous synthesis, alteration of pH, ligand length, concentration or charge, and Cd:S ratio all produced changes in nanoparticle size, fluorescent emission wavelength, and quantum yield. Most notably, optimal quantum yields (~15%) were produced for intermediate particle sizes (~2 nm). We discuss possible causes of these variations and their dependences on particle growth patterns. From this work, we determined the optimum synthesis conditions and particle sizes for our system.

In **Chapter 4**, two methods of attaching nanoparticles to cell surface receptors using biorecognition molecules are described. The first method uses antibodies conjugated to the quantum dot surface to create interfaces with neurons. Conjugation was accomplished by condensing carboxyl groups on the nanoparticle surface with amines in the antibody, producing amide bonds. [33] Antibody binding to the particle surface was

confirmed through absorbance measurements. Additionally, binding was verified using fluorescence microscopy of neurons (i.e., SK-N-SH neuroblastoma cells) labeled with a two antibody technique. A primary antibody that recognizes and binds to extracellular matrix receptors (i.e., vitronectin receptors) on the cell membrane surface was applied. Secondary antibodies that recognize and bind to this primary antibody were linked to nanoparticles, as described previously, and the quantum dot–antibody conjugates were incubated with the cells. Binding was evidenced only in the presence of both antibodies. This system demonstrates the ability to link quantum dots directly to a desired receptor. Further, because the secondary antibody attached to the nanoparticle will bind a wide class of primary antibodies, the system is easily adapted by simply changing the primary antibody to one that targets a different receptor.

In the second system, peptide molecules were used to mediate attachment of nanoparticles to cells. Peptides were incorporated directly onto the quantum dot surface using thiol chemistry, and this binding was confirmed through absorbance measurements, FTIR spectroscopy, and fluorescence anisotropy. Two peptides were investigated, CGGGRGDS and CDPGYIGSR, both of which adhere to extracellular matrix receptors (i.e., fibronectin [34] and laminin [35] receptors, respectively). Interfaces were created by exposing neurons to peptide-nanocrystal conjugates and confirmed using fluorescence microscopy. Interfaces were only formed in the presence of peptides known to adhere to the cell surface. This work demonstrated the ability to attach quantum dots to specific receptors on the cell surface. Additionally, since peptides are significantly smaller than proteins (e.g., antibodies) [36], the separation distance between the electrical components and the receptor targets was greatly reduced.

Chapter 5 explores the relationships between nanoparticle synthesis conditions and material properties, non-specific binding of the cell surface, and cell viability and

behavior. We altered the methods developed in Chapter 4 for use with a primary cell line (i.e., rat neonatal cortical cells, RNCs). We explored the effect of washing conditions, solvent, and quantum dot material on cell viability. We established that primary cells are extremely sensitive to environmental conditions, and found that some materials (e.g. CdTe) that are compatible with other cell types produce toxicity in these cells. We also investigated the effect of different cell compatible buffer systems on the solubility, non-specific binding, and cytocompatibility of quantum dots. Increasing the number of additives (e.g., salt ions or dextrose) in a buffer system reduced particle solubility and decreased non-specific binding. This reduction in solubility most likely occurs because increased additives can limit the effectiveness of solvating molecules. Also, we examined the ability of neurons to take up, or endocytose, nanoparticles. This factor contributes to the long-term stability of quantum dot–neuron interfaces. It was determined that particles are endocytosed within 30 minutes unless the cells are metabolically suppressed (i.e., by exposing them to cold temperatures, ~4 ºC).

This factor is extremely liming in the development of stable quantum dot-neuron interfaces; therefore, we developed two additional binding methods using non-specific interactions. First, we utilized non-specific binding to create delocalized labeling of the cell surface. We characterized quantum dot affinity for the cell surface as a function of synthesis conditions. Quantum dots of increasing size exhibited an increase in binding, whereas nanoparticles with the highest quantum yield (~2 nm, as determined in our synthesis experiments, Chapter 3) produced the least non-specific binding. As an alternative material, we also examined CdTe nanoparticles created using an organic synthesis. CdTe produced diffuse non-specific binding on cell surfaces. Increased binding appears to result from reduced ligand passivation on the nanocrystal surface. We discuss the likely relationship between particle surface coverage, cell viability, and non-specific

binding. Next, we investigated endocytosis of non-specifically bound particles. Although endocytosis occurred at a lower rate than for recognition molecule binding, particles were internalized. Thus, this method is not suitable for long-term neuroelectronic interfacing.

Finally, we developed an additional interfacing technique using tethered nanoparticle films. Although this technique does not produce specific binding to receptors, it is likely that uniform films would create some interfaces with ion channels of cells cultured on their surfaces. Quantum dots were attached to glass surfaces with siloxanes [37] and poly-D-lysine [38] chemistries. Films were analyzed for stability in cell culture medium and with cells. Although films displayed excellent compatibility in medium, films demonstrated diminished and red-shifted fluorescence in the presence of cells. This most likely resulted from Ostwald ripening of the particles, which may have been accelerated by oxidizing agents released from the cells. On the other hand, these interfaces did not produce endocytosis and represent a viable method for interfacing nanoparticles with cell surfaces. From all of these results, we were able to optimize the nanoparticle size, buffer system, and binding conditions to produce nanoparticle-cell interfaces with good cell viability and a minimum of non-specific binding and endocytosis.

In **Chapter 6**, we discuss two measurement systems that could be used to explore the influence of excited nanoparticles on the cell membrane potential. We explored whole-cell clamping as a system for measuring the neuronal membrane potential. We discuss modification of our interface to this measurement technique, and our initial results. Creation of an interface with sufficient stability for measurement was extremely difficult, and we offer some suggestions for improvement. However, whole-cell clamping is an invasive technology that cannot be used to create a long-term device. Therefore, we also investigated microelectrode arrays. We demonstrated the ability to create arrays

using electron beam lithography, which can produce feature sizes compatible with ion channels. [24] Additionally, we demonstrated that the resist layer (i.e., poly (methyl methacrylate)) can be used as an insulating layer, eliminating a manufacturing step, and that this resist layer supports cell adhesion and growth. From this work, we identified two possible measurement systems for exploring the neuron-quantum dot interface and discuss implementation of each system.

In **Chapter 7** our results are summarized, conclusions presented, and recommendations for future work are made.

1.5 REFERENCES

1. D.T. Chiu. "The Development of Autogenous Venous Nerve Conduit as a Clinical Entity," in P and S Medical Review vol. 3, issue 1. Columbia-Presbyterian Medical Center, Dec. 1995.

2. J.O. Winter and C.E. Schmidt. "Biomimetic Strategies and Applications in the Nervous System," in Biomimetic Materials and Design, A.K. Dillow and A.M. Lowman, Eds., Marcel-Dekker, New York: 2002.

3. B. Alberts, D. Bray, J. Lewis, M. Raff, K. Roberts, and J.D. Watson. Molecular Biology of the Cell, 3rd Ed., Garland Publishing, New York: 1994, pp. 1129-1130.

4. B. Alberts, D. Bray, J. Lewis, M. Raff, K. Roberts, and J.D. Watson. Molecular Biology of the Cell, 3rd Ed., Garland Publishing, New York: 1994, pp. 523-525.

5. G. Pollak and H. Zakon. Vertebrate Physiology, Spring 2000 Ed., University Co-op Press, Austin, TX: 2000, p. 25.

6. E.R. Kandel, J.H. Schwartz, and T.M. Jessel. Principles of Neuroscience, 4th Ed., McGraw Hill, New York: 2000, pp. 140-186.

7. W.L.C. Rutten. "Selective Electrical Interfaces with the Nervous System." Annu. Rev. Biomed. Eng. 4: 407, 2002.

8. A. L. Hodgkin and A. F. Huxley. "A Quantitative Description of Membrane Current and its Application to Conduction and Excitation in Nerve." J. Physiol. 117: 500, 1952.

9. A.L. Hodgkin, A.F. Huxley, and B. Katz. "Measurement of Current-Voltage Relations in the Membrane of the Giant Axon of *Loligo*." J. Physiol. 116: 424, 1952.

10. E. Neher and B. Sakmann. "Single-Channel Currents Recorded from Membrane of Denervated Frog Muscle Fibres." Nature. 260(5554): 799, 1976.

11. B. Alberts, D. Bray, J. Lewis, M. Raff, K. Roberts, and J.D. Watson. Molecular Biology of the Cell, 3rd Ed., Garland Publishing, New York: 1994, pp. 181-183.

12. A. Molleman. Patch Clamping: An Introductory Guide to Patch Clamp Electrophysiology. John Wiley and Sons, West Sussex, England: 2003, p. 126.

13. G.W. Gross. “Simultaneous Single Unit Recording in vitro with a Photoetched Laser Deinsulated Gold Multimicroelectrode Surface.” IEEE Trans. on Biomed. Eng. 26(5): 273, 1979.

14. J.L. Novak and B.C. Wheeler. “Multisite Hippocampal Slice Recording and Stimulation Using a 32 Element Microelectrode Array. J. Neurosci. Meth. 23: 149, 1988.

15. P. Heiduschka and S. Thanos. “Implantable Bioelectronic Interfaces for Lost Nerve Functions.” Prog. Neurobio. 55: 433, 1998.

16. P.C. Loizou. “Introduction to Cochlear Implants.” IEEE Eng. Med. Bio. 18(1): 32, 1999.

17. G.T. Kovacs, C.W. Storment, and J.M. Rosen. “Regeneration Microelectrode Array for Peripheral Nerve Recording and Stimulation.” IEEE Trans. Biomed. Eng. 39(9): 893, 1992.

18. R. Douglas, M. Mahowald, and C. Mead. “Neuromorphic Analogue VLSI.” Ann. Rev. Neurosci. 18: 255, 1995.

19. A. Watson. “Why Can’t a Computer Be More Like a Brain?” Science 277: 1934, 1997.

20. R.A. Kaul, N.I. Syed, and P. Fromherz. “Neuron-Semiconductor Chip with Chemical Synapse between Identified Neurons.” Phys. Rev. Lett. 92: 038102, 2004.

21. S.A. Makohliso, P. Aebischer, L. Giovangrandi, H.J. Bühlmann, and M. Dutoit. “A Biomimetic Materials Approach Towards the Development of a Neural Cell-Based Biosensor.” Proceedings of the 18th Annual International Conference of the IEEE Engineering in Medicine and Biology Society, Amsterdam, 1996, pp. 81-82.

22. X. Cui, V.A. Lee, Y. Raphael, J.A. Wiler, J.F. Hetke, D.J. Anderson and D.C. Martin. “Surface Modification of Neural Recording Electrodes with Conducting Polymer Biomolecule Blends.” J. Biomed. Mat. Res. 56(2): 261, 2001.

23. B. Alberts, D. Bray, J. Lewis, M. Raff, K. Roberts, and J.D. Watson. Molecular Biology of the Cell, 3rd Ed., Garland Publishing, New York: 1994, p. 996.

24. G.R. Brewer, Ed., Electron Beam Technology in Microelectronic Fabrication. Academic Press, New York: 1980.

25. H. Lodish, A. Berk, S.L. Zipursky, P. Matsudaira, D. Baltimore, and J.E. Darnell. Molecular Cell Biology, 4th ed., W. H. Freeman & Co, New York: 2000, Section 21.3.

26. A.P. Alivisatos. “Perspectives on the Physical Chemistry of Semiconductor Nanocrystals.” J. Phys. Chem. 100: 13226, 1996.

27. T.J. Bukowski and J.H. Simmons. “Quantum Dot Research: Current State and Future Prospects.” Crit. Rev. Solid State Mat. Sci. 27(3): 119, 2002.

28. C.J. Murphy and J.L. Coffer. “Quantum Dots: A Primer.” App. Spect. 56(1): 16A, 2002.

29. C.A. Mirkin. “Programming the Assembly of Two- and Three-Dimensional Architectures with DNA and Nano-scale Inorganic Building Blocks.” Inorg. Chem. 39: 2258, 2000.

30. C. Loo, A. Lin, L. Hirsch, M.H. Lee, J. Barton, N. Halas, J. West, and R. Drezek. “Nanoshell-Enabled Photonics-Based Imaging and Therapy of Cancer.” Tech. Cancer Res. Treat. 3(1): 33, 2004.

31. K. Kalyanasundaram, E. Borgarello, D. Duonghong, and M. Grätzel. “Cleavage of Water by Visible-Light Irradiation of Colloidal CdS Solutions: Inhibition of Photocorrosion by RuO_2” Angew. Chem. Int. Ed. Engl. 20(11): 987, 1981.

32. C.B. Murray, D.J. Norris, and M.G. Bawendi. “Synthesis and Characterization of Nearly Monodisperse CdE (E = S, Se, Te) Semiconductor Nanocrystallites.” J. Am. Chem. Soc. 115: 8706, 1993.

33. G.T. Hermanson. Bioconjugate Techniques. Academic Press, San Diego: 1996, pp. 170-173.

34. M.D. Pierschbacher and E. Ruoslahti. “Cell Attachment Activity of Fibronectin Can Be Duplicated by Small Synthetic Fragments of the Molecule.” Nature 309: 30, 1984.

35. J. Graf, R.C. Ogle, F.A. Robey, M. Sasaki, G.R. Martin, Y. Yamada, and H.K. Kleinman. “A Pentapeptide from the Laminin B1 Chain Mediates Cell Adhesion and Binds the 67,000 Laminin Receptor.” Biochem. 26(22): 6896, 1987.

36. T. E. Creighton. Proteins: Structures and Molecular Principles. W. H. Freeman and Co., New York: 1983.

37. C. Abdelghani-Jacquin, A. Abdelghani, G. Chmel, M. Kantlehner, and E. Sackmann. “Decorated Surfaces by Biofunctionalized Gold Beads: Application to Cell Adhesion Studies.” Eur. Biophys. J. 31: 102, 2002.

38. F. Patolsky, Y. Weizmann, O. Lioubashevski, and I. Willner. “Au-Nanoparticle Nanowires Based on DNA and Polylysine Templates.” Angew. Chem. Int. Ed. 41(13): 2323, 2002.

Chapter 2: Quantum Dots and Their Applications

Quantum dots, also known as semiconductor nanoparticles, have generated a great deal of interest as a result of their small sizes (i.e., ~1-10 nm [1]) and unique optical and electrical properties. These properties, resulting from quantum confinement, include electron transfer, strong dipole moments, and size-tunable absorbance and fluorescent emission. [1] Although still in nascent stages, the applications of these materials have been widespread. Quantum dots have been integrated into a number of electrical devices, including LEDs, solar cells, and lasers, [2] and also show great potential in the biological sciences. [3] They exhibit size scales comparable to or smaller than the fundamental components of living systems. For example, the diameter of DNA is ~2 nm, a cell surface receptor is ~10 nm, and a virus is ~50 nm. [4] The ability to manufacture electronic materials with these biologically compatible feature sizes allows for the development of new sensing technologies, treatments, and therapeutics. Already, quantum dots have been utilized as fluorescent dyes for cell labeling [5-6], biosensors for chromosomal mapping [7], and chemotherapy alternatives [8]. With continued improvement of quantum dot coatings to enhance biocompatibility, in vivo applications are just on the horizon. Because of their small size and demonstrated success in electronic and biological systems, quantum dots provide a model material for the creation of nano-scale neuroelectronic interfaces.

In this chapter, the properties and applications of nanoparticles are reviewed. First, the motivation for the development of nano-scale bio-electronic systems is considered. Then, a brief description and history of the nanocomponents used in our work, semiconductor quantum dots, are supplied. Next, we examine the impact of size on material attributes. The requirements for quantum confinement, as well as the changes in

the energy band structures, are discussed. These are related to the resulting electrical and optical phenomena, and contrasted with the properties of bulk materials. Additionally, we discuss applications of nanoparticles in both electrical and biological contexts. Finally, we present our proposed system, and the mechanism of its interaction with the cell surface.

2.1 NANOCOMPONENTS AND NANOPARTICLES

To produce electronic interfaces with individual cell receptors it is necessary to employ components at the nanometer length scale. Most existing devices are based on the microelectrode array platform, which includes micron-sized (~10 μm [9]) components. These devices are manufactured using photolithography techniques, and the current length scale limitation of this technology is ~90 nm. [10] Electrodes of this size are still almost an order of magnitude larger than the average ion channel (~10 nm [11]). Alternative patterning technologies, such as electron beam lithography (EBL), can produce electrodes of the correct dimension (e.g., as small as 10 nm). [12] However, EBL is a time consuming process, and is not well adapted to mass production. Furthermore, any patterned structure will have to address the difficulty of forming controlled interfaces between migrating cells and fixed electrode surfaces. [9] The number of electrodes required to ensure an interface through random cell placement could be quite large, and each would have to be individually addressed to a much larger electrical contact. For these reasons, optically addressable nanoparticles pose an attractive alternative to patterned electrode systems.

Nanoparticles have many advantages over patterned devices. They are typically produced in solution and can be directly linked to cellular components. [5] They can also be absorbed or tethered to a substrate, forming thin films. [13] Additionally, nanoparticles can be manipulated non-invasively to produce photocurrent, photo-induced electric fields, or electro-luminescence. [2] All of these factors eliminate the need for fixed wires and contacts, rendering cell adhesion and migration minor concerns. For our experiments, we chose to examine the ability of a particular class of nanoparticle, semiconductor quantum dots, to form neuroelectronic interfaces.

Quantum dots are crystalline solids that typically average less than 10 nm in diameter. [1] Because of their small size, the particles exhibit quantum confinement; giving them several unique optical and electronic features (see Section 2.2 for more details). They display many attributes indicative of quantum mechanical principles, as opposed to bulk materials, which follow traditional Newtonian laws. Quantum dots can be made from a variety of materials including metals and semiconductors. [14] For our experiments, we examined two materials from the semiconductor class: Cadmium Sulfide (CdS) and Cadmium Telluride (CdTe). These were selected because of their documented electrical and optical properties. [1] Additionally, both materials can be excited optically in the UV or visible range of wavelengths, allowing for visualization of the cell interface using fluorescence microscopy.

2.2 Optical and Electronic Properties of Quantum Dots

2.2.1 A Brief History

Quantum dots were initially discovered in 1981, during the development of materials for the photo-cleavage of water. [15] Bulk cadmium sulfide is known to be an ideal electrode material; however it experiences photocorrosion upon irradiation. It was believed that colloidal particles of cadmium sulfide, coated with a protective agent (i.e., RuO_2), would be more resistant to corrosion. Therefore, a synthesis method was developed to produce colloidal CdS through aqueous precipitation. The resulting particles displayed unique properties not found in the bulk, including fluorescent emission. These properties were determined to be the result of quantum size effects, [16] and were found to be tunable by altering the size of the particle. [17-18] This provided a method for selecting excitation and emission wavelengths, and particle band gaps.

2.2.2 Quantum Confinement and Size Effects

Quantum effects occur in colloidal nanoparticles for a number of reasons. Small particles can experience quantum confinement of the excited state. In bulk semiconductor materials, an excited electron leaves behind a positive charge in the crystal lattice, known as a hole. The excited electron, now in the conduction band, can be coupled with the hole in the valence band through Coulombic attractions (e.g., electrostatic attraction) to create an exciton, an electron-hole pair that are bound together (Figure 6A). In quantum mechanics, the positions of electrons and holes are described as wavefunctions, or probability distributions. The exciton has a certain size, determined by the combined probability distribution functions, and if this size exceeds the particle diameter, quantum confinement occurs (Figure 6B).

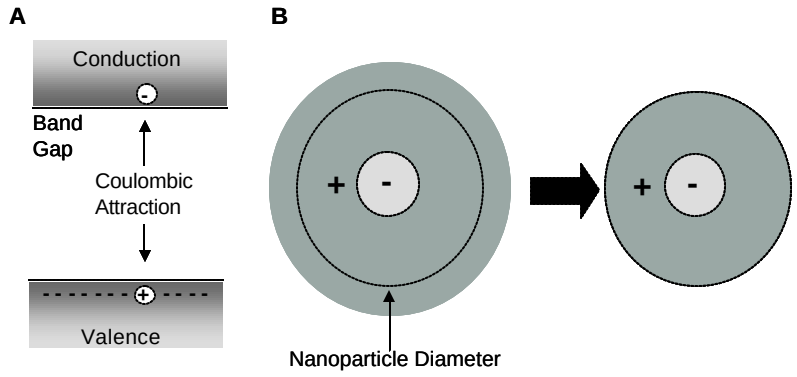

Figure 6: Exciton Formation and Quantum Confinement.

(A) An excited electron in the conduction band is coupled to a vacancy (hole) in the valence band creating an exciton. (B) If the electron probability distribution of the exciton exceeds the nanoparticle diameter, then quantum confinement will result. The exciton probability distribution is forced to remain within the confines of the nanoparticle.

The size limit for quantum confinement is given by the diameter of the bulk Bohr exciton, [19] which can be calculated from the Schrödinger equation. [20] However, it

can be approximated from a modified version of the De Broglie wavelength equation for a free electron (Equation 1), [21-22]

$$\text{De Broglie } l = \frac{h}{mv} = \frac{h}{m_e v} \qquad \text{[Equation 1]}$$

where h is Planck's constant, and m and v are the mass and velocity of the excited electron, respectively. Modification of this equation is required because bulk semiconductor materials do not contain truly free electrons; charge screening effects of neighboring atoms in the crystal lattice must be taken into account. This is accomplished by noting the symmetry of each lattice position. If we assume an infinite system, each position is equivalent. We can model a single position by utilizing the equations for free electron systems, but approximating the mass of an electron with m_e, the effective mass, which includes the averaged effects of attraction, repulsion, and shielding from neighboring atoms. [22]

Nanocrystals contain many fewer atoms than found in the bulk, and as atoms are removed, charge screening effects are reduced. The effective mass declines, and the De Broglie wavelength can become uncharacteristically large, up to several nanometers. For cadmium sulfide and cadmium telluride, the materials we examined; these wavelengths are 5.5 [16] and 7.5 [23] nm, respectively. For particles that exhibit sizes smaller than this wavelength, the exciton "feels" restricted. Thus, the nanocrystal will display a band gap and associated optical and electrical features proportional to its size.

An additional feature of shrinking nanoparticle diameter is the formation of discrete bands within the potential energy diagram of the particle (Figure 7). Bulk semiconductor materials are characterized by bands of allowed potential energy values. An electron in the ground state may occupy any state within the valence band; while

electrons in the excited state may occupy any state in the conduction band (Figure 7A). The region between the two bands is forbidden. For an electron to be excited, it must absorb at least enough energy to be carried from the highest energy state in the valence band to the lowest energy state in the conduction band. Energies below this minimum value (i.e., the band gap) will not produce an excited state. However, a continuum of values greater than the band gap will produce an excited state. [24]

When we examine a system consisting of only two atoms, the molecular orbitals formed create discrete potential energy states (Figure 7B). Electrons will only be excited if energy is absorbed in discrete quantities. Other values are not permitted and will not produce excited states. [25] Quantum dots occupy the interval between discrete and continuous energy levels (Figure 7C). [1] As the number of atoms in the particle is reduced, the potential energy bands split and shrink, eventually collapsing to the discrete values of the atomic state. Thus, electrons in quantum dots may be excited by energies in discrete intervals, rather than a continuum.

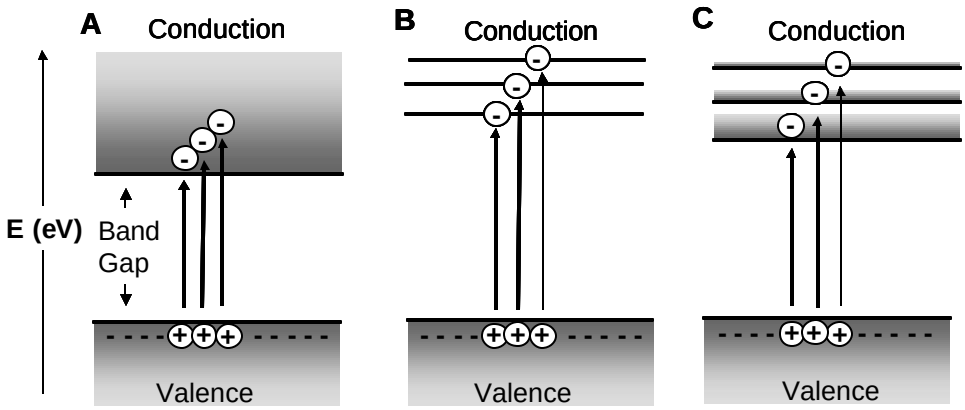

Figure 7: Potential Energy States and Particle Size.

(A) Bulk materials have continuous energy bands, and absorb energy at a value greater than the band gap. (B) Molecular materials possess discrete energy levels and only absorb energy with certain values. Additionally, the band gap is greater than that of a bulk material as a result of shrinking and splitting of the energy bands. (C) Quantum dots lie between the extremes (A, B). They possess discrete energy bands and absorb energy in discrete intervals. The band gap is greater than that of a bulk material, but less than that of a molecular material.

2.2.3 Electrical Properties Resulting from Quantum Confinement

For bulk semiconductors, the band gap of a uniform material is fixed. However for quantum dot systems, splitting and shrinking of the bands produces an increase in band gap with decreasing particle size, approaching the value for an atomic system. Thus, gap energies are size dependant, and electrical properties that depend on this difference will display size dependence as well. One such property is electron transfer. [26] Electrons with no additional energy added prefer to move to lower energy states within a given material. Because there are no energy states in the band gap, the electron will decay until it reaches the lowest state in the conduction band, and then return to the valence band through another mechanism (i.e., electron-hole recombination, non-radiative energy

loss, etc.). [27] However, if the electron encounters a material with lower available energy states (i.e., values within the band gap); it can transfer its electron to that material (Figure 8). This process is dependant upon the band gap. As the band gap increases, excited electrons occupy higher energy levels, and can decay to a greater number of lower state values. As a result of size-tunable band gaps within the particle, electron transfer can be optimized to many materials.

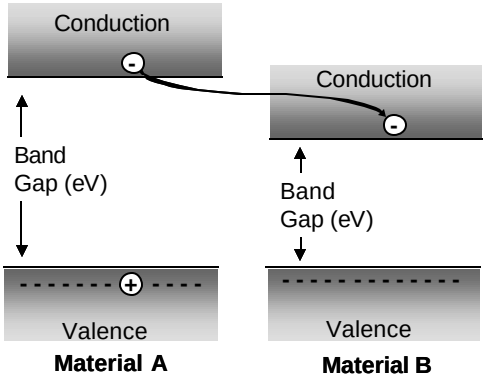

Figure 8: Electron Transfer and Band Gap Energy.

If an excited electron in one material (A) encounters a second material (B) with a lower band gap energy, it can transfer its electron to that material.

Another property resulting from small nanocrystal sizes is the presence of large excited state dipole moments. When an electron in a quantum dot is excited, the probability functions of both the electron and the hole are altered. [28] One possibility is the formation of a state where the wavefunctions of the electron and hole are concentric (Figure 9A). [29] This would result in radial symmetry producing a net dipole moment of 0 Debye. However, it is also possible for the electron to get trapped at the particle surface (Figure 9B). This usually occurs as a result of defects in the crystal lattice (e.g., interstitial atoms, adsorbed species, dopants, etc.). Electron trapping results in a fixed charge separation, producing a dipole moment dependant on the size of the crystal (e.g., 192 Debye for 4 nm CdSe [29]). Cadmium-based nanocrystals exhibit a mixing of these two states, with dipole moments of more modest, but still quite large values (~ 30 Debye for nanocrystals [29] vs. 5 Debye for bulk material [30]). Dipole moments are of interest

in electronic applications because each dipole moment has an associated electric field that can be used to influence ions outside of the particle (see Section 2.5).

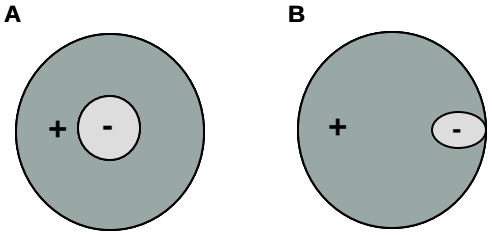

Figure 9: Formation of a Dipole Moment in the Excited State.

(A) Excited state exciton wavefunction for a perfect nanocrystal. (B) Excited state exciton wavefunction with a surface-trapped electron. Surface-trapping results in charge separation, producing a transient dipole moment.

2.2.4 Optical Properties Resulting from Quantum Confinement

Additionally, quantum confinement affects the optical properties of nanoparticles. The electrical and optical energies of the band gap are equivalent through the following conversion: [31]

$$E = hn = \frac{hc}{l} \qquad \text{[Equation 2]}$$

where E is the band gap energy difference, h = Planck's constant, ν = the frequency of the incident light, c = the speed of light, and λ = the wavelength of incident light. Thus, the energy difference of the band gap is inversely proportional to the wavelength of incident light. Nanoparticles will only absorb light of wavelengths shorter than that determined by the band gap value. For example, CdS (bulk) has a band gap of 2.42 eV, which corresponds to a wavelength of 512 nm. [15] CdS begins to adsorb light at 512 nm and absorbs continuously into the UV (e.g., shorter wavelengths). As particle size declines, the band gap increases, and the absorbance onset shifts to shorter wavelengths (Figure 10). Thus, onset of absorbance is directly related to particle size.

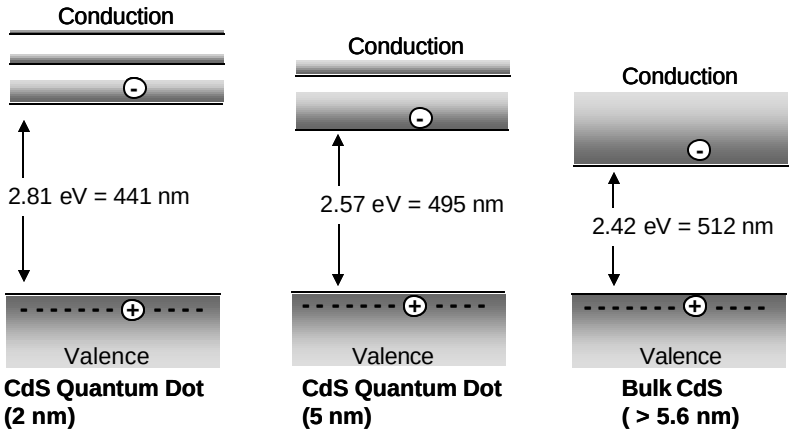

Figure 10: Band Gap Energy and Optical Absorption.

The band gap (eV) increases with decreasing nanoparticle size. Band gap is inversely related to absorbance onset (λ) through the relationship $E=hc/\lambda$. Therefore, smaller particles begin to absorb at shorter wavelengths. [32]

The influence of particle size on optical properties is not limited to absorbance. Particle fluorescence is also a function of the band gap. After an electron is excited, some of its energy is lost to atomic vibrations, satisfying the second law of thermodynamics. Typically, this energy is converted to heat. When the electron decays into the ground state, it will emit light, or fluoresce, at a longer wavelength because of this energy loss (Figure 11A). [33] As the band gap decreases, a smaller amount of energy is dissipated through fluorescent emission to return to the ground state, and the wavelength of emitted light will shift to the red (Figure 11B). Because band gap is inversely proportional to nanocrystal size, larger nanocrystals display red-shifted emission. Additionally, the energy lost to heat decreases in a size-dependant manner.

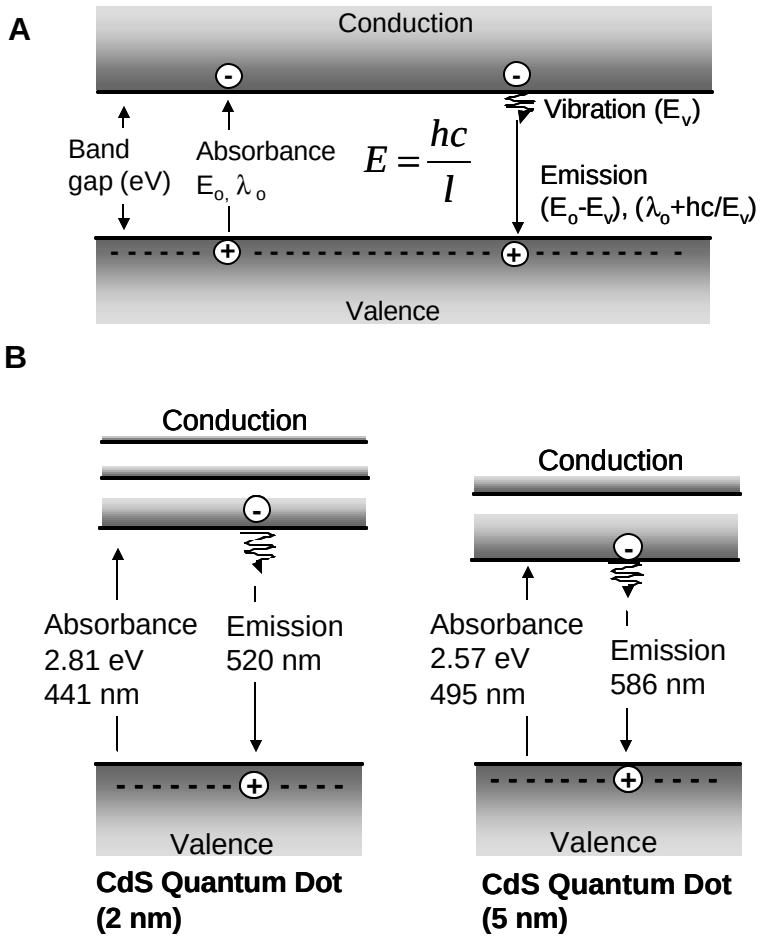

Figure 11: Fluorescent Emission and Particle Band Gap.

(A) Photon absorption creates an excited electron. This electron loses some energy to heat; then decays to ground, emitting a photon. The emitted photon has a longer wavelength than the absorbed photon because of the energy lost to heat. (B) As the band gap (e.g., ΔE) decreases, the particle will absorb at longer wavelengths. This will produce a concomitant red-shift in particle fluorescent emission.

Finally, nanoparticles can exhibit a unique type of fluorescent emission resulting from the trapping of an electron at the crystal surface. [34] When a defect is introduced into the crystal, it can introduce a potential energy state in the forbidden zone (Figure 12). Electrons that enter into this state will become trapped (Figure 9), as photonic emission from this level is forbidden by classical physics. However, quantum mechanics allows for emission from this state, albeit at a low probability, and the electron can eventually decay to the ground state through this mechanism. Because of this delay, the lifetime of an excited electron in a trapped state is significantly longer than that of an electron in an exciton or band gap state, as much as 3 orders of magnitude. [28] Additionally, the shift

between the absorbance wavelength and the emitted wavelength will be larger as a result of the energy lost in decaying to the trapped state.

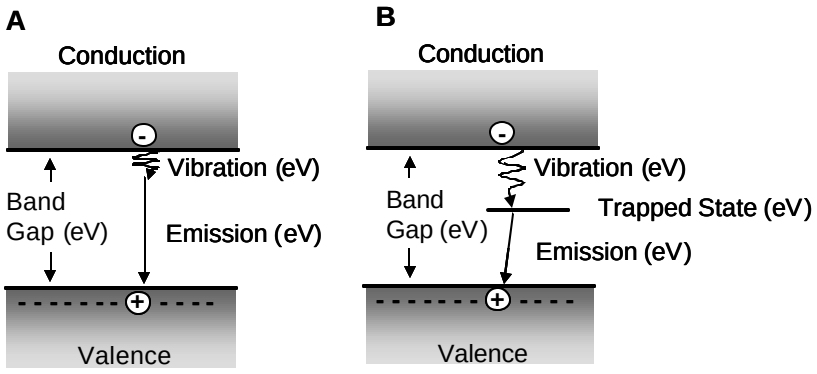

Figure 12: Trapped State Fluorescent Emission.

(A) After absorption of a photon at the band gap energy/wavelength, an excited electron loses some energy to vibration and recombines with the hole, emitting a photon at a slightly longer wavelength. (B) In a system with a trap, the electron first decays into the trap, and then recombines with the hole producing a photon at a longer wavelength than in (A).

2.3 Applications of Quantum Dots in Electronic Devices

Exceptional optical properties make quantum dots attractive components for integration into devices. One significant asset of quantum dots over traditional optoelectronic materials is that they exist in the solid state. Solids tend to be more compact, easily cooled, and allow for direct charge injection. [35] Additionally, quantum dots can interconvert light and electricity in a tunable manner dependant on crystal size, allowing for facile wavelength selection. This is a significant improvement over silicon-based materials, which require modification of their chemical composition (i.e., doping) to alter optical properties. [35] Thus, researchers have experimented with quantum dots in lasers, LEDs, and photovoltaics. Most of these applications are still in early development; however, the benefits of quantum dot components are evident. Our proposed

neuroelectronic interface also converts optical energy into an electrical signal; thus, a study of these applications provides successful models for the development of our system.

2.3.1 Quantum Dot Lasers

The primary employment of quantum dots in optoelectronic devices has been for the development of lasers. [35] Lasers operate through stimulated light emission; as opposed to the spontaneous light emission discussed earlier (see Section 2.2.4). Spontaneous emission occurs when an electron decays from an excited state to the ground state, releasing a photon. However, if an excited electron is bombarded with a photon of the same wavelength as that emitted spontaneously, it may be encouraged to decay to the ground state and release a second photon (Figure 13A). Thus, one photon interacting with an electron can produce two photons of emitted light. Additionally, these two photons will be coherent (i.e., possess the same wavelength and phase) as a result of their interaction. Lasing occurs when these emitted photons can bombard other excited state electrons to produce a sustained chain reaction and amplification of coherent emitted light through stimulated emission. [36]

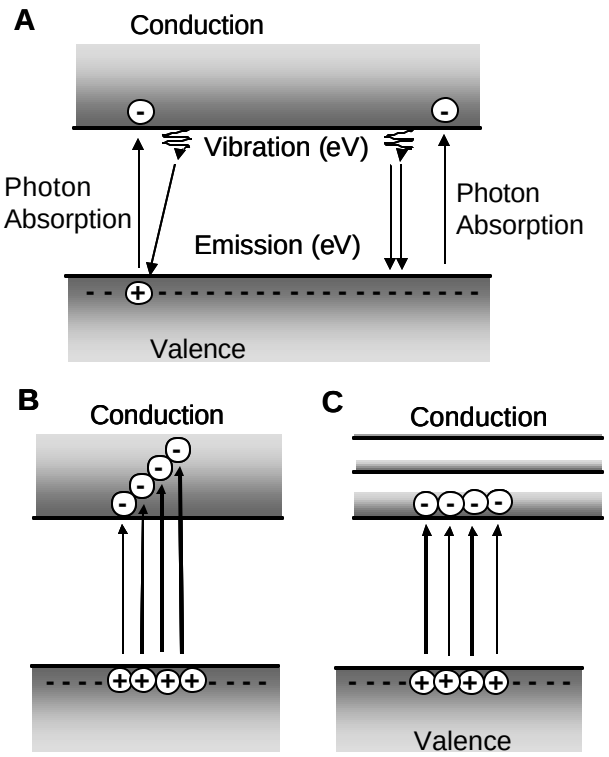

Figure 13: Spontaneous versus Stimulated Emission.

(A) Spontaneous fluorescent emission occurs when an electron is excited from ground to valence and then decays spontaneously back to ground (left). Stimulated emission occurs when a previously excited electron absorbs a photon with the same energy. The electron decays, releasing two coherent photons with the same wavelength (right). (B) Bulk materials can absorb at multiple wavelengths, making it difficult to place electrons at the same energy level. (C) Quantum dots have narrower energy bands; therefore, it is easier to establish electrons in the same energy level.

In order for lasing to occur, there must be more electrons in the excited state than in the ground, and they must all occupy the *same* excited state. Otherwise different wavelengths of light will be required to stimulate electrons in each energy level (Figure 13B), and lasing will be difficult to maintain. The main advantage of quantum dot lasers is that they posses fewer energy states than bulk materials, reducing the "spread" of electrons (Figure 13C). [2] It is thus much easier to create lasing. Additionally, quantum dots can be tuned to a specific emission wavelength by altering the size of the particle, and can be operated within a narrow excitation wavelength range. [35] All of these advantages have led to the development of numerous types of quantum dot lasers.

2.3.2 Quantum Dot Light Emitting Diodes

A second optoelectronic device that utilizes quantum dots is the light emitting diode (LED). A diode is a material that contains positive charges on one side, and negative charges on the other. Under forward bias (voltage), the positive and negative charges meet in the center of the material, annihilating each other and producing emitted light. LEDs are important components used in many technologies, including display elements in cell phones and laptop computers. Currently, these devices are composed of microfabricated semiconductor materials that emit a fixed light wavelength based on their chemical composition. Quantum dots provide a novel alternative to these materials because emission wavelengths can be selected simply by changing the size of the particle. Additionally, because of their small size, quantum dots can easily be encapsulated into conducting organic polymers, allowing for the development of flexible displays. [37] These two advantages will allow for quantum dot LEDs to be utilized in many additional technologies. One exciting prospect is the replacement of incandescent lights with paper thin materials that could produce illumination at a variety of wavelengths and could be molded into any shape. [37]

2.3.3 Quantum Dot Photovoltaics

A third use of quantum dots in electronics is for the creation of advanced photovoltaics, or solar cells. Solar cells convert absorbed light energy into electrical current. Electrons in the material are excited by light absorption, which in turn produces a current that can be conducted away from the device. [2] The primary difficulty with photovoltaic devices is the efficient conversion of light to energy. Light with a wavelength below the value of the band gap will not be adsorbed, and is not converted to energy. Further, any electron excited with a photon greater than the band gap value, will

dissipate the extra energy as heat. Only the portion of energy corresponding to the band gap will produce a current. The advantage of quantum dot photovoltaics is that multiple particles can be incorporated into a single solar cell, and each particle can have a different band gap. [2] Thus, a solar cell can be constructed that is responsive to the entire spectrum of emitted solar light.

2.3.4 Summary of Quantum Dot Electronic Devices

The advantages of quantum dots in optoelectronic devices are significant. Their size-tunable emission wavelengths, continuous adsorption, and small sizes have already provided impetus for the development of lasers, LEDs, and solar cells. As improvements continue to be made in quantum dot synthesis and crystal structure, the optical properties of nanoparticles are enhanced. Thus, quantum dots increasingly become a viable and preferable alternative to microfabricated semiconductor materials. All of these applications establish the utility of quantum dots to interconvert light and energy, and pave the way for the development of future applications, including optically excited quantum dot-neuroelectronic devices.

2.4 Applications of Quantum Dots in Biology

Nanoparticles have also been explored in a number of biological uses. The first demonstration of their utility in a biological context occurred in 1998 by A.P. Alivisatos, et al. [5] and S. Nie, et al. [6] Both groups employed CdSe/ZnS quantum dots as fluorescent labels. Coupling the quantum dots directly to biorecognition molecules (e.g., antibodies, proteins), the particles could be targeted to particular parts of the cell, producing a fluorescent indicator. Fluorescent labeling is an important tool in biology

that is used to track the positions of entire cells, intracellular structures, and disease markers in tissue specimens. This application has become the primary biological use for quantum dots because of their advantageous optical characteristics.

Quantum dots offer several enhancements over the organic fluorescent dyes that are typically used for biological labeling. Organic dyes can exhibit a low quantum yield, or brightness, because of molecular interactions with themselves, each other, and the solvent. Quantum dots are also susceptible to these limitations, but the particles may be passivated with protective insulating materials to produce quantum yields that are > 50%. [38] Another limitation of organic dyes is the loss of fluorescence that occurs when dye molecules react irreversibly with each other or the solvent, producing a non-fluorescent product. This process, known as photobleaching, can occur in aqueous solution on the order of minutes. [6] However, photobleaching in quantum dots is diminished, as the same passivating layer that enhances quantum yield also protects particles from external interactions. Most notably, passivation reduces photooxidation of the particle core, which can produce free ions (e.g., Cd^{2+} in our case) and eventually particle dissolution. [39] As a result of reduced photobleaching, quantum dots can exhibit continuous fluorescence for a time period an order of magnitude greater than organic fluorescent dyes. [6]

Also, organic fluorescent dyes typically exhibit fixed, narrow excitation spectra. Fluorescent excitation spectra reflect absorbance spectra; and as discussed earlier, quantum dot absorbance is continuous after the size-tunable onset. Thus, quantum dots may be excited in a range of wavelengths selected by their size. Additionally, the emission bandwidth (e.g., wavelength range of emitted light) for nanoparticles can be particularly narrow (~20-30 nm) when compared with organic dyes (> 40 nm, often with a tail into red wavelengths). [5] This results from the shrinking and splitting of potential energy bands as particle size decreases (Figure 7). Photon emission can only occur from

an allowed energy state in the conduction band to an allowed energy state in the valence band. As the width of these bands decreases, the number of acceptable energy transitions declines and the range of emitted wavelengths are diminished. All of these properties have led to quantum dot applications in diverse biological fields, including biosensing, cellular labeling, and *in vivo* fluorescent detection and therapeutics.

2.4.1 Quantum Dots Biosensors

Biosensors detect molecules of biological significance through an optical or electrical signal produced upon analyte recognition. Although their initial use was primarily for disease detection and monitoring, there has been a recent resurgence in the detection of bio-warfare agents; and a great deal of federal funding has been directed to this purpose. [40] Most biosensors operate on the principle of molecular recognition. Antibodies, peptides, proteins, and DNA sequences all bind tightly to their target biomolecules with high specificity. [41] Dyes can be coupled to these recognition molecules to produce a fluorescent event when binding occurs. Quantum dot biosensors offer many benefits to those based on dye molecules. The surface of quantum dots can be easily altered, providing a facile route for conjugation to recognition molecules. [1] Additionally, their small size allows for incorporation into existing electronic devices. Several types of biosensors have been studied, but the most common utilize fluorescence resonance energy transfer (FRET) or the aggregation of fluorescent probes to detect analytes.

2.4.1.1 FRET-Based Biosensors

The simplest method for detection using fluorescent molecules is a system that produces an on or off signal upon binding. This can be accomplished using FRET. First, an electron in a fluorescent molecule is excited. Then, instead of decaying through photon emission, the energy in that electron is dissipated by transfer to a second molecule. This quenches the fluorescence of the first molecule. FRET is a distance dependant event. As the FRET donor and acceptor move away from each other, transfer no longer occurs and fluorescence in the donor is restored. [42] If a conformational change can be introduced upon analyte binding that separates the two molecules, a fluorescent on/off signal can be produced.

This has been accomplished in a number of systems. A combination of gold quantum dots (which do not fluoresce) and organic fluorophores have been utilized to create DNA sensors. [43] Gold quantum dots were bound to single stranded DNA sequences, which were terminated with fluorescent molecules, or fluorophores. The fluorophores formed an arched structure that interacted with the nanoparticle surface, quenching fluorescence (Figure 14). However, when the complement DNA was introduced, binding occurred and the conformation changed. The fluorophore migrated away from the quantum dot surface and its fluorescence was restored. This technique is very accurate, the mismatch of a single base pair in a 30 amino acid DNA sequence could be detected. [43]

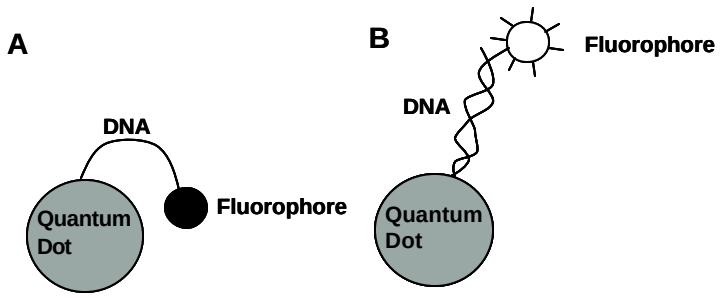

Figure 14: Detection of DNA Binding Through FRET.

(A) Fluorophore-conjugated single stranded DNA is bound to a quantum dot, forming an arched structure with the nanoparticle surface. Fluorophore fluorescence is quenched through FRET with the nanoparticle. (B) When the complement DNA is added, the DNA structure changes, moving the fluorophore away from the nanoparticle and restoring fluorescence.

A second, similar system utilized fluorescent CdSe/ZnS quantum dots to detect sugar binding. [44] The initial configuration contained cyclodextrin molecules conjugated to a non-fluorescent FRET acceptor. The cyclodextrin adhered to maltose (i.e., sugar) binding protein, which was present on the quantum dot surface. FRET between the nanoparticle and the acceptor molecule quenched quantum dot fluorescence. However, when maltose was introduced, the cyclodextrin was displaced, restoring fluorescence to the quantum dot. Although maltose sensing was demonstrated, these sensors could eventually be adapted to detect glucose, a crucial molecule to monitor in the management of diabetes.

Finally, systems need not be hybrids, incorporating nanoparticles and fluorescent dyes; homogeneous systems have also been constructed. [45] Two types of CdTe quantum dots were bound to model proteins. Red-emitting quantum dots were conjugated to bovine serum albumin (BSA), while green-emitting quantum dots were conjugated to an antibody that binds BSA (i.e., anti-BSA). When the two quantum dots were incubated together, the green fluorescence was quenched, as excited electrons transferred their energy to the red-emitting particles. Further, the red fluorescence was enhanced because

energy transferred from the green-emitting quantum dots was dissipated through the red-emitting quantum dot.

FRET-based quantum dot biosensors are elegant, and in theory can provide analyte detection of as few as 10 parts per trillion. [45] Additionally, the signal is easy to interpret: fluorescence indicates the presence of an analyte. FRET-based biosensors can also provide quantitative information, as fluorescent intensity can be correlated to the number of molecule binding events. Although FRET systems could be constructed entirely from fluorescent dye molecules, quantum dots provide an excellent alternative. They display high quantum yield; and their acceptor energy and emission wavelengths can be tailored by changing the size of the particle.

2.4.1.2 Aggregation-Based Biosensors

Another type of biosensor constructed using quantum dots is based on particle aggregation. Many biomolecules possess recognition sites for different binding targets. These biomolecules can be used to link quantum dots together. If one population of nanoparticles is conjugated to target A, and another to target B, when a biomolecule recognizing A and B is introduced, aggregation of the particles will result. Depending on the type of quantum dot, this can produce increased fluorescence or a change in color. CdSe/ZnS quantum dots have been used to identify DNA molecules with this technique. [46] Two types of 15 amino acid single stranded DNA were conjugated to the nanoparticle surface. When 30-amino acid DNA complementary to both sequences was introduced, aggregation of the nanoparticles occurred. This change could be easily visualized with a fluorescence microscope. A second system is based on gold quantum dots, which do not fluoresce, but change visible color upon aggregation. [47] Again two types of single stranded DNA were conjugated to nanoparticles. When the complement

was introduced, the color of the nanocrystal solution changed from red to blue as a result of particle aggregation.

While these systems are functional, they are not as elegant as FRET-based biosensors. They require a greater quantity of analyte to produce detection, and the signal is not quantitative. However, they may offer improvements to biosensors constructed using fluorescent dyes because the nanocrystal surface chemistry can be easily altered, [1] aiding in bioconjugation. Quantum dot biosensors are still in early development, but already present a viable alternative to dye-based systems. With their unique optical properties, there is no doubt that they will continue to be utilized in these devices.

2.4.2 Quantum Dot Fluorescent Labels for Cells

The most prevalent biological use of quantum dots has been fluorescent labeling of cells. In this function, quantum dots are not only superior to fluorescent dyes, but have also extended the potential applications of fluorescent labels in biological systems. For example, they have been used to investigate the motion of biomolecules, detect cell phenotype, and study cell migration. In each of these uses, they present several enhancements over systems employing fluorescent dyes. Most importantly, their small size and high resistance to photobleaching have allowed quantum dots to be used in a number of high throughput systems with real-time monitoring, [48] a difficult feat with dye molecules.

One new use of quantum dot labels has been the detection of single molecules within the cellular environment. Normally, single molecule tracking is accomplished using fluorescent beads (e.g., rhodamine on polystyrene) that can have sizes from tens of nanometers to a micron. [49] However, these beads cannot be used in all situations; in some cases, they cannot penetrate the confined spaces to be monitored. With their small

size, quantum dots can be employed to track and study the motion of molecules in these locations. For example, quantum dots have been used to investigate the movement of neurotransmitter receptors in the synaptic cleft. Researchers were able to study the diffusion dynamics of glycine receptors over several minutes, an achievement that would have been nearly impossible using fluorescent beads. [49] This technique has also been used to detect transferrin uptake, the transport of charged dye molecules, and oligonucleotide motion. [50] Thus, quantum dots have been shown to provide real-time monitoring of biomolecules in living cells. This approach can provide new insights into cell function and promote novel methods of disease treatment.

Another unique use of quantum dots is for the identification of particular cell types in a mixed population. This is critical for cancer detection, as well as drug screening. [48] Commonly, cells are distinguished by observation of phenotype or by fluorescently tagging uniquely expressed bio-markers. However, the implementation of these techniques has been difficult in practice. Phenotype distinction requires detailed inspection of individual cells and is difficult to automate, limiting its use in high-throughput applications. On the other hand, fluorescent molecules must possess a wide range of distinct emission wavelengths to label all of the desired cell types in a population. The emission wavelengths of organic dyes are difficult to modify because they are determined by the composition of the material. Additionally, dyes can have large emission bandwidths, creating difficulty in distinguishing individual colors. Quantum dots, with their narrow emission bandwidths and size tunable fluorescence are ideal labels for cell detection. Multi-plexed imaging of cells has been demonstrated for up to 5 different cell types, and could in theory be expanded to detect over 100 distinct types of cells. [48] This system was also used to provide monitoring in real time, with the simultaneous observation of calcium levels in three different cell types. High-throughput

identification of individual cells in a heterogeneous environment will improve cancer diagnosis, whereas real-time monitoring of biomolecule expression in different populations could provide new insights into drug metabolism and function.

A final, notable use of quantum dots as cellular labels is in the study of cell motion. The detection of increased migration is important, especially when estimating the metastatic potential of cancer cells. Migrating cells can ingest molecules as they move over them, leaving behind a path known as a phagokinetic track. [51] In the past, phagokinetic tracks have been monitored using gold particles with diameters from microns to several hundred nanometers. However, these particles do not adhere well to the substrate, and their large size can perturb cell mobility. Because of their high resistance to photobleaching, quantum dots are the first fluorescent labels that have demonstrated the potential for detection of phagokinetic tracts. Additionally, they can be easily placed on the substrate and have sizes unlikely to affect cell mobility. In early experiments, quantum dots were able to distinguish between cancerous and non-cancerous cells and remained luminescent for over one week. [51]

The unique optical properties of quantum dots have not only produced superior fluorescent labels, but also have expanded the use of labeling technologies into new fields. To capitalize on the success of quantum dot labeling, two commercial companies, Quantum Dot Corporation (Hayward, CA) and Evident Technologies (Troy, NY), have both begun to produce nanoparticle–bioconjugates, making this technology easily accessible to biologists. With continuing improvements in biocompatibility and stability, quantum dot labels will continue to find use in new applications.

2.4.3 *In Vivo* Applications of Quantum Dot Labels

The most exciting possibility for quantum dot labels has been their use *in vivo.* This is no small task. The penetration of excitation and emission light can be difficult *in vivo,* as tissue is transparent to light only in a limited spectral range, mostly at longer, infrared wavelengths. [52] Additionally, the metabolism and biocompatibility of nanocrystals *in vivo* have proven to be much more complicated than in single cells. The majority of nanoparticles used in biological applications have been based on a Cd–X structure, where X = tellurium, sulfur, or selenium. Cadmium is known to interfere with DNA mismatch repair [53], can inhibit certain types of neuronal firing [54], and is a known carcinogen [55]. Therefore, toxicity of the particles has been a major concern. Surface passivation can significantly reduce the risk of exposure to free cadmium, [56] and although the long-term effects of nanoparticle exposure have not yet been investigated; short-term *in vivo* studies do not demonstrate any acute effects. [8, 57-62] Quantum dots have been utilized in a number of *in vivo* procedures that would not be possible with organic fluorescent dyes. Many of these take advantage of the longevity of their fluorescence, as a result of resistance to photobleaching; [57-60] while others exploit their electrical properties to deliver therapeutic treatment. [8, 61-62]

One novel use of quantum dots *in vivo* has been to monitor embryogenesis. [57] When quantum dots were injected into frog (i.e., *Xenopus*) embryos, they were transferred from parent to daughter cells upon cell division. The particles maintained their fluorescence over many cell division cycles and did not appear to be toxic. They were used to track the movement of different structures in the embryonic frog, as the embryo matured to a tadpole. The use of fluorescent dyes in this system would have been very demanding because of high levels of photobleaching. Thus, the utilization of quantum dots presented a significant advance that allowed for long-term monitoring of

embryonic growth. Ultimately, this technique will allow developmental biologists to form a better understanding of growth in the early embryo and thus elucidate the nature of specific birth defects.

Another use of quantum dots *in vivo* has been to image structures within the body. Currently, vasculature is visualized using fluorescent dextrans. Some of the most challenging regions to image with these molecules are skin and adipose (i.e., fat) tissue because of their high degree of light scattering. Using quantum dots in living mice, researchers were able to visualize capillaries several hundred micrometers below the surface of the skin. [58] Producing the same image with dextran dyes required five times as much power and was much less detailed. With their narrow bandwidths and high quantum yields, nanoparticles provide improved imaging capabilities to dextran dyes. Thus, quantum dots have been shown to present viable alternatives to current clinical practice.

Quantum dots have also been used to track the *in vivo* motion of biomolecules and cellular structures over time. [59] Fluorescent dyes, with their high susceptibility to photo-bleaching, are difficult to use in this context. However, nanoparticles can be used to monitor the motion of proteins, peptides, antibodies, or therapeutic agents in real time. [59] For example, when quantum dots were conjugated to peptides that bound the lung and tumor vasculature, they could be visualized *in vivo.* [60] Eventually, these techniques could be used to improve drug delivery and understand biomolecule circulation in the body.

Finally, quantum dots have been evidenced in limited therapeutic contexts. Quantum dots can be used to image and even penetrate cancer cells, through receptor-mediated endocytosis. [62] Particles can be coupled to therapeutic agents, which are activated in the presence of light excitation. Gold nanoshells conjugated to recognition

molecules can be used to image tumors. [8] When they are optically excited they produce heat. Depending on the size of the nanoshell, heat production can be significant enough to kill the attached cells. Additional systems are envisioned that could release therapeutic agents, including chemotherapy drugs, upon light activation. [61] By only targeting the cells of interest, systems for localized drug delivery could significantly reduce the toxic effects of chemotherapy. These ideas take advantage of the combined electrical and optical properties of quantum dots, and serve as models toward the development of other combined optoelectronic systems, including neuroelectronic interfaces.

2.4.4 Summary of Quantum Dot Biological Applications

With their high quantum yields, resistance to photobleaching, narrow bandwidths, and size-tunable spectra, quantum dots have significant advantages over fluorescent dyes. This has made fluorescent labeling the primary application of quantum dots in biology. In this context, they have been demonstrated as biosensors, fluorescent labels for cells and tissue, and even as *in vivo* therapeutic agents. Many of these applications are not possible with fluorescent dyes. For example, quantum dots have been used for high-throughput and long-term imaging, techniques that are difficult to implement with fluorescent dyes. Additionally, combined systems that utilize both electrical and optical properties have been developed. These systems provide models for future development of neuroelectronic interfaces. As improvements in biocompatibility and optical properties continue to be made, quantum dots will find even more uses in biology.

2.5 PROPOSED QUANTUM DOT-NEURONAL RECEPTOR INTERFACE

Our proposed system combines aspects of quantum dot optoelectronic devices and biological uses to create the first system capable of producing *electrical* interactions with cells. Specifically, we anticipate that electrical signals from the nanoparticle can modulate the behavior of neuronal voltage-gated ion channels. These channels are the primary mechanism of signal propagation in a neuron. They consist of four repeated subunits containing six transmembrane spanning regions. These transmembrane regions include positively-charged alpha helices that are normally attracted to the negatively-charged interior of the cell, producing a closed pore (Figure 15A). However, when the membrane experiences a localized change in voltage (Chapter 1, Section 1.1), the alpha helices move toward the exterior cell surface, opening the pore (Figure 15B). [63] Quantum dots could potentially be used to produce these local changes in membrane potential.

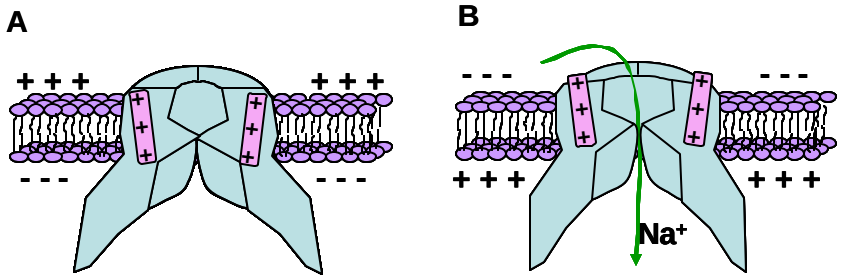

Figure 15: Voltage-Gated Ion Channel.

(A) At rest, the positively charged alpha helices of the ion channel are attracted to the cell interior, closing the channel pore. (B) When a localized membrane depolarization occurs, the alpha helices move to the exterior cell surface, opening the pore and allowing ions to pass.

There are several possible mechanisms for quantum dot electrical interaction with ion channels. For example, electron transfer has already been demonstrated between quantum dots and methylviologen [64-65], a biomolecule. However, we believe that the most likely method of ion channel stimulation is through the nanoparticle electric field,

which is a result of the optically-created transient dipole moment (Section 2.2.3). [28] If this electric field is strong enough, an induction response may elicit changes in the local cell potential (Figure 16). Previous groups have used induction to stimulate neurons and to measure existing signals, leading to microarray devices that communicate with the cell. [66]

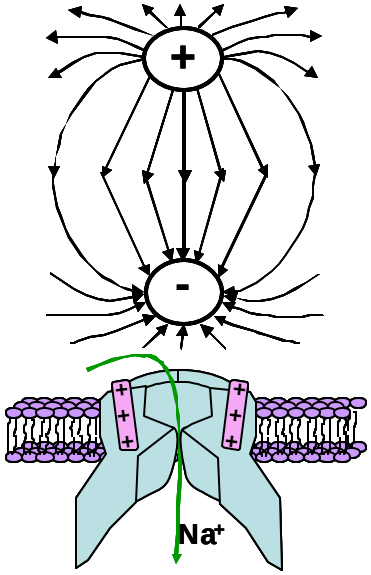

Figure 16: Nanoparticle Dipole Moment and Ion Channel Activation.

The dipole moment of an optically excited nanoparticle (black) produces an electric field (arrows). That field may be strong enough to attract alpha helices in the ion channel (pink) to the membrane surface, opening the ion channel pore. This allows Na^+ ions to enter the cell (green), eliciting an action potential.

Nanoparticle dipole moments result from charge separation between the electron and hole in the exciton (Section 2.2.3). This occurs primarily because of electron trapping at the nanoparticle surface. These dipole moments create an electric field and associated potential.[28] A simplistic view allows us to approximate the dipole as a point source (Figure 17A). The voltage between it and any given point is supplied by the following equation: [67]

$$V = \frac{kp\cos q}{r^2} \qquad \text{[Equation 3]}$$

where k is $(4\pi\varepsilon_o)^{-1}$ = 8.98 x 10^9 N-m^2/C^2, p is the dipole moment in C-m (1 Debye = 3.336 x 10^{-30} C-m), and r and θ are the distance and angle between the center of the dipole and the point of interest.

However, this equation assumes that the separation of charges in the dipole (d) is much less than the distance of the dipole to the point of interest (r). This is not rigorously correct for our interface. The separation of charges in the dipole is approximately the diameter of the nanoparticle (i.e., 1-5 nm), while the ion channel may be as close as a few nanometers. Thus, a more appropriate means to determine the dipole voltage field treats each charge as a point source. With this method, the voltage between the dipole and point of interest is given by: [67]

$$V = kq\left[\frac{r_- - r_+}{r_+ r_-}\right] \qquad \text{[Equation 4]}$$

where k is $(4\pi\varepsilon_o)^{-1}$ = 8.98 x 10^9 N-m^2/C^2, q is the charge of an electron = 1.602 x 10^{-19} C, and r_+ and r_- are the distances between the point of interest and the positive and negative charges of the dipole, respectively (Figure 17B). If we examine a point directly opposite one of the charged poles, this equation reduces to:

$$V = \left[\frac{kp}{r^2 - d^2/4}\right] \qquad \text{[Equation 5]}$$

where k is $(4\pi\varepsilon_o)^{-1}$ = 8.98 x 10^9 N-m^2/C^2, p is the dipole moment in C-m (1 Debye = 3.336 x 10^{-30} C-m), r is the separation distance from the center of the dipole to the point of interest, and d is the separation of the positive and negative dipole charges.

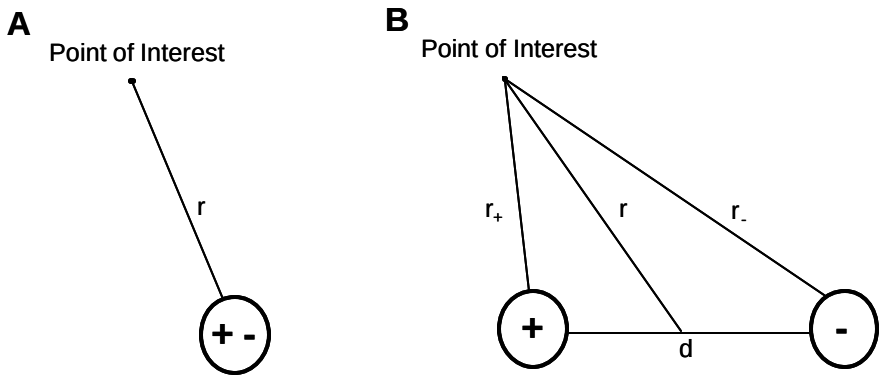

Figure 17: Calculating the Electrical Potential of a Dipole Moment.

(A) If r >> d, the dipole is approximated as a point source. (B) If r ~ d, then we must represent each pole as a point source.

Using this equation, we estimated the potential created by dipole moments from 20-40 Debye at various separation distances. These dipole strengths represent similar magnitudes to published values (i.e., ~30 Debye [29]). Our calculations (Figure 18) showed that voltage potentials capable of stimulating ion channels (i.e., > 15 mV [6]) could be obtained for separation distances of ~ 10 nm or less, and measurable potentials (i.e. > ~ 5 mV) were produced at separation distances of ~ 15 nm or less. Many linker molecules (e.g., antibodies or peptides) can produce separation distances of this magnitude [68-69], thus it is theoretically possible for nanoparticles to activate ion channels.

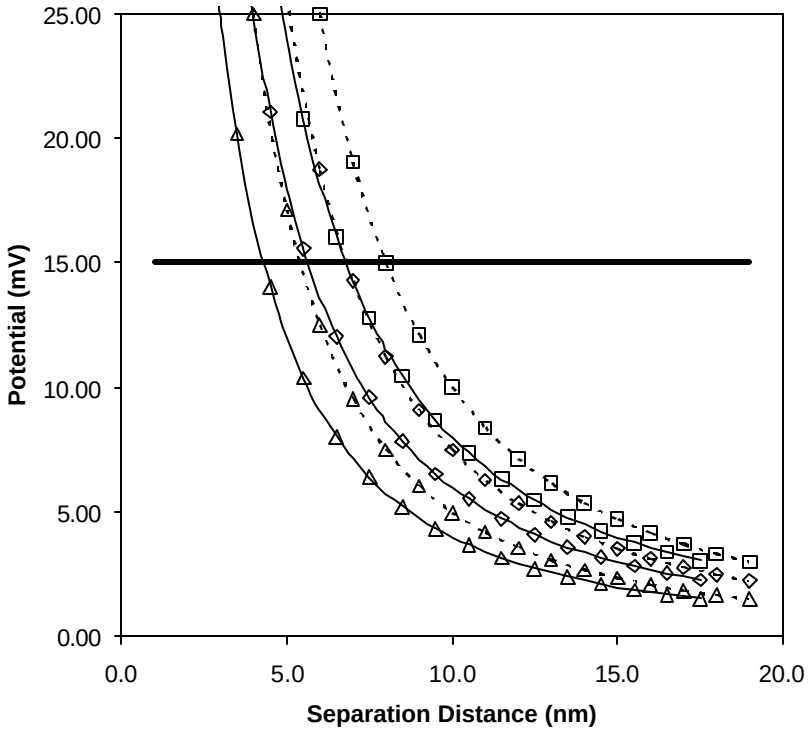

Figure 18: Electric Dipole Potential.

The potential of an electric dipole moment is plotted for values of Δ = 20, ◊ = 30, and □ = 40 Debye and nanoparticle sizes of 2 (dashed) and 5 (solid) nm. Higher dipole moments and smaller nanoparticle sizes produce a stronger potential. A potential of 15 mV (bold line) is required to activate an ion channel.

However, these results apply to interactions taking place in deionized water. Biological systems require a particular osmotic pressure, provided by ~150 mM saline [70], for survival. The addition of salt ions can produce a screening effect (Figure 19) that reduces the electric field strength of the dipole. This screening is described by the Debye Length, which is the distance required for the potential intensity to drop by a value of *e*. [71] The Debye length of normal saline is 0.8 nm. [72] We can account for screening by

incorporating the Debye length into our equations through the following relationship: [71]

$$\text{Equation 6: } V = EXP\left(\frac{-r_{pole}}{0.8}\right)\left[\frac{kp}{r^2 - d^2/4}\right]$$

where k is $(4\pi\varepsilon_o)^{-1}$ = 8.98 x 10^9 N-m^2/C^2, p is the dipole moment in C-m (1 Debye = 3.336 x 10^{-30} C-m), r is the separation distance from the center of the dipole to the point of interest, r_{pole} is the separation distance from the closest pole to the point of interest, and d is the separation of the positive and negative dipole charges.

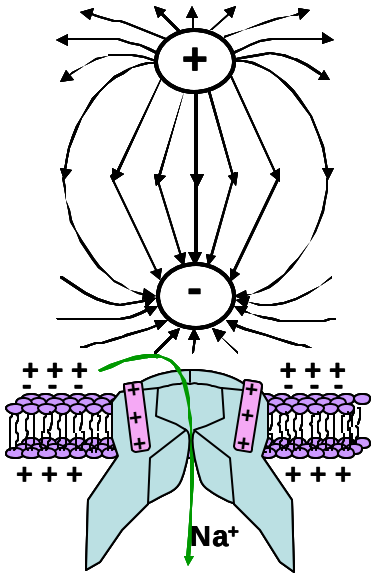

Figure 19: Charge Screening and the Nanoparticle Dipole Moment.

The addition of normal saline (~150 mM), which is required for cell survival, produces a layer of salt ions between the dipole and the cell surface. This ion layer reduces the electric field of the dipole moment, decreasing the likelihood of ion channel stimulation.

When we include the effects of charge screening, the minimum separation distance required to create an action potential declines significantly (Figure 20). Distances of less than ~2 nm can theoretically produce an action potential, and distances of less than ~2.5 nm can create a measurable voltage change in the membrane. This

separation can be achieved with certain linker molecules (i.e., peptides [69]), but is difficult to produce. However, there are several mitigating factors that are not considered in this approximation. For example, we are estimating the field for one nanocrystal, but it is highly probably that multiple nanoparticles will be bound to a single ion channel. Depending on nanoparticle alignment, the collective dipole could be many times that of a single nanocrystal. Additionally, the cell membrane is not a static surface; it is a capacitor that separates internal negative charge from external positive charge (Figure 20). [73] These charges would be influenced by the presence of the dipole and could augment the potential. When we include these factors, it is quite possible that nanoparticles produce dipole moments of sufficient intensity to modulate neuronal ion channels. Through optimization of the most important limitations: the strength of the dipole moment, the size of the nanocrystal and its separation distance from the ion channel, we believe that a viable system can be created.

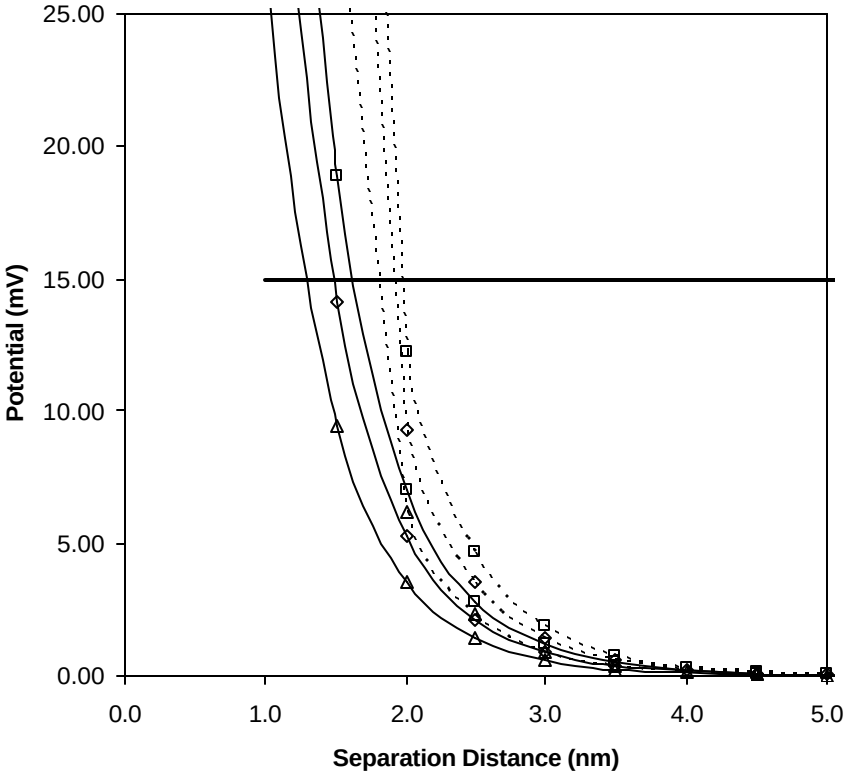

Figure 20: Electric Dipole Potential with Charge Screening.

The potential of a screened electric dipole moment in normal saline (~150 mM) is plotted for values of Δ = 20, ◊ = 30, and □ = 40 Debye and nanoparticle sizes of 2 (dashed) and 5 (solid) nanometers. A potential of 15 mV (bold line) is required to activate an ion channel.

2.6 CONCLUSIONS

Quantum dots, or nanocrystals, have many unique properties that result from their small size. The properties occur because of quantum confinement in the nanocrystal, which leads to a reduction in the density of potential energy states and a size-tunable band gap. Electrical and optical properties that result from these features include electron transfer, the formation of a transient dipole moment, continuous absorption at

wavelengths smaller than a size-tunable onset, size tunable emission wavelengths, and trapped-state emission. The combination of these properties has led to numerous applications in optoelectronics. Quantum dot lasers, light emitting diodes, and photovoltaics have all been investigated. However, the influence of quantum dots has not been limited to engineering; several significant biological technologies have been developed. Biosensing, monitoring of live cells, and *in vivo* imaging have all been demonstrated. These techniques rely upon the use of quantum dots primarily as fluorescent labels.

Our interface would combine these two functionalities to create electrical systems that could modulate biological entities. Particularly, stimulation of neuronal ion channels could be provoked with the electric field produced by an optically excited nanoparticle. Our application represents the first system that combines these electrical and biological features. Future directions will likely lead to a greater integration of these two phenomena to create new classes of biological optoelectronic devices possessing the capability to interact with cells at increasingly smaller length scales.

2.7 REFERENCES

1. A.P. Alivisatos. “Perspectives on the Physical Chemistry of Semiconductor Nanocrystals.” J. Phys. Chem. 100: 13226, 1996.

2. T.J. Bukowski and J.H. Simmons. “Quantum Dot Research: Current State and Future Prospects.” Crit. Rev. Solid State Mat. Sci. 27(3): 119, 2002.

3. C.J. Murphy and J.L. Coffer. “Quantum Dots: A Primer.” App. Spect. 56(1): 16A, 2002.

4. B. Alberts, D. Bray, J. Lewis, M. Raff, K. Roberts, and J.D. Watson. Molecular Biology of the Cell, 3rd Ed., Garland Publishing, New York: 1994, pp. 101, 275, 996.

5. M. Bruchez, Jr., M. Moronne, P. Gin, S. Weiss, and A.P. Alivisatos. “Semiconductor Nanocrystals as Fluorescent Biological Labels.” Science 281: 2013, 1998.

6. W.C.W. Chan and S. Nie. “Quantum Dot Bioconjugates for Ultrasensitive Nonisotopic Detection.” Science 281: 2016, 1998.

7. X. Gao and S. Nie. “Molecular Profiling of Single Cells and Tissue Specimens with Quantum Dots.” Trends Biotech. 21(9): 371, 2003.

8. C. Loo, A. Lin, L. Hirsch, M.H. Lee, J. Barton, N. Halas, J. West, and R. Drezek. “Nanoshell-Enabled Photonics-Based Imaging and Therapy of Cancer.” Tech. Cancer Res. Treat. 3(1): 33, 2004.

9. W.L.C. Rutten. “Selective Electrical Interfaces with the Nervous System.” Annu. Rev. Biomed. Eng. 4: 407, 2002.

10. S.A. Campbell. The Science and Engineering of Microelectronic Fabrication, 2nd Ed., Oxford University Press, New York: 2001, p. 153.

11. B. Alberts, D. Bray, J. Lewis, M. Raff, K. Roberts, and J.D. Watson. Molecular Biology of the Cell, 3rd Ed., Garland Publishing, New York: 1994, p. 996.

12. G.R. Brewer, Ed., Electron Beam Technology in Microelectronic Fabrication. Academic Press, New York: 1980.

13. F. Patolsky, Y. Weizmann, O. Lioubashevski, and I. Willner. “Au-Nanoparticle Nanowires Based on DNA and Polylysine Templates.” Angew. Chem. Int. Ed. 41(13): 2323, 2002.

14. C.B. Murray, C.R. Kagan, and M.G. Bawendi. "Synthesis and Characterization of Monodisperse Nanocrystals and Close-Packed Nanocrystal Assemblies." Ann. Rev. Mat. Sci. 30: 545, 2000.

15. K. Kalyanasundaram, E. Borgarello, D. Duonghong, and M. Grätzel. "Cleavage of Water by Visible-Light Irradiation of Colloidal CdS Solutions: Inhibition of Photocorrosion by RuO_2" Angew. Chem. Int. Ed. Engl. 20(11): 987-988, 1981.

16. R. Rossetti, S. Nakahara, and L.E. Brus. "Quantum Size Effects in the Redox Potentials, Resonance Raman Spectra, and Electronic Spectra of CdS crystallites in aqueous solution." J. Chem. Phys. 79(2): 1086, 1983.

17. L.E. Brus. "A Simple Model for the Ionization Potential, Electron Affinity, and Aqueous Redox Potentials of Small Semiconductor Crystallites." J. Chem. Phys. 80(9): 5566, 1983.

18. R. Rossetti, J.L. Ellison, J.M. Gibson, and L.E. Brus. "Size Effects in the Excited Electronic States of Small Colloidal CdS Crystallites." J. Chem. Phys. 80(9): 4464, 1984.

19. S.A. Empedocles, R. Neuhauser, K. Shimizu, and M.G. Bawendi. "Photoluminescence from Single Semiconductor Nanostructures." Adv. Mats. 11(15): 1243, 1999.

20. L.E. Brus. "Electron-Electron and Electron-Hole Interactions in Small Semiconductor Crystallites: The Size Dependence of the Lowest Excited Electronic State." J. Phys. Chem. 80(9): 4403, 1984.

21. P. Atkins. Physical Chemistry, 5th Ed., W.H. Freeman and Co., New York: 1994, pp. 367-368.

22. R.H. Bube. Electrons in Solids, 2nd Ed., Academic Press, Boston: 1988, p. 120.

23. W.E. Buhro and V.L. Colvin. "Semiconductor Nanocrystals: Shape Matters." Nat. Mats. 2: 138, 2003.

24. W.D. Callister, Jr. Materials Science and Engineering: An Introduction. John Wiley and Sons, New York: 2000, pp. 610-612.

25. W.D. Callister, Jr. Materials Science and Engineering: An Introduction. John Wiley and Sons, New York: 2000, pp. 608-610.

26. R. Rossetti, S.M. Beck, and L.E. Brus. "Direct Observation of Charge-Transfer Reactions Across Semiconductor: Aqueous Solution Interfaces Using Transient Raman Spectroscopy." J. Am. Chem. Soc. 106: 980, 1984.

27. R.G. Mortimer. Physical Chemistry. Benjamin/Cummings Publishing Co., Redwood City, California: 1993, p. 614.

28. Y. Wang and N. Herron. "Nanometer-Sized Semiconductor Clusters: Materials Synthesis, Quantum Size Effects, and Photophysical Properties." J. Phys. Chem. 95: 525, 1991.

29. V.L. Colvin and A.P. Alivisatos. "CdSe Nanocrystals with a Dipole Moment in the First Excited State." J. Chem. Phys. 97(1): 730, 1992.

30. S.G. Raptis, M.G. Papdopolous, and A.J. Sadlej. "The Correlation, Relativistic, and Vibrational Contributions to the Dipole Moments, Polarizabilities, and First and Second Hyperpolarizabilities of ZnS, CdS, and HgS." J. Chem. Phys. 111(17): 7904, 1999.

31. P. Atkins. Physical Chemistry, 5th Ed., W.H. Freeman and Co., New York: 1994, pp. 540-541.

32. H. Weller, H.M. Schmidt, U. Koch, A. Fojtik, S. Baral, A. Henglein, W. Kunath, K. Weiss, and E. Dieman. "Photochemistry of Colloidal Semiconductors. Onset of Light Absorption as a Function of Size of Extremely Small CdS Particles." Chem. Phys. Lett. 124(6): 557, 1986.

33. P.W. Atkins. Physical Chemistry, 1st Ed., WH Freeman and Co., San Francisco: 1978, p. 595.

34. A. Hässelbarth, A. Eychmüller, and H. Weller. "Detection of Shallow Electron Traps in Quantum Sized CdS by Fluorescence Quenching Experiments." Chem. Phys. Lett. 203(2-3): 271, 1993.

35. C. Weisbuch, H. Benisty, and R. Houdré. "Overview of Fundamentals and Applications of Electrons, Excitons, and Photons in Confined Structures." J. Luminescence. 85: 271, 2000.

36. C.B. Hitz. Introduction to Lasing Technology. IEEE Press, Piscataway, NJ: 2001, pp. 67-69.

37. S. Coe-Sullivan, W.-K. Keung, J.S. Steckel, M. Bawendi, and V. Bulovic. "Tuning the Performance of Hybrid Organic/Inorganic Quantum Dot Light-Emitting Devices." Org. Elec. Phy. Mats. Appl. 4(2-4): 123, 2000.

38. M.A. Hines and P. Guyot-Sionnest. "Synthesis and Characterization of Strongly Luminescing ZnS-Capped CdSe Nanocrystals." J. Phys. Chem. 100: 468, 1996.

39. L. Spanhel, M. Haase, H. Weller, and A. Henglein. “Photochemistry of Colloidal Semiconductors. 20. Surface Modification and Stability of Strong Luminescing CdS Particles.” J. Am. Chem. Soc. 109: 5649, 1987.

40. S. Bunk. “Sensing Evil.” The Scientist. 16(15): 13, 2002.

41. J.A. McCammon. “Theory of Biomolecular Recognition.” Curr. Opin. Struct. Biol. 8(2): 245, 1998.

42. L. Stryer and R.P. Haugland. “Energy Transfer: A Spectroscopic Ruler.” Proc. Natl. Acad. Sci. 58(2):719, 1967.

43. D.J. Maxwell, J.R. Taylor, and S. Nie. “Self-Assembled Nanoparticle Probes for Recognition and Detection of Biomolecules.” J. Am. Chem. Soc. 124: 9606, 2002.

44. I.L. Mendintz, A.R. Clapp, H. Mattoussi, E.R. Goldman, B. Fisher, and J.M. Mauro. “Self-Assembled Nano-scale Biosensors Based on Quantum Dot FRET Donors.” Nature Mats. 2: 630, 2003.

45. S. Wang, N. Mamedova, N.A. Kotov, W. Chen, and J. Studer. “Antigen/Antibody Immunocomplex from CdTe Nanoparticle Bioconjugates.” Nano Letts. 2(8): 817, 2002.

46. J. Taylor and S. Nie. “Probing Specific DNA Sequences with Luminescent Semiconductor Quantum Dots,” in Nanoparticles and Nanostructured Surfaces: Novel Reporters with Biological Applications, C.J. Murphy, Ed.,, Proceedings of SPIE., vol. 4258, 2001, p. 16.

47. C.A. Mirkin. “Programming the Assembly of Two- and Three-Dimensional Architectures with DNA and Nano-scale Inorganic Building Blocks.” Inorg. Chem. 39: 2258, 2000.

48. L.C. Mattheakis, J.M. Dias, Y.-J. Choi, J. Gong, M.P. Bruchez, J. Liu, and E. Wang. “Optical Coding of Mammalian Cells Using Semiconductor Quantum Dots.” Anal. Chem. 327: 200, 2004.

49. M. Dahan, S. Lévi, C. Luccardini, P Rostaing, B. Riveau, and A. Triller. “Diffusion Dynamics of Glycine Receptors Revealed by Single-Quantum Dot Tracking.” Science 302: 442, 2003.

50. T.A. Byassee, W.C.W. Chan, and S. Nie. “Probing Single Molecules in Single Living Cells.” Anal. Chem. 72: 5606, 2000.

51. W.J. Parak, R. Boudreau, M. Le Gros, D. Gerion, D. Zanchet, C.M. Micheel, S.C. Williams, A.P. Alivisatos, and C. Larabell. “Cell Motility and Metastatic Potential

Studies Based on Quantum Dot Imaging of Phagokinetic Tracks." Adv. Mats. 14(12): 882, 2002.

52. S. Stolik, J.A. Delgado, A. Perez, and L. Anasagasti. "Measurement of Penetration Depths of Red and Near Infrared Light in Human "ex vivo" Tissues." J. Photochem. Photobiol. B 57: 90, 2000.

53. A. Hartwig and T. Schwedtle. "Interactions by Carcinogenic Metal Compounds with DNA Repair Processes: Toxicological Implications." Toxic. Lett. 127: 47, 2002.

54. J.B. Lansman, P. Hess, and R.W. Tsien. "Blockade of Current Through Single Calcium Channels by Cd^{2+}, Mg^{2+}, and Ca^{2+}. J. Gen. Physiol. 88: 321, 1986.

55. M.P. Waalkes. "Cadmium Carcinogenesis." Mut. Res. 533: 107, 2003.

56. A.M. Derfus, W.C.W. Chan, and S.N. Bhatia. "Probing the Cytotoxicity of Semiconductor Quantum Dots." Nano Lett. 4(1): 11, 2004.

57. B. Dubertret, P. Skourides, D.J. Norris, V. Noireaux, A.H. Brivanlou, and A. Libchaber. "In Vivo Imaging of Quantum Dots Encapsulated in Phospholipid Micelles." Science 298: 1759, 2002.

58. D.R. Larson, W.R. Zipfel, R.M. Williams, S.W. Clark, M.P. Bruchez, F.W. Wise, and W.W. Webb. "Water-Soluble Quantum Dots for Multiphoton Fluorescence Imaging In Vivo." Science 300: 1434, 2003.

59. W.C.W. Chan, D.J. Maxwell, X. Gao, R.E. Bailey, M. Han, and S. Nie. "Luminescent Quantum Dots for Multiplexed Biological Detection and Imaging." Curr. Opin. Biotech. 13: 40, 2002.

60. M.E. Åkerman, W.C.W. Chan, P. Laakkonen, S.N. Bhatia, and E. Ruoslahti. "Nanocrystal Targeting In Vivo." Proc. Nat. Acad. Sci. 99(20): 12617, 2002.

61. C. Seydel. "Quantum Dots Get Wet." Science 300: 80, 2003.

62. X. Wu, H. Liu, J. Liu, K.N. Haley, J.A. Treadway, J.P. Larson, N. Ge, F. Peale, and M.P. Bruchez. "Immunofluorescent Labeling of Cancer Marker Her2 and Other Cellular Targets with Semiconductor Quantum Dots." Nature Biotech. 21: 41, 2003.

63. E.R. Kandel, J.H. Schwartz, and T.M. Jessel. Principles of Neuroscience, 4th Ed., McGraw Hill, New York: 2000, pp. 140-186.

64. Y. Nosaka and Y. Nakaoka. "Effect of the Amount of Reactant on the Photon-fluence Dependence in Laser-Induced Transient Formation at the Surface of Colloidal Semiconductor Particles." Langmuir 11(4): 1170, 1995.

65. M. Hamity and R.H. Lema. "The Effect of Methylviologen on the Photoluminescence Bands of Quantum-Sized CdS." J. Photochem. Photbio. A 99: 177, 1996.

66. P. Fromherz, A. Offenhäusser, T. Vetter, and J. Weis. "A Neuron-Silicon Junction: A Retzius Cell of the Leech on an Insulated-Gate Field-Effect Transistor." Science 252: 1290, 1991.

67. http://hyperphysics.phy-astr.gsu.edu/hbase/electric/dipole.html. Accessed July 2004.

68. S. Kimura, W. Laosinchai, T. Itoh, X. Cui, and R.M. Brown, Jr. "Immunogold Labeling of Rosette Terminal Cellulose Synthesizing Complexes in a Vascular Plant (*Vigna angularis*)." Plant Cell 11(11): 2075, 1999.

69. T. E. Creighton. Proteins: Structures and Molecular Principles. W. H. Freeman and Co., New York, 1983.

70. R.I. Freshnay. Culture of Animal Cells, 3rd Ed., John Wiley and Sons, New York: 1994, pp. 84-85.

71. P. Atkins. Physical Chemistry, 5th Ed., W.H. Freeman and Co., New York: 1994, p. A8.

72. P. Bongrand. "Adhesion of Cells," in Handbook of Biological Physics, vol. 1, R. Lipowsky and E. Sackmann, Eds., Elsevier, Amsterdam: 1995, p. 767.

73. G. Pollak and H. Zakon. Vertebrate Physiology, Spring 2000 Ed., University Co-op Press, Austin, TX: 2000, p. 25.

Chapter 3: Quantum Dot Synthesis and Analysis[2]

This chapter discusses selection criteria and synthesis methods for nanoparticles employed in the neuroelectronic interface. The motivation for our choice of cadmium–X quantum dots, where X = sulfur or tellurium, is presented. Next, we discuss synthesis methods for these particles: organic phase precursor decomposition and aqueous arrested precipitation. The advantages of each technique are discussed, and in particular, those factors impacting the development of the neuroelectronic interface.

Then, we present our optimization and characterization of the aqueous method utilized in our work: arrested precipitation of $CdCl_2$ and Na_2S in the presence of a thiolated passivating ligand. We investigated this system thoroughly, studying the effects of the reactant ratios and concentrations; ligand concentration, length and charge; and reaction pH on the optical properties of the quantum dots produced. Altering each of these variables produced changes in the absorbance onset wavelength, which has been linked to nanocrystal size, and particle quantum yield. Most notably, we discovered that particles with intermediate sizes have the highest quantum yield (~15%). As quantum yield and particle size determine the conversion efficiency of optical input to electrical output, [1] they are critical variables in the development of neuroelectronic interfaces.

[2] Portions of this material have been submitted for publication to Journal of Colloids and Surfaces A.

3.1 MATERIALS SELECTION

The selection of a specific material for any quantum dot application is crucial, as it determines the optical and electrical properties of the particle. [2] Our system requires high quantum yields and resistance to photobleaching, along with biocompatibility. High quantum yields (i.e., conversion of absorbed photons into emitted photons) are important because they are related to the number of particles in the excited dipole state. [3] Hence, a high percentage of the particles will be available to interact with the nerve membrane. Photobleaching not only reduces our ability to detect particles from their fluorescent signal, but can quench the dipole state entirely. [2] Therefore, resistance to photobleaching is a critical component of a long-term neuroelectronic interface. Finally, particles must be water-soluble and non-toxic to *living* neurons.

The majority of previous biological systems have utilized cadmium-based nanoparticles. Most commonly cadmium selenide (CdSe) has been explored, although cadmium sulfide (CdS) and cadmium telluride (CdTe) have also been studied. [4] Cadmium-based particles are a good selection for biological systems because their excitation and emission wavelengths lie in the UV-visible region of the spectrum. This is the area typically employed for organic fluorescent dyes; therefore, most biological equipment (i.e., fluorescence microscopes, microplate readers, etc.) operates in this wavelength range. [For further discussion of cadmium toxicity see Chapter 5, Section 5.1.2] Although metallic particles (i.e., gold and silver) have been used for a limited number of applications (e.g., biosensing, *in vivo* therapeutics); they do not fluoresce and produce undesirable quantities of heat. [5] Therefore, they are not suited to the development of neuroelectronic interfaces. Thus, to create a system that could be readily

reproduced in biological laboratories, we selected two types of cadmium-based particles for analysis: CdS and CdTe particles.

3.2 PARTICLE SYNTHESES

In addition to selecting a particle material, the method of synthesis is of great importance. Synthesis techniques for quantum dots have advanced significantly since their discovery in the early 1980's. [6] Methods have shifted from arrested precipitation in aqueous solution to precursor decomposition in organic solution. [7] The majority of changes were instituted in order to improve nanoparticle quantum yield, resistance to photobleaching, and size distribution. Nanoparticles synthesized with current techniques can exhibit quantum yields >50%, [8] fluorescence that can last for hours under continuous excitation, [9] and size distributions as narrow as 5%. [7]

These improvements arose largely from the introduction of a new synthesis method: precursor decomposition at high temperature. [7] Prior to this time, nanoparticles were produced primarily at room temperature, a condition that does not permit adequate annealing of defects on the nanoparticle surface. Defects are undesirable because they can serve as traps for excited electrons, increasing the probability of electron decay through vibration, as opposed to fluorescent emission. The introduction of high temperatures not only addressed this problem, but also allowed for controlled nanoparticle growth and nucleation, thus limiting the size distribution. All of these improvements provide desirable increases in quantum yield and photostability.

However, these particles are produced in organic solvents that are not compatible with biological systems. Thus, additional steps are required to confer water-solubility. This can be accomplished by altering the surface chemistry of the nanoparticle, either through exchanging the capping ligand or by coating the particle with a water-soluble

shell. These techniques have both been used to create particles that have been demonstrated in biological labeling. [9-10] However, the process for transferring particles into water can be time-consuming and requires equipment outside the reach of most biological laboratories.

3.2.1 Organic Synthesis Methods for Cadmium–Based Quantum Dots

3.2.1.1 Synthesis with Dimethyl Cadmium in Trioctylphosphine

The organic syntheses currently used for cadmium-based nanoparticle production are primarily based on a technique, pioneered by Murray, et al., [7] which produces trioctylphosphine oxide (TOPO)–capped CdSe nanoparticles. Briefly, dimethyl cadmium and selenium shot are each placed in a solution of trioctylphosphine (TOP) in a glove box. [A variation of this procedure uses tributylphosphine (TBP) instead of TOP. [11]] Next, a solution TOPO is degassed at 200ºC under vacuum for 20 minutes, melting the TOPO and removing oxygen. Then, the solution temperature is raised to 300ºC under argon. When temperature has been reached, the cadmium and selenium solutions are combined into one syringe, quickly removed from the glove box, and injected into the hot TOPO solution. The temperature declines to ~180ºC upon injection, but is gradually raised to 230-260ºC.

Particle size is controlled largely through the final temperature, with higher temperatures leading to larger particles. Additionally, TOPO molecules coordinate with the surface of the nanoparticle limiting its growth. Depending on the reaction time and final temperature, particles from 1-11 nm may be produced. [7] Optical characteristics are favorable, with excitation wavelengths tunable across the visible spectra (i.e., from 400-700 nm) and emission wavelengths that are red-shifted ~10 nm from excitation. [7] The

small magnitude of the shift between emission and excitation wavelengths indicates that emission does not occur from deep surface trap states, and that the crystal contains few electronic defects. The quantum yield of these particles is ~10%. [7]

These traits make CdSe quantum dots that are produced using this method appealing choices for the development of neuroelectronic interfaces. However, there are several difficulties to their direct use. First, particles are produced in TOP and are TOPO-capped. They are soluble in chloroform and other organic solvents, but not in alcohols or aqueous solution. [7] Further, TOPO is a weakly bound ligand and can disassociate from the particle over time, and TOPO is toxic to cells. [12] The loss of ligand coverage can expose the core of the particle to oxidative attack, limiting quantum yield and producing photobleaching. [13] Further, the synthesis requires the use of a glove box and Schlenk line, not common equipment in biological laboratories, and exposure to extremely toxic chemicals that can be explosive (i.e., dimethyl cadmium and TOPO).

3.2.1.2 Synthesis with Cadmium Oxide in Trioctylphosphine and Tetradecylphosphonic Acid

A common variation of the standard method, developed by Peng, et al., [14] replaces dimethyl cadmium with cadmium oxide (CdO) as a precursor. Additionally, TOPO ligands are augmented with tetradecylphosphonic acid (TDPA) or hexylphosphonic acid (HPA); both of which bind strongly to the cadmium core. Briefly, CdO, TOPO, and either TDPA or HPA are heated above 60ºC (the melting point of TOPO). Additionally, selenium shot is placed in TOP and heated above 150ºC (to produce dissolution). The TOPO solution is degassed for several hours. Next, the temperature of the CdO solution is raised to 340ºC. Then, the temperature of both

solutions is lowered: to 300ºC for CdO and to 120ºC for Se. Finally, the Se is injected into the hot CdO solution, producing nanoparticles.

These variations reduce exposure to toxic agents and produce high quality particles. [14] CdO is much less toxic than dimethyl cadmium and does not require the use of a glove box. Additionally, the optical properties of the previous synthesis are improved or retained. Emission wavelengths are minimally shifted from absorption, indicating a high quality crystal surface, and quantum yield is improved to as much as 20%. [14] However, a Schlenk line is required for particle production; and although reaction temperatures are reduced, they are > 200ºC. Particles are not soluble in water and partially capped with TOPO. Thus, despite the reduced toxicity of this method, it is still not ideal for use in creating neuroelectronic interfaces.

3.2.1.3 Core-Shell Syntheses

The particles made from the organic syntheses described above are often modified with a shell of a wider band gap material (i.e., more insulating material). This change protects the particle core from photooxidation and surface reactions and further confines the exciton. Additionally, a shell can be used to confine potentially toxic cadmium ions on the surface of the particle to the interior. The majority of the particles used in biological applications contain a shell, with the most common material being zinc sulfide (ZnS). [4] ZnS is an ideal shell material as it is substantially less toxic than cadmium, possesses a larger band gap than CdSe, and does not easily form alloys with CdSe. [8, 13]

The production of core-shell particles is based in large part on the standard organic methods. [8] Solutions of dimethyl cadmium and selenium shot are prepared in TOP, as described before. However, dimethyl zinc is also prepared, along with bis (trimethylsilyl) sulfide (a sulfur source), in a separate TOP solution. [Alternatively

diethyl zinc has also been used as a zinc source. [15]] Particles are produced as described previously, except that injection occurs at 350ºC, instead of 300ºC. The temperature after Cd/Se injection is allowed to decline to 300ºC, at which time the Zn/S solution is injected in 5 aliquots over 20 s intervals. The injection of small aliquots over time allows the temperature to be held fairly constant during this period. The ratio of Zn solution to Cd solution is ~1:4.

Core-shell particles offer many benefits over those produced with standard organic methods. The quantum yield is substantially increased, from 20% for CdSe to 50% for CdSe/ZnS. [8] Additionally, CdSe normally presents a tail in the emission band toward red wavelengths, but this tail is eliminated with capped particles. Otherwise, particles exhibit spectra that would be expected from uncapped CdSe, indicating that the core is largely unaffected by the presence of the ZnS shell, which averages less than a nanometer in thickness. Instead, improvements in quantum yield and bandwidth likely result from the reduction of surface traps in the CdSe core. Further, the presence of a shell protects the core particle from photooxidation and reduces the likelihood of cadmium dissolution at the particle surface. Thus, CdSe/ZnS capped particles are stable for months, even in the presence of oxygen and are less toxic than uncapped particles. [13]

Nonetheless, core-shell particles are still not ideal for neuroelectronic interfaces. The final product contains TOPO ligands on the surface, which are insoluble in water and toxic. Additionally, the chemistry involved can be complex and requires equipment that is outside the reach of most biological laboratories. However, the most important limitation to the use of core-shell particles in neuroelectronic interfaces is the effect of the shell on the particle dipole moment. Unless the shell is epitaxially aligned with the core, it would not participate fully in the formation of a dipole moment. [16] Thus, it would

have some insulating properties. With a Debye length of ~1 nm, [17] even a thin shell could significantly reduce electrical interactions with the neuron. Although core-shell particles may make excellent biological labels, they are not ideal for systems requiring *electrical* interactions.

3.2.2 Water-Soluble Particles Produced Using an Organic Synthesis

Organic particles have many advantages to their use in biological applications, and in particular neuroelectronic interfaces. They possess high quantum yields and good resistance to photobleaching. [8] Both of these qualities present the potential for a high conversion of optical energy into an electrical signal, a requirement for optically activated neuroelectronic devices. The main limitation of organic particles is their lack of water solubility. Several techniques have been offered to confer water solubility, but all rely on modification of the nanoparticle surface. This can be accomplished by altering the nature of the passivating ligands or augmenting the crystal with a shell material that is biocompatible.

3.2.2.1 Ligand Exchange

The most common method for producing water-soluble particles using an organic synthesis includes an additional post-processing step known as ligand exchange. During ligand exchange, the existing chemical surface coating of the particle is replaced with one that can alter the solubility of the colloid. [18] There are a number of variations in the ligand exchange technique; however the basic premise remains the same. First, particles are dried to remove unreacted ligand and the organic solvent. This can be accomplished using either a rotary evaporator or precipitation in a counter-solvent. In the case of

TOPO-capped particles, the addition of anhydrous methanol will cause flocculation of the particles; and centrifugation can be used for separation. [7] Next, the particles are introduced into a solution containing a gross excess of the new ligand. After an incubation of several hours, exchange occurs. Exchange can be confirmed by altered solubility of the particles, or through analytical techniques like FTIR (Fourier Transfer Infrared Spectroscopy) and XPS (X-ray Photoelectron Spectroscopy).

The most common ligand exchange used to produce biologically compatible quantum dots exchanges TOPO, bound to CdSe/ZnS core-shell particles, for mercaptoacetic acid (MAA=HS-CH_2-COOH). [9, 18] The binding of MAA occurs through the sulfur group at the molecule's terminus, which adheres to Zn atoms on the ZnS coating. [18] The carboxyl end of MAA provides water solubility. In addition to MAA, a number of other thiolated chemicals have been examined, including mercaptopropionic acid (MPA= HS-$(CH_2)_2$-COOH), mercaptoethylamine (MEA, HS-$(CH_2)_2$-NH_2), and β-mercaptoethanol (MBE, HS-CH_2-CHOH). In fact, any molecule which binds to the surface of the particle and is water-soluble can be used, thus allowing for a range of surface chemistries that can be explored.

This technique allows researchers to use high-quality particles produced with an organic synthesis in a biological context, and addresses many of the limitations of an organic process alone. However, there are still some disadvantages. For example, the initial synthesis of CdSe/ZnS particles requires access to a Schlenk line and possibly a glove box. Exposure to toxic and potentially explosive chemicals still occurs. Additionally, ligand exchange is a long, multi-step process spanning as many as three days. The particles are only stable for 1-3 weeks; [18] indicating possible loss of ligand coverage over time. If the ligands are toxic (i.e., MBE [19]) or bioactive (MEA [20]), desorption can have deleterious effects on the cells in contact with the particles. Despite

these concerns, this technique could be used to produce particles for a neuroelectronic interface. Nonetheless, there are other techniques that can be used to make particles more quickly, and that are more accessible to a biological audience.

3.2.2.2 Additional Surface Coatings

Another method to create water-soluble nanoparticles alters the surface by applying a biocompatible shell material. An example of this technique, developed by Alivisatos, et al., [10, 21] coats TOPO-capped CdSe/ZnS particles with silica, although any TOPO-capped particle could be used. The particles are created using the standard method. Then, they are precipitated in anhydrous methanol, dried, and re-dissolved in mercaptopropyltris(methyloxy)silane (MPS) to which tetramethylammonium hydroxide (TMAH) has been added. The pH of the mixture is altered to pH 10 and the entire contents are placed under nitrogen at 60ºC. Additional MPS and TMAH are added, along with (trihydroxysilyl)propyl methylphosphonate (to provide stability in water) and the cycle is repeated. The silanization reaction is quenched using chlorotrimethylsilane. Finally, the solution is stirred under nitrogen for several days, and filtered using a combination of rotary evaporation, dialysis, and centrifugation.

Silica-coated particles meet several of the criteria for biological applications. For example, the advantageous optical properties of the particle core remain largely unchanged. Despite a silica shell averaging 2-5 nm in thickness, emission wavelengths are similar to uncoated CdSe/ZnS. [21] Quantum yields average 5-20%, and are 60-80% of the original values. [10, 21] Unlike particles that undergo ligand exchange, silica coated nanocrystals exhibit stability for months, with little loss of quantum yield. [10, 21] Additionally, biomolecules can be readily conjugated to silica using well-established techniques developed for chromatography. However, despite all of these advantages,

these particles are not ideally suited for neuroelectronic interfaces. Silica shells are insulating and increase the separation distance of the cell and the particle by several nanometers. Given a Debye length of ~1 nm, [17] this can reduce electronic interactions significantly. Thus, additional strategies must be pursued.

3.2.3 Aqueous Synthesis Methods for Cadmium–Based Quantum Dots

An obvious route to water-soluble nanocrystals is their production in aqueous solvents. Nanocrystal synthesis in water occurs through a process known as arrested precipitation. For example, the solubility constant of CdS in water is ~10^{-29}, [22] indicating that the bulk material is relatively insoluble. If a water-soluble thiol is added to the reaction mixture, some cadmium ions complex with this chemical. As crystal growth occurs, it is hindered by the steric presence of the thiol compounds. Eventually, free sulfur anions cannot overcome the steric forces of the thiol and particle growth is terminated. If the surface is well passivated with water-soluble thiol ligands, the crystals can remain suspended in water. This process is controlled by many factors, including the reactant ratios, the thiolated ligand in question, and the pH of the reacting mixture; all of which contribute to nanoparticle size and uniformity. [23]

Aqueous syntheses are very flexible. A variety of materials can be used as reactants. The first CdS nanocrystals were produced using $Cd(SO_4)$ as a cadmium source [6], although $Cd(ClO_4)_2$ [24] and $CdCl_2$ [23] have also been used. Sulfur can be introduced through a variety of mechanisms, and $(NH_4)_2S$ [6], Na_2S [24], and H_2S [25] have all been investigated. Thiolated ligands investigated range widely, including MAA, MPA, MEA, and MBE. [23, 26-27] Although thiolated ligands are used most commonly, any ligand that binds to Cd^{2+} ions and promotes water solubility of the particle may be

employed. Initially, polymers, such as maleic hydride/styrene, [6] silicon dioxide sol, [24] and polyphosphate, [25] served this purpose.

Nanoparticles produced using aqueous syntheses offer many benefits for biological studies. For example, they have the unique ability of being manufactured using simple bench-top chemistry, requiring only a fume hood. These requirements can be easily met by most biological laboratories. Additionally, particle surfaces may be readily altered through the use of thiolated biomolecules, or by performing post-synthetic conjugation chemistry on a ligand functional group. The main limitations of this procedure are the reduced optical properties and large particle size distribution. Particle quantum yields average only ~10-15%, [28-29] and the majority of emission occurs through trapped states, meaning that the emission bandwidth can be very large. [30] The size distribution is an issue because it can increase with time, developing a tail at larger sizes, indicating particle instability. [31] This is likely a result of Ostwald ripening, the growth of larger particles at the expense of the thermodynamically less stable smaller ones. [27] However, we have observed that only solutions of larger particles exhibit this behavior; solutions containing smaller particles (i.e., ~3 nm and less) can be stable in aqueous solution for months. Thus, the particles can exhibit remarkable stability, comparable only to silica-capped CdSe/ZnS. [10, 21] Although these factors could be limiting for other technologies, particles created through aqueous methods are suitable for use in neuroelectronic interfaces.

3.3 SYNTHESIS SELECTION AND CHARACTERIZATION

3.3.1 Synthesis Selection

Direct aqueous-phase synthesis of semiconductor nanocrystals with a high photoluminescence (PL) quantum yield provides a convenient, economic, and environmentally friendly alternative to the labor-intensive method of organic-phase synthesis followed by ligand exchange CdS nanocrystals, created using arrested precipitation in aqueous media, represent one such system with properties suitable for neuroelectronic interfaces. They can be manufactured quickly, using readily available laboratory equipment, and with minimal exposure to toxic chemicals. Additionally, CdS nanocrystals can be both fabricated and functionalized with biomolecules in a single synthetic step.

Although there are some limitations in their optical properties, these are not problematic for their use in neuroelectronic interfaces. For example, it is true that quantum yields are substantially lower than those for core-shell systems (e.g., CdSe/ ZnS: quantum yields ~50% [8]); however, core-shell particles are not ideal for this application as a result of the possible insulating nature of the shell. Thus, quantum yields are low (~15% [29]), but compare well with other available systems (e.g., CdSe averages ~20% [7]).

Also, trapped state emission, the other major limiting factor, is less important in neuroelectronic interfaces. Trapped state emission indicates the presence of trapped electrons at crystal defect sites. The presence of a trap can permit electrons to decay through non-radiative methods (e.g., crystal vibrations). This would be reflected in a reduced quantum yield for the particle. However, trapped states can also increase the lifetime of the exciton, [2] thus increasing the amount of time that the particle is in the

transient dipole moment state. In this case, trapped state emission is an advantage for neuroelectronic interfaces.

Finally, CdS possesses a relatively large band gap (i.e., 2.42 eV [6]). PL emission is limited to the upper energy half of the visible spectrum, requiring UV or blue (350 to 425 nm) excitation wavelengths, which could damage the cells. However, this wavelength range is often used for labeling applications, particularly those employing the organic dye DAPI (λ_{exc}=350, e.g., Molecular Probes, D-1306), which binds cellular nuclear components. Thus, CdS nanocrystals are comparable to commercially available organic dyes and other semiconductor nanocrystals (e.g., CdSe, CdTe) and provide a suitable system for the development of neuroelectronic interfaces.

3.3.2 Motivation for Synthesis Characterization

Our ongoing efforts to use aqueous CdS nanocrystals conjugated to biomolecular recognition components [29] for the development of neuroelectronic interfaces has revealed that subtle variations in synthesis parameters, such as pH, concentration and ligand length, lead to unpredictable differences in PL emission wavelength, quantum yield and dispersibility. Despite the fact that many studies have examined the aqueous arrested precipitation of CdS nanocrystals using thiolate [26, 32-33] and phosphate [30] terminated ligands, we found that the key synthetic parameters controlling the particle size and PL quantum yield were not adequately identified. Here, we report a systematic study of the effects of reactant concentration, Cd:S mole ratios, Cd:ligand mole ratios, ligand chain length, pH, and ligand R group on the nanocrystal size and PL for CdS nanocrystals synthesized by aqueous-phase arrested precipitation. The acid/base equilibrium of free ligands is coupled to ligand surface adsorption, Cd-thiolate complex formation, and CdS precipitation. By decoupling the effects of pH and concentration, we

obtained a predictive understanding of nanocrystal growth, which will allow us to produce controlled, reproducible nanocrystal populations for use in the neuroelectronic interface.

3.3.3 Materials and Methods

The absorbance and PL spectra of CdS nanocrystals produced under conditions of altered reactant concentrations, reactant and ligand ratios, ligand length, pH, and ligand R group were measured and evaluated. All chemicals were used as received from either Sigma-Aldrich or Fluka Chemical Companies and all water was doubly distilled and deionized.

3.3.3.1 Standard CdS Nanocrystal Synthesis

As a standard case, mercaptoacetic acid-stabilized CdS nanocrystals were synthesized by the methods developed by Feng, et al. [34] 50 µL mercaptoacetic acid (MAA, $HOOCHCH_2SH$) (Fluka) were added to 10 mL of 5 mM $CdCl_2$ (Sigma) for a final MAA concentration of 55 mM and pH of 2.15-2.30. The pH was raised by drop wise addition of concentrated 10 M NaOH to pH 4.5, and then incremented further through drop wise addition of 1 M NaOH to a final pH of 7.0 ± 0.05 (total addition ~600 µL 1 M equivalents). 10 mL of 2 mM $Na_2S{\cdot}9H_2O$ (Sigma) solution were added to this solution with rapid stirring, which raises the pH to ~8.2. The reaction mixture was stirred for 4 hours prior to analysis. Table I summarizes the reaction conditions and variables examined in this study.

Table I: Experimental Synthesis Conditions Examined

Parameter[3]	Ligand	[$CdCl_2$] (mM)	[Ligand] (mM)	[Na_2S] (mM)	pH
Control	MAA	5	55	2	pH^1 = 7
Concentration	MAA	1-20	11-220	0.4-9.5	pH^1 = 7
Ratio	MAA	5	55	0.5-20	pH^1 = 7, pH^2 = 8.2
Ligand Conc.	MAA	5	1-500	2	pH^1 = 7, pH^2 = 8.2
Ligand Length	-OH terminated[4]	10	98.5	10	pH^1 = 7, pH^2 = 8.2
pH	MAA	5	55	2	pH^1 = 5-11, pH^2 = 8.2
Ligand R Group	MAA, MBE, MEA	5	55	2	pH^1 = 3-11

[1] pH before Na_2S addition, pH after Na_2S addition fluctuates freely
[2] pH after Na_2S addition, held constant through drop wise 1 M HCl or 1 M NaOH addition
[3] All reactions were carried out in a total volume of 20mL.
[4] $HS(CH)_xOH$, with x = 2, 3, 4, 6.

3.3.3.2 Reactant Concentration

Overall reactant concentration was examined by carrying out particle growth in a total volume of 20 mL with constant molar ratios of [$CdCl_2$]:[Na_2S]=2.5 and [MAA]:[$CdCl_2$]=11. $CdCl_2$ concentrations ranged from 1 to 20 mM, with corresponding MAA addition ranging from 11 to 220 µL. In these experiments, the pH was raised to 7 using NaOH prior to Na_2S addition.

3.3.3.3 Cadmium:Sulfur Ratio

The [$CdCl_2$]:[Na_2S] molar ratios were altered, while [MAA]:[$CdCl_2$] = 11 was kept constant. Two classes of experiments were performed with initial pH (prior to Na_2S

addition) = 7.0 and (1) reaction pH fluctuates freely and (2) reaction pH (after Na_2S addition) = 8.2. The reaction pH was adjusted to 8.2 using rapid drop wise addition of 1 M NaOH or 1 M HCl. These experimental conditions were selected to differentiate the effect of pH changes from that produced by the variable alone.

3.3.3.4 Ligand Concentration

The [MAA]:[$CdCl_2$] molar ratio was altered from 0.2 to 100, while holding the [$CdCl_2$]:[Na_2S] ratio constant at 2.5. MAA was added to 10 mL of 5 mM $CdCl_2$ to achieve the desired [MAA]:[$CdCl_2$] ratio. After MAA addition, the pH was raised to 7.0 by drop wise addition of 10 M and 1 M NaOH. In some of the experiments, the reaction pH was adjusted to 8.2 after Na_2S was added, using drop wise addition of either 1 M NaOH or 1 M HCl.

3.3.3.5 Ligand Chain Length

Ligand chain length was investigated using –OH terminated ligands. Alcohol terminated ligands were selected because a wide range of chain lengths, from 2 to 6 carbons long, were commercially available, which was not the case for carboxyl-terminated ligands. We examined β-mercaptoethanol (2-mer, $HS(CH_2)_2OH$) (Sigma), 3-mercaptopropanol (3-mer, $HS(CH_2)_3OH$) (Sigma), 4-mercapto-1-butanol (4-mer, $HS(CH_2)_4OH$) (Sigma), and 6-mercapto-1-hexanol (6-mer, $HS(CH_2)_6OH$) (Fluka). For these experiments, the $CdCl_2$ and Na_2S concentrations were modified from the standard conditions, as the –OH ligands produced CdS nanocrystals with significantly blue-shifted absorbance that did not fluoresce. 10 mM $CdCl_2$, [$CdCl_2$]:[Na_2S]=1, and [MAA]:[$CdCl_2$]=9.85 were used for the reactions. The pH was raised to 7.0 with NaOH

solution after adding capping ligand, and prior to Na_2S addition. In some cases, the pH was adjusted to 8.2 after sulfide addition by drop wise addition of either 1 M NaOH or 1 M HCl.

3.3.3.6 pH Adjustment

50 μL MAA was added to 10 mL of 5 mM $CdCl_2$ solution following the standard procedure. 10 M and 1 M NaOH were added to obtain the desired initial pH value, ranging from 5 to 11, prior to Na_2S addition. In one set of experiments, the reaction pH after adding the Na_2S solution was adjusted to 8.2 by drop wise addition of either 1 M NaOH or 1 M HCl.

3.3.3.7 Ligand R Group

Three different capping ligands were explored: MAA, MBE, and β-mercaptoethylamine hydrochloride (MEA, $HSCH_2CH_2NH_2{\cdot}HCl$, Fluka). MAA is an acid, MBE is neutral, and MEA is a base. Each ligand was added to 10 mL of 5 mM $CdCl_2$ solution as per the standard preparation to a final concentration of 55 mM ([Ligand]:[$CdCl_2$]=11). After ligand addition, the pH was raised to values ranging from 3 to 11 by adding 10 M and 1 M NaOH. 10 mL of 2 mM $Na_2S{\cdot}9H_2O$ (Sigma) solution were added to this solution with rapid stirring.

3.3.3.8 Absorbance and Photoluminescence Spectroscopy

Room temperature absorbance spectra of CdS nanocrystals dispersed in DI-H_2O were obtained using a Beckman DU500 spectrophotometer (Beckman Coulter, Fullerton, CA). Room temperature PL spectroscopy was performed using a Quanta Master Model C

Cuvette-based scanning spectrofluorometer (Photon Technology International, Lawrenceville, NJ) with a Xenon lamp source and monochromator scanning. Bandpass filters were set to 4 nm. Spectra were obtained from CdS nanocrystals dispersed in water with optical densities adjusted to 0.1 at the excitation wavelength in standard quartz cuvettes. PL quantum yield was measured using a quinine sulfide standard (QY= 0.55, λ_{exc}=366) in 0.5 M H_2SO_4. The room temperature PL quantum yield of CdSe nanocrystals obtained from Evident Technologies (Troy, NY) dispersed in toluene was measured using carboxytetramethylrhodamine (TAMRA) as a standard in methanol (QY=0.68, λ_{exc}=543).

3.3.4 Results and Discussion

MAA-stabilized CdS nanocrystals were synthesized through aqueous-phase arrested precipitation. Nanocrystals created using the standard procedure luminesce at 366 nm with a quantum yield of 15%. This quantum yield compares well with commercially available CdSe nanocrystals (Evident Technologies) that we found to emit with PL quantum yields of 1.2% and reported values of ~20%. [7] Changes in optical properties resulting from altered reactant concentration, Cd:S and Cd:ligand mole ratios, ligand length, pH, and R group chemistry from control procedure were examined (Table II).

Table II: Summary of Experimental Synthesis Results

Variable	Abs. Edge	PL Peak λ	PL Intensity[4]
⇑ Conc.	NC[3]	NC	NC
⇑ Ratio	⇓ [1,2]	⇓ [1,2]	Max at 2:1, 4:1[1,2]
⇑ Ligand Concentration	NC[1] ⇑ [2]	NC[1] ⇑ [2]	Max. at 55, 100 mM[1,2]
⇑ Ligand Length	⇓ [1,2]	⇓ [1,2]	⇓ [1] ⇑ [2]
⇑ pH	⇑ [1] NC[2]	⇑ [1] NC[2]	Max. at pH 7[1,2]
Ligand R Group	Varied with pH	N/A*	Max. for MAA, MEA*

(NC) =No Change
*N/A. No fluorescence occurred for MBE samples.
[1]Reaction pH fluctuates freely
[2]Reaction pH = 8.2
[3]Peak energy is unchanged; intensity increases
[4]OD=0.1, Control (see Table I) quantum yield = 15%.

3.3.4.1 Overall Reactant Concentration

Figures 21A-B show absorbance and PL emission spectra for CdS nanocrystals synthesized with the standard Cd:S and MAA:Cd mole ratios of 2:1 and 11:1, respectively, at different overall reactant concentrations. In these experiments, the solution pH did not vary appreciably from 8.2 after Na_2S addition. Increased overall reactant concentration increased the absorbance; however, the exciton peak energy did not vary significantly (Figure 21C). The spectra indicate that nanocrystal number density increases with more reactant, while the particle size distribution does not change. Additionally, the PL emission peak energy did not vary with overall concentration (Figure 21B), providing further support that nanocrystals of the same size are formed in

each preparation. Furthermore, increasing particle concentration in the synthesis does not significantly alter the PL quantum yield (Figure 21D).

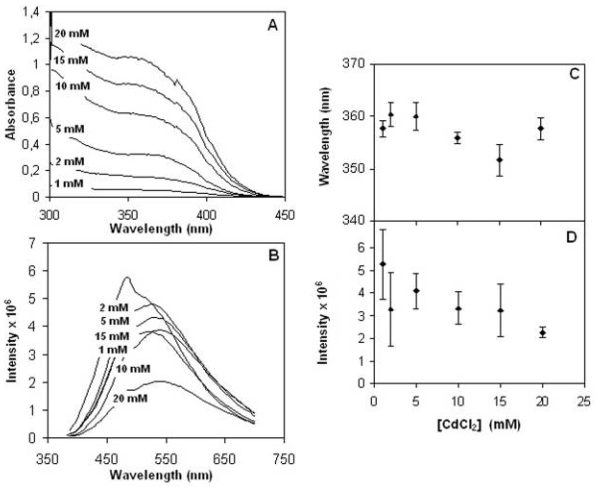

Figure 21: Absorbance and Excitation Spectra for Increased Reactant Concentrations.

Room temperature (A) absorbance spectra and (B) PL emission spectra (λ_{exc}=366 nm, OD=0.1) for aqueous CdS nanocrystals synthesized with increasing [$CdCl_2$] while maintaining the Cd:S and MAA:Cd mole ratios of 2.5 and 11, respectively. (C) The exciton peak energies observed in the absorbance spectra and (D) the PL intensity averaged over 3 experiments (OD=0.1 for all samples). Exciton peak energy remains approximately constant as overall reactant concentration is increased, whereas PL intensity experiences a slight decline at higher concentration.

Although CdS nanocrystals synthesized at different overall reactant concentrations exhibit similar optical properties and size, the dispersion stability was significantly higher for nanocrystals produced at lower concentrations. Particles created at higher concentrations (e.g., 15 mM, 20 mM) generally precipitated within one week. Decreased stability most likely results from higher ionic solution strength and increased particle proximity. As reactant concentration increases, additional Na^+ and Cl^- ions are available to screen the repulsive charge between more closely-packed carboxyl-coated nanocrystals — a combination which results in particle aggregation and precipitation. Dispersion stability is a concern for biological labeling applications, as less-soluble particles are more likely to adhere non-specifically to cellular and substrate surfaces.

3.3.4.2 Cd:S Ratio

The [$CdCl_2$]:[Na_2S] was varied from 10:1 to 1:4. For these experiments, the stock $CdCl_2$/MAA solution was prepared according to the standard procedure, with a solution pH adjusted to 7.0 prior to Na_2S addition. Figures 22A-D shows absorbance and PL spectra of the CdS nanocrystals. The relationship between the absorbance onset and CdS nanocrystal size is well studied and can be used as a measure of particle diameter. [35] Increasing Cd:S ratio decreases the particle size (Figures 22A,B,E). These results are consistent with past findings in the literature. [28, 36-37] To ensure that these observations were not related to solution pH variations, nanocrystals were also synthesized by adjusting the pH to 8.2 after Na_2S addition (Figures 22B and 22D). This final pH readjustment did not change the nanocrystal optical properties.

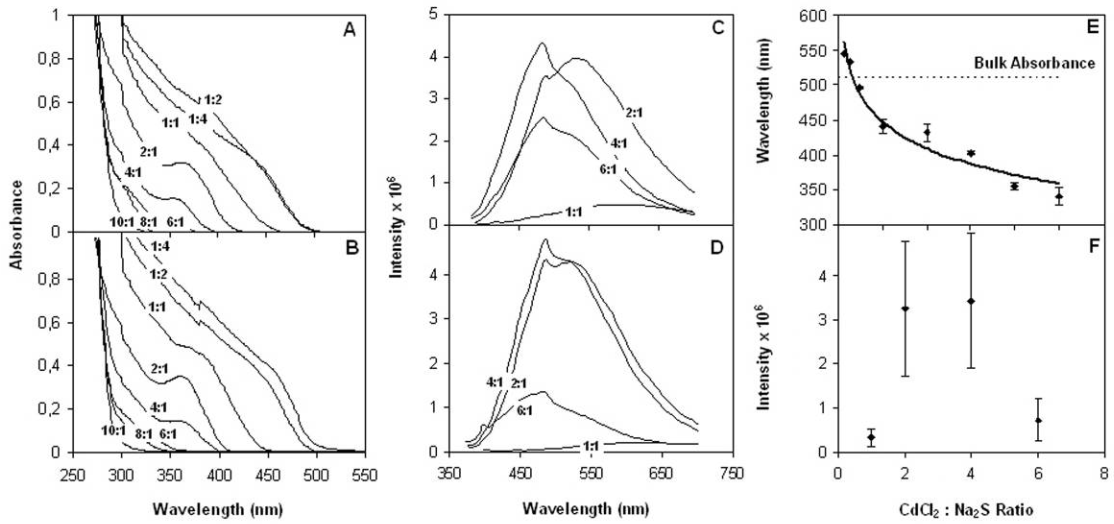

Figure 22: Absorbance and Excitation Spectra for Increased Cd:S Ratio.

Room temperature (A,B) absorbance and (C,D) PL emission spectra (λ_{exc}=exciton peak, OD=0.1) for aqueous CdS nanocrystals synthesized with different [$CdCl_2$]:[Na_2S] mole ratios. For these experiments, [$CdCl_2$]=5 mM, [MAA]:[$CdCl_2$]=11, and the pH is adjusted to 7.0 prior to Na_2S addition. In one set of experiments (B,D), the pH was also adjusted to 8.2 after Na_2S addition. (E) Absorbance onset averaged over 3 preparations as a function of [$CdCl_2$]:[Na_2S] ratio for the samples with pH adjusted to 8.2 after Na_2S addition. For reference, the band gap energy of bulk CdS is identified with a dotted line. The curve fit in (E) is a logarithmic fit to the data points (R^2 = 0.956, λ_{onset} = -55 ln(Cd:S ratio) + 486). (F) PL emission peak intensity (OD=0.1 for all samples) plotted as a function of [$CdCl_2$]:[Na_2S] ratio. Nanocrystals formed with [$CdCl_2$]:[Na_2S]>6 and [$CdCl_2$]:[Na_2S]<1 did not fluoresce.

The decrease in size with increasing [$CdCl_2$]:[Na_2S] results from competition between MAA and SH^- anions (Na_2S exists primarily as SH^- for the pH range investigated) for Cd^{2+} binding sites at the nanocrystals surface: [36, 38]

$$(CdS)_n + Cd^{2+} + SH^- \longleftrightarrow (CdS)_{n+1} + H^+$$

$$(CdS)_n + Cd^{2+} + mRSH \longleftrightarrow (CdS)_n (Cd(SR)_m)^{(m-2)-} + mH^+$$

SH^- condenses with Cd^{2+} ions or Cd dangling bonds on the nanocrystal surface to produce CdS, whereas RSH terminates nanocrystals surfaces or stabilizes new nuclei by forming Cd-SR complexes. As [Na_2S] increases, more SH^- becomes available for CdS formation and particle growth. As [$CdCl_2$] increases, a greater proportion of Cd atoms are available for surface reaction with the capping ligand — a situation resulting in the stabilization of smaller particles. An insoluble precipitate with bulk spectral properties forms below a lower Cd:S limit (1:1), whereas at the upper end of Cd:S ratios (Cd:S > 6:1), particles that formed did not fluoresce and exhibited significantly blue-shifted absorbance. Nosaka [23] proposed that these high Cd:S ratios yield molecular clusters, as opposed to nanocrystals with bulk crystal structure. The PL intensity is also a strong function of Cd:S ratio (Figure 22F), with maximum emission occurring for Cd:S ratio ranging between 2 and 4 and absorbance onsets that correspond to a size of ~2 nm. [35] This appears to indicate that surface passivation is best for mid-size (or mid-spectral) CdS nanocrystals. The presence of a size-specific maximum in PL intensity has been observed before in several other systems, including CdTe [39], CdSe [39-41], InAs [39], and CdS [28, 42-43].

3.3.4.3 Ligand Concentration

MAA-stabilized CdS nanocrystals were synthesized at different [$CdCl_2$]:[MAA] ratios, with [$CdCl_2$]=5 mM and [$CdCl_2$]:[Na_2S]=2. The pH was raised to 7.0 after adding MAA to the $CdCl_2$ solution, and prior to Na_2S addition. In one set of experiments, the reaction pH was not controlled; and in a separate set of experiments, the pH was adjusted to 8.2 after sulfide addition. As seen in the absorbance and PL spectra in Figures 23A-D, when the reaction pH was not readjusted to 8.2 after sulfide addition, the ligand concentration had little effect on the nanocrystal size for the majority of the conditions tested. Slight increases in size were seen at the highest ligand concentration (500 mM), and insoluble bulk material formed at the lowest concentration (1 mM). These observations are consistent with previously reported results for MAA-stabilized CdS nanocrystals. [34] However, when the reaction pH was adjusted to 8.2 after Na_2S addition, a small *increase* in particle size occurred with increasing ligand concentration (Figures 23B, D, E). Prior to adjustment, the reaction pH ranged from 7 (for 10:1) to 10 (for 1:4).

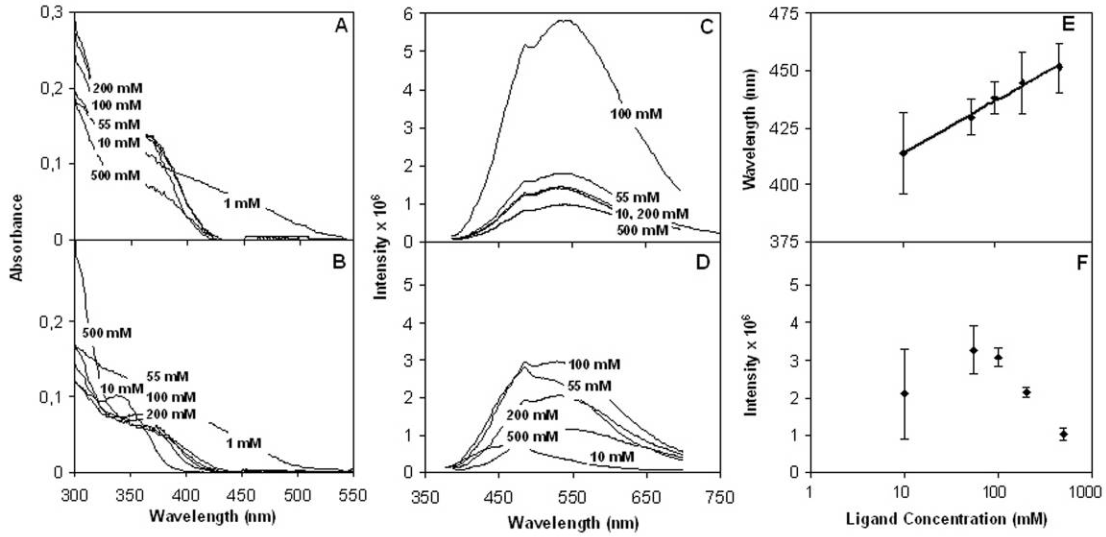

Figure 23: Absorbance and Excitation Spectra for Increased Ligand Concentrations.

Representative room temperature (A, B) absorbance and (C, D) PL emission (λ_{exc}=exciton peak, OD=0.1) spectra of aqueous CdS nanocrystals synthesized with different [MAA] concentration. For these reactions, [$CdCl_2$]=5 mM; and [MAA]=55 mM, corresponding to [MAA]:[$CdCl_2$]=11. The pH was set to 7.0 prior to Na_2S addition. The spectra in (B) and (D) correspond to particle growth experiments where the pH was also adjusted to 8.2 after sulfide addition. (E) The absorbance onset of nanocrystals synthesized with pH adjusted to 8.2 plotted as a function of ligand concentration on a semi-log plot, fitted to a logarithmic curve: (R2 = 0.97, λ_{onset} = 8.24 ln([MAA (mM)]) + 396). (F) PL intensity (OD=0.1 for all samples) as a function of ligand concentration for reaction pH adjusted to 8.2 (semi-log plot). PL intensity was maximum for the range, 55 mM<[MAA]<100 mM.

The observed increase in particle size with increasing ligand concentration is consistent with only one study in the literature. In that study, increased oleic acid concentration in octadecene [44] gave rise to larger CdS particles. The majority of work examining the effect of ligand concentration on particle size has found that increasing ligand concentration either decreased particle size (β-mercaptoethanol-stabilized CdS) [26-27, 45] or had little effect (CdS nanocrystals stabilized with β-mercaptoethanol (high

concentration), sodium hexametaphosphate, ethylene glycol, and ethanol). [27] One would expect that nanocrystal size would decrease with increased ligand concentration, to be consistent with the proposed competitive binding mechanism [26, 38] between RSH and SH^-. However, pH also plays a critical role in particle growth, as it determines the equilibrium species and concentrations of all the reactants. In fact, it is possible that some of the trends reported earlier in the literature occurred in part as a result of changes in reaction pH (e.g., addition of more acidic ligand lowers reaction pH) and not because of increases in ligand concentration.

The PL and absorbance spectra both follow similar trends with ligand concentration. Without adjusting pH after sulfide addition, the PL peak energy is not affected by the [MAA]:[$CdCl_2$] ratio (Figure 23C); however, the PL intensity varies considerably for both adjusted and unadjusted pH after sulfide addition. The maximum PL intensity was found for [MAA] in the range of 55 to 100 mM (Figure 23F), concentrations that produce particles in the 2 nm size range. This corresponds to [MAA]:[Na_2S] ratios ranging from 22:1 to 44:1—the same ratios that gave rise to the highest PL emission intensity in the [Cd]:[S] experiments shown in Figure 22. Although the particle size is not affected by changes in ligand concentration (when pH is not adjusted), the PL quantum yield can change by almost an order of magnitude.

3.3.4.4 Ligand Length

CdS nanocrystals were synthesized in the presence of $HS(CH_2)_xOH$ with varying hydrocarbon chain length, x=2, 3, 4, and 6. For these reactions, $[CdCl_2]$=10 mM, $[CdCl_2]$:$[Na_2S]$=1, and $[HS(CH_2)_xOH]$:$[CdCl_2]$=9.85. The pH was raised to 7.0 prior to Na_2S addition. In one set of experiments, the pH was adjusted to 8.2 after Na_2S was added. Figure 24A-D shows the absorbance and PL emission spectra of the CdS nanocrystals synthesized using ligands of varying chain length. The 6mer produced a white insoluble precipitate—most likely due to the formation of an insoluble hydrophobic Cd-SR complex [8]—and is therefore not included in the spectra. Increasing chain length led to decreased particle size, as found in a previous study (Figures 24A, B). [7] The trend is more dramatic without the pH readjustment after sulfide addition (Figure 24A). Consistent with suggestions by others, [7, 46] it appears that the added bulkiness associated with the longer ligands leads to slightly smaller nanocrystals. Similar results have also been observed in a number of nanocrystal materials synthesized in both organic and aqueous phases, including CdSe, CdTe, CdS [7], Ag [47], InP, InAs [48].

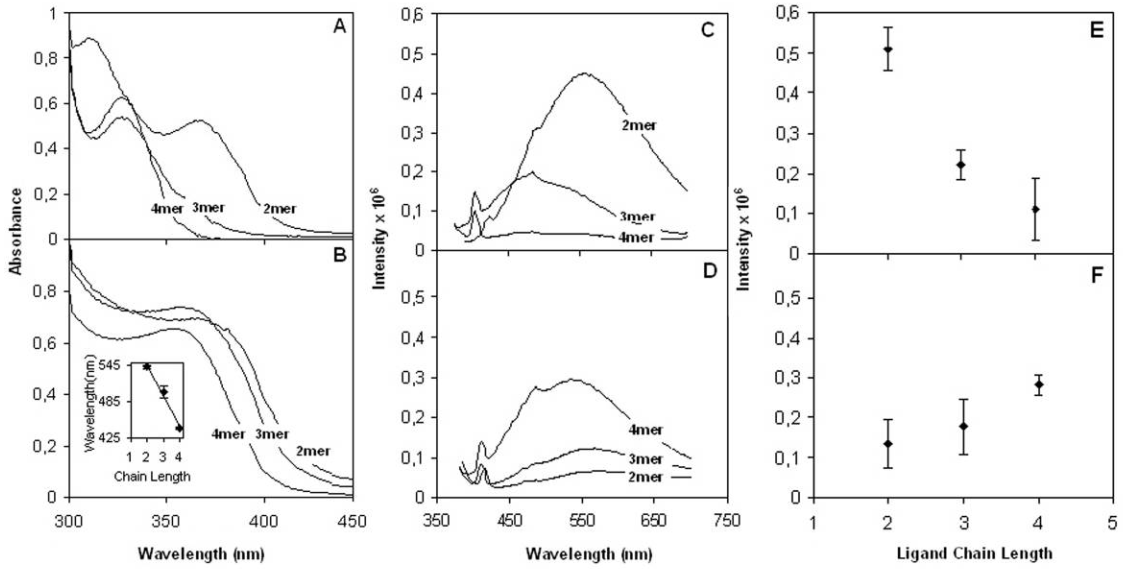

Figure 24: Absorbance and Excitation Spectra for Increased Ligand Length.

Room temperature (A,B) absorbance and (C,D) PL emission spectra (λ_{exc}=exciton peak, OD=0.1) for aqueous CdS nanocrystals stabilized by $HS(CH_2)_xOH$ ligands with varying hydrocarbon chain length, x. The nanocrystals were synthesized with [$CdCl_2$]=10 mM, [$CdCl_2$]:[Na_2S]=1, and [Ligand]:[$CdCl_2$]=9.85. In one set of experiments (B,D), the pH was adjusted to 8.2 after adding Na_2S. (B, Inset) Three experiment average of absorbance onset plotted against ligand chain length for the samples adjusted to 8.2 after adding Na_2S. The curve corresponds to a linear fit of the data (R^2 = 0.99, λ_{onset} = -50.6(Ligand Length) + 647.) PL intensity (OD=0.1 for all samples) plotted versus ligand chain length for CdS nanocrystals formed without (E) and with (F) pH readjustment to 8.2 for three experiments.

The longer chain length capping ligand also shifts the PL emission peak to the blue, as expected based on the absorbance spectra (Figures 24C, 4D). Without readjusting the pH after adding the sulfide reagent, the CdS nanocrystals show quantum yield efficiencies that decrease with increasing chain length (Figure 24E). On the other hand, when the pH was adjusted to 8.2, the PL intensity increased with increasing chain length (Figures 24F). These trends appear to be related to the particle size differences rather than the ligand length. When PL intensity is correlated to nanoparticle size, we see that a

maximum in PL intensity occurs for particles with similar sizes, ~2 nm (Figure 24A, 2mer; Figure 24B, 4mer).

3.3.4.5 pH Effects

MAA-stabilized CdS nanocrystals were synthesized at different solution pH values prior to Na_2S addition. The pH was varied between 5 and 11 prior to adding Na_2S, because pH values less than 4.5 led to the formation of insoluble $CdCl_2$/MAA complexes [34, 49] and the pH of Na_2S solutions exhibit an upper pH limit of 12. The exciton and PL emission peak wavelengths monotonically shift to the blue with decreased pH (Figures 25A, C), which is consistent with previous findings in the literature. [23, 50] The exciton peak wavelength varies sigmoidally with the pH prior to sulfide addition (Figure 25E) and parabolically with the pH after sulfide addition (Figure 25F). The sigmoidal trend resembles a titration curve for Na_2S (pK_a = 6.90 [51]), further indicating that SH^- anions mediate nanocrystal formation.

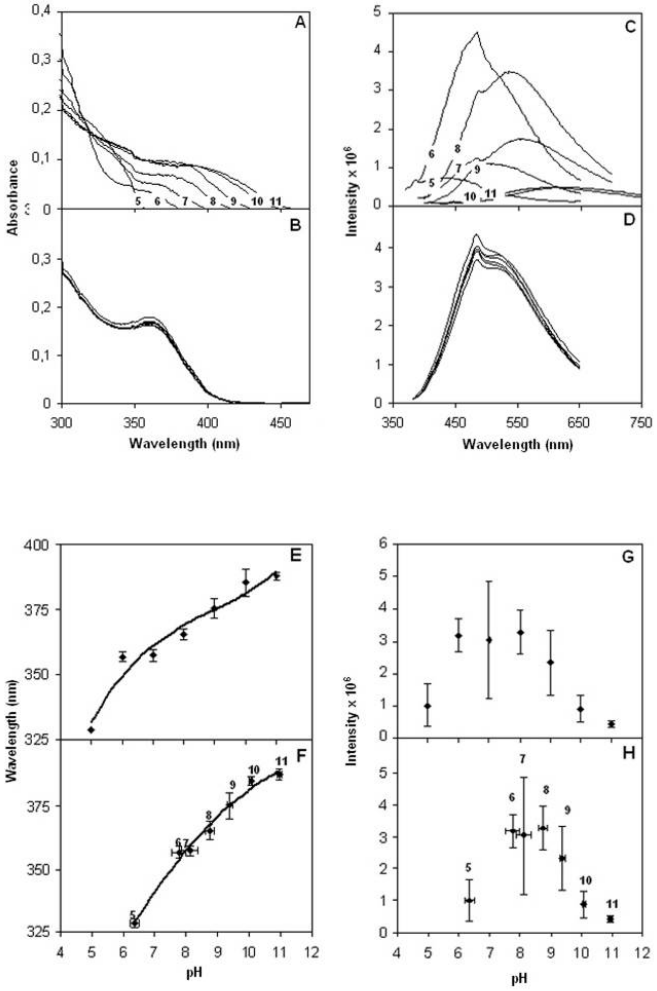

Figure 25: Absorbance and Excitation Spectra for Increased Reaction pH.

Room temperature (A, B) absorbance and (C,D) PL emission spectra (λ_{exc}=exciton peak, OD=0.1) for aqueous CdS nanocrystals synthesized at different solution pH prior to Na_2S addition. The nanocrystals were synthesized with [$CdCl_2$]=5 mM, [$CdCl_2$]:[Na_2S]=2, [MAA]:[$CdCl_2$]=11. The pH was adjusted to 8.2 after sulfide addition for the samples with absorbance and PL plotted in (B) and (D). (E) Exciton peak energy plotted as a function of pH prior to sulfide addition—the curve is a sigmoidal fit to the data: R^2 = 0.955, $\lambda_{peak} = 0.347(pH)^3 - 9.27(pH)^2 + 88.3(pH) + 78.1$. (F) Exciton peak energy plotted as a function of solution pH after Na_2S addition—the labels above the data points are the pH values prior to Na_2S addition and the curve is a parabolic fit to the data: R^2 = 0.989, $\lambda_{peak} = -1.47(pH)^2 + 38.7(pH) + 142.5$. PL intensity (OD=0.1 for all samples) plotted against the solution pH before (G) and after (H) Na_2S addition. In (H), each data point is labeled with the pH value prior to sulfide addition.

Again, the PL emission spectra exhibit a peak in intensity in the mid-size, or mid-spectral range, whereas the peak energy increases with declining pH (Figures 25G-H). Interestingly, CdS nanocrystals synthesized at a solution pH of 7.0 (prior to sulfide addition) exhibited a large standard deviation in PL intensity, perhaps as a result of the competition for the formation of different Cd-SR complexes in this pH range. Nanocrystals synthesized at different initial pH, but with the pH adjusted to 8.2 after Na_2S addition, exhibited identical absorbance and PL curves. This indicates that the reaction pH, and not the pH prior to Na_2S addition, is the pH that determines the size.

The pH dependent size shift of the nanocrystals also depends on the ligand concentration. The sigmoidal pH versus exciton energy curve shown in Figure 25E shifts to lower pH values with increasing ligand concentration (data not shown). Thus, when using a solution of 220 mM MAA for the capping ligand, it is necessary to decrease reaction pH by 2 units to produce nanocrystals with similar spectroscopic properties to those created with 55 mM MAA. This is in part because the pH required to dissolve the precipitate formed upon MAA addition to $CdCl_2$ solution is also a function of ligand concentration, with solutions of higher [MAA] dissolving at lower pH (e.g., pH 3 for 220 mM MAA vs. pH 4.5 for 55 mM MAA).

3.3.4.6 Ligand R Group

Previous studies [23, 37] have reported *increasing* particle size with decreasing pH for *basic* ligands (i.e., polyphosphate, mercaptoethylamine hydrochloride (MEA)). Upon further exploration, we found that the relationship between the pH and size is more complicated than a simple monotonic increase or decrease, especially for CdS nanoparticles stabilized with basic or neutral ligands. Figure 26A shows the exciton peak

energy for CdS nanocrystals synthesized using three different thiolate ligands containing acidic (i.e., -COOH (MAA)), neutral (-CH_2OH (MBE)), and basic (–CH_2NH_2 (MEA)) R groups. The nanocrystals were grown using standard solution conditions, with variation of the pH prior to Na_2S addition ranging between 3 and 10 for MBE and MEA and 5 to 11 for MAA.

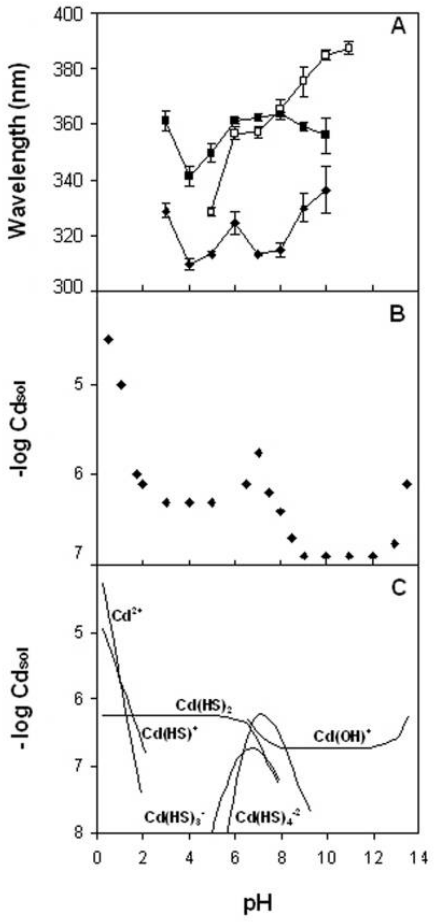

Figure 26: Effects of Altered Ligand Charge.

(A) Exciton peak energy plotted as a function of ligand R group: (♦) MBE; (■) MEA; and (□) MAA. (B) The negative log of the total concentration for all soluble free Cd^{2+} and Cd complexes formed in an excess of Na_2S is plotted versus pH. (C) The negative log of concentration for individual soluble Cd species present in an excess of Na_2S is plotted versus pH. [Plots in B and C are adapted from J. Ste-Marie, A.E. Torma, A.O. Gübeli. Can. J. Chem. 42: 662, 1964.]

At low pH (<5), the peak absorbance energies for neutral MBE and basic MEA stabilized nanocrystals exhibit the same trend. In the mid-pH range (5 to 8), basic MEA and acidic MAA-stabilized particles show similar peak energy dependence on pH. At high pH (>8), the peak energy increases with increasing solution pH for acidic MAA and

neutral MBE stabilized particles; whereas, the peak energy of MEA-stabilized nanocrystals decreases with increasing pH. Taking into account the charge of the functional group on each ligand, the pH-dependence of the nanocrystal size appears to correlate with R group acidity/alkalinity. At low pH the "unique" curve is the acidic ligand, in the median pH range it is the neutral ligand, and at high pH it is the basic ligand.

Further, the "W"-shaped pH curve for the neutral MBE ligand is strikingly similar to the pH-dependent solubility curve for Cd-S complexes reported in the literature (Figure 26B-C). [51] Although, Figures 26B-C describe water-soluble Cd-S species formed in the presence of excess Na_2S and not Cd-RSH, the complexes formed by ligands appear to be qualitatively similar. These complexes play an important role in the formation of CdS particles. Since free Cd^{2+} only appears at pH lower than 2.0 (Figure 26C), CdS nanocrystal formation must be mediated by Cd-thiol species. The ligand R group can modulate the concentration and nature of these Cd-thiol complexes and thereby influence particle formation.

For example, between pH 5 and 10, two Cd-thiol species are seen: $Cd(HS)_3^-$ and $Cd(HS)_4^{-2}$, with a maximum concentration of both near pH 7. We believe that these Cd-thiol species play a critical role in crystal growth for several reasons. First, MBE capped nanocrystals display a local maxima in size at pH 6-7. Also, MAA-coated particles synthesized in this pH region (i.e., pH 6-7, Figure 25G) exhibit maximum PL intensity. Finally, molecular studies show that Cd-HSR complexes formed in the process of nanocrystal growth generally demonstrate Cd coordination numbers of 3, 4, or their multiples. [52-54] Based on our data and these observations, we propose that $Cd(HS)_3^-$ and $Cd(HS)_4^{-2}$ and $Cd(HSR)_x^{2-x}$ based complexes are the most likely intermediates for CdS nanocrystal formation. Thus, the maximum concentration of these intermediates at

pH 7 corresponds to the observed increase in MBE particle size and MAA PL intensity around pH 6-7. As these concentrations decline, MBE particle size also declines, reaching a minimum around pH 7-8.

The presence of a charged R group (e.g., MAA, MEA) could alter the interactions between the ligand and Cd^{2+} producing deviations from the behavior of the neutral ligand described above. It is particularly notable that both the acidic and basic curves resemble that of MBE (neutral), except in the region where the ligand would be charged. Thus, the Cd-thiol complexes present in solution before Na_2S addition are a major factor in determining particle size, and the presence of charged R groups will influence Cd-HSR complex formation. However, these complexes are not the sole determinant of particle size; competition between the capping ligand and SH^- for Cd surface binding also plays a role, as evidenced in the ratio experiment.

3.3.5 Summary of Synthesis Characterization

The effects of reactant concentration, Cd:S and Cd:ligand mole ratios, ligand length, pH, and R group chemistry on the optical properties of CdS nanocrystals synthesized by aqueous-phase arrested precipitation were analyzed (Table II). For the majority of variables examined, a size-dependant PL intensity maximum occurs at intermediate particle sizes (i.e., absorbance onset = 430 nm, diameter ~ 2 nm). This implies that as the PL emission peak is adjusted to produce tunable fluorescence, quantum yield may be sacrificed. The PL intensity is linked to particle surface quality, [39-40, 43] which is dependent upon the nanocrystal growth mechanism. We believe that optimal surface quality occurs from growth mediated by selected Cd-thiol nucleating complexes. Because these complexes appear to be present only under certain synthesis conditions (e.g., pH 6-8, Figure 26C), which are linked to a particular nanocrystal size

and emission wavelength, the ability to manipulate the location of the PL intensity maximum by tuning synthetic conditions can potentially be limited.

This is extremely important for the development of bio-labels because the ability to produce particles with a variety of narrow bandwidth emission wavelengths is desired for viewing multiple labeled components of a cell in a single image. Although the decline in PL intensity that occurs at these varied wavelengths may not be substantial enough to inhibit visualization with a microscope, it is relevant to consider this effect when designing particles for these applications. An alternative approach is to tune the color of the qdot by altering composition, either through varying the semiconductor (e.g., CdSe, CdTe [7]) or by adding dopants (e.g., Mg [45], Cu [55], Zn [56]). Additionally, capping the particles with a material of larger band gap can significantly improve quantum yields by enhanced exciton confinement, but even in this case, the epitaxial interfacing at the surface must be optimized. [7]

3.3.6 Relevance to Neuroelectronic Interfaces

Based on these results, CdS quantum dots produced using an aqueous synthesis display characteristics that are favorable to the development of neuroelectronic interfaces. Particles with high quantum yields (~15%) can be created reproducibly by controlling the reactant ratios and reaction pH. Particles can be capped with a variety of ligands, including acids, bases, and neutral molecules. This allows for a range of surface conjugation strategies that could be used to link particles to the cell receptor of interest. Additionally, a variety of particle sizes can be produced, allowing for modulation of the magnitude of the transient dipole moment; and hence the electric field to which the cell is exposed. Thus, through characterization of the arrested precipitation of CdS in aqueous

media, a thorough understanding of the relationship between synthesis conditions and the relevant physical properties of the resultant quantum dots was obtained.

3.4 CONCLUSIONS

Cadmium-based semiconductor nanocrystals offer many benefits to the development of neuroelectronic interfaces. Although metallic and other semiconductor materials could be used, cadmium-based particles provide high quantum yields with excitation and emission wavelengths in the UV and visible regions of the spectra. Additionally, these particles have been used in other biological applications, demonstrating their compatibility with aqueous media and living components. There are several synthesis strategies for producing these particles. Organic syntheses provide the best optoelectronic properties (e.g., high quantum yield, resistance to photobleaching); however, these particles are not water-soluble and are made from toxic materials. Although several strategies exist for producing water-soluble particles from an organic synthesis, aqueous routes offer a convenient, non-toxic alternative to nanocrystal production. The main limitations of nanoparticles produced using an aqueous synthesis are lower quantum yields and trapped state emission. However, these factors are not crucial to the development of a neuroelectronic interface. Quantum yields for aqueous particles compare well with the usable organic systems, and trapped state emission may in fact lengthen the transient dipole moment state, increasing the time of electrical contact with the nerve cell.

Our initial efforts to utilize these particles evidenced a lack of reproducibility in the optical properties. Through systematic analysis of nanocrystal synthesis conditions, we were able to determine the critical factors in nanoparticle production. Increased reactant concentrations do not alter the nanoparticle size or emission wavelength, but can

affect quantum yield and stability in water. Reactant and ligand ratios, ligand length, and pH control particle emission wavelength and quantum yield. Finally, the charge of the ligand can alter the emission wavelength and quantum yield, especially for the reaction pH values in which the molecule is charged. We also discovered that regardless of the synthesis variable altered, particle quantum yield is size-dependant, with a maximum at intermediate sizes (~2 nm). This may represent a thermodynamic preference for nanocrystal growth from certain molecular precursors: clusters of Cd-ligand with ligand coordination numbers of 3, 4, or their multiples. These results allow us to create reproducible nanoparticles with a range of sizes and optical characteristics; thus providing us with several options to implement in a neuroelectronic interface.

3.5 REFERENCES

1. T.J. Bukowski and J.H. Simmons. “Quantum Dot Research: Current State and Future Prospects.” Crit. Rev. Solid State Mat. Sci. 27(3): 119, 2002.

2. A.P. Alivisatos. “Perspectives on the Physical Chemistry of Semiconductor Nanocrystals.” J. Phys. Chem. 100: 13226, 1996.

3. Y. Wang and N. Herron. “Nanometer-Sized Semiconductor Clusters: Materials Synthesis, Quantum Size Effects, and Photophysical Properties.” J. Phys. Chem. 95: 525, 1991.

4. W.C.W. Chan, D.J. Maxwell, X. Gao, R.E. Bailey, M. Han, and S. Nie. “Luminescent Quantum Dots for Multiplexed Biological Detection and Imaging.” Curr. Opin. Biotech. 13: 40, 2002.

5. C. Loo, A. Lin, L. Hirsch, M.H. Lee, J. Barton, N. Halas, J. West, and R. Drezek. “Nanoshell-Enabled Photonics-Based Imaging and Therapy of Cancer.” Tech. Cancer Res. Treat. 3(1): 33, 2004.

6. K. Kalyanasundaram, E. Borgarello, D. Duonghong, and M. Grätzel. “Cleavage of Water by Visible-Light Irradiation of Colloidal CdS Solutions: Inhibition of Photocorrosion by RuO_2” Angew. Chem. Int. Ed. Engl. 20(11): 987-988, 1981.

7. C.B. Murray, D.J. Norris, and M.G. Bawendi. “Synthesis and Characterization of Nearly Monodisperse CdE (E = S, Se, Te) Semiconductor Nanocrystallites.” J. Am. Chem. Soc. 115: 8706, 1993.

8. M.A. Hines and P. Guyot-Sionnest. “Synthesis and Characterization of Strongly Luminescing ZnS-Capped CdSe Nanocrystals.” J. Phys. Chem. 100: 468, 1996.

9. W.C.W. Chan and S. Nie. “Quantum Dot Bioconjugates for Ultrasensitive Nonisotopic Detection.” Science 281: 2016, 1998.

10. M. Bruchez, Jr., M. Moronne, P. Gin, S. Weiss, and A.P. Alivisatos. “Semiconductor Nanocrystals as Fluorescent Biological Labels.” Science 281: 2013, 1998.

11. J.E. Bowen Katari, V.L. Colvin, and A.P. Alivisatos. “X-ray Photoelectron Spectroscopy of CdSe Nanocrystals with Applications to Studies of the Nanocrystal Surface.” J. Phys. Chem. 98: 4109, 1994.

12. Tri-octyl phosphine Oxide MSDS Product Number 223301, version 1.5, 6/28/2004, from Sigma Aldrich.

13. A.M. Derfus, W.C.W. Chan, and S.N. Bhatia. "Probing the Cytotoxicity of Semiconductor Quantum Dots." Nano Lett. 4(1): 11, 2004.

14. Z.A. Peng and X. Peng. "Formation of High-Quality CdTe, CdSe, and CdS Nanocrystals Using CdO as Precursor." J. Am. Chem. Soc. 123: 183, 2001.

15. B.O. Dabbousi, J. Rodriquez-Viejo, F.V. Mikulec, J.R. Heine, H. Mattoussi, R. Ober, K.F. Jensen, and M.G. Bawendi. "(CdSe)ZnS Core-Shell Quantum Dots: Synthesis and Characterization of a Size Series of Highly Luminescent Nanocrystallites." J. Phys. Chem. B 101: 9463, 1997.

16. Personal Communication from Fred Mikeluc, Innovalight, Austin, Texas, June 29, 2004.

17. P. Bongrand. "Adhesion of Cells," in Handbook of Biological Physics, vol. 1, R. Lipowsky and E. Sackmann, Eds., Elsevier, Amsterdam: 1995, p. 767.

18. W.C.W. Chan, T.L. Prendergast, M. Jain, and S. Nie. "One-Step Conjugation of Biomolecules to Luminescent Nanocrystals," in Molecular Imaging: Reporters, Dyes, Markers, and Instrumentation, Darryl J. Bornhop, Kai Licha, Eds., Proceedings of SPIE., vol. 3924, 2000, p. 2.

19. β-Mercaptoethanol MSDS Product Number M7522, version 1.12, 4/6/2004, from Sigma Aldrich.

20. J.A. Schneider, B. Katz, and R.B. Melles. "Update on Nephropathic Cystinosis." Pediatr. Nephrol. 4(6): 645, 1990.

21. D. Gerion, F. Pinnand, S.C. Williams, W.J. Parak, D. Zanchet, S. Weiss, and A.P. Alivisatos. "Synthesis and Properties of Biocompatible Water-Soluble Silica-Coated CdSe/ZnS Semiconductor Quantum Dots." J. Phys. Chem. B 105: 8861, 2001.

22. R.C. Weast and M.J. Astle, Eds., CRC Handbook of Chemistry and Physics, 60th Ed. CRC Press, Boca Raton, Florida: 1979, p. B-220.

23. Y. Nosaka, N. Ohta, T. Fukuyama, and N. Fujii. "Size Control of Ultrasmall CdS Particles in Aqueous Solution by Using Various Thiols." J. Col. Interface Sci. 155: 23, 1993.

24. A. Henglein. "Photo-Degradation and Fluorescence of Colloidal Cadmium Sulfide in Aqueous Solution." Ber. Bunsenges. Phys. Chem. 86: 301, 1982.

25. A. Eychmüller, A. Hässelbarth, L. Katsikas, and H. Weller. "Fluorescence Mechanism of Highly Monodisperse Q-Sized CdS Colloids." J. Luminescence. 48-49: 745, 1991.

26. Y. Nosaka, K. Yamaguchi, H. Miyama, and H. Hayashi. "Preparation of Size-Controlled CdS Colloids in Water and Their Optical Properties." Chem. Lett. 4: 605, 1988.

27. K. Kundu, A.A. Khosravi, S.K. Kulkarni, and P. Singh. "Synthesis and Study of Organically Capped Ultra Small Clusters of Cadmium Sulphide." J. Mat. Sci. 32: 245, 1997.

28. A. Hässelbarth, A. Eychmüller, and H. Weller. "Detection of Shallow Electron Traps in Quantum Sized CdS by Fluorescence Quenching Experiments." Chem. Phys. Lett. 203(2-3): 271, 1993.

29. J.O. Winter, T.Y. Liu, B.A. Korgel, and C.E. Schmidt. "Recognition Molecule Directed Interfacing Between Semiconductor Quantum Dots and Nerve Cells." Adv. Mat. 13: 1673, 2001.

30. A. Fojtik, H. Weller, U. Koch, and A. Henglein. "Photo-Chemistry of Colloidal Metal Sulfides 8. Photo-Physics of Extremely Small CdS Particles: Q-State CdS and Magic Agglomeration Numbers." Ber. Bunsenges. Phys. Chem. 88: 969, 1984.

31. R. Rossetti, J.L. Ellison, J.M. Gibson, and L.E. Brus. "Size Effects in the Excited Electronic States of Small Colloidal CdS Crystallites." J. Phys. Chem. 80(9): 4464, 1984

32. Y. Nosaka, H. Shigeno, and T. Ikeuchi. "Formation Steps of CdS Clusters in Aqueous Solution Containing 2-mercaptoethanol." Surf. Rev. Let. 3:1209, 1996.

33. D. Hayes, O.I. Micic, M.T. Nenadovic, V. Swayambunathan, and D. Meisel. "Radiolytic Production and Properties of Ultrasmall CdS Particles." J. Phys. Chem. 93: 4603, 1989.

34. H.M. Chen, X.F. Huang, L. Xu, J. Xu, K.J. Chen, and D. Feng. Superlattices and Microstructures. "Self-Assembly and Photoluminescence of CdS-Mercaptoacetic Clusters with Internal Structures." 27: 1, 2000.

35. H. Weller, H.M. Schmidt, U. Koch, A. Fojtik, S. Baral, A. Henglein, W. Kunath, K. Weiss, and E. Dieman. "Photochemistry of Semiconductor Colloids. 14. Photochemistry of Colloidal Semiconductors-Onset of Light Absorption as a Function of Size of Extremely Small CdS Particles." Chem. Phys. Lett. 124: 557, 1986.

36. N. Herron, Y. Wang, and H. Eckert. "Synthesis and Characterization of Surface-Capped, Size-Quantized CdS Clusters – Chemical Control of Cluster Size." J. Am. Chem. Soc. 112: 1322, 1990.

37. H. Weller. "Colloidal Semiconductor Q-Particles – Chemistry in the Transition Region Between Solid-State and Molecules." Angew. Chem. Int. Ed. Engl. 32: 41, 1993.

38. V. Swayambunathan, D. Hayes, K.H. Schmidt, Y.X. Liao, and D. Meisel. "Thiol Surface Complexation of Growing CdS Clusters." J. Am. Chem. Soc. 112: 3831, 1990.

39. D.V. Talapin, A.L. Rogach, E.V. Shevchenko, A. Kornowski, M. Haase, and H. Weller. "Dynamic Distribution of Growth Rates within the Ensembles of Colloidal II-VI and III-V Semiconductor Nanocrystals as a Factor Governing Their Photoluminescence Efficiency." J. Am. Chem. Soc. 124: 5782, 2002.

40. C. de Mello Donegá, S.G. Hickey, S.F. Wuister, D. Vanmaekelbergh, and A. Meijerink. "Single-Step Synthesis to Control the Photoluminescence Quantum Yield and Size Dispersion of CdSe Nanocrystals." J. Phys. Chem. B. 107: 489, 2003.

41. L. Qu and X. Peng. "Control of Photoluminescence Properties of CdSe Nanocrystals in Growth." J. Am. Chem. Soc. 124: 2049, 2002.

42. G.R. Bradburn, T.J. Trentler, S.C. Goel, W.E. Buhro, and J.M. Jean. "Dependence of Quantum Yield from the Deep Trap States of CdS Nanoparticles on Particle-Size and Capping Group." 210th ACS National Meeting, PHYS-322 (Pt. 2): Chicago, 1995.

43. D.V. Bavykin, E.N. Savinov, and V.N. Parmon. "Specific Features of Luminescence of Q-CdS Colloids with Different Sizes." Russ. Chem. Bul. 47: 629, 1998.

44. Y.W. William and X. Peng. "Formation of High-Quality CdS and Other II-VI Semiconductor Nanocrystals in Noncoordinating Solvents: Tunable Reactivity of Monomers." Angew. Chem. Int. Ed. 41: 2368, 2002.

45. A.A. Khosravi, M. Kundu, B.A. Kuruvilla, G.S. Shekhawat, R.P. Gupta, A.K. Sharma, P.D. Vyas, and S.K. Kulkarni. "Manganese-Doped Zing-Sulfide Nanoparticles by Aqueous Method." Appl. Phys. Lett. 67: 2506, 1995.

46. C. Barglik-Chory, E. Dieman, A.F. Münster, H. Strohm, C. Remenyi, and G. Müller. "Influence of Synthesis Parameters on the growth of CdS Nanoparticles in Colloidal Solution and Determination of Growth Kinetics using Karhunen-Loeve Decomposition." Chem. Phys. Lett. 374: 319, 2003.

47. P. Shah, S. Husain, K.P. Johnston, and B.A. Korgel. "Role of Steric Stabilization on the Arrested Growth of Silver Nanocrystals in Supercritical Carbon Dioxide." J. Phys. Chem. B. 106: 12178, 2002.

48. D. Battaglia and X. Peng, Nano. Lett. "Formation of High Quality InP and InAs Nanocrystals in a Noncoordinating Solvent." Nano Lett. 2: 1027, 2002.

49. V.L. Colvin, A.N. Goldstein, and A.P. Alivisatos. "Semiconductor Nanocrystals Covalently Bound to Metal-Surfaces with Self-Assembled Monolayers." J. Am. Chem. Soc. 114: 5221, 1992.

50. L. Spanhel, M. Haase, H. Weller, and A. Henglein. "Photochemistry of Colloidal Semiconductors. 20. Surface Modification and Stability of Strong Luminescing CdS Particles." J. Am. Chem. Soc. 109: 5649, 1987.

51. J. Ste-Marie, A.E. Torma, and A.O. Gübeli. "The Stability of Thiocomplexes and Solubility Products of Metal Sulphides." Can. J. Chem. 42: 662, 1964.

52. Y. Nosaka, H. Shigeno, and T. Ikeuchi. "Formation of Polynuclear Cadmium-Thiolate Complexes and CdS Clusters in Aqueous-Solution Studied by Means of Stopped-Flow and NMR Spectroscopies." J. Phys. Chem. 99: 8317, 1995.

53. H.-B. Bürgi. "Stereochemistry of Polynuclear Cadmium (II) Thioglycolates: Crystal Structure of Cadmium (II) Bisthioglycolate." Helv. Chim. Acta. 57: 515, 1974.

54. V.S. Gurin. "Large Clusters with Cadmium Sulfide Cores: Simulation of Thiolate Ligands on the Surface by ab initio MO LCAO Calculation." Surf. Rev. Lett. 7: 161, 2000.

55. J.M. Huang and C.J. Murphy. Materials Research Society Luminescent Materials Symposium; San Francisco, 1999, pp. 33.

56. P.J. Sebastian. "ZnCdS Films for Solar Cell and Photodetector Applications Deposited by in situ Chemical Doping of CdS with Zn." Adv. Mat. Opt. Elec. 5: 269, 1995.

Chapter 4: Quantum Dot Bioconjugation and Directed Cell Binding[3]

The formation of interfaces with individual neuronal ion channels requires nanoparticle binding in close proximity to channel proteins. Although this could be accomplished through non-specific binding, a more promising method utilizes the native biorecognition capabilities of proteins and peptides to adhere to targets on the cell surface. [1] Several strategies have already been developed to conjugate these recognition molecules to fluorescent dyes, [2] and these strategies can be directly applied to nanocrystals. Previous to our studies, quantum dots had been conjugated to both proteins [3] and antibodies [4], although only proteins had been used with living systems. Here, we describe our efforts to develop additional methods to produce targeted cell binding with quantum dots.

Using CdS quantum dots, we have conjugated antibodies and peptides to nanoparticle surfaces for targeted cell binding. As a model system, we investigated the ability of these nanoparticles to bind integrins (e.g., extracellular matrix receptors [5]) on the cell surface. Antibody binding to the quantum dot surface was confirmed using UV-visible absorbance spectroscopy, while peptide binding was verified using UV-visible absorbance spectroscopy, fluorescence anisotropy and Fourier transform infrared spectroscopy (FTIR). Finally, both nanoparticle-conjugates were attached to cells, establishing the ability of quantum dots to form controlled interfaces with cell surfaces. Although these results represent a model system, they can be extrapolated to a variety of cell surface receptors, including ion channels. Thus, these strategies have the potential to

[3] Portions of this material have been previously published in the following reference: J.O. Winter, T.Y. Liu, B.A. Korgel, C.E. Schmidt. "Recognition Molecule Directed Interfacing Between Semiconductor Quantum Dots and Nerve Cells." Advanced Materials 13: 1673, 2001.

create controlled neuroelectronic interfaces between nanocrystals and neuronal ion channels.

4.1 FORMATION OF MOLECULAR–CELL INTERFACES

Present neuroelectronic devices establish contact through the direct or random placement of cells over device electrodes. [6] However, the small size of nanoparticles precludes this approach for binding cell receptors controllably. Additional strategies are needed to bring nanoparticles into the proximity of cell surface receptors. Several techniques have already been developed to link fluorescent molecules and microbeads to various parts of the cell. [2] At the time of this work, two of these strategies had been employed to bind nanocrystals to proteins [3] and antibodies. [4] These and other methods can potentially be applied to the development of controlled neuroelectronic interfaces.

4.1.1 Requirements for Forming Receptor–Scale Neuroelectronic Interfaces

Quantum dots average 1-10 nm in diameter, [7] and the average cell surface receptor is 10 nm. [8] However, the cell body is typically 10-30 *microns* in size. [9] Although several methods of controlled placement exist for entire cells (e.g., micropositioners), none have nanometer scale resolution. [6] Thus, precise electrical connections cannot be established by situating receptors over individual quantum dots. Biorecognition techniques provide an alternative strategy that allows direct presentation of nanoparticles to cells. In this method, nanoparticles are coupled to molecules that recognize and bind receptors on the cell surface. Nanocrystal-conjugates are then exposed to cells in solution, and are capable of forming precise interfaces with their receptor targets.

These techniques are well-established, as biorecognition has been used extensively to link other small molecules with selected cell components. [2] However, to develop active *electronic* interfaces between nanoparticles and cells, two additional factors must be considered. First, the conjugation of a biorecognition molecule to the nanocrystal must not interfere with its optoelectronic properties. Second, it is crucial that the distance between the nanoparticle and the cell surface receptor be minimized. This is because the nanoparticle electric field, which interacts with ion channels in the cell membrane, decays as a function of separation distance (Chapter 2, Section 2.5). Standard biorecognition techniques, combined with modification of the nanocrystal surface, can be combined to meet both of these needs.

4.1.2 Biomolecular Recognition

Biorecognition describes the strong and highly specific binding that exists between a receptor and its ligand target. This binding is not completely understood, but is believed to arise from a combination of electrostatic attractions, hydrogen bonding, and hydrophobic/hydrophilic interactions. [1] The cumulative interaction of these forces, which are individually weak, produces tight binding. Additionally, this affinity is unique to the ligand and its analogs, as only molecules with a certain conformation can access the binding site and form the appropriate bonds. Thus, the interfaces formed through biomolecular recognition are highly specific and controlled.

A number of molecules have been identified as biorecognition elements, and can be used to connect small molecules to components of the cell. Typically, these fall into three classes: antibodies, proteins, and peptides. [1] Antibodies recognize components that are foreign to their host system, and can be produced for almost any cellular component. A wide range of antibodies are commercially available, and their large size

and high number of functional groups allow for ready conjugation to many surfaces. Antibodies are by far the most commonly used biorecognition element in conjugate chemistry. [10] However, when antibodies cannot be applied, alternatives such as proteins and peptides may be employed. Because protein or peptide binding will produce a cellular response, these methods are often utilized to impose a specific cellular function (e.g., receptor-mediated endocytosis [4]) to the attached molecule. Proteins can be linked to these molecules through chemistry techniques, the success of which depends widely on the nature of the protein employed. For applications where an entire protein might be too large or expensive, protein fragments, known as peptides, can be employed. Peptides can be synthesized with additional amino acids to allow for conjugation to a chosen molecule.

4.1.3 Conjugation Strategies Using Biorecognition Molecules

Several different chemistry strategies have been developed to link recognition molecules to surfaces. [11] The majority of these techniques rely upon the presence of primary amines and carboxylic acid residues, common functional groups in antibodies and proteins. For many materials, conjugation to these groups is straightforward. However, if there are no or only a few functional groups that can be chemically linked to amines or carboxyl groups, modification of the material's structure may be required. One advantage of quantum dots is that their surfaces can be readily modified through ligand selection, and their conjugation to biorecognition molecules is not limited to a particular functional chemistry. Thus, nanoparticles can draw upon the full range of previously developed conjugation techniques. Two of the most frequently used methods are described below as examples.

4.1.3.1 Carbodiimide Conjugation

By far the most commonly employed approach for establishing links between proteins and other molecules is carbodiimide chemistry [12]. This method produces amide bonds (i.e., -CO-NH_2-) between free amines and carboxylic acid groups with no additional elements contributed to the molecule (Figure 27). Briefly, carboxylic acids are activated using EDC (1-ethyl-3-(3-dimethylaminopropyl)carbodiimide) to produce a urea intermediate. Then, this complex reacts with primary amines to produce an amide bond and an isourea by-product. This technique is highly effective; however, it has many limitations. The most common problem associated with EDC chemistry is the direct relationship between cross-linking efficiency and yield. When the EDC concentration is increased more protein is attached to the material of interest. However, additional, unintended bonds may also form between conjugates, creating networks of agglomerated molecules. Extreme care must be taken to ensure near unimolecular attachment, and the amount of protein that can be incorporated without aggregation is low.

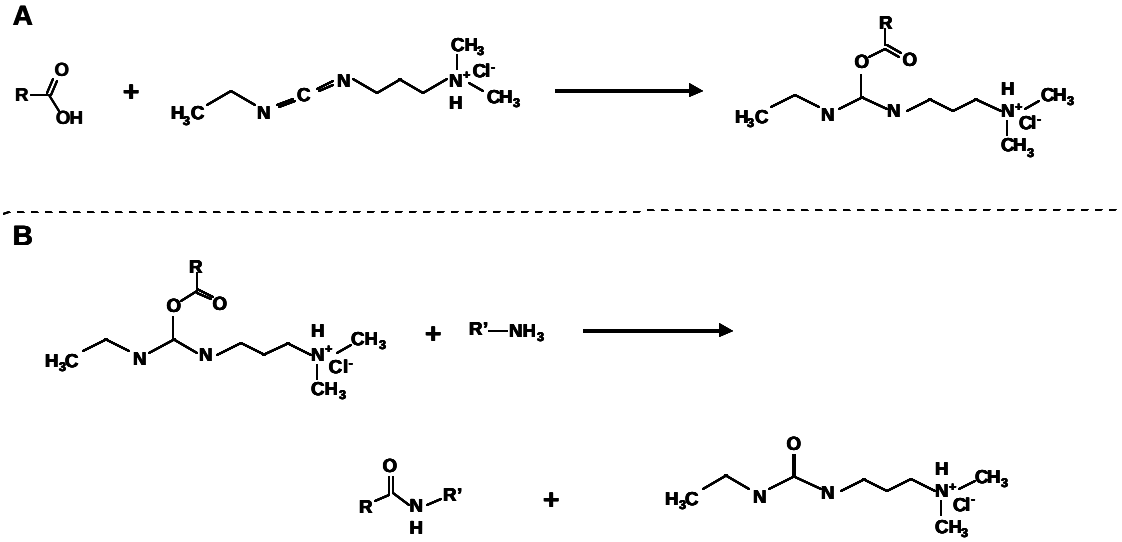

Figure 27: Carbodiimide Conjugation Chemistry.

(A) Carboxylic acid residues are activated with EDC. (B) This complex reacts with primary amines to produce amide bonds and isourea. [Adapted from Figure 106, G.T. Hermanson. Bioconjugate Techniques. Academic Press, San Diego: 1996, p. 171.]

4.1.3.2 Avidin-Biotin Interactions and Conjugation

A second commonly used approach to link proteins to a surface employs avidin and biotin [13], two naturally occurring proteins that display a remarkable affinity for each other. Conjugation of avidin to one molecule and biotin to the other can be used to produce tight binding between two unrelated components. This approach is frequently coupled with antibody binding to create systems that can recognize almost any cellular protein. A large variety of biotinylated antibodies are commercially available for this purpose. Conjugation of biotin to a surface is straightforward, and frequently occurs through reaction of a commercially available, activated biotin molecule (i.e., biotinamidocaproic acid 3-sulfo-N-hydroxysuccinimide ester) with primary amines.

Conjugation of avidin can be accomplished through many mechanisms, the most common utilizing primary amines in both the avidin molecule and the material of interest. In this method, free amines in avidin are activated with 2-iminothiolane to produce a sulfhydryl (-SH) leaving group (Figure 28). Then, the surface in question is modified to contain maleimides using SMCC (succinylimidyl-4-(N-maleimidomethyl)cyclohexane–1-carboxylate). This reaction proceeds through primary amines on the material surface and the NHS group (N-hydroxylsuccinyl group) of the SMCC molecule. Finally, the –SH group of avidin reacts with maleimides in the SMCC-conjugated material to produce a thioether bond. As both components initially contain amines, this reaction can also occur in reverse (i.e., SMCC reacting with avidin and 2-iminothiolane activation of the material surface).

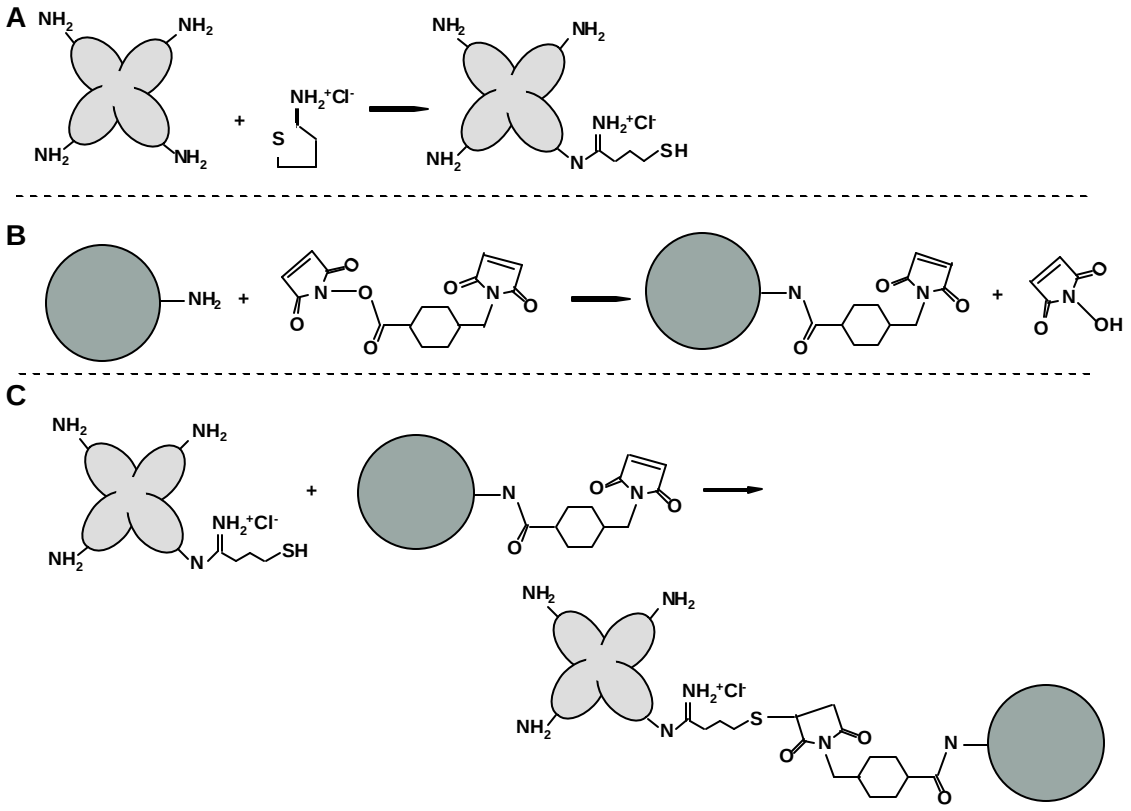

Figure 28: Streptavidin and Avidin Conjugation Chemistry.

(A) Avidin (light gray) is activated with 2-iminothiolane, producing an activated thiol complex. (B) The molecule of interest (dark gray) reacts with SMCC to produce a free NHS molecule and an activated maleimide complex. (C) The activated thiol-avidin complex and the activated SMCC-conjugate react, creating an avidin-conjugate. [Adapted from Figures 158 and 363, G.T. Hermanson. Bioconjugate Techniques. Academic Press, San Diego: 1996, p. 234, 577]

4.2 PREVIOUSLY EMPLOYED CONJUGATION STRATEGIES FOR QUANTUM DOTS

At the initiation of our work, there were only two significant publications describing quantum dots in a biological setting, [3-4] and both of these papers investigated nanoparticles as potential biolabels. Quantum yield is the main consideration for this use, and the particles employed were created using the highly luminescent (e.g., quantum yields ~ 50% [14]) core-shell synthesis. This synthesis produces TOPO-capped particles in organic solution. Thus, additional processing was introduced to provide water solubility and to attach biomolecules. Conjugation strategies, such as those described above, were some of the first approaches utilized for biofunctionalization of these quantum dots.

4.2.1 Biofunctionalization of Silica-Coated Nanocrystals

The first paper, by Alivisatos, et al., [3] utilized CdSe-CdS core-shell nanocrystals. Particles were enclosed in a silica shell, which not only conferred water-solubility on the particle, but also provided functional groups for bioconjugation. This was accomplished through variation of the silanization agent employed. For example, trimethoxysilylpropyl urea ($(CH_3O)_3$-Si-$(CH_2)_3$NH-CO-NH_2) and 3-aminopropyl trimethoxysilane ($(CH_3O)_3$-Si-$(CH_2)_3NH_2$) both introduce positively charged amine residues onto the particle surface. This modification can be exploited to produce cell labeling through either electrostatic or specific interactions.

To demonstrate non-specific binding, the silica coating was modified with trimethoxysilylpropyl urea (urea = NH_2-C-NH_3^+ at neutral pH), which binds negatively charged acetate groups (-CH_2-COO^- at neutral pH) in the cell nucleus. Nanocrystal

binding was displayed at the nucleus, as evidenced through fluorescence microscopy measurements. Binding was suppressed with the addition of a negatively-charged reagent or sodium dodecylsulfate (SDS), indicating that it was mediated primarily through non-specific electrostatic interactions.

To demonstrate specific binding, biotin was conjugated to the nanocrystal surface (Section 4.1.3.2). First, the silica coating of the nanocrystal was modified to include primary amines using 3-aminopropyltrimethoxysilane. Then, biotinamidocaproic acid 3-sulfo-N-hydroxysuccinimide ester was introduced. The NHS ester group of the activated biotin reacts quickly with primary amines to produce amide bonds, linking the nanocrystals to biotin molecules. To produce interfacing between these conjugates and cells, a complicated duel-biotin/streptavidin system was used. The cells were exposed to a separate solution of biotinylated-phalloidin, which adhered to F-actin filaments in the cytoskeleton. Then, streptavidin was introduced, binding the biotin component of biotin-phalloidin. Finally, cells were incubated with the biotinylated-nanocrystals, which bound to the phalloidin-biotin-streptavidin complexes at avidin sites. Using this system, specific nanoparticle binding of F-actin filaments was produced.

4.2.2 Biofunctionalization of Mercaptoacetic Acid-Coated Nanocrystals

The second paper, by S. Nie, et al., [4] used a slightly different approach to investigate CdSe-ZnS core-shell particles as potential biolabels. Particles were altered through mercaptoacetic acid ligand exchange, placing carboxyl groups on the surface. Using EDC (i.e., carbodiimide chemistry, Section 4.1.3.1), those carboxyl groups were conjugated to the reactive amines of IgG antibodies and transferrin, a surface protein that promotes uptake of iron molecules through receptor-mediated endocytosis. Because aggregation is a side-effect of EDC chemistry, conjugates were examined with

transmission electron microscopy and were found to be primarily single particles. Additionally, fluorescence optical microscopy confirmed that conjugated particles maintain their initial optical properties.

To demonstrate biorecognition, IgG conjugates were shown to aggregate in the presence of a specific polyclonal antibody known to bind IgG fragments. These particles were not, however, examined with living cells. On the other hand, transferrin-conjugated particles were incubated with living cells. Transferrin-conjugated particles were found in intracellular vesicles, as would be expected following receptor-mediated endocytosis.

4.2.3 Summary of Previous Quantum Dot Strategies and Applicability to the Neuroelectronic Interface

Although the previously used techniques are highly successful for biolabeling applications, many limitations exist to their application in a neuroelectronic interface. Quantum dot binding was achieved through *non-specific* interactions [3] or through *secondary* binding to molecular receptors. [3-4] Neither of these strategies can produce the specificity or close-proximity binding required for the neuroelectronic interface. Non-specific interactions (e.g., positively charged molecules binding nuclear proteins) can provide disperse labeling over large portions of the cell membrane, and may even produce connections with ion channels. However, they do not provide the control to interface nanoparticles with a *chosen* receptor of interest. Alternatively, indirect attachment methods (i.e., avidin-biotin systems and 2º antibodies), while specific, give rise to significant cell-quantum dot separation distances, on the order of 30 nm, [15] reducing electrical contact. Furthermore, at the initiation of our work, only intracellular labeling had been demonstrated with *living* cells. Thus, new methods were needed to produce close proximity binding to targeted receptors on the extracellular surface.

4.3 RECEPTOR-NANOPARTICLE INTERFACES USING RECOGNITION MOLECULES

4.3.1 Strategies for Creating Quantum Dot–Receptor Interfaces

A limited number of biorecognition molecules can produce separation distances of less than 10 nanometers between their conjugates and cells. In fact, the majority of proteins are several nanometers in size. For example, a single antibody is approximately 15 nm in diameter. [16] Considering that the Debye screening length for biological saline is on the order of 1 nm, [17] this distance is too large to allow for direct nanoparticle influence on the cell membrane potential. Both of the nanocrystal conjugation technologies discussed previously utilize large protein molecules (Sections 4.2.2 and 4.2.3), producing untenable separation distances. [3-4] Thus, we developed two additional routes to interface the receptors of living neurons with semiconductor quantum dots. The first employs known antibody-antigen recognition and the second, a new approach, utilizes peptide recognition groups.

4.3.1.1 Antibody-Based Approach

The first method expands the quantum dot-antibody conjugation chemistry demonstrated by Nie, et al. [4] to create more intimate cell connections. As discussed above, antibodies themselves are too large to create neuroelectronic interfaces; however, an alternative is to use antibody Fab fragments, the smallest portion of an antibody that retains its binding capability. These fragments are ~5 nm in diameter. [16] Fab fragments are commercially available for many cell targets, and can be created using papain digestion. [18] Although antibodies have been demonstrated previously by Nie, et al. [4] to link quantum dots to biomolecules, this work did not demonstrate cell compatibility.

Additionally, the particles studied were not produced using aqueous methods. Instead, organic CdSe-ZnS TOPO-capped quantum dots were made water-soluble through a complicated ligand exchange process. Thus, we expanded this method to bind particles manufactured using aqueous synthesis and demonstrated connections to *living* cells.

As a model system, we conjugated aqueous CdS quantum dots to IgG secondary antibodies using the technique described by Nie, et al. [4] (Figure 29A). IgG antibodies recognize and bind a variety of primary antibodies that are specific to targets on the cell surface. In particular, we chose to investigate integrins (i.e., extracellular matrix receptors on the cell surface) because of their abundance and documented expression pattern. [19] Integrins are not electrically active, but expansion of this technique to ion channels is straightforward through selection of the appropriate antibody. Although this system produces a large separation distance (~30 nm [15]), it demonstrates the utility of antibody intermediates for quantum dot-cell interfacing. Ultimately, this method could be expanded to include Fab fragments, which possess a more appropriate size for the neuroelectronic interface. Thus, the model system is not ideal for neuroelectronic interface creation, but can be easily altered to create components of the proper dimensions and binding capabilities.

4.3.1.2 Peptide-Based Approach

In addition to the antibody method, a second, novel approach utilizing peptides was developed (Figure 29B). Biorecognition peptides are protein fragments that promote attachment of bulk protein to the active site. The advantage of employing peptides, as opposed to the whole protein molecule, is their large reduction in scale. The minimum peptide length for recognition depends on the protein selected, but can be as short as 3-5

amino acids (e.g., 1-1.5 nm). [20-21] Additionally, peptides can be manufactured to almost any length, with each amino acid roughly corresponding to 3 angstroms (0.3 nm) for a straight chain conformation. [22] Thus, the separation distance between the particle and the cell surface can be tuned through altering the length of the peptide. Their small size and tunable length make peptides ideal alternatives to large conjugation molecules.

For our model system, we investigated aqueous CdS nanoparticles and selected peptides. In particular, we chose to investigate peptides containing some of the shortest sequences necessary for recognition, RGDS [20] and YIGSR, [21] which bind to integrin receptors. These sequences bind the same receptor class as the antibody-based method, allowing for direct comparison between the two techniques. Peptides were linked to the quantum dot through a novel approach: thiolated ligand binding using cysteine residues. They were used as sole passivating agents and in combination with mercaptoacetic acid, a traditional ligand. In this method, peptide attachment to the quantum dot surface occurs during synthesis, providing a single-step technique for nanocrystal synthesis and bioconjugation. Although our model system binds to integrins, which are not electrically active, it can be expanded to include ion channels. Given these advantages, peptide bioconjugation presents a superior approach for forming close-range interfaces between semiconductor quantum dots and cellular receptors.

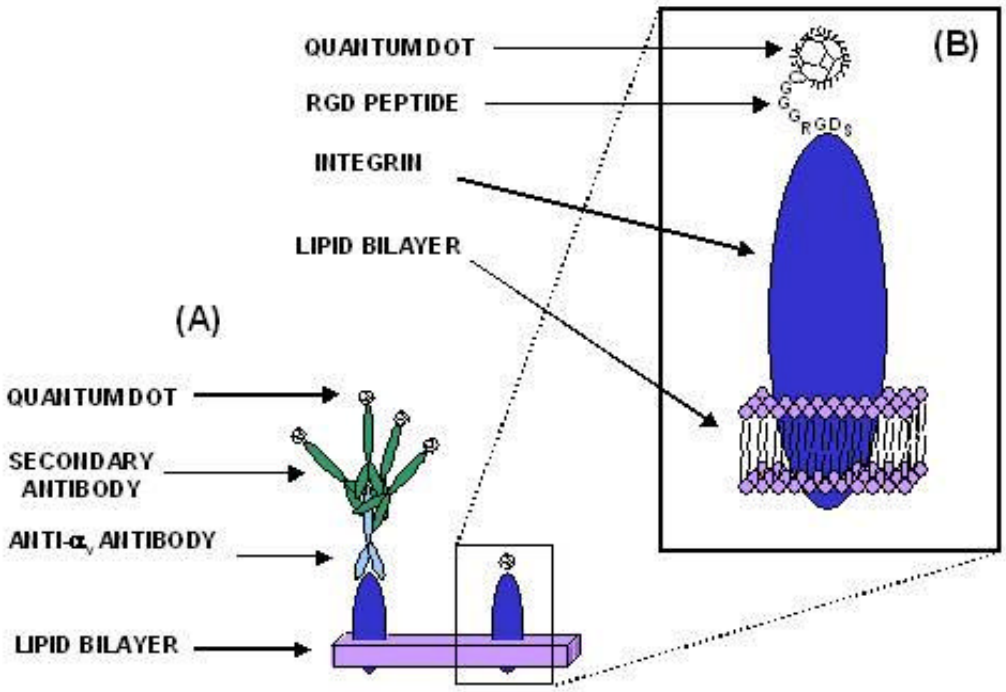

Figure 29: Recognition Molecule-Directed Interfacing Between Quantum Dots and Nerve Cells.

(A) Antibody Technique. A primary antibody binds to specific cell surface receptors. Multiple secondary antibodies bind to the primary antibody. Quantum dots are attached to the secondary antibody through amine bonds. The expected separation distance between the quantum dot and the cell is ~30 nm [15] assuming no crosslinking of secondary antibodies and a linear attachment. Actual distances may be smaller. (B) Peptide Technique. Peptide recognition sequences bind to specific cell surface receptors. These sequences are embedded in the capping layer of the quantum dots producing primary attachment. Based on stoichiomentric and chemical considerations, a monolayer of peptide and mercaptoacetic acid is expected. The maximum expected separation distance between the quantum dot and the cell is ~3 nm [22] based on an octomer peptide recognition sequence.

4.3.1.3 Summary of Quantum Dot–Recognition Molecule Approaches

Unlike previous methods, our approaches are capable of creating extremely close connections between quantum dots at cell receptors. Additionally, these connections are localized to the specific receptor of interest. Given the commercial availability of antibodies, a wide variety of receptors may be investigated at separation distances of ~5 nm. Although peptides are not as widely available as antibodies, the peptide approach could theoretically produce separation distances of 1 nm or less. Thus, these techniques are the first to allow for electrical interactions between the receptors of living cells and nano-scale inorganic particles. Although our interest is the development of a neuroelectronic interface, these methods could be used to study a myriad of other processes, including ox-redox reactions, mitochondrial respiration, and cell metabolism.

4.3.2 Materials and Methods

4.3.2.1 Synthesis of CdS Quantum Dots (and Peptide-Coated CdS Dots)

Dots were synthesized using previously published methods. [23] Briefly, carboxyl-stabilized CdS nanocrystals were produced through arrested precipitation at room temperature in aqueous solution. Mercaptoacetic acid served as the colloidal stabilizer. All chemicals were used as obtained from Sigma Chemical Co. (St. Louis, MO). Nanocrystals were prepared from a stirred solution of 0.009 g $CdCl_2$ (5 mM) in 10 ml of pure distilled, deionized water. Then, 200 µL of mercaptoacetic acid were added to the solution (220 mM MAA) lowering the pH to ~2.00. The pH was raised to 7 with concentrated NaOH (~1760 µL 1 M equivalents); and 10 ml of 2.5 mM $Na_2S{\bullet}9H_2O$ (0.00575 g) were added, raising the final pH to ~8.13. The solution turned yellow shortly

after sulfide addition due to CdS nanocrystal formation, which was qualitatively confirmed using a UV lamp to observe fluorescence.

Three types of peptide-coated quantum dots were produced: RGD-quantum dots, RGD/MAA-quantum dots, and YIGSR/MAA-quantum dots. The specific peptides utilized were Acetyl-CGGGRGDS and CDPGYIGSR. Both peptides were synthesized and purified at the University of Texas Protein Microanalysis facility and were used as supplied. For RGD-quantum dots, RGD peptide was added at 10 mM (i.e., 8 mg/mL $CdCl_2$) to the $CdCl_2$ solution in place of MAA. For RGD/MAA- and YIGSR/MAA-quantum dots, peptide was added at 0.6 mM (i.e., 0.5 mg/mL for RGD and 0.65 mg/mL for YIGSR) to the $CdCl_2$ solution in addition to the 220 mM MAA. Quantum dots containing a control sequence, CGGGRVDS, were also synthesized following the procedure for RGD/MAA-nanoparticles. This sequence, which does not bind the cell, [20] was used to demonstrate the specificity of peptide binding. Final incorporation rates of the peptides were not measured explicitly, but incorporation was qualitatively confirmed using analytical techniques.

4.3.2.2 Conjugation of Quantum Dots to IgG Antibody

Goat IgG antibody (Jackson Immunochemistry) was covalently linked to CdS quantum dots at the carboxyl terminus of the quantum dot capping ligand (i.e., MAA). Antibody was added to MES (2-(N-Morpholino)ethanesulfonic acid, Sigma) 50 mM buffer at a concentration of 0.3 mg/ml. Then, an equal volume of 1.2 μM (post-synthesis concentration diluted by a factor of 6) quantum dots was added to the solution. After a 15 minute incubation period, EDC (1-Ethyl-3-(3-Dimethylaminopropyl)-Carbodiimide Hydrochloride, Sigma) was added at 4 mg/ml. Next, the pH was adjusted to pH 6.5 ± 0.2. Following two hours in an orbital shaker, the reaction was quenched using glycine at 7.5

mg/ml. Conjugated quantum dots were isolated via repeated centrifugation (3000 g) and stored in 10 mM phosphate buffered saline (PBS, Table III) at pH 7.4.

Table III: 10 mM Phosphate Buffered Saline (PBS)

Component[1]	Concentration
Sodium Phosphate Monobasic	0.131 g
Sodium Phosphate Dibasic	0.575 g
Sodium Chloride	4.5 g
Distilled, De-ionized Water	500 mL

[1]All components were purchased from Fisher

Control experiments exposing quantum dots to antibody without EDC revealed noticeable physisorption of IgG on quantum dots, as evidenced by pellet formation during centrifugation. However, absorbance measurements of these nanocrystals revealed substantially less IgG binding than in the presence of EDC. Additionally, when the pH of the nanoparticle solution was raised above 6.5, the physisorbed antibody dissociated from the nanocrystals, as evidenced by the inability to form a pellet at high pH. Therefore, prior to all nerve cell labeling experiments, the nanocrystals were transferred to 1 ml of PBS (pH 7.4). As a result of EDC-induced crosslinking, some agglomeration of particles occurred; however, the aggregates were eliminated through sterile filtration. Remaining aggregates were small enough to remain suspended in solution.

4.3.2.3 Absorbance Measurements

Absorbance spectra of antibody-quantum dot conjugates were used to confirm antibody binding. Measurements were collected using a Beckman DU500 series spectrophotometer. Unmodified antibody and quantum dot spectra were collected as

standards and compared to the antibody-quantum dot conjugates. Additionally, MAA-quantum dots, RGD/MAA-quantum dots, and RGD-quantum dots were all examined to determine the degree of peptide binding. All measurements were acquired at optical densities less than 1.

4.3.2.4 Fluorescence Anisotropy

Fluorescence anisotropy is commonly employed to confirm the attachment of biomolecules to fluorescent species. The technique uses polarized light to obtain the solution tumbling rate for a fluorescent compound. Larger molecules display slower tumbling rates, thus conjugates can be distinguished from unmodified quantum dots. Anisotropy measurements were collected with a Sim Aminco Bowman Series 2 Luminescent Spectrophotometer with λ_{exc}=400 and λ_{em}=600. Measurements were repeated ten times for each sample.

4.3.2.5 Fourier Transform Infrared Spectroscopy (FTIR) Measurements

FTIR spectroscopy was used to confirm peptide conjugation to the nanocrystal surface. Quantum dots were obtained as a solid through the addition of a 1-propanol anti-solvent and centrifugation. Approximately 10 mg of this solid were mixed with an excess of potassium bromide (KBr) and pressed into a transparent pellet. Pellets were analyzed using a Thermo Mattson Affinity Gold FTIR with Winfirst Software in a nitrogen atmosphere. Measurements were not collected until the concentration of water and CO_2 in the chamber were negligible (~30 minutes), as determined by FTIR baseline spectra. As a control, 10 mg of dry peptide were also pelleted and evaluated under the same conditions.

4.3.2.6 Cell Culture

SK-N-SH neuroblastoma cells (American Type Culture Collection #HTB-11) were cultured in DMEM cell culture medium (Sigma) with 10% fetal bovine serum (FBS, Gibco) and 1% penicillin-streptomycin (pen-strep, Gibco). Cells were plated at densities of 1:8 and passaged every 6 days. Medium was changed every 2 days. Cells with passage numbers greater than 20 were discarded. SK-N-SH cells exhibit both neuronal and fibroblast morphologies. [24] Dense cultures produce the neuronal morphology; plating densities were selected to maximize this morphology.

4.3.2.7 CdS Morbidity Studies

To establish the cytocompatibility of CdS quantum dots, particles were added to culture medium and exposed to cells for one passage period. Cells were incubated with CdS dots at concentrations of $3x10^{-11}$, $1.5x10^{-11}$, and $0.75x10^{-11}$ M in DMEM cell culture medium with FBS and pen-strep added. These concentrations reflect multiples of the relative number of quantum dots added to the cells in the attachment procedure, up to ten times in excess. After adjustment to biocompatible salt concentrations (9 g/L), cell death did not occur with CdS quantum dot addition. Cells were studied for five days, monitoring proliferation and attachment. No differences from controls were observed.

4.3.2.8 Attachment of Quantum Dot Complexes to Cells

Quantum dot complexes were attached to cells using standard immunocytology techniques. [1] Briefly, cells were placed on 22x22 mm no. 1 thickness coverslips using imaging chambers (Sigma, Cat. No. Z36,585-4) to retain fluid. Cells were cultured at densities of 1 x 10^4 cells/mL in DMEM medium (Sigma) at 37 ºC and 5% CO_2 in sterile

conditions. After the cells reached ~70% confluency (~2 days), they were washed with Dulbecco's PBS (DPBS, Table IV) Then, the cells were blocked with 5% Bovine Serum Albumin in DPBS (BSA-DPBS,) for one hour at 4ºC. Following blocking, cells were washed with DPBS.

For antibody attachment (Figure 29A), primary antibody (anti-CD51, Accurate Chemical) was added at 10 µg/ml in BSA-DPBS and incubated for 30 minutes at 4ºC. Cells were washed three times with DPBS. Then, antibody-quantum dot conjugate was added to cells filling the imaging chamber (~1 ml/chamber). Cells were incubated for 30 minutes at 4ºC then washed with DPBS three times.

For peptide attachment (Figure 29B), peptide-quantum dot conjugates were first modified to pH 7.4 and dispersed in DPBS. The pH was adjusted using 1M and 0.1 M NaOH or HCl, as required. DPBS suspensions were obtained through either the addition of powdered DPBS salts, resuspension in DPBS following anti-solvent addition and centrifugation, or dilution with an equal volume of 2X DPBS. The best results occurred with 2X DPBS dilutions. The imaging chamber was filled with peptide-quantum dot conjugate solution (~1 ml/chamber), and cells were incubated for 30 minutes at 4ºC. Then, cells were washed three times with DPBS.

Following staining with either antibody- or peptide-conjugates, cells were stored in DPBS at 4ºC until observation. Imaging chambers were sealed with a 25 x 25 mm no. 1 square coverslip.

Table IV: Dulbecco's Phosphate Buffered Saline (DPBS)

Component[1]	Concentration
Potassium Chloride	0.100 g
Calcium Chloride	0.050 g
Magnesium Chloride * 6 H_2O	0.050 g
Potassium Phosphate Monobasic	0.100 g
Sodium Phosphate Dibasic	0.575 g
Sodium Chloride	4 g
Distilled, De-ionized Water	500 mL

[1]All components were purchased from Fisher

4.3.2.9 Fluorescence Microscopy

Fluorescence and phase contrast images were obtained using an Olympus IX70 inverted microscope with a mercury arc lamp and UV (λ_{exc}=330-385) and wideband blue (λ_{exc}=450-480) filter sets. Images were collected immediately after formation of the quantum dot-cell interfaces, employing a 100X objective with oil immersion. The use of coverslips, in conjunction with imaging chambers, eliminated the requirement of sample inversion. All images were collected with an exposure time of 496 ms. Some images were modified for brightness and contrast using Adobe Photoshop version 5.5.

4.3.3 Results and Discussion

4.3.3.1 CdS Nanocrystal Synthesis and Cytocompatibility

Cadmium sulfide (CdS) quantum dots (Figure 30A) were selected for these studies because of their straightforward single-step preparation, [26] which was easily modified for recognition molecule addition. The synthesis yields nanocrystals coated with exposed carboxyl groups on the particle surface that provide water solubility and convenient linking sites for amine-terminated antibodies. [12] The CdS quantum dots exhibit robust photoluminescence (PL) in visible wavelengths with photoluminescence excitation energies (PLE) just above those that induce cell damage (Figures 30B, C). To confirm that CdS quantum dots could be used successfully in conjunction with *living* cells, cells were exposed to quantum dot concentrations up to ten times in excess of that applied during labeling for five days. Cells were monitored for attachment and proliferation. No differences were seen from controls, suggesting that quantum dots were not toxic to cells over this time frame.

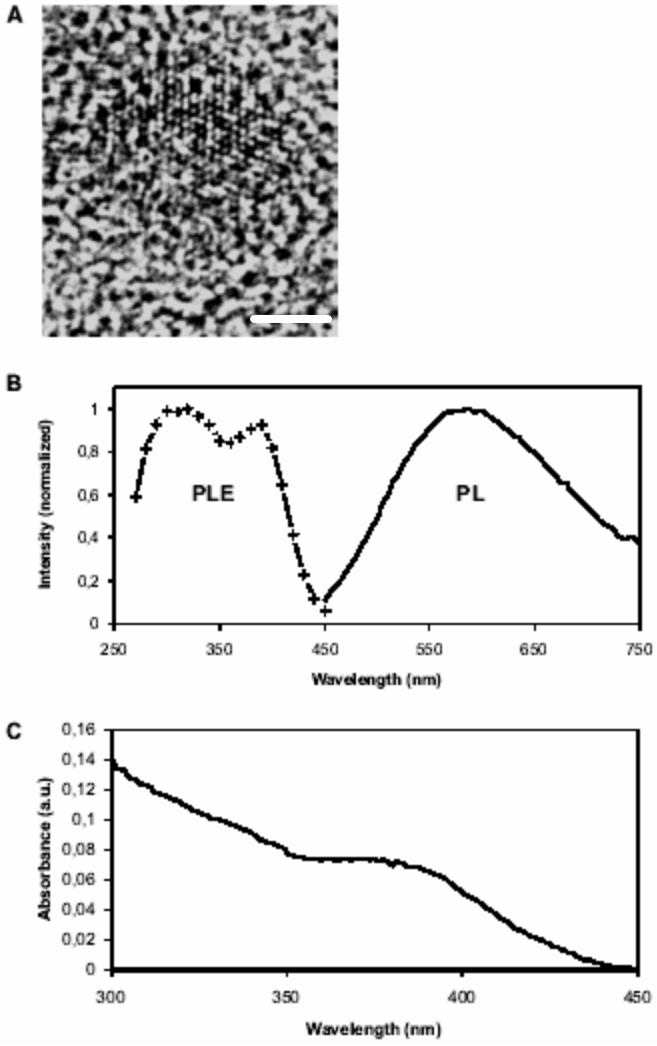

Figure 30: Properties of CdS Quantum Dots Employed for Bioconjugation Studies.

(A) TEM of CdS Quantum Dots. The nanocrystals have an average diameter of 30 Å with a 3.1 Å lattice spacing characteristic of wurtzite CdS. Scale bar = 1 nm. (B) Room temperature photoluminescence, PL, (λ_{exc}=400 nm) and photoluminescence excitation, PLE, (λ_{em}= 600 nm) spectra of CdS quantum dots dispersed at pH 7.4 in phosphate buffered saline (PBS). (C) Room temperature absorbance spectrum of an aqueous dispersion of CdS quantum dots. The exciton peak at 380 nm (3.6 eV) corresponds to an average particle size of 20 Å. [27]

4.3.3.2 Quantum Dot–Neuron Interfaces Using Antibody Recognition

To extend previous nanoparticle-conjugate work [3,4] to the receptors of living neurons, quantum dots were attached to SK-N-SH neuroblastoma cells (American Type Culture Collection #HTB-11) using an indirect immunofluorescence approach without fixation. [24] Antibody-nanoparticle conjugates were produced through the covalent linkage of nanoparticle surface carboxyl groups to Immunoglobulin G (IgG) secondary

antibodies (2ºAb) using EDC chemistry. [12] Attachment of IgG 2ºAbs to quantum dots was confirmed through UV-visible absorbance spectroscopy (Figure 31). Quantum dot-IgG conjugates exhibit absorbance peaks indicative of both antibody and quantum dots; controls do not.

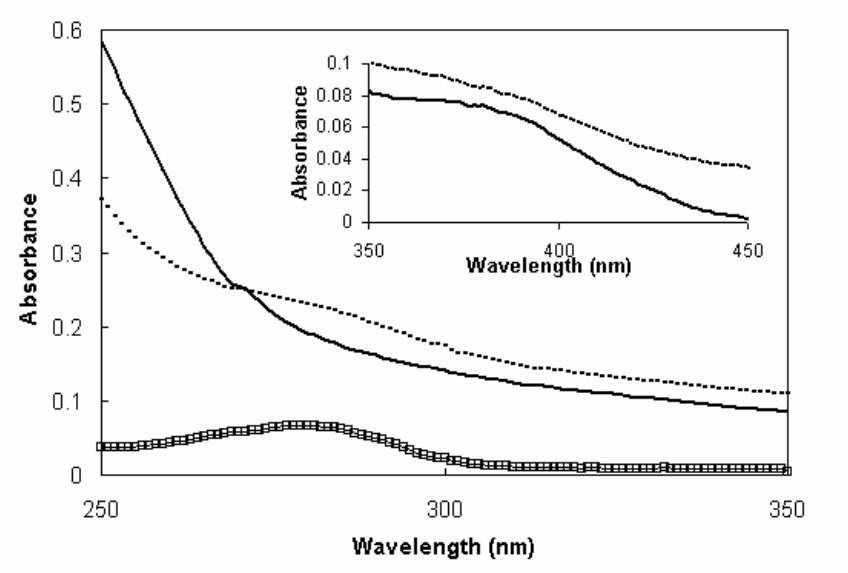

Figure 31: Room Temperature Absorbance Spectra of CdS Quantum Dots and CdS-Antibody Complexes.

IgG absorbs at 280 nm (squares). After binding IgG, the quantum dot absorbance spectrum (dashed) exhibits this feature, which is absent in bare quantum dots (solid). (Inset) CdS quantum dots bound to IgG (dashed) exhibit the same exciton peak as bare quantum dots (solid) at 380 nm. All materials were dispersed in PBS buffer (pH 7.4).

These conjugates were then attached to SK-N-SH neuroblastoma cells using a two-antibody method. The human neuronal SK-N-SH cell line was selected because they are the closest approximation to the primary cells that will ultimately be used in a neuroelectronic interface. In the two-antibody approach, a primary antibody (1ºAb), targeting the α_v portion of integrin receptors (anti-CD51, Accurate Chemical) was attached to the cell surface. The integrin α_v subunit binds both vitronectin and fibronectin

in the form of $\alpha_v\beta_1$ and $\alpha_v\beta_3$ complexes. It was chosen as the attachment site because of its location on the exterior of the cell [28] and the high expression levels of the $\alpha_v\beta_1$ complex in the SK-N-SH cell type. [24] Following primary antibody exposure, quantum dot-IgG 2°Ab conjugates were exposed to 1°Ab-labeled SK-N-SH cells (Figure 29A).

Attachment of the antibody complexes to the cells was verified through phase contrast and fluorescence optical microscopy images (Figure 32A and 32B respectively). Controls establishing the location of the α_v subunits on the SK-N-SH nerve cells were performed in a series of separate experiments (Figure 32C) using IgG 2°Ab attached to a common fluorescent dye, Alexa-488 (Molecular Probes), and compared with published results. [19] Quantum dot-IgG conjugates and Ab-Alexa-488 controls demonstrate binding only on the cell exterior, where integrin proteins are located. [28] Without 1°Ab tagging of the cell, no observable binding of IgG/CdS quantum dots occurred (Figure 32D). Also, bare quantum dots (i.e., quantum dots coated with carboxyl groups only) did not attach to the cells (Figure 32E). These results further confirm that antibodies mediate the attachment of quantum dots to living cells.

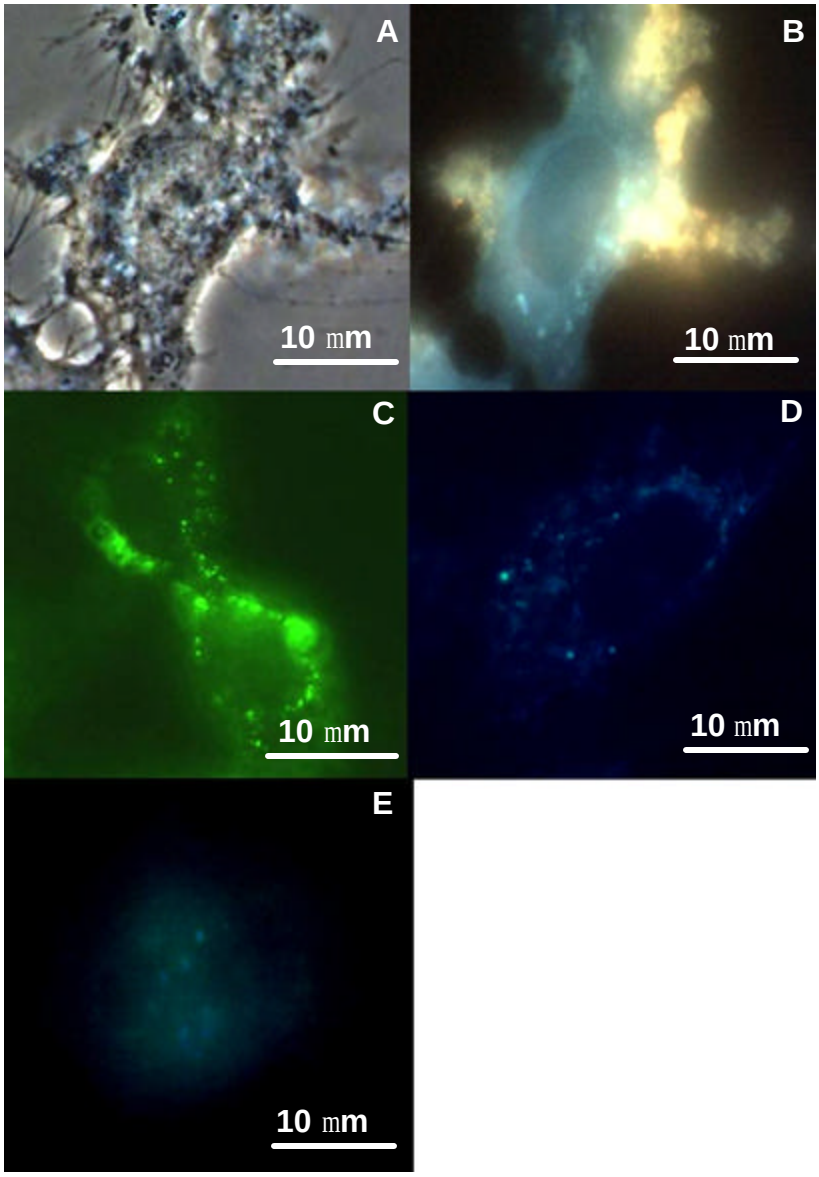

Figure 32: Quantum Dot Attachment to Neurons Using Antibody Binding Techniques.

(A) Phase contrast and (B) fluorescence (λ_{exc}=330-385 nm) optical microscopy images of SK-N-SH human neuroblastoma cells labeled with CdS quantum dots. Quantum dots were functionalized with IgG 2°Abs that bind anti-α_v integrin subunit 1° Abs. In (B,D,E) the blue color is the native autofluorescence of the cytoplasm of the cell—common in near UV excitation. (B) The yellow/orange color is CdS quantum dot luminescence. (C) Fluorescence image (λ_{exc}=450-480 nm) of control labeled with anti-α_v 1ºAb and Alexa-488 conjugated-IgG 2ºAb. Green fluorescence shows location of integrin receptors. (D,E) Fluorescence images ((λ_{exc}=330-385 nm) of controls incubated with (D) 2º antibody-quantum dot conjugates in the absence of 1º antibody. and (E) unconjugated quantum dots.

4.3.3.3 Quantum Dot–Neuron Interfaces Using Peptide Recognition

To reduce quantum dot-neuron separation distances beyond those achieved with the antibody method, peptide recognition molecules were attached to the CdS quantum dots. Two peptide sequences known to bind integrins were selected for further study. One of these peptides, RGD (Arg-Gly-Asp), binds the $\alpha_v\beta_1$ and $\alpha_v\beta_3$ integrins studied in our antibody model system, and was used for direct comparison. [20] The actual sequence used, CGGGRGDS, included the tetramer, RGDS, which has been found to adhere to the receptor more effectively than the trimer. [29] A terminal cysteine residue was added to attach the RGDS recognition group to the particle surface through its exposed atoms. The three intermediate glycines are intended to serve as molecular spacers, potentially reducing steric hindrance to cell binding that could result from the mercaptoacetic acid groups and the nanocrystal itself (Figure 29B). A second integrin binding sequence, the naturally occurring laminin peptide CDPGYIGSR, [21] was also studied for comparison. This sequence binds $\alpha_4\beta_1$ integrin receptors through the YIGSR pentapeptide, while the terminal cysteine residue allows for attachment to the nanoparticle surface.

CdS nanocrystals were synthesized through a *single-step* arrested precipitation in the presence of peptide. Because of cost limitations and their blue fluorescence, quantum dots that utilize only peptide as a ligand are not practical for final implementation in a neuroelectronic interface. Therefore, three types of nanoparticles were created. To demonstrate cell binding, RGD/MAA-quantum dots and YIGSR/MAA-quantum dots containing only small amounts of peptide were developed; while RGD-quantum dots were created to verify peptide incorporation onto the nanoparticle surface.

Peptide was added to the $CdCl_2$ precursor solution either at 10 mM concentration (RGD-quantum dots) or in a 0.6:220 molar ratio with MAA (RGD/MAA- and

YIGSR/MAA-quantum dots). The addition of MAA to RGD/MAA- and YIGSR/MAA-conjugates stabilizes the quantum dot size and prevents unwanted particle aggregation, while the peptide groups supply sites for cell surface receptor binding. Both MAA and the peptide bind CdS particle surfaces through sulfur atoms, creating either disulfide bonds or additional CdS bonds. There are no additional binding molecules exposed, and no chemical activators added. For peptide/MAA-quantum dots, peptide is added in a low stoichiometric ratio; and a monolayer is expected to form. Additional peptide ratios were not examined, but since peptide and mercaptoacetic acid compete for binding sites, it is expected that a minimum value for binding exists.

The resulting nanocrystals exhibit absorbance and PL spectra similar in shape but blue-shifted from those of quantum dots made without peptide (Figure 33). This is expected because our previous studies (Chapter 3, section 3.3.4.4) demonstrated that increased ligand length results in smaller (i.e., blue-shifted) particles as a result of ligand steric hindrance to nanocrystal growth. As the concentration of peptide is increased, this effect is more pronounced, indicating additional peptide binding.

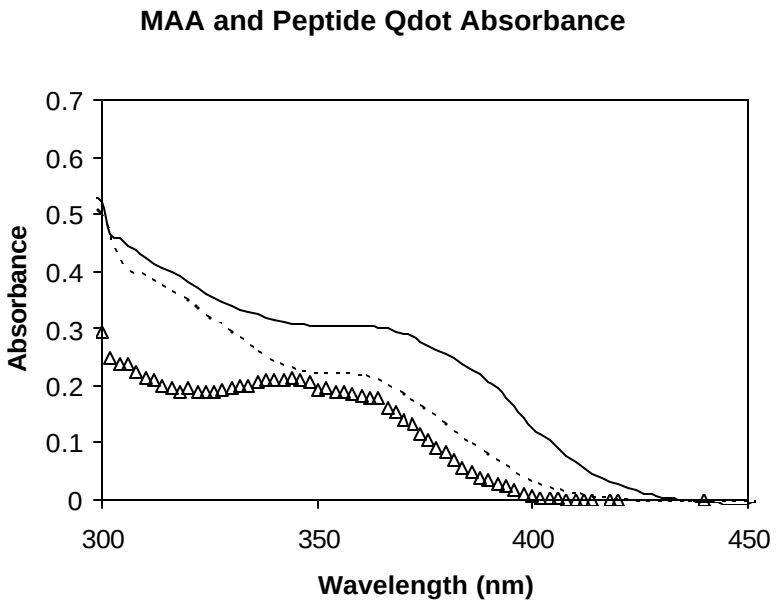

Figure 33: Absorbance Spectra of Peptide-Conjugated Quantum Dots.

Absorbance spectra of RGD-quantum dots (triangles) and RGD/MAA-quantum dots (dashed) are blue shifted from that of MAA-coated particles (solid). Increased concentrations of peptide (triangles vs. dashed) evidence a more pronounced shift in the absorbance edge.

To further confirm peptide conjugation, RGD/MAA-quantum dots were examined using anisotropic fluorescence spectroscopy (or tumbling fluorescence spectroscopy), which measures changes in fluorescence polarization that result from differing rotational rates in solution. [30] Heavier molecules rotate less frequently, and therefore exhibit more anisotropy in their fluorescence. Quantum dots functionalized with CGGGRGDS peptide demonstrated statistically higher anisotropy than mercaptoacetic acid-coated quantum dots ($p<0.0001$, Figure 34) indicating peptide attachment.

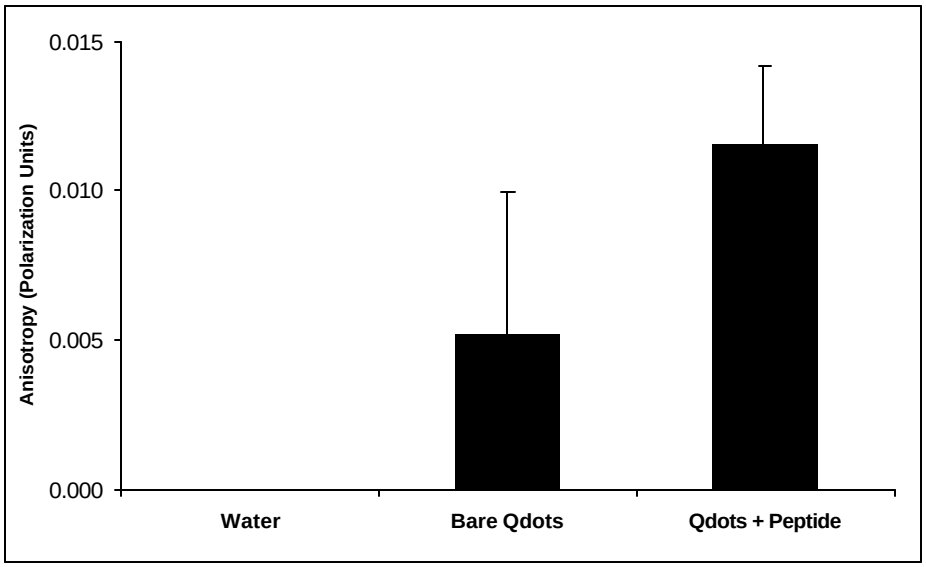

Figure 34: Fluorescence Anisotropy of CdS Quantum Dots.

Peptide-quantum dot conjugates demonstrate a greater degree of anisotropy than bare quantum dots (i.e., quantum dots coated with only mercaptoacetic acid). This occurs due to the bulkier size of the CGGGRGDS peptide. Peptide-quantum dot complexes displayed an anisotropy of $(1.16 \pm 0.3) \times 10^{-2}$ polarization units, versus $(5.17 \pm 4.79) \times 10^{-3}$ polarization units for the bare quantum dots ($p<0.0001$), confirming peptide attachment to the quantum dots ($p<0.0001$). [N=10]

Additionally, peptide binding was confirmed using Fourier transform infrared spectroscopy (FTIR). This technique evaluates the atomic vibrations of a molecule in the infrared spectrum. Results can be compared to standards or known spectra to determine the composition of a molecule. As MAA molecules would provide additional vibrations in the spectra, FTIR spectra were collected for RGD-quantum dots. These results were compared to a control consisting of CGGGRGDS peptide powder (Figure 35). The spectra for the peptide control and the RGD-quantum dots overlap, as would be expected for peptide-conjugated nanocrystals. For example, amide II and III peaks indicative of peptide amide bonds are seen at wavenumbers of 1550 and 1650, respectively. [31]

Vibrations specific to the nanocrystal occur at lower wavenumbers, beyond the sensitivity of most IR instruments, and are therefore not evidenced in the spectrum. [32]

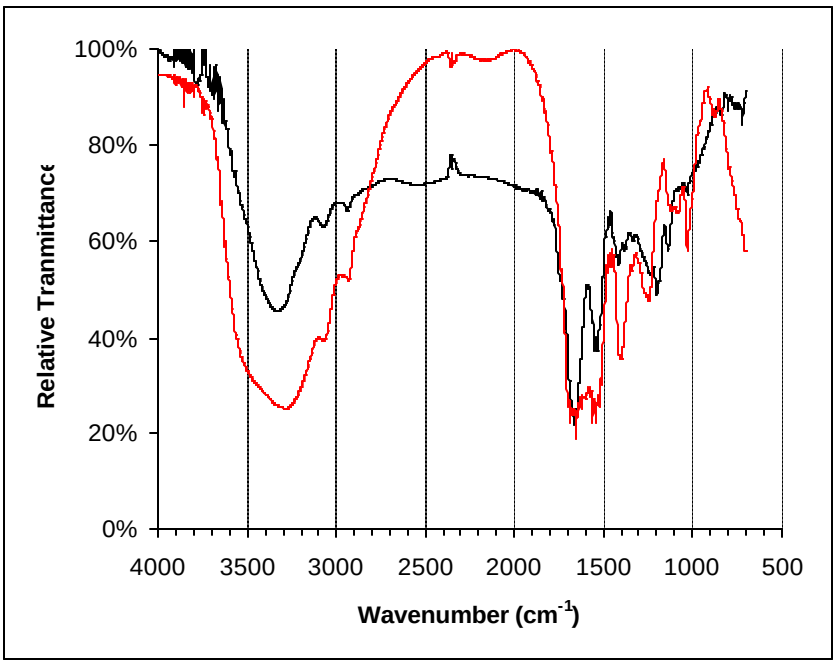

Figure 35: FTIR of RGD-Quantum Dots.

FTIR spectra of powdered peptide (black) and RGD-quantum dots (red) demonstrate similar peaks, indicating the presence of peptide on the nanocrystal surface.

The combined results of absorbance, anisotropy, and FTIR confirm peptide binding to the nanoparticle surface. This binding appears to occur in proportion to the amount of peptide added, as the absorbance onset is further blue-shifted (i.e., smaller particles) for increased peptide quantities. Although we did not investigate additional peptide ratios, these results confirm the ability to control the amount of peptide bound to the nanocrystal surface. Thus, peptide conjugation to quantum dots not only occurs, but is tunable depending on the concentration of peptide added to $CdCl_2$ solution.

The procedure for attaching peptide-coated quantum dots to the cell resembles that used for the antibody labeling method, [24] the key difference being that only a *primary* incubation was needed, as peptide-coated quantum dots do not require an intermediate linker. RGD/MAA-quantum dots and YIGSR/MAA-quantum dots were

exposed to cells to produce quantum dot-receptor interfaces. RGD-quantum dots were not used as their blue-fluorescence cannot be distinguished from the native autofluorescence of the cell. Brightfield and fluorescence microscopy images of the cells following exposure to RGD/MAA-quantum dots (Figures 36A and 36B, respectively) demonstrate nanoparticle binding. A yellow/orange layer of CdS quantum dots coats the blue autofluorescent cell. The quantum dots surround the exterior of the cell as expected, given the surface location of the integrin proteins. [19]

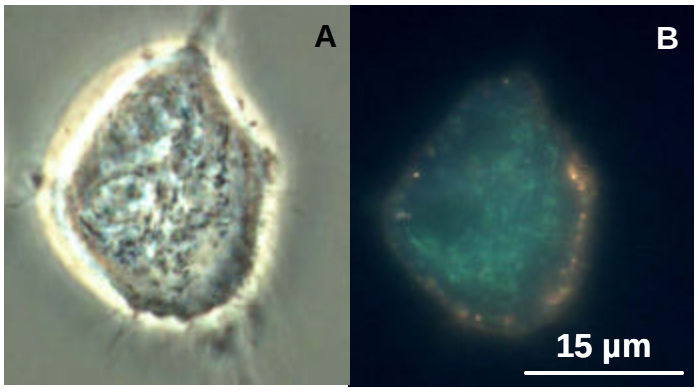

Figure 36: Quantum Dot Attachment to Neurons Using Peptide Binding Techniques.

(A) Brightfield and (B) fluorescence (λ_{exc}=330-385 nm) optical microscopy images of SK-N-SH human neuroblastoma cells. CdS quantum dots conjugated to CGGGRGDS peptide and MAA ligands are on the surface of the cell. In (B), the blue color is the native autofluorescence of the cytoplasm of the cell—common in near UV excitation—and the yellow/orange color is CdS quantum dot luminescence.

To further confirm the ability of peptides to form quantum dot–neuronal receptor interfaces, YIGSR/MAA-quantum dots were exposed to cells (Figure 37). YIGSR binding was similar to that of the RGD peptide. Fluorescence was localized to the cell surface, the location of the integrin binding targets. [19]

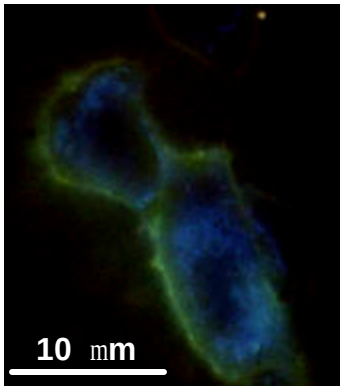

Figure 37: YIGSR-Quantum Dot Labeling of Neuroblastoma Cells.

Fluorescence (λ_{exc}=330-385 nm) optical microscopy image of SK-N-SH human neuroblastoma cells labeled with CdS quantum dots functionalized with CDPGYIGSR peptide and MAA. The blue color is the native autofluorescence of the cytoplasm of the cell—common in near UV excitation—and the yellow color is CdS quantum dot luminescence.

Compared to nerve cells labeled with IgG-functionalized quantum dots (Figure 32B), peptide-coated quantum dots (Figure 36B, Figure 37) experience significantly lower aggregation. Antibody-labeled quantum dots were more susceptible to aggregation than the peptide-quantum dot conjugates because of multiple secondary antibody binding and chemically induced cross-linking. This resulted in increased steric hindrance and clustering compared to the peptide approach. Both antibody- and peptide-conjugated quantum dot solutions demonstrate the same initial PL spectra intensity and are applied at the same concentration.

Therefore, we conclude that the reduced overall luminescence intensity from the peptide-coated quantum dots compared to the antibody-labeled quantum dots results from *primary*, specific binding (i.e., lower signal amplification), and not from differing material properties of the quantum dots. To ensure that the peptide sequences indeed recognize specific receptors on the cell surface, peptide/MAA-quantum dots were synthesized with a non-binding control peptide sequence, [20] CGGGRVDS, and then exposed to the nerve cells. Quantum dot binding was not observed in this case, as expected.

4.3.4 Summary of Peptide and Antibody Quantum Dot Conjugation

We have attached semiconductor quantum dots to living neurons utilizing both antibody and peptide recognition molecules. Unlike previous work interfacing nerve cells and electronic materials, [6] these techniques do not require *directed* neuronal growth. Instead, the electronic materials are brought to specific cell surface targets on the nerve. Furthermore, peptide recognition molecules provide nanometer-scale control over the targeting and separation distance between the quantum dot and the cell. Antibody methods could be adapted to produce similar separation distances using Fab fragments. [16, 18]

Although these techniques were demonstrated using integrin-binding as a model system, the methods can be adapted to neuronal ion channels. Antibodies for a variety of ion channels are available commercially, and can be treated to create Fab fragments. [18] Additionally, if suitable antibodies are not available for the desired ion channel, they may be manufactured directly. [33] To ensure proper interface formation, the antibody selected must bind the cell on the extracellular surface, and must not inhibit or activate the ion channel under study.

Expansion of the peptide method to ion channels is slightly more difficult than with the antibody system. The majority of known ion channel binding peptides affect the function of the channel. [34-37] However, two possibilities may allow for peptide use. Binding peptides that do not inhibit channel function could be identified using phage display techniques, [38] or the ion channel itself could be genetically modified to express a molecule with a known peptide binding sequence. [39] Either of these techniques would allow for close-proximity binding to ion channels.

The ability to design devices with specific, known attachment sites and controllable nanometer-length separation distances opens the door to developing future

bioelectronic devices. These techniques can be adapted to bind ion channels, enabling the development of receptor-scale neuroelectronic interfaces. Additionally, previous work (i.e., Chan and Nie [4]) has demonstrated the capacity of quantum dot complexes to enter the interior of the cell. Thus, it is possible to utilize optically activated quantum dots as intracellular probes to study internal electrochemical reactions. The future of bioelectronic devices hinges upon the ability to make controlled, specific interfaces, such as those described here, between biological components and semiconductor devices.

4.4 Additional Conjugation Strategies

Since the completion of this work, two promising additional strategies have been published for close-range nanoparticle-cell interfacing. [40-42] The first of these strategies is an extension of our work, relying on peptides to produce quantum dot-receptor binding. Our technique is ideal for water-soluble systems, adding peptides as passivating ligands during the initial synthesis. However, it is not compatible with organic media, as peptides are generally hydrophilic. To adapt our process to organic particles, Ruoslahti, et al. [40] introduced a passive ligand exchange that relies on the sulfur groups of thiolated peptides to produce nanocrystal binding. This technique exchanges peptides for TOPO ligands through overnight incubation in pH 7.4 phosphate-buffered saline (PBS). Nanocrystals altered using this method maintain all the benefits of peptide modification described for our process and could be employed to develop neuroelectronic interfaces.

A second technique, developed by two separate groups, uses the natural electrostatic interactions of proteins to produce nanoparticle-receptor interfaces. In one variation of this approach, [41] negatively-charged lipoic acid capped-quantum dots (-COO^- terminal) are attached to positively-charged leucine-zipper fusion proteins (surface

$-NH_3^+$ exposed) through electrostatic interactions. The leucine zipper proteins were genetically modified to be expressed in combination with the target biorecognition molecule, in this case maltose binding protein (MBP). Conjugation did not interfere with enzyme function, as evidenced by the ability of the complexes to bind maltose sugars.

A second variation of this approach [42] utilizes bacterially derived cohesin protein to produce nanocrystal self-assembly. Cohesin protein is used by bacteria to construct cellusome complexes (i.e., a cellulose binding complex on the bacteria surface). When this protein was incubated with quantum dots, it resulted in quantum dot incorporation into protein-nanoparticle compounds. Through conjugation of other proteins or peptides to cohesin, this technique could be used to produce nanocrystal-receptor binding.

Both of these variations capitalize on the specific binding that occurs between proteins and their target molecules. Additionally, both strategies can be applied to a wide range of molecules of varying lengths, thus providing control of the neuroelectronic interface separation distance. Although demonstrated on organic particles (i.e., CdSe-ZnS); these methods could be adapted to aqueous syntheses, and are therefore versatile. The main limitation of these techniques is that they both require genetically engineered molecules, which may be difficult to obtain.

4.5 CONCLUSIONS

Previously, laboratories have attempted micron-scale neuroelectronic interfaces using patterned semiconductor device structures with biocompatible features to favor neuron growth in desired locations. [43-48] This approach meets two major challenges: (a) reproducible neuron/device interfacing is difficult due to uncontrollable neuronal growth; and (b) the relatively large separation between the cell and the device (on the

order of 100 nm [49]) leads to poor electronic coupling. [50-51] These devices operate primarily through induction (Chapter 1, Section 1.1), the movement of separated charges. Coulomb's law, describing the field between separated charges, is dependant on the inverse of the radius squared. Thus, to achieve high fields, small separation distances are desired.

Patterning a surface with the nanometer-size features needed to interface electronic materials with specific cellular receptors is impossible using current technologies. [6, 52] Furthermore, the location of such receptors is varied, unpredictable, and dynamic from cell-to-cell. Semiconductor quantum dots attached to biological recognition molecules with short length scales can be positioned within nanometers of the cell surface, and direct attachment to the receptor of interest eliminates the need to control cell growth on a substratum. Thus, quantum dots provide a "smart" approach: wiring neurons directly with electronic structures through designated cell surface receptors.

The interfacing of materials and cells using bio-recognition molecules, such as antibodies and peptides, has been investigated extensively. Recognition molecules have even been utilized to link quantum dots to certain cell structures and proteins. [3-4] However, none of these systems is capable of interacting *electrically* with living cells to provide stimulation. Our approach represents one of the first systems that can both attach a material to the cell *and* optimize parameters that enhance electrical interactions, particularly at the nanometer scale.

4.6 REFERENCES

1. J.A. McCammon. “Theory of Biomolecular Recognition.” Curr. Opin. Struct. Biol. 8(2): 245, 1998.

2. See for example: G.T. Hermanson. Bioconjugate Techniques. Academic Press, San Diego: 1996.

3. M. Bruchez, Jr., M. Moronne, P. Gin, S. Weiss, and A.P. Alivisatos. “Semiconductor Nanocrystals as Fluorescent Biological Labels.” Science 281: 2013, 1998.

4. W.C.W. Chan and S. Nie. “Quantum Dot Bioconjugates for Ultrasensitive Nonisotopic Detection.” Science 281: 2016, 1998.

5. B. Alberts, D. Bray, J. Lewis, M. Raff, K. Roberts, and J.D. Watson. Molecular Biology of the Cell, 3rd Ed., Garland Publishing, New York: 1994, p. 995.

6. W.L.C. Rutten. “Selective Electrical Interfaces with the Nervous System.” Annu. Rev. Biomed. Eng. 4: 407, 2002.

7. A.P. Alivisatos. “Perspectives on the Physical Chemistry of Semiconductor Nanocrystals.” J. Phys. Chem. 100: 13226, 1996.

8. B. Alberts, D. Bray, J. Lewis, M. Raff, K. Roberts, and J.D. Watson. Molecular Biology of the Cell, 3rd Ed., Garland Publishing, New York: 1994, p. 996.

9. B. Alberts, D. Bray, J. Lewis, M. Raff, K. Roberts, and J.D. Watson. Molecular Biology of the Cell, 3rd Ed., Garland Publishing, New York: 1994, p. 18.

10. G.T. Hermanson. Bioconjugate Techniques. Academic Press, San Diego: 1996, pp. 456-460.

11. See for example: L.J. Kricka, Ligand-Binder Assays, Marcel Dekker, Inc., New York, 1985.

12. G.T. Hermanson. Bioconjugate Techniques. Academic Press, San Diego: 1996, pp. 170-173.

13. G.T. Hermanson. Bioconjugate Techniques. Academic Press, San Diego: 1996, pp. 235-237, 570-572, 575-578.

14. M.A. Hines and P. Guyot-Sionnest. "Synthesis and Characterization of Strongly Luminescing ZnS-Capped CdSe Nanocrystals." J. Phys. Chem. 100: 468, 1996.

15. S. Kimura, W. Laosinchai, T. Itoh, X. Cui, and R.M. Brown, Jr. "Immunogold Labeling of Rosette Terminal Cellulose Synthesizing Complexes in a Vascular Plant (*Vigna angularis*)." Plant Cell 11(11): 2075, 1999.

16. V.R. Sarma, E.W. Silverton, D.R. Davies, and W.D. Terry. "The Three-Dimensional Structure at 6 Å Resolution of a Human γG1 Immunoglobulin Molecule." J. Bio. Chem. 246(11): 3753, 1971.

17. P. Bongrand. "Adhesion of Cells," in Handbook of Biological Physics, vol. 1, R. Lipowsky and E. Sackmann, Eds., Elsevier, Amsterdam: 1995, p. 767.

18. R.R. Porter. "The Hydrolysis of Rabbit γ-globulin and Antibodies with Crystalline Papain." Biochem. J. 73: 119, 1959.

19. M.C. Willingham. An Atlas of Immunofluorescence in Cultured Cells, Academic Press, Orlando, 1985.

20. M.D. Pierschbacher and E. Ruoslahti. "Cell Attachment Activity of Fibronectin Can Be Duplicated by Small Synthetic Fragments of the Molecule." Nature 309: 30, 1984.

21. J. Graf, R.C. Ogle, F.A. Robey, M. Sasaki, G.R. Martin, Y. Yamada, and H.K. Kleinman. "A Pentapeptide from the Laminin B1 Chain Mediates Cell Adhesion and Binds the 67,000 Laminin Receptor." Biochem. 26(22): 6896, 1987.

22. T. E. Creighton. Proteins: Structures and Molecular Principles. W. H. Freeman and Co., New York, 1983.

23. H.M. Chen, X.F. Huang, L. Xu, J. Xu, K.J. Chen, and D. Feng. Superlattices and Microstructures. "Self-Assembly and Photoluminescence of CdS-Mercaptoacetic Clusters with Internal Structures." 27: 1, 2000.

24. T. Yoshihara, N. Esumi, M. J. Humphries, and S. Imashuku. "Unique Expression of Integrin Fibronectin Receptors in Human Neuroblastoma Cell Lines." Int. J. Cancer 51: 620, 1992

25. M.C. Willingham, in Methods in Molecular Biology, Vol 115: Immunocytochemical Methods and Protocols, L.C. Javois, Ed., Humana Press Inc., Totowa, NJ: 1999, ch. 16.

26. B. A. Korgel and H.G. Monbouquette. "Quantum Confinement Effects Enable Photocatalyzed Nitrate Reduction at Neutral pH Using CdS Nanocrystals." J. Phys. Chem. B 101: 5010, 1997.

27. B.A. Korgel and H.G. Monbouquette. "Synthesis of Size-Monodisperse CdS Nanocrystals using Phosphatidylcholine Vesicles as True Reaction Compartments." J. Phys. Chem. 100: 346, 1996.

28. M. Hemler. "VLA Proteins in the Integrin Family: Structures, Functions, and Their Role on Leukocytes." Annu. Rev. Immunol. 8: 365, 1990.

29. S.L. Goodman, S.L. Cooper, and R.M. Albrecht. "Integrin Receptors and Platelet Adhesion to Synthetic Surfaces." J. Biomed. Mats. Res. 27: 683, 1993.

30. T.L. Mann and U.J. Krull. "Fluorescence Polarization Spectroscopy in Protein Analysis." Analyst. 128: 313, 2003.

31. S.Y. Venyaminov and N.N. Kalnin. "Quantitative IR Spectrophotometry of Peptide Compounds in Water (H2O) Solutions. I. Spectral Parameters of Amino Acid Residue Absorption Bands." Biopolymers. 30(13-14): 1243, 1990.

32. H. Hu, P.K. Nair. "Chemical Deposition of Photosensitive CdS Thin Films on Polyester Foils." J. Cryst. Growth 152: 150, 1995.

33. E. Harlow and D. Lane. Antibodies: A Laboratory Manual. Cold Spring Harbor Press, Plainview, New York: 1988, pp. 53-135.

34. W.A. Catterall. "Molecular Mechanisms of Gating and Drug Block of Sodium Channels." Novartis Found Symp. 241: 206, 2002.

35. G.M. Nicholson, M.J. Little, and L.C. Birinyi-Strachan. "Structure and Function of Delta-Antracotoxins: Lethal Neurotoxins Targeting the Voltage-Gated Sodium Channel." Toxicon. 43(5): 587, 2004.

36. G.I. Hatton and Z. Li. "Mechanisms of Neuroendocrine Cell Excitability." Adv. Exp. Med. Biol. 449: 79, 1998.

37. H.R. Guy and S.R. Durell. "Structural Models of Na^+, Ca^{2+}, and K^+ Channels." Soc. Gen. Physiol. Ser. 50: 1, 1995.

38. See for example: C.F. Barbas, D.R. Burton, J.K. Scott, and G.J. Silverman. Phage Display: A Laboratory Manual. Cold Spring Harbor Laboratory Press, Cold Spring Harbor, New York: 2001.

39. See for example: L.M. Diaz, R. Maiya, S.L. Boehm, H.A. Scott, S.E. Bergeson, R.D. Mayfield, and R.A. Morrisett. "Sindbis Viral Delivery of eGFP Labeled Dopamine D1 Receptors into Primary Cultured Neurons, Brain Slice Culture and in vivo." Res. Soc. Alcoholism Abstr., 27: 93, 2003.

40. M.E. Åkerman, W.C.W. Chan, P. Laakkonen, S.N. Bhatia, and E. Ruoslahti. "Nanocrystal Targeting In Vivo." Proc. Nat. Acad. Sci. 99(20): 12617, 2002.

41. H. Mattoussi, J.M. Mauro, E.R. Goldman, G.P. Anderson, V.C. Sundar, F.V. Mikeluc, and M.G. Bawendi. "Self-Assembly of CdSe-ZnS Quantum Dot Bioconjugates Using an Engineered Recombinant Protein." J. Am. Chem. Soc. 122: 12142, 2000.

42. S.-Y. Ding, M. Jones, M.P. Tucker, J.M. Nedeljkovic, J. Wall, M.N. Simon, G. Rumbles, and M.E. Himmel. "Quantum Dot Molecules Assembled with Genetically Engineering Proteins." Nano Lett. 3(11): 1581, 2003.

43. G.W. Gross. "Simultaneous Single Unit Recording in vitro with a Photoetched Laser Deinsulated Gold Multimicroelectrode Surface ." IEEE Trans. Biomed. Eng. 26: 273, 1979.

44. P. Fromherz and A. Stett. "Silicon-Neuron Junction: Capacitive Stimulation of an Individual Neuron on a Silicon Chip." Phys. Rev. Lett. 75: 1670, 1995.

45. J.L. Novak and B.C. Wheeler. "Multisite Hippocampal Slice Recording and Stimulation Using a 32 Element Microelectrode Array." J. Neurosci. Meth. 23: 149, 1988.

46. D. Kleinfeld, K.H. Kahler, and P.E. Hockberger. "Controlled Outgrowth of Dissociated Neurons on Patterned Substrates." J. Neurosci. 8: 4098, 1988.

47. P. Connolly, P. Clark, A.S.G. Curtis, J.A.T. Dow, and C.D.W. Wilkinson. "An Extracellular Microelectrode Array for Monitoring Electrogenic Cells in Culture." Biosens. Bioelec. 5: 223, 1990.

48. M.P. Maher, J. Pine, J. Wright, and Y-C. Tai. "The Neurochip: A New Multielectrode Device for Stimulating and Recording from Cultured Neurons." J. Neurosci. Meth. 87: 45, 1999.

49. P. Fromherz. "Electrical Interfacing of Nerve Cells and Semiconductor Chips." Chem. Phys. Chem. 3: 276, 2002.

50. S. Vassanelli and P. Fromherz. "Neurons from Rat Brain Coupled to Transistors." App. Phys. A 65: 85, 1997.

51. P. Fromherz, V. Kiessling, K. Kottig, and G. Zeck. "Membrane Transistor with Giant Lipid Vesicle Touching a Silicon Chip." App. Phys. A 69: 571, 1999.

52. G.R. Brewer, Ed., Electron Beam Technology in Microelectronic Fabrication. Academic Press, New York: 1980.

Chapter 5: Optimization of Directed Quantum Dot-Cell Binding and Non-Specific Binding Alternatives[4]

As discussed in the previous chapter (Chapter 4), biorecognition molecule-directed binding produces nanometer-scale connections between quantum dots and cellular receptors, addressing many of the issues in receptor-based neuroelectronic interface design. However, substantial challenges remain. The development of neuroelectronic devices requires primary, harvested neurons that can be integrated into components lasting up to several months. Previous work has not established the ability of quantum dot–cell attachments to meet this requirement.

We examined the ability of biorecognition techniques to produce stable, non-toxic connections between primary cells and CdS or CdTe quantum dots. CdTe particles exhibited greater cell toxicity than CdS, most likely because of free Cd^{2+} ions released through surface oxidation. Additionally, we researched the role of endocytosis in junction longevity, and determined that attachment to fixed receptors is required for maximum stability. As an alternative system, we investigated non-specific binding to cellular surfaces. Particle synthesis conditions were shown to play a large role in non-specific binding, particular those combinations which decreased ligand coverage on particle surfaces. However, endocytosis also occurred in non-specific cellular attachments. Therefore, we developed a fixed system, using poly-D-lysine- or mercaptosilane-modified substrates, to produce tethered-nanoparticle films. Both films displayed some stability in cell culture medium and were able to promote cell growth. Here, we present these three possible methods for the formation of neuroelectronic interfaces.

---

[4] Portions of this material have been previously published in the following reference: J.O. Winter, C.E. Schmidt, B.A. Korgel. Proceedings of the 2003 Fall MRS Meeting. Quantum Dots: Nanoparticles, and Nanowires. P. Guyot-Sionnest, N.J. Halas, H. Mattoussi, Z.L. Wang, U. Woggon, eds. 789: N.6.1, 2004.

5.1 Requirements for Long-Term Neuroelectronic Interfaces

The quantum dot-cell binding methods developed in Chapter 4, address many of the limitations in forming controlled interfaces between cell receptors and electronics. However, challenges to practical implementation remain. Typically, neuroelectronic interfaces are formed using primary neurons harvested from the brain or spinal cord. [1] These cells do not divide, and can therefore be integrated into devices lasting up to several months. Additionally, these cells are more sensitive to environmental conditions, and are more reflective of the *in vivo* atmosphere. [2] For a functional receptor-based interface, electrical components must create controlled, *long-lasting* connections at the nanometer-scale. Quantum dot-receptor binding has yet to meet these conditions. Here, we discuss the requirements for receptor-based neuroelectronic interfaces and the limitations of existing quantum dot–cell attachment methods.

5.1.1 Cell Type

Neuroelectronic interfaces are designed to serve as prosthetic devices, laboratory models of neuron signaling, or computational systems. [1] Most interfaces are developed or implemented *ex vivo*, using cultured cells. In prosthetic devices, *ex vivo* systems approximate *in vivo* conditions, whereas in laboratory models and computational systems, *ex vivo* systems provide a controlled environment for scientific questioning. Each of these applications requires cells that are plastic (e.g., capable of altering and forming new neuron-neuron connections) and non-proliferating. Also, certain uses (e.g., prosthetics, biosensors) necessitate that cells can survive for long periods of time in culture. Immortalized, cultured cells do not meet these requirements. The mechanisms that produce immortal cells introduce changes that can alter ion channel expression and the ability to fire action potentials. [3-5] Additionally, immortal cells continue to divide;

disrupting attachment to the device and requiring periodic transfer to a new growth substrate. [2]

Current neuroelectronic interfaces are manufactured using primary cells, taken directly from tissue. [1] Typically, this tissue is derived from the spinal cord or brain; and the most commonly employed cell types are hippocampal cells, cortical cells, and dorsal root ganglia. To preserve plasticity, cells are often isolated from embryonic, neo-natal, or juvenile animals. These cells maintain the ability to form and alter neuronal connections in culture. [6-8] Additionally, primary cells do not divide and can be cultured for up to several months. Thus, primary cells meet all the requirements of interface design.

Few researchers have examined quantum dots in living systems, and the majority of these investigations have used immortal, cultured cell lines. [9] The only study employing primary cells examined liver cells (i.e., hepatocytes) and not neurons. [10] Primary cells are much more sensitive to culture conditions than immortal cells. [2] Therefore, binding techniques that are compatible with immortal cells may require adaptation for primary culture systems. Further, primary cells are isolated from tissue, which results in associated debris. In our previous studies, we have observed that quantum dots adhere to dead, immortal cells, producing a fluorescence signal considerably brighter than that of directed binding. Debris may serve as a target for non-specific binding, obscuring biorecognition-mediated adhesion. Additional work is required to establish the feasibility of using quantum dots to form interfaces with primary, neuronal cultures.

5.1.2 Toxicity

Several groups have reported using quantum dots in living systems with no ill effects. [11-16] However, in the one study that specifically examined interactions

between semiconductor quantum dots and primary cells, [10] the cells utilized (i.e., hepatocytes) exhibited marked cell death in the presence of nanocrystals under certain conditions. This was attributed to the release of free Cd^{2+} ions following oxidation of the particle core. Cd^{2+} ions have well-established health risks, [17] and have been the chief concern in quantum dot toxicity. However, recent reports have implicated other nano-scale particulates in lung-toxicity [18] and oxidative stress in the brain. [19] Although these effects may be reduced by the presence of a suitable surface coating, [10, 20] these insulating layers may interfere with the operation of neuroelectronic interfaces. Thus, a careful study of nanoparticle toxicity on primary cells is required to identify those particles that may be employed in a neuroelectronic device. Briefly, we review the available data for toxicity of nanoparticulates and cadmium-based compounds.

5.1.2.1 Nanoparticulate Toxicity

Very few studies have examined the potential health risks of nanoparticles and other nano-sized materials. However, there is limited evidence that risks are present, particularly through inhalation. A recently published study demonstrated that inhaled carbon nanotubes can produce asbestos-like lesions in the lung. [18] Among the highest dose group, the mortality rate was 55% [N=9] after only 7 days of exposure. Although these results were for pulmonary tissue, a separate set of studies examining carbon [19, 21-22], graphite [22], and iridium [23] particulates established the ability of nanomaterials to damage other tissues, including the immune system [21] and brain [19, 22]. Particle effects on the brain included an increase in lipid peroxidation and damage to lipid-rich tissues. [19] The most troubling finding of these studies is that particle clearance proceeds slowly. A low level (i.e., 6% in lung) of particulates remained in tissue a full six months after exposure. [23]

However, it is unclear if these results will apply to semiconductor quantum dots. Most of these investigations examined toxicity through inhalation, but quantum dots are produced in solution-phase. A more likely route of exposure is through ingestion or skin contact. [20] To date, only a single study [10] has confirmed that quantum dots may be cytotoxic to cells when presented in aqueous solution. Additionally, the materials studied (i.e., carbon particulates and nanotubes) bear little similarity to quantum dots other than size, but there are indications that nanoparticle toxicity is not necessarily a function of composition. The most certain fact is that a full understanding of the effects of quantum dot exposure via *any* route has yet to be established. To develop viable neuroelectronic interfaces, thorough knowledge of quantum dot toxicity must be obtained.

5.1.2.2 Cadmium Exposure

One of the greatest concerns for the biocompatibility of semiconductor quantum dots is the well-established toxicity of cadmium, a key component of most particles. Cadmium is a known carcinogen, and has been linked to lung, testicular, adrenal, liver, and kidney cancer. [24] Although the exact mechanism of carcinogenicity is not understood, cadmium has been shown to interfere with DNA mismatch repair. [25] It also binds strongly to the sulfhydryl groups of mitochondrial proteins, [26] and this is the believed source of toxicity observed for the primary hepatocytes studied previously. [10] Additionally, cadmium is a commonly used blocking agent in patch-clamp studies that interferes with neuronal firing. [27]

A number of groups have employed quantum dots *in vitro* and *in vivo* without noticeable cell damage; [11-16] however, none of these studies specifically examined cadmium toxicity. A single study [10] has measured cadmium levels *in vitro* suggesting that significant release occurred with nanoparticle oxidation, resulting in cell death. It is

well known that nanoparticles are susceptible to oxidation and photooxidation, [10, 28-32] particularly with UV exposure. Reaction of oxygen with group VI elements (e.g., S, Se, Te) produces oxides, [30] that can disassociate from the particle surface. Free Cd atoms are left behind and may eventually enter solution. In these published studies, free cadmium levels were elevated for poorly-capped particles and particles exposed to prolonged UV excitation. [10]

Given all of these factors, the stability of the nanoparticle core is of great concern in the development of the neuroelectronic interface. Modifying particles with a strongly-bound passivating ligand, an inorganic layer (e.g., ZnS), or a polymer coating can increase particle stability by preventing the entry of oxygen. [10, 20] All of the reports on quantum dot use for living systems utilize some coating of this nature. [11-16] However, these techniques have limited application in the neuroelectronic interface. Coatings can reduce nanoparticle electrical signals by producing an insulating layer or increasing the separation distance between the particle and the receptor. Thus, the development of a non-toxic, yet electrically active, nanoparticle system for neuroelectronic interface development is challenging.

5.1.3 Longevity of the Interface: Endocytosis

Adaptability to primary cells and biocompatibility remain the main requirements for neuroelectronic interface development. However, it is also important that the interface have a useful lifetime, preferably on the order of weeks or months. If the chief location of nanoparticle attachment is the cell membrane, this is a point of concern. Cells recycle their membrane and membrane-bound receptors regularly through a process known as endocytosis. [33]

Quantum dots bound to cell surfaces may be internalized through the endocytotic pathway, limiting interface longevity. In fact, several groups have exploited a particular type of endocytosis (i.e., receptor-mediated endocytosis) specifically for the purpose of introducing quantum dots to the interior of the cell. [10, 14, 34-35] Endocytosis can be suppressed by performing experiments at low temperature. [36] However, neurons do not experience normal signal propagation at low temperature, [37] and endocytosis resumes rapidly when cells are warmed to physiological temperatures. Further, endocytosis is not limited to receptor-bound ligands; non-specifically bound nanoparticles have also been internalized. [12, 38-39]

Internalization could limit the use of biorecognition methods in forming long-term neuroelectronic interfaces. Only those molecules which bind fixed receptors or those recycled at a very low rate (i.e., lactoferrin receptor) would create long-term connections. The primary proteins targeted for binding (i.e., ion channels) are regulated on the membrane surface. [40] However, this process occurs slowly, and direct binding to ion channels should not pose a problem for interface longevity. Nonetheless, in cases where such binding is not permitted, an alternative method of stable interface formation will be required.

5.1.4 Motivation for Examining Biorecognition-Directed Quantum Dot–Neuron Interfacing and Development of Alternatives

Our previous work (Chapter 4) demonstrated the ability of biorecognition molecules to form controlled interfaces with cell surface receptors. Specifically, we utilized antibodies and peptides to bind quantum dots to the integrin receptors of SK-N-SH neuroblastoma cells. This system has two major limitations to implementation in a neuroelectronic interface. First, the cells examined were immortal, cancer cells. Thus,

they do not engage in normal signal propagation and divide continuously, significant impediments to the development of a device. [2-5] The second challenge is that the antibodies and peptides used, anti-CD51 and RGDS respectively, can be internalized through receptor-mediated endocytosis, [41-42] minimizing long-term stability.

The ability of quantum dots to form long-term interfaces with the cell surface has not been thoroughly explored. Quantum dots have been employed in living systems, [11-16] but their potential toxicity is not well understood. Previous research is confined mainly to applications using immortal, cultured cell lines or *in vivo* studies of short duration. In either case, long-term toxic effects would be unlikely to surface during the course of these studies. A single study has investigated quantum dot toxicity to primary cells, [10] which are more sensitive to environmental conditions. [2] A direct relationship between cadmium released from the nanoparticle surface and cell death was established. Additionally, the stability of quantum dot-neuron interfaces is not well-explored. It is known that internalized particles can persist for several weeks; [14] however, nanoparticles bound to cell surfaces may be subject to endocytosis.

Here we present our efforts to produce long-term, stable interfaces between quantum dots and cell surface receptors. We investigated the toxicity of both CdS and CdTe particles to primary, neuronal cells. We also examined the role of endocytosis for both receptor-bound and non-specifically adherent quantum dots. Finally, we developed three separate methods to produce nanoparticle interfaces with the cell surface and characterized the long-term stability of each junction.

5.2 MATERIALS AND METHODS

5.2.1 Quantum Dot Synthesis

5.2.1.1 CdS Synthesis

Standard and peptide-bound CdS quantum dots were synthesized as described previously (Chapter 3, Section 3.3.3.1 and Chapter 4, Section 4.3.2.1). Briefly, a solution of 55 mM mercaptoacetic acid was created in 5 mM aqueous $CdCl_2$. The pH was raised to 7 using NaOH (~ 600 µL of 1 M equivalents), and 2 mM aqueous $Na_2S * 9H_2O$ was added. Nanocrystals formed immediately and continued to grow for up to four hours after sulfur addition.

For peptide-conjugated nanoparticles, peptide was added to the $CdCl_2$ solution at 10 mM or, in combination with 55 mM MAA, at 0.6 mM. Additionally, the reaction pH was increased to 12, producing green-yellow nanocrystals that could be distinguished from blue cellular autofluorescence. Otherwise, synthesis proceeded as described. For the non-specific binding studies, synthesis reactant concentrations and ratios, ligand concentration, and pH values were varied. Table V describes these changes in detail. For tethered quantum dot films, $CdCl_2$ concentrations from 2-20 mM were examined while maintaining constant Cd:S ratio, and with reaction pH values of 7 or 11.

Table V: Particle Synthesis Conditions for Non-Specific Binding Studies.

Parameter[1]	Ligand	[$CdCl_2$] (mM)	[Ligand] (mM)	[Na_2S] (mM)	pH[2]
Control	MAA	5	55	2	pH = 7
pH	MAA	5	55	2	pH = 5-11
Ratio	MAA	5	55	0.83-5	pH = 7
Ligand Conc.	MAA	5	10-500	2	pH = 7
Concentration	MAA	2-20	22-220	0.8-8	pH = 7

[1] All reactions were carried out in a total volume of 20mL.
[2] pH before Na_2S addition.

5.2.1.2 CdTe Synthesis

CdTe particles were produced using the synthesis method developed by Peng, et al. [43] with the modifications of Donegá, et al. [44] Cadmium oxide (CdO, Aldrich) precursor (0.056 g) was placed in a 50 mL, 14/20, three-neck round bottom flask equipped with an RTD port, along with 0.230 g of tetradecylphosphonic acid (TDPA, Alfa Aesar) and 3.7 g of trioctylphosphine oxide (TOPO, Aldrich). In addition, 0.066 g of tellurium powder (Te, Aldrich) and 2.5 mL of trioctylphosphine (TOP, Fluka) were added to a separate 50 mL, 14/20, three-neck round bottom flask. A condenser was placed in the middle neck of each flask and secured with Teflon tape or vacuum grease, while the two remaining necks were sealed with silicone septa (Sigma).

The CdO-containing flask was then placed in a heating mantle connected to a variable transformer and temperature controller. An RTD probe from the temperature controller was inserted into the RTD port, and the entire flask was wrapped with glass wool and aluminum foil. The CdO solution was degassed on a Schlenk line at 60ºC for two hours under 300-500 mtorr of vacuum. Meanwhile, the Te flask was placed on a hot

plate. A thermometer was inserted through one of the silicone septa and secured with Teflon tape and vacuum grease.

After the CdO solution had been under vacuum for 2 hours, it was placed under nitrogen and heated to 340ºC. Additionally, the Te solution was attached to the Schlenk line, placed under N_2, and heated to 150ºC. When both solutions had completed heating, the temperatures were lowered to 300ºC (CdO) and 120ºC (Te) for injection. A 10 mL glass syringe was used to remove the Te solution. Te was quickly injected into the CdO, producing a black solution of TOPO-capped particles. The temperature was reduced to 60ºC and the solution was allowed to stir for 30-45 minutes. After this time, 5 mL of chloroform was injected.

To create water-soluble particles, 16 mL of 0.5 M mercaptopropionic acid (MPA, Fluka) in basic methanol (pH = 12) were added to 5.2 mL of the TOPO-capped particles. The temperature was reduced to 37ºC, and particles were left to stir under nitrogen overnight. Following incubation, particles were extracted and placed in a 50 mL centrifuge tube. A ~3 fold excess of 2-propanol was added as an anti-solvent, and the solution was placed in a -20ºC freezer for at least two hours. Then, the mixture was centrifuged at 6000 g for 10 minutes at 4ºC. The supernatant was decanted, producing a pellet of black nanocrystalline CdTe particles that could be resuspended in aqueous solvents (e.g., phosphate buffered saline). Aqueous CdTe particles exhibited an excitation peak of 512 nm, an emission peak of 665 nm, and displayed quantum yields of ~15-30%, decreasing with particle age.

Peptide-conjugated nanocrystals were produced through an additional partial ligand exchange. MPA-capped nanocrystals were removed from nitrogen and divided into 500 µL aliquots without anti-solvent extraction. Each aliquot was placed in a 2 mL microcentrifuge tube and left in a vacuum oven overnight to remove excess fluid. Dry

particles were stored in a glove box under nitrogen. For peptide conjugation, 6 mg of CGGGRGDS peptide were dissolved in 2 mL of PBS (to 4 mM). This solution was then added to one 2 mL tube of dry particles. Particles were vortexed and placed in a 10 mL, 14/20, single-neck round bottom flask. A condenser was placed in the neck, and the flask was purged under nitrogen overnight to produce reaction. Peptide conjugation was confirmed through increases in fluorescence anisotropy (Chapter 4, Section 4.3.3.4) and quantum yield. Quantum yields were amplified because the peptide does not completely displace MPA ligands; but instead supplements existing ligand coverage, augmenting particle passivation. Following peptide binding, anisotropy of the particles increased from 3.57×10^{-2} to 3.73×10^{-2} (~5%); while quantum yields increased from 11.2% to 15.2%.

5.2.2 Cell Culture and Isolation

5.2.2.1 SK-N-SH Neuroblastoma Cells

SK-N-SH neuroblastoma cells were cultured as described previously (Chapter 4, Section 4.3.3.6). Briefly, cells were grown in DMEM cell culture medium (Sigma) with 10% fetal bovine serum (FBS, Gibco) and 1% penicillin-streptomycin (pen-strep, Gibco). Cells were plated at densities of 1:8 and passaged every 6 days. Medium was changed every 2 days. Cells with passage numbers greater than 20 were discarded. SK-N-SH cells exhibit neuronal and fibroblast morphologies. [45] Dense cultures produce the neuronal morphology, and plating densities were selected to maximize this morphology.

5.2.2.2 Isolation and Culture of Rat Neonatal Cortical Cells (RNCs)

Several days prior to harvest, slides were prepared for cell adhesion. Mouse laminin (BDBiosciences) was incubated with slides for 20 minutes at 3.03 μg/mL in

distilled, deionized water (ddH_2O). The solution was then aspirated, and slides were dried under UV for at least 1 hour. Next, slides were exposed to poly-D-lysine hydrochloride (Sigma, Mol. Wt. > 300,000) for one hour at 0.5 mg/mL in ddH_2O. Slides were rinsed three times for 10 minutes in ddH_2O and dried under UV overnight. MEM (Gibco, without L-Glutamine) was placed on cells at least 24 hours prior to harvest.

Rat neonatal cortical cells were obtained from 1-2 day old Sprague-Dawley rat pups. Twenty minutes before harvest, a protease solution of 3 mg Pronase (Calbiochem) in 5 mL of MEM was prepared and incubated at 37ºC. To obtain cells, rat pups were rapidly decapitated in a tissue culture sterile hood. The skull was opened, and the brain was removed and placed in medium at 4ºC. After 1-2 minutes, the cortex of the brain was transected from the temporal lobe and hippocampal structures using a razor blade. The cortex was homogenized and incubated in Pronase solution for 20 minutes with frequent mixing (i.e., tube inversion every 3 minutes).

After this time, the mixture was centrifuged at 200 g for 3 minutes, and the supernatant was aspirated. The cells were rinsed with 3 mL of meglumine buffer (Table VI) and centrifuged at 200 g for 3 minutes, followed by supernatant aspiration. This was repeated two additional times. Washed cells were resuspended in 1.5 mL of meglumine buffer and triturated using a series of 2-3 increasingly smaller-diameter, flame-pulled, capillary pipettes. Triturated cells were added to 10 mL of warm supplemented neurobasal medium (Table VII). Cells were counted using a hemocytometer and plated at concentrations of 2×10^5 cells/cm. Cells were fed 24 hours after initial plating, and every 2 days thereafter using supplemented neurobasal medium. Cells began to extend processes over the course of 2-3 days, and were not used until at least 5 days of age. Cells clustered and exhibited rounded morphologies after 3 weeks, and were discarded after this time.

Table VI: Meglumine Buffer

Component[1]	Concentration
0.5 M Magnesium Sulfate	600 μL
N-Methyl-Glucamine	7.5 g
Sodium Chloride	0.173 g
HEPES	0.704 g
Dextrose	0.533 g
Distilled, De-ionized Water	300 mL

[1]All components were purchased from Sigma

Table VII: Supplemented Neurobasal Medium

Component	Concentration	Manufacturer
Neurobasal Medium	500 mL	Gibco
B-27 Supplement	10 mL	Gibco
200 mM L-Glutamine	125 μL	Fisher
Penicillin-Streptomycin[1]	4800 μL	Gibco

[1] 10000 units/mL of activity

To examine quantum dot toxicity, 20 mM $[Cd]_{initial}$ solutions of nanoparticles were precipitated through anti-solvent addition (i.e., 1- propanol for CdS, 2- propanol for CdTe) and centrifugation at 6000 g. Pellets were dried in a vacuum oven for at least one hour and resuspended in supplemented neurobasal medium. Cells were cultured in nanoparticle-containing medium for five days. Medium was changed every two days. Cell viability was confirmed using fluorescence microscopy (Section 5.2.5).

5.2.3 Attachment of Quantum Dot Complexes to Cells

For SK-N-SH cells, the control labeling procedure was performed as described previously (Chapter 4, Section 4.3.3.8). Prior to exposure, quantum dots were modified to pH 7.4 using 1 M and 0.1 M NaOH or HCl as required. Additionally, normal saline conditions were obtained through resuspension of dried particle pellets in Dulbecco's PBS (DPBS; Chapter 4, Table IV) or dilution of particle solutions with an equal volume of 2X DPBS. Cells were incubated with 5% BSA in DPBS (BSA-DPBS) at 4ºC for one hour, followed by one rinse in cold DPBS. Next, quantum dots were introduced and exposed to cells for 30 minutes at 4ºC. Then, cells were rinsed three times with cold DPBS. Binding was confirmed using fluorescence microscopy (see Section 5.2.5).

For primary cells, several alterations to the initial procedure were investigated. To examine solvent compatibility, artificial cerebrospinal fluid (aCSF, Table VIII) was studied as an alternative to DPBS. The effect of shear forces on cells was analyzed by modifying the rinsing procedure. The relationship between culture dish size and shear was established using 3, 6, and 10 cm dishes, in place of the 1 cm control. Additionally, the number of rinses following BSA-DPBS incubation and quantum dot exposure was reduced from 1 and 3 to 0 and 1, respectively. For these studies, cell viability was confirmed using phase contrast microscopy (Section 5.2.5) and live-dead staining (Section 5.2.3.1). To evaluate endocytosis, experiments were performed at 37ºC in a 5% CO_2 environment. With this modification, the impact of reduced quantum dot incubation times were also studied (i.e., from 30 minutes to 5 minutes). Both of these conditions were evaluated with phase contrast and fluorescence microscopy (Section 5.2.5).

Table VIII: Artificial Cerebrospinal Fluid (aCSF)

Component	Concentration
Magnesium Sulfate	0.058 g
Calcium Chloride	0.040 g
Sodium Chloride	1.402 g
Dextrose	0.360 g
Potassium Chloride	0.049 g
Sodium Phosphate Monobasic	0.034 g
HEPES	1.19 g
Distilled, Deionized Water	200 mL

Non-specific quantum dot-cell interfacing was investigated using CdS and CdTe nanocrystals on SK-N-SH neuroblastoma and RNC cells. CdS particles were prepared as described above (Section 5.2.1.1) and in Table V. CdTe particles were manufactured following the synthesis in Section 5.2.1.2. Quantum dot solutions were created through anti-solvent addition (i.e., 1-propanol for CdS and 2-propanol for CdTe) and centrifugation at 6000 g. The supernatant was decanted, and particles were dried in a vacuum oven for at least one hour. Particles were resuspended in DPBS. To assay binding, cells were first incubated in BSA-DPBS solution for one hour; and then quantum dot-DPBS solutions for 30 minutes. Cells were rinsed with DPBS following aspiration of the quantum dot solution, and evaluated using fluorescence microscopy (Section 5.2.5).

5.2.3.1 Live-Dead Staining

Cell viability was confirmed using a live-dead cell staining kit containing calcein AM and ethidium homodimer-1 dyes (Molecular Probes). Non-fluorescent calcein dye permeates cell membranes, where it is converted into a green fluorescent product

(λ_{em}=515) by living cells. Ethidium enters dead or damaged cells through gaps in the plasma membrane and binds to nuclear proteins with a significant enhancement in fluorescence (λ_{em}=635). Ethidium is excluded from living cells by their intact membrane. Calcein-AM and ethidium homodimer-1 dyes were added to cells at concentrations of 0.25 and 2 μL/mL in DPBS, respectively. Cells were incubated with the dyes for 20 minutes, and then washed twice with DPBS. Cells were immediately observed using fluorescence microscopy (Section 5.2.5).

5.2.4 Formation of Tethered Quantum Dot Films

5.2.4.1 Siloxane-Based Films

As an alternative to direct quantum dot-cell attachment, two types of tethered films were developed. The first of these utilized published methods [46] to create mercaptosilane substrates for quantum dot attachment. Briefly, glass slides were cleaned in a 1:3 mixture of concentrated hydrochloric acid:nitric acid for 30 minutes. Then, slides were rinsed with ddH_2O until the pH = 7.0, and blown dry with argon. The slides were further dried in a vacuum oven at 75ºC for at least 3 hours.

Next, clean, dried slides were placed into solutions ranging from 1–50 mM of (3-mercaptopropyl) trimethoxysilane (MTS, Fluka) in anhydrous toluene. All solutions were prepared in an anhydrous environment under argon. Slides were incubated in MTS overnight on a rocker plate. Following incubation, MTS-coated slides were rinsed three times with anhydrous toluene, three times with ethanol, and blown dry with argon. Then, they were further dried in a vacuum oven at 40ºC for at least 3 hours. Siloxane layer formation was confirmed using ellipsometry (Section 5.2.4.3).

Then, silanized slides were incubated with quantum dot solutions overnight on a rocker plate. Quantum dots were synthesized with $CdCl_2$ concentrations (Section 5.2.1.1) ranging from 2-20 mM and reaction pH values of 7 or 11, while maintaining constant Cd:S ratio. Quantum dots were exposed to slides 4-24 hours after synthesis. Following incubation, slides were rinsed three times with ddH_2O, three times with ethanol, and blown dry with argon. Quantum dot tethering was confirmed using fluorescence microscopy (Section 5.2.5).

5.2.4.2 Ellipsometry

The presence of siloxane on slide surfaces was confirmed using a J.A. Woollam Co., Inc (Lincoln, NE) EC-400 ellipsometer equipped with an M-2000D spectrophotometer and XLS-100 stage. Measurements were performed at wavelengths from 400-700 nm at an angle of incidence of 70º. Results were analyzed using a Cauchy fit, with no backscattering correction, and an assumed index of refraction of 1.5. [46]

5.2.4.3 Poly-D-Lysine-Based Films

As an alternative to siloxane, poly-D-lysine was used as an adhesion substrate. Poly-D-lysine is positively charged at neutral pH because of its $-NH_3^+$ functional groups, while quantum dots capped with mercaptoacetic acid (MAA) are negatively charged. Using electrostatic interactions, films of tethered quantum dots were formed. Poly-D-lysine hydrochloride (Sigma, Mol. Wt. > 300,000) was incubated with slides at 0.5 mg/mL in ddH_2O for one hour. Then, slides were rinsed three times for 10 minutes in ddH_2O and dried under UV overnight. Next, sterile-filtered quantum dots were incubated with slides for one hour. Quantum dots were prepared with $CdCl_2$ concentrations ranging

from 2-20 mM and reaction pH values of 7 or 11, while Cd:S ratio was held constant (Section 5.2.1.1). Following incubation, slides were rinsed three times with sterile ddH_2O and dried in a sterile tissue culture hood. Quantum dot tethering was confirmed using fluorescence microscopy (Section 5.2.5).

5.2.4.4 Tethered Quantum Dot Film Stability

To ascertain the stability of tethered films, the fluorescence of quantum dot-coated slides was analyzed after exposure to cell culture medium over six days. First, slides were prepared for sterile culture. Silanized slides were soaked in absolute ethanol for 20 minutes and air dried in a sterile tissue culture hood. As described previously (Section 5.2.4.2), poly-D-Lysine slides were exposed to UV overnight prior to quantum dot adhesion and prepared with sterile solvents thereafter. Following sterilization, slides were incubated with supplemented neurobasal medium and observed at 1-2 day intervals using fluorescence microcopy (Section 5.2.5). Medium was changed every 2 days.

5.2.4.5 Cell Culture on Tethered Films

To establish the ability of quantum dot films to support cell growth, rat neonatal cortical cells (RNCs) were cultured on their surfaces. RNCs were isolated as described previously (Section 5.2.2.2); however, slide surfaces were not prepared with laminin and poly-D-lysine. Instead, RNCs were cultured directly on sterile siloxane-quantum dot or poly-D-lysine-quantum dot films (Sections 5.2.4.3 and 5.2.4.4). Cells were grown following standard protocols (Section 5.2.2.2) in supplemented neurobasal medium, which was changed one day after initial harvest and every two days thereafter. Film-coated slides were observed every 1-2 days following harvest for cell growth, extension

of neuronal connections, and layer stability using phase contrast and fluorescence microscopy (Section 5.2.5).

5.2.5 Microscopy

Fluorescence and phase contrast images were obtained using an Olympus IX70 inverted microscope with a mercury arc lamp and UV (λ_{exc}=330-385), wideband blue (WB, λ_{exc}=450-480), and narrowband green (NG, λ_{exc}=530-550) filter sets. Cell viability following rinsing and quantum dot toxicity (Section 5.2.3) were evaluated using a 20X objective and phase contrast. Additionally, live-dead cell staining (Section 5.2.3.1) was performed using a 20X objective in phase contrast and in fluorescence with the WB (calcein AM) and NG (ethidium homodimer-1) filter sets. Images for the endocytosis, incubation length, and non-specific binding studies (Section 5.2.3) were collected using phase contrast and fluorescence microscopy with a 60X or 100X objective and oil immersion. For all of the above experiments, the UV filter set was employed for CdS analyses, and the NG filter set was utilized for CdTe. All images were collected with an exposure time of 496 ms. The evaluation of quantum dot tethered films (Section 5.2.4) was conducted using fluorescence microscopy with a 100X objective, oil immersion, and the UV filter set. Exposure time for all images was 733 ms. Some images were modified to enhance brightness and contrast using Adobe Photoshop version 5.5. In this case, all images from the same experimental set were treated equally.

5.3 RESULTS AND CONCLUSIONS

5.3.1 Optimization of Biorecognition Molecule–Directed Interfacing for Primary Cells

Our model system for neuroelectronic interface formation utilized the SK-N-SH neuroblastoma cell line, a cancer-derived line that is unsuitable to final implementation in the device. Therefore we chose to adapt our methods to primary rat neonatal cortical cells (RNCs), a commonly employed cell type in neuroscience. Primary cells were harvested directly from tissue, in this case the cortex of 1-2 day old rat pups. They are known to be more sensitive to environmental conditions than immortalized cells, [2] and this was evidenced in our attempts to integrate them into a quantum dot interface. Thus, optimization of our procedure was required to maximize cell viability.

5.3.1.1 Isolation and Culture of RNCs

Our initial attempts to culture RNCs met with little success. Although cells were harvested, they exhibited an unfavorable glial morphology (Figure 38A). [47] This morphology indicates either selective glial survival or is a response of neurons to unfavorable environmental conditions. It is unlikely that the culture consisted of glia, as the medium selected (supplemented neurobasal) is designed to inhibit glial growth. [48] Upon further investigation, we determined that shear stresses in the medium, introduced by two factors, contributed to the glial morphology. First, during harvest, cells were triturated with increasingly smaller diameter metal needles (e.g., 16, 18, 21, and 23 gauge), rather than the fire-polished glass capillary pipettes recommended. Second, the exchange of medium was performed rapidly, introducing shear forces. When these two factors were corrected, cells of the proper morphology [47] were obtained (Figure 38B).

These results demonstrate the extreme sensitivity of primary cells, and their suitability to evaluate quantum dot toxicity. Similar results were not obtained with SK-N-SH cells.

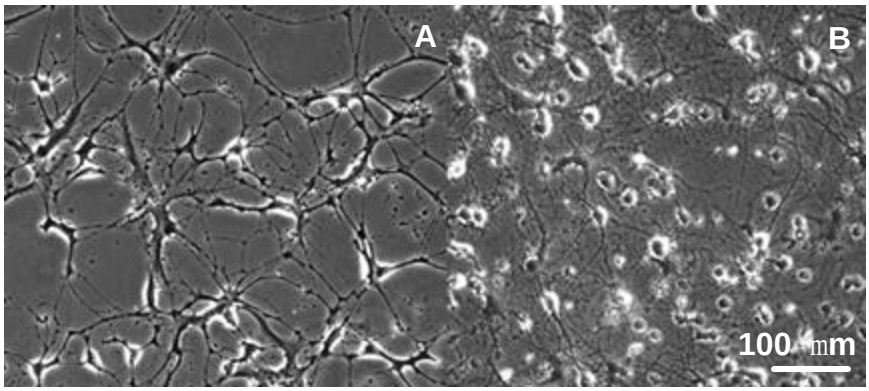

Figure 38: Rat Neonatal Cortical Cells in Culture.

Phase contrast images of (A) initial cultures exhibiting glial morphologies and (B) normal cells exhibiting a neuronal morphology. Glial morphologies appear to be the result of shear forces in the liquid introduced during harvest and medium exchange.

5.3.1.2 Rinsing Protocol for Interface Formation

Based on our findings for the harvesting protocol, we examined methods to reduce shear stress in the quantum dot-receptor interfacing procedure. The most significant sources of shear are the DPBS washing steps, which are used to ensure complete removal of the BSA-DPBS blocking agent and the quantum dot solution. Therefore, we investigated methods to reduce shear at these steps.

First, we examined the role of culture dish size in the rinsing procedure. The hypothesis was that a larger culture dish would protect cells from shear forces by increasing the distance between the liquid entry point and cells elsewhere on the dish. Culture dishes of 3, 6, and 10 cm diameters were compared to the 1 cm diameter dish used in the model system. Cells were observed following three rinses with DPBS. Surprisingly, we determined that *increased-diameter* dishes produced the least viable cells (Figure 39). Prior to DPBS washing cells had attained ~100% confluency, however

significant areas of the larger diameter dishes (Figure 39 B-D) display no cells or cell debris.

To establish the viability of remaining cells, live-dead staining was performed. Live cells can be identified by delocalized green fluorescence in the cytoplasm, and dead cells can be located through red nuclear fluorescence. The majority of cells on all dishes were living, as evidenced by wide-spread green fluorescence (Figure 40). However, cell death appeared to increase with dish diameter and was localized primarily to areas with reduced cell adhesion. These regions probably experienced the greatest shear, as evidenced by cell detachment. These results demonstrate that the volume of fluid in a rinse (e.g., 1 ml/cm dish diameter) is a more significant factor to cell adhesion and viability than the localized forces introduced at the point of fluid application. Thus, for all future interface formation procedures, 1 cm diameter dishes were employed.

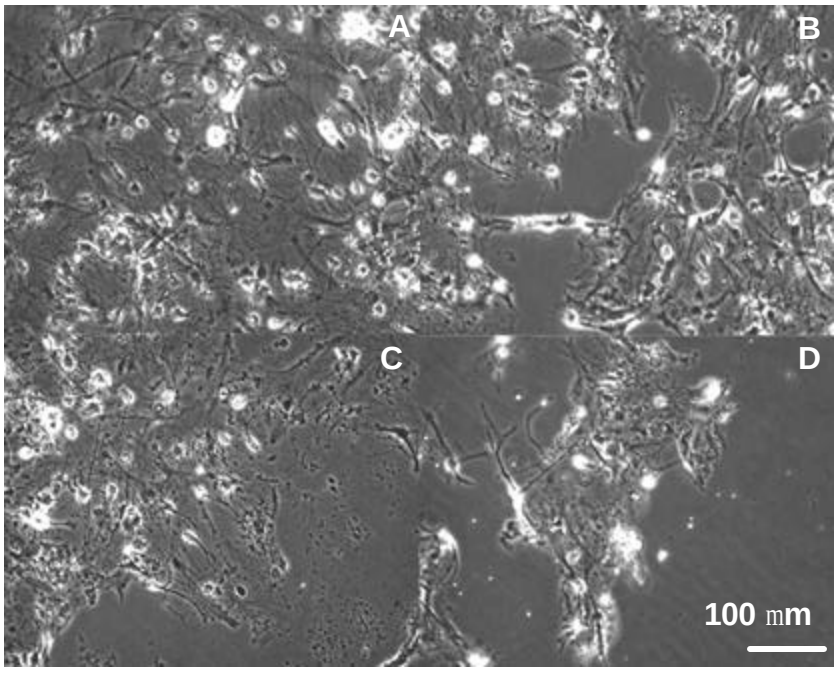

Figure 39: Effect of Increased Culture Dish Diameter on RNC Viability.

Phase contrast images of RNC cells on (A) 1 cm, (B) 3 cm, (C) 6 cm, and (D) 10 cm diameter culture dishes following three rinses in DPBS. Increased dish size reduced the number of adherent cells.

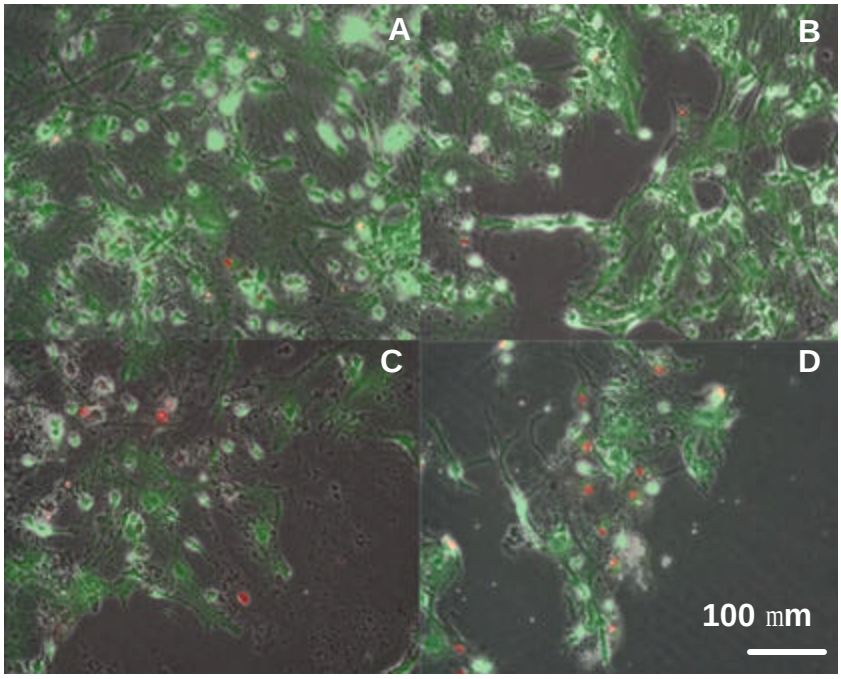

Figure 40: Live-Dead RNC Staining for Culture Dishes of Increased Diameter.

Fluorescence-phase contrast images of RNC cells on (A) 1 cm, (B) 3 cm, (C) 6 cm, and (D) 10 cm diameter culture dishes following three rinses in DPBS. Green and red staining indicate living and dead cells, respectively. Cell death increased with culture dish diameter, and was most pronounced in areas where cell adhesion was diminished.

In addition to the dish diameter, the number of DPBS rinses was investigated. In the initial protocol, cells were rinsed with DPBS once following BSA-DPBS incubation and three times after quantum dot incubation. This process resulted in significant cell death for RNCs (Figure 41A). The main purpose of rinsing is to eliminate any non-specific binding that may result from the presence of excess quantum dots in solution. Therefore, we eliminated the rinse following BSA-DPBS incubation and decreased the number of post-quantum dot incubation rinses from three to one. This procedure resulted in a significant improvement in cell viability (Figure 41B), with no increase in non-specific binding (not shown).

These results demonstrate the extreme sensitivity of primary cells to environmental factors, including shear stress. Similar shear stress exposure did not

impact our model system, SK-N-SH neuroblastoma cells. All further attempts to create quantum dot–RNC interfaces utilized the modified DPBS washing procedure.

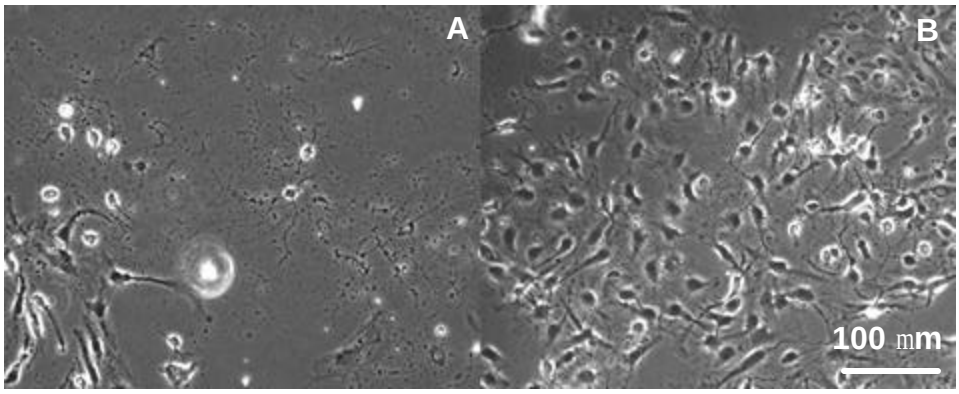

Figure 41: Effect of Reduced Rinsing Steps on RNC Viability.

Phase contrast images of cells prepared following the (A) initial and (B) modified DPBS washing procedures. Cells with a reduced number of rinses evidenced a significant increase in viability.

5.3.1.3 Quantum Dot Solvent

To further improve RNC viability, we also examined the effect of quantum dot solvent. In our previous interfacing procedure, the standard solvent used was DPBS (Table IV), which consists of phosphate buffered saline with calcium and magnesium salts added. As alternatives, we examined PBS (phosphate buffered saline with no calcium or magnesium added, Table III) and artificial cerebrospinal fluid (aCSF, Table VIII), a commonly used buffer for RNC culture. In our analysis, we evaluated each buffer against three criteria: quantum dot solubility, RNC viability, and non-specific binding.

CdS quantum dots were obtained as solids and resuspended in PBS, DPBS, or aCSF. Solubility was evaluated after initial resuspension and also following sterile-filtration (0.22 μm cellulose acetate filter), using a UV lamp to observe fluorescence. Quantum dot solubility was highest in PBS and lowest in aCSF (i.e., quantum dot

solubility PBS> DPBS> aCSF). Although this might first appear to be an effect of increased charge screening, the total ionic salt concentration *decreases* from PBS to aCSF (PBS = 172 mM, DPBS = 160 mM, aCSF = 132 mM). Thus, it is more likely that decreased quantum dot solubility results from an increase in the size and number of dissolved species. In addition to the phosphate and sodium salts of PBS, DPBS contains Ca and Mg salts; while aCSF includes Ca, Mg, dextrose, and HEPES buffer. The bulk of additional solutes may limit the number of water molecules available to solvate the particles. Particle-particle collisions would also be more likely to occur, resulting in nanocrystal aggregation.

These solutes are added to increase cell viability, and their removal may be detrimental to cells. Therefore, we evaluated the effect of each solvent on RNC and SK-N-SH viability. Quantum dot-containing solutions were prepared and exposed to cells according to the modified protocol (i.e., protocol with reduced rinses). Cells incubated in PBS-quantum dot solutions (i.e., without Ca^{2+} and Mg^{2+}) exhibited rounded morphologies and detached from the dish during DPBS washing (not shown). This was not unexpected, as the removal of Ca^{2+} and Mg^{2+} is known to promote cell detachment. [49] Therefore, despite its superior solvating properties, PBS cannot be used for quantum dot-receptor interface formation. Cells incubated in DPBS and aCSF did not display any difference in viability from control cells that remained in medium (not shown); therefore, there does not appear to be any viability benefit to the additional solutes added to aCSF buffer.

The other major concern in altering the quantum dot solvent is a potential increase in non-specific binding. Non-specific binding could interfere with the operation of a receptor-specific neuroelectronic interface by activating additional types of ion channels. To determine the degree of unwanted binding, we compared SK-N-SH cells labeled with

quantum dots in either DPBS or aCSF solvents. SK-N-SH cells were examined because they contain less debris than RNC cultures. Quantum dots display a high affinity for debris and dead cells that could obscure subtle binding to living components.

Cells labeled with DPBS-quantum dots exhibited more non-specific binding than those labeled with aCSF-quantum dots (Figure 42). In DPBS solutions, quantum dot binding appears as diffuse yellow labeling surrounding the exterior of the cell (Figure 42A); while aCSF solutions produce aggregate binding primarily confined to the substrate (Figure 42B). The apparent binding reduction in aCSF most likely results from a decline in the total number of particles, rather than a decrease in cell affinity. The concentration of quantum dots in aCSF is reduced because many aggregated particles are unable to pass through the 0.22 μm sterile filter. Additionally, aggregation of the remaining particles decreases the number of surfaces available for binding.

These results demonstrate the importance of solvent selection for interfacing methods. While PBS solvents produced the least quantum dot aggregation, they did not support cell adhesion. However aCSF solvents, which are frequently used with RNCs, produced considerable particle aggregation. Thus, the benefits of increased cell compatibility must be balanced against the requirements of an optimal quantum dot environment. Given the significant quantum dot aggregation in aCSF solution and no perceivable increase in cell viability, we did not alter the quantum dot solvent used in our original method. Quantum dot incubations continued to be performed in DPBS solution.

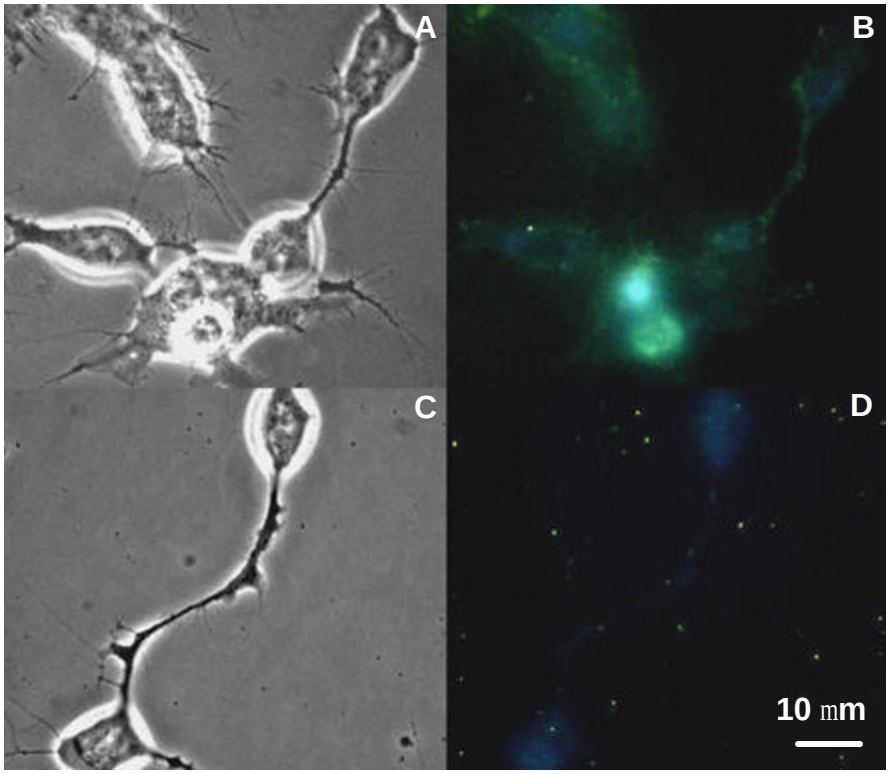

Figure 42: Solvent Effects on Quantum Dot Non-Specific Binding.

Phase contrast (A,C) and fluorescence images (B,D) of non-specific binding in DPBS (A,B) and aCSF (C,D) quantum dot solutions. Non-specific binding is increased in DPBS (B), appearing as diffuse yellow labeling surround blue cellular autofluorescence. In aCSF solvents (D), quantum dots appear aggregated and bind to the substrate, not the cell. It should be noted that the image contrast was significantly enhanced in Figure 42 to demonstrate the slight increase in fluorescence produced in DPBS. The non-specific binding in either solvent is still far less than that generated by biorecognition molecule-directed interfacing (Chapter 4, Figures 36-37).

5.3.1.4 Quantum Dot Composition

To compare the toxicity of various quantum dot materials, we examined CdS produced using aqueous synthesis (Section 5.2.1.1) and CdTe produced using organic synthesis (Section 5.2.1.2). Both particles were capped with thiol-acids containing carboxyl terminal groups (i.e., mercaptoacetic acid for CdS and mercaptoproprionic acid

for CdTe). Additionally, both particles were cleaned using anti-solvents and centrifugation, dried in a vacuum oven, and resuspended in DPBS. Solutions were sterile-filtered, added to supplemented neurobasal medium at similar concentrations (0.1 mg/ mL medium), and placed on RNC cells. Medium was changed every two days, and cells were observed over five days.

Cells incubated with CdS quantum dots exhibited no differences over controls cultured only in neurobasal medium. However, cells incubated with CdTe particles exhibited a rounded morphology by Day 1 and complete cell death by Day 2 (not shown). CdTe particles are not stable in air, with a near complete loss of fluorescence and water solubility within 48 hours. [44] Low stability most likely results from oxidation of Te atoms, which reduces ligand adhesion sites and releases Cd^{2+} in the core. Te has been shown to be more susceptible to oxidation than CdS and CdSe materials. [50] Oxidation of Cd^{2+} has been linked directly with reduced cell viability, [10] and could explain the cell morbidity observed at Day 2. Thus, as prepared, CdTe particles cannot be employed in a long-term neuroelectronic interface, and should be used with caution for short-term applications.

These results underscore the importance of shielding the particle core from oxidation. Most commonly protection is provided through the addition of a shell, either of an inorganic material (e.g., ZnS) or a biocompatible passivating layer (e.g., poly (ethylene) glycol, BSA.). [10] However, most biocompatible passivating layers are insulating, reducing the electrical properties of the particle; and inorganic shells do not provide complete protection. [10] The development of a long-term neuroelectronic interface will require alternative approaches, including enhancement of existing synthesis techniques to increase stability of the particle core.

5.3.1.5 Endocytosis

While cell viability is the primary concern in development of a neuroelectronic interface, longevity is also an important consideration. One of the most significant limiting factors in interface longevity is recycling of the plasma membrane and its receptors through a process known as the exocytosis-endocytosis cycle. [51] The endocytosis portion of this cycle (i.e., ingesting of components on the extracellular surface) can produce particle internalization, negating the ability of particles to manipulate the cell membrane potential. Recycling of the plasma membrane can be suppressed at low temperature, [36] and our initial experiments (Chapter 4) were conducted under these conditions. However, decreased temperatures also affect neuronal signaling. [37] To evaluate the effect of endocytosis on interface longevity, we evaluated our initial system using both SK-N-SH and RNC cells at physiological temperatures.

Aqueous CdS quantum dots passivated with the RGDS recognition sequence were prepared as described above (Section 5.2.1.1). Particles did not contain any additional chemical linkers (i.e., MAA), were manufactured with a reaction pH of 12, and exhibited a yellow-green fluorescence. Nanocrystals were incubated with SK-N-SH cells following the standard protocol, with the exception of incubation temperature, which was held at 37ºC. After the 30 minute incubation period, significant internalization occurred (Figure 43A). Green-yellow quantum dots appear as vesicular structures within the cytoplasm. This pattern is consistent with that of endocytotic vesicles and not dead cells or specific labeling because particles are excluded from the nucleus. Particle internalization most likely occurred through receptor-mediated endocytosis as the RGD peptide has been shown to promote this type of internalization. [41-42]

Additionally, we developed a second type of interface, formed through non-specific binding of cell surfaces. We discovered that MPA-capped CdTe particles exhibit

low levels of non-specific binding to cortical cells (Section 5.3.2.6). Comparing this binding to directed binding produced by CdTe particles with peptide/MPA surface coatings (Section 5.2.1.2), we examined the effects of membrane ingestion and receptor-mediated endocytosis. Despite the toxicity of CdTe, incubation times were sufficiently short (~30 minutes) to preclude cell death. Red CdTe particles conjugated to RGD peptide exhibited similar endocytotic labeling to that for CdS (Figure 43B). The increase in fluorescent intensity for CdTe is a result of increased particle quantum yield. Unconjugated nanocrystals (i.e., MPA-CdTe particles) bound to cell surfaces non-specifically displayed a considerable reduction in fluorescence (Figure 43C), but were also internalized.

Thus, internalization occurred for particles linked to both endocytotic receptors and the cell membrane. The implications for a long-term neuroelectronic interface are considerable. Non-specific binding to cell surfaces cannot be used to form stable interfaces, and biorecognition molecule-directed interfacing must be used with caution. *Only those biorecognition molecules that bind fixed receptors with low recycle rates (e.g., lactoferrin [38]) can be used to create long-term quantum dot-receptor interfaces.* Ion channels are recycled as a means of controlling specific neuronal response, [40] but using a different mechanism and over longer time scales than receptor-mediated endocytosis. Thus, directed-recognition methods could still be used to form long-term neuroelectronic interfaces.

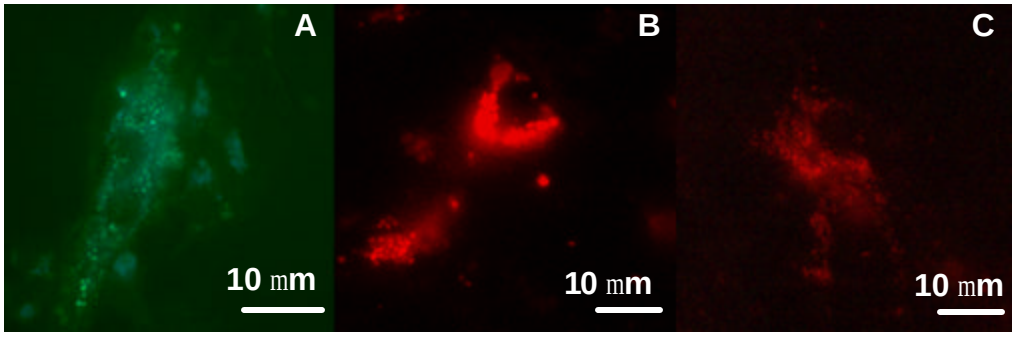

Figure 43: Endocytosis of CdS and CdTe Quantum Dots.

Fluorescence images of (A) SK-N-SH cells labeled with CdS RGD-quantum dots, (B) RNCs labeled with CdTe RGD/MPA-quantum dots, and (C) RNCs labeled with CdTe MPA-quantum dots at physiological temperature (37 ºC). Green (A, CdS) and red (B and C, CdTe) particles are seen as vesicular structures in the cytoplasm, indicating endocytotic uptake. Uptake is more pronounced in the presence of peptide (A,B), most likely due to receptor-mediated endocytosis.

5.3.2 Non-Specific Binding for Quantum Dot-Receptor Interface Formation

Given the limitations of direct labeling of cellular receptors, we chose to investigate additional methods of nanoparticle presentation. One possibility is the use of delocalized, non-specific interfacing to produce generalized interactions. Particles may be tethered directly to the substrate to prevent endocytosis, and cells can be cultured on their surfaces. The electrical implications of a delocalized interface are unclear. The Debye length is less than one quantum dot or receptor diameter; [52] therefore, it is unlikely that particles will interact with each other. However, competing signals may be conducted through the membrane or the cytoplasm, reducing electrical response. If non-specific interactions appeared to stimulate more than one type of ion channel, particles could still be used to explore cell responses in the presence of blocking agents, [53] which limit the number of active ion channels, or for small portions of membrane (i.e., using patch-clamp techniques). On the other hand, there is some evidence that particle films produce an

increase in collective dipole moment through the formation of aligned structures. [54] This could augment the electrical signal to the cells.

The first step in producing non-specific interfaces is to determine which variables modulate nanocrystal attraction to the cell surface. These generally fall into two categories: properties of the nanocrystal and contributions from the incubation method. We selected one quantum dot material, CdS, and thoroughly studied the role of synthesis conditions on non-specific binding to SK-N-SH cells. SK-N-SH cells were selected because they exhibit significantly lower levels of debris that could produce false positive signals. Then, we investigated the role of cell type, quantum dot material, and incubation length on nanoparticle attraction to SK-N-SH and RNC cells. These results were used to develop tethered quantum dot films, but also demonstrate limitations to direct quantum dot labeling of cell surfaces.

5.3.2.1 Effect of Nanocrystal Reaction pH

We investigated the role of synthesis pH on quantum dot-cell affinity. Reaction pH prior to Na_2S addition was varied from 6 to 11 (Section 5.2.1.1). This range was chosen because reaction pH values less than 6 produce blue-emitting nanocrystals whose fluorescence cannot be distinguished from cellular autofluorescence. Particles with varied synthesis pH values were characterized previously (see Chapter 3), and found to increase in size with increasing reaction pH. Maximum quantum yield occurred for nanoparticles with a reaction pH of 7. Non-specific binding was evaluated through quantum dot incubation with SK-N-SH neuroblastoma cells following the modified interface formation procedure (Section 5.2.3).

Fluorescence images (Figure 44) demonstrate that nanocrystal binding is directly related to reaction pH, with increased cell affinity at higher values (Figure 44C-F).

Binding is widespread, with attachment to both the cells and the substrate. At the highest reaction pH values, quantum dots appear to form a film that covers all surfaces (Figures 44E-F). It is likely that this binding is the result of reduced surface passivation. As pH increases, larger particles are produced, yet the concentration of ligand remains the same. Thus, an increased surface area must be passivated with a fixed amount of ligand. Our previous results (Chapter 3) demonstrating a decrease in quantum yield at high reaction pH values support this conclusion.

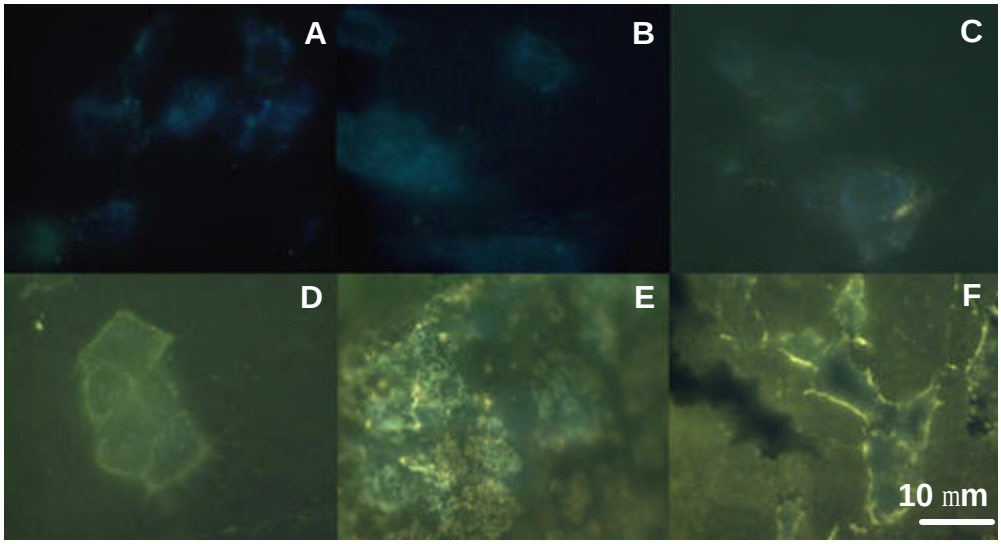

Figure 44: Effect of Nanocrystal Synthesis pH on Cellular Non-Specific Binding.

Fluorescence microscopy images of CdS quantum dot non-specific binding to SK-N-SH neuroblastoma cells with nanocrystal synthesis pH values of (A) 6, (B) 7, (C) 8, (D) 9, (E) 10, and (F) 11, prior to Na_2S addition. Binding increases with reaction pH, and is not limited to cellular structures.

5.3.2.2 Effect of Nanocrystal Cd:S Ratio

To further investigate the relationship between nanocrystal size and non-specific binding, we examined nanocrystals produced with Cd:S ratios ranging from 6:1 to 1:1 (Section 5.2.1.1). Our earlier work (Chapter 3) established that particle size is inversely

related to Cd:S ratio, with 6:1 producing the smallest particles. Quantum yield maxima occurred for intermediate sized particles (i.e., Cd:S ratio = 4:1 and 2:1). Results were similar to those for reaction pH; larger particles displayed a higher affinity for cells than smaller particles (Figure 45). As in syntheses with varied reaction pH, Cd:S variations are not accompanied by an increase in ligand concentration. Thus, larger particles are expected to exhibit reduced passivation. These results support our previous conclusion that cell affinity is related to a reduction in ligand surface coverage.

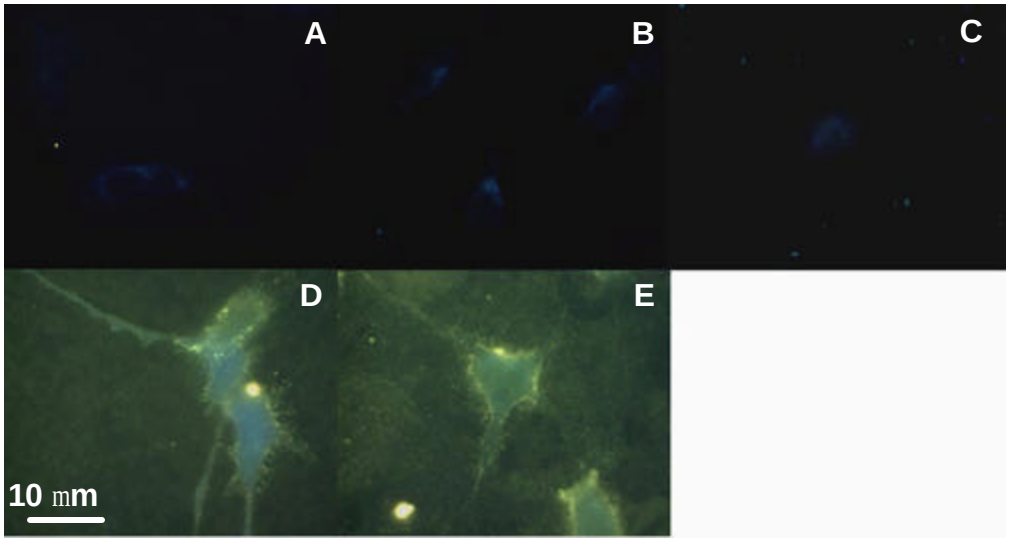

Figure 45: Effect of Nanocrystal Synthesis Cd:S Ratio on Cellular Non-Specific Binding.

Fluorescence microscopy images of CdS quantum dot affinity to SK-N-SH neuroblastoma cells with nanocrystal Cd:S ratios of (A) 6:1, (B) 4:1, (C) 2:1, (D) 1.5:1, and (E) 1:1. Particles with the lowest Cd:S ratios produce the most non-specific binding.

5.3.2.3 Effect of Nanocrystal Cd:Ligand Ratio

Next, we analyzed the effect of Cd:ligand ratio on nanoparticle non-specific binding. In our synthesis experiments (Chapter 3), we determined that particle sizes *increase* with increasing ligand concentration (i.e. [MAA]) and constant [$CdCl_2$] and

[Na_2S]. If non-specific binding is a function of nanoparticle size, we should see increased cell affinity for particles with the highest concentrations. However, if binding is a product of reduced ligand passivation, we would expect reduced or no non-specific binding at larger particle sizes.

Quantum dots with [MAA] ranging from 10-500 mM were synthesized (Section 5.2.1.1) and investigated for non-specific binding to SK-N-SH neuroblastoma cells. Control particles produced using the standard synthesis (i.e., [MAA] = 55 mM) did not display non-specific binding (not shown), consistent with previous observations (Figure 44B and Figure 45C). In fact, the only sample that did exhibit consistent non-specific binding was that with the lowest [MAA] (i.e., 10 mM, Figure 46). However, this binding was slight when compared to the dramatic increases seen for reaction pH and Cd:S ratio. Although further study is needed to measure actual ligand surface coverage values, these results support our hypothesis that reduced passivation exposes the particle core, promoting non-specific binding.

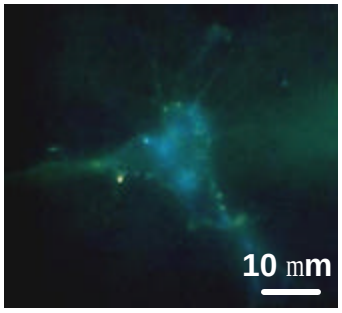

Figure 46: Effect of Nanocrystal Synthesis Ligand Concentration on Cellular Non-Specific Binding.

Fluorescence microscopy image of CdS quantum dot non-specific binding to SK-N-SH neuroblastoma cells with nanocrystal ligand concentration = 10 mM. Slight non-specific binding is evidenced.

5.3.2.4 Effect of Nanocrystal Reactant Concentrations

In addition to ligand passivation, non-specific binding may also be related to quantum dot concentration. This is definitely true for fluorescent dyes, which frequently require concentration optimizations before they are used to label specific cellular

structures. To explore this possibility, we studied CdS quantum dots at a range of concentrations using SK-N-SH cells. CdS quantum dots were prepared using the standard procedure (Section 5.2.1.1), except that the $[Cd]_{initial}$ was varied from 2-20 mM with constant Cd:S and constant Cd:ligand (Table V). Particles did not exhibit non-specific binding at any concentration (not shown), including the control value ($[Cd]_{initial}$ = 5 mM). Thus, we can conclude that particles manufactured with the standard synthesis do not exhibit non-specific binding, regardless of the concentration at which they are applied. Further investigation of the relationship between non-specific binding and concentration was performed using CdTe particles, which do have an affinity for RNC cells (Section 5.3.2.6).

5.3.2.5 Cell Type

We have shown that nanoparticle properties play an active role in their affinity for cells. However, to investigate the role of cell type in binding, we compared SK-N-SH neuroblastoma and RNC cells exposed to CdS quantum dots manufactured with a reaction pH of 11. These particles were selected for their known binding affinity to SK-N-SH cells.

Both cell types displayed nanocrystal affinity, but SK-N-SH cell binding was more diffuse than that of RNCs (Figure 47A-B). This may be a result of different substrate preparations for the two cell types. RNC cells are plated onto laminin and poly-D-lysine-coated glass slides that have been exposed to medium for at least 24 hours; whereas SK-N-SH cells are plated on polystyrene tissue culture dishes. However, the cellular labeling has a different character as well. Binding of RNCs is confined primarily to debris surrounding the cell (Figure 47C-D). Debris is a common element of primary cell cultures because it is difficult to separate cells from the homogenized tissue they are

derived from. The bright, localized labeling of RNCs is exhibited only for dead cells in SK-N-SH cultures (not shown).

Thus, despite initial appearances, non-specific binding of *living cells* appears to be lessened in RNC cultures. This decrease may result from a different complement of sugars or proteins on the cell surfaces. [55] Additional experiments are required to distinguish cell and substrate labeling in SK-N-SH cultures. Nonetheless, debris in RNC cultures creates a potential problem for neuroelectronic interface formation, as nanocrystal binding is localized and uncontrolled. This is primarily a problem for systems requiring direct binding to the cell surface; however, it may also reflect an affinity of tethered quantum dot films for debris.

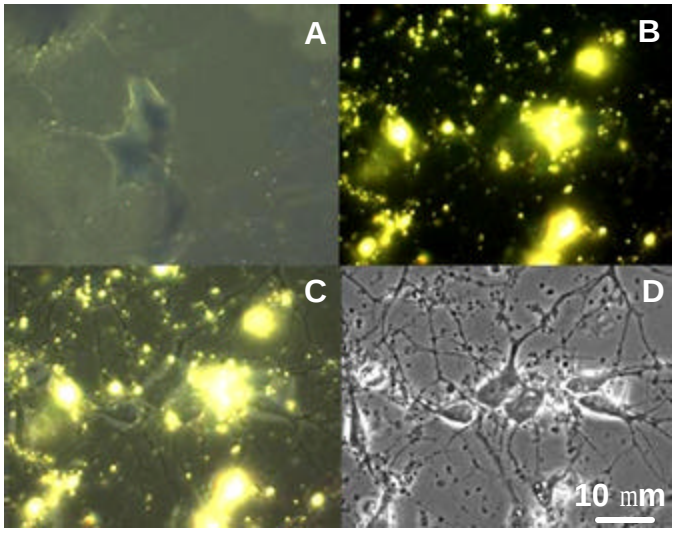

Figure 47: Effect of Cell Type on CdS Non-Specific Binding.

(A) Fluorescence image of CdS quantum dots exposed to SK-N-SH cells. (B) Fluorescence, (C) fluorescence/phase contrast composite and (D) phase contrast images of CdS quantum dots exposed to RNC cells. RNCs exhibited less non-specific binding, particular on the substrate.

5.3.2.6. Quantum Dot Composition

To compare the cellular affinity of different quantum dot materials, we exposed RNCs to CdS and CdTe particles. CdS particles were manufactured following the standard procedure (Section 5.2.1.1.) with reaction pH values of 11. CdTe particles were prepared in organic solution with ligand exchange (Section 5.2.1.2). This synthesis

produces dense nanoparticle solutions, which were diluted over the range of 2-20 mM $[Cd]_{initial}$. Cells were labeled with particles following the modified interface formation procedure (5.2.3) and viewed using fluorescent microscopy (Section 5.2.5).

CdS particles labeled debris surrounding the cell as in previous experiments (Figures 47C, 48A); however, CdTe quantum dots displayed a high affinity for cells and their extensions (Figure 48D,G,J). Additionally, unlike CdS with a reaction pH = 7, fluorescent intensity was proportional to the concentration of quantum dots applied (Figures 48 C,F,I and D,G,J). Examination of fluorescent images for the highest CdTe concentrations (i.e., 20 mM and 4 mM $[Cd]_{initial}$) (Figure 48C,F) reveal cellular shaped voids displaying no binding. These regions are surrounded by brightly labeled structures. Inspection of phase contrast images (Figure 48B,E) for the same regions shows that voids are primarily composed of cellular debris. Most cells in these samples are not intact, and remaining cells exhibit rounded morphologies. These facts indicate a toxic effect of CdTe particles at these concentrations. CdTe particles at lower concentration values (i.e., 2 mM $[Cd]_{initial}$) did not demonstrate this behavior (Figure 48H-J).

The cell death observed is most likely caused by the osmotic pressure of highly concentrated CdTe solutions. Although the $[Cd]_{initial}$ is similar in magnitude to values used for CdS, CdTe solutions appeared to a have higher reaction yield. Synthesis of CdS resulted in only 17% yield, and produced clear, yellow solutions; while synthesis of CdTe produced opaque brown-black solutions. Additionally, post-cleaning pellet sizes were significantly larger than those of CdS for the same volume and $[Cd]_{initial}$. These results indicate an upper limit to the number of quantum dots that may be applied without inducing cell death. All further CdTe experiments were conducted using 2 mM $[Cd]_{initial}$.

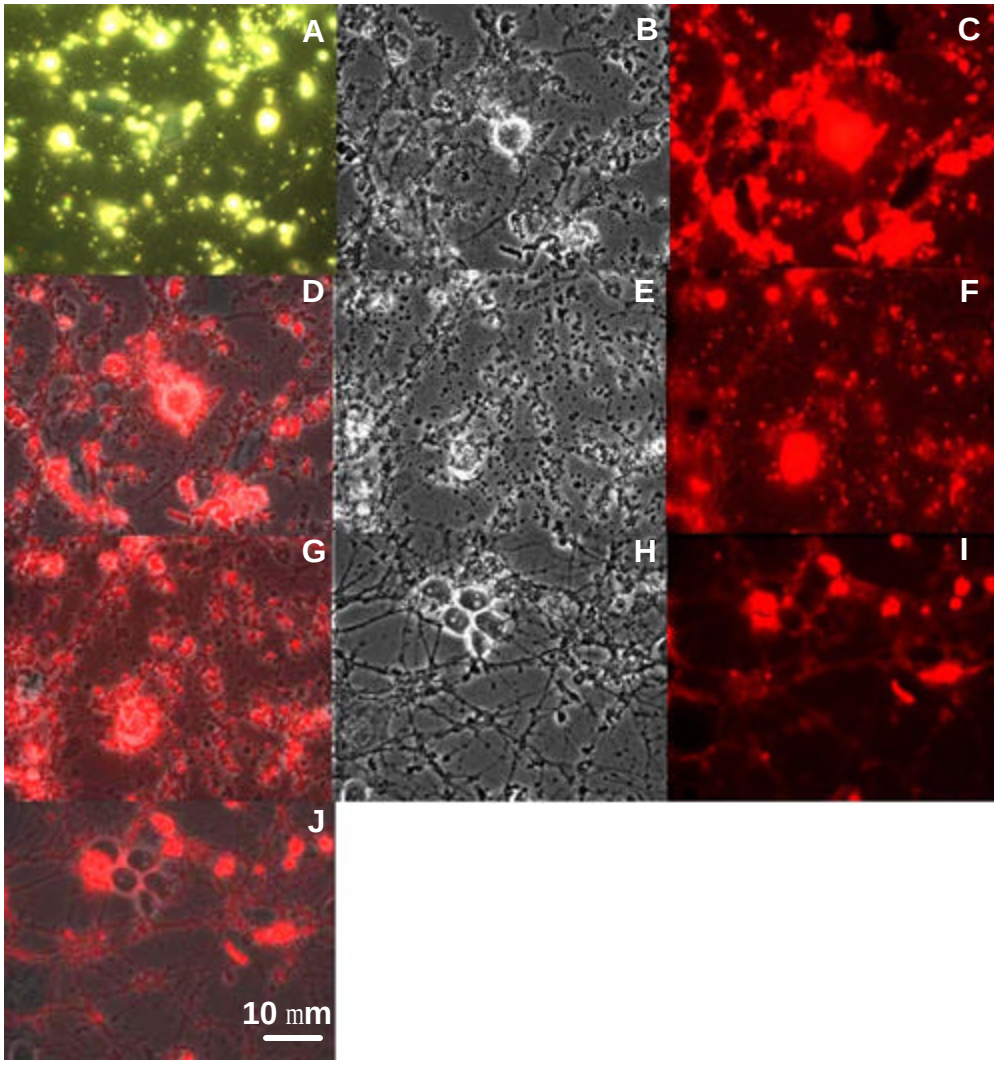

Figure 48: Effect of Quantum Dot Composition on RNC Non-Specific Binding.

Fluorescence images of non-specific binding to RNC cells using (A) CdS quantum dots (reaction pH = 11, 5 mM $[Cd]_{initial}$) (B-D) CdTe quantum dots (20 mM $[Cd]_{initial}$), (E-G) CdTe quantum dots (4 mM $[Cd]_{initial}$), and (H-J) CdTe quantum dots (2 mM $[Cd]_{initial}$). Fluorescence/phase contrast composite images (A,D,G,J) show that CdS labeling (A) is confined primarily to debris surrounding the cell, while CdTe particles (D,G,J) bind cells and their extensions. Comparing CdTe phase contrast (B,E) and fluorescence images (C,F), cellular shaped regions devoid of binding appear to be locations where cells have exploded, most likely as a result of osmotic pressures. Bright regions surrounding these voids contain cellular debris.

5.3.2.7 Incubation Length

Non-specific binding of debris by CdS quantum dots could prove problematic for the development of a neuroelectronic interface. To establish how quickly non-specific binding of debris occurs in RNC cultures, we examined the effect of reduced incubation length for CdS particles with a reaction pH of 11 and CdTe quantum dots with 2mM $[Cd]_{initial}$. After only 5 minutes of exposure, CdS particles displayed binding of cellular debris (Figure 49A-B). CdTe particles, which label living cells and their extensions, exhibited significantly less binding in the same time frame (Figure 49C-D). However, endocytosis of CdTe particles was already evident (Figure 49C, arrow). These data indicate that uptake of particles by dead cellular material is extremely rapid. Additionally, while cellular labeling takes place over a longer time frame, endocytosis begins almost immediately. The binding of undesirable components and endocytosis are unavoidable, presenting significant limitations to use of non-specific methods for labeling cell surfaces. However, tethered-films can overcome these challenges.

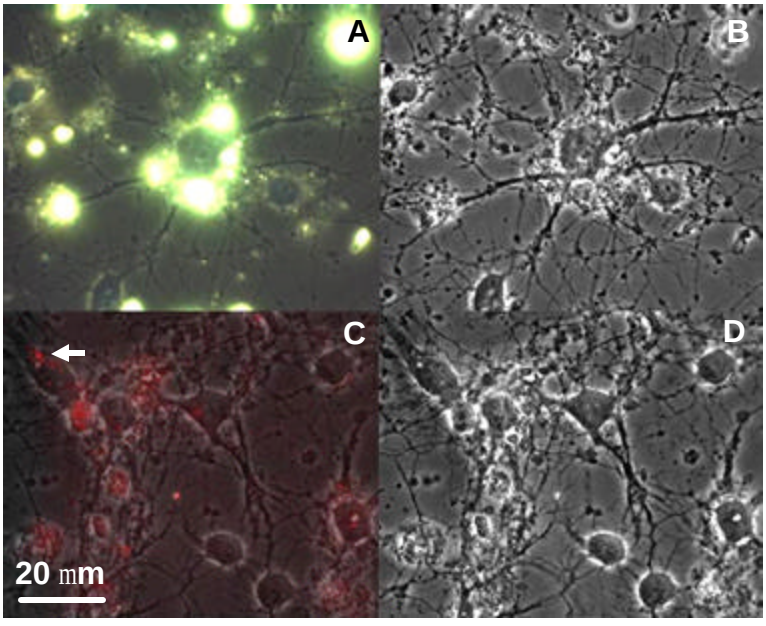

Figure 49: Effect of Reduced Quantum Dot Incubation Time on RNC Non-Specific Binding.

Fluorescence/Phase contrast (A,C) and phase contrast (B,D) images of RNCs incubated with (A,B) CdS and (C,D) CdTe particles for five minutes. CdS particles non-specifically bind debris; CdTe binding is much less pronounced. However, endocytosis is evident in the CdTe sample (C, arrow).

5.3.3 Tethered Quantum Dot Films

Films of glass-tethered quantum dots were developed, based on the results of our non-specific binding studies, with two separate adhesion technologies. In the first method, the silane terminus of a mercaptosilane compound was used to bind a glass substrate (SiO_2), whereas the mercaptan terminus (-SH) provided a surface for quantum dot adhesion. Cd-based quantum dots bind strongly to thiols through exposed core Cd^{2+} ions and disulfide interactions. The second method utilized electrostatic attractions between poly-D-lysine ($-NH_3^+$ side chains) adsorbed on glass and quantum dot surface ligands (COO^-) to produce binding.

These films offer several advantages for neuroelectronic interface formation. Tethered quantum dots considerably limit the probability of endocytosis, increasing interface longevity. Additionally, films can introduce a greater number of quantum dots to a cell than directed recognition or non-specific binding. However, the films also present limitations, the most significant of which is the inability to control quantum dot-receptor interface formation. It is unclear how quantum dot–membrane interfaces affecting multiple ion channel types would influence cell signaling. Nonetheless, tethered films offer a viable strategy to demonstrate the ability of quantum dots to modulate cellular receptors.

5.3.3.1 Previous Nanoparticle Tethered Films

Tethered nanoparticle films have been developed before, chiefly as methods of particle self-assembly. These techniques primarily rely upon the strong interactions between gold particles and alkanethiols to produce films, [46, 56-58] although silver [59]

and Cd-based nanoparticles have also been explored. [60-63] Two basic strategies for film formation have been utilized. In the first method, silica substrates (glass [46] or SiO_2-coated silicon substrates [56, 58]) are coated with siloxanes (i.e., (3-mercaptopropyl)-trimethoxysilane [46, 56] and (3-aminopropyl) trimethoxysilane [58]) to produce nanocrystal binding surfaces. The second method utilizes thiol-containing organics, which self-assemble on gold-coated substrates, to provide functional groups that bind nanoparticles. [57, 59-63]

Both methods have been used to create well-characterized particle films. However, the siloxane-based method is more compatible with development of a neuroelectronic interface because the gold films required for thiol self-assembly may interfere with electrical signals produced by the quantum dots. Additionally, siloxane-based films have already demonstrated compatibility with cell culture techniques. [46] Therefore, we chose to utilize siloxane-based chemistry to produce nanoparticle films for neuroelectronic interface development.

In addition to siloxane-based films, we developed an alternative using poly-D-lysine. These films offer some potential advantages to siloxane-based films, as they are substantially easier to fabricate. Also, because attachment occurs through charge attraction, the films can incorporate a higher number of nanocrystals than siloxane monolayer surfaces.

Poly-D-lysine has been used in a limited number of applications to create gold and silver nanoparticle films. [54, 64-67] Although it has not been examined as a substrate for Cd-based quantum dot assembly, results from metal films suggest poly-D-lysine strategies are promising for neuroelectronic interface development. Polylysine substrates promoted nanoparticle alignment into 1-D structures and nanowires, [54, 64-

65, 67] producing an increase in cumulative dipole moment. [54] This could create a greater cellular response than un-tethered nanoparticle interfaces.

5.3.3.2 Siloxane Films

Siloxane-based films were prepared as described previously [46] (Section 5.2.4.1). Mercaptosilane was incubated overnight with cleaned glass slides. Then, slides were rinsed and exposed to quantum dots overnight. Siloxane concentrations ranging from 1 to 50 mM were investigated. The presence of siloxane was confirmed using ellipsometry (Section 5.2.4.2). Films formed from 1 mM mercaptosilane were not uniform, and the thickness could not be established. 10 mM mercaptosilane produced films with thicknesses from 1-3 monolayers (1 nm – 3 nm).

Quantum dot attachment was confirmed using fluorescence microscopy (Figure 50). Because silanization techniques produce particle films only a few monolayers in thickness, fluorescence intensity is low and difficult to distinguish from the background. However, when compared to an unsilanized control (Figure 50A), quantum dot binding is evident (Figure 50B-E). Maximal binding occurred for 10 mM mercaptosilane (Figure 50C). This indicates that coverage of the substrate is essentially complete at a 10 mM concentration; therefore, no benefit is derived from additional silanization chemical. Future experiments utilized 10 mM mercaptosilane.

Figure 50: Effect of Increased Siloxane Concentration on Siloxane-Tethered Quantum Dot Films.

Fluorescence images of glass with (A) 0 mM, (B) 1 mM, (C) 10 mM, (D) 20 mM, and (E) 50 mM mercaptosilane after CdS quantum dot incubation (standard synthesis, reaction pH = 11). Quantum dot adhesion is apparent on silanized sides (B-E). Binding was maximal at intermediate concentrations (C), indicating complete surface coverage.

Next, we analyzed the role of increasing quantum dot concentration on surface coverage. CdS particles with reaction pH = 7 were manufactured with $[Cd]_{initial}$ ranging from 2-20 mM. Quantum dots at the highest concentration investigated (i.e., 20 mM) demonstrated the greatest binding affinity (Figure 51F), indicating that surface sulfhydryl groups may not be saturated with particles. Additional experiments are needed to study higher concentrations; however, these solutions may be difficult to produce as nanoparticle solubility declines with concentration (Chapter 3).

Figure 51: Effect of Increased CdS Concentration on Siloxane-Tethered Quantum Dot Films.

Fluorescence images of 10 mM mercaptosilane films with (A) 0 mM, (B) 2 mM, (C) 5 mM, (D) 10 mM, (E) 15 mM, and (F) 20 mM CdS quantum dots applied. The greatest degree of binding occurs at the highest quantum dot concentration (F, 20 mM).

Additionally, we investigated the role of quantum dot reaction pH on substrate binding. Previously (Section 5.3.2.1), we established that particles with higher reaction pH values have a greater affinity for glass substrates. We therefore created solutions at the highest pH value (i.e., pH 11) with concentrations of 10, 15, and 20 mM $[Cd]_{initial}$. Similar to results for pH 7 particles (Figure 51), increased quantum dot concentrations produced higher degrees of binding (Figure 52), with 20 mM particles exhibiting maximal affinity (Figure 52D). Additionally, pH 11 particles displayed a greater degree of binding than pH 7 particles of the same concentration (Figure 51 vs. 52). This may result from reduced surface passivation of the pH 11 particles. To maximize nanoparticle binding, remaining experiments were conducted using 20 mM $[Cd]_{initial}$ CdS quantum dots with a reaction pH of 11.

Figure 52: Effect of CdS Concentration and pH on Siloxane-Tethered Quantum Dot Films.

Fluorescence images of (A) 0 mM, (B) 10 mM, (C) 15 mM, and (D) 20 mM CdS quantum dots with a reaction pH of 11 bound to mercaptosilane films. Quantum dot binding increases with concentration and is more pronounced at higher pH (compare to Figure 51).

5.3.3.3 Poly-D-Lysine Films

Poly-D-lysine films were prepared through adsorption onto glass surfaces (Section 5.2.4.3), followed by quantum dot incubation. The concentration and molecular weight of poly-D-lysine were the same as those used to promote RNC cell adhesion (Section 5.2.2.2). Other concentrations were not investigated. The presence of polylysine

was confirmed by qualitatively observing the contact angle. Polylysine-coated surfaces are significantly less wetting than uncoated glass.

To optimize quantum dot adhesion, solutions of 2-20 mM $[Cd]_{initial}$ CdS quantum dots were prepared and incubated with polylysine surfaces for one hour. Quantum dot adhesion was visible for concentrations of 10 mM and greater (Figures 53D-F), and films persisted after three washes in ddH_2O indicating tethered binding. As expected, binding was greater than that of siloxane-based films (Figure 52 vs. 53), but particle aggregation also increased. Aggregation was not random, favoring the formation of circular structures on top of a more uniform background adhesion layer (Figure 53F). These structures may indicate the presence of circular nanowires, which were produced under similar circumstances using gold nanoparticles. [67] However, gold nanowires were ~0.5 μm in diameter, while our structures approach 2 μm in size. Additional AFM or TEM analysis is required to determine the nature of these aggregates. If these regions prove to contain nanowires, they could provide favorable electronic properties to the film. [54] Nonetheless, to avoid the presence of aggregates remaining experiments were conducted with 10 mM quantum dot concentrations.

Figure 53: Effect of CdS Concentration on Polylysine-Tethered Quantum Dot Films.

Fluorescence images of glass slides following exposure to (A) a 5 mM quantum dot solution and (B-F) polylysine followed by (B) 2 mM, (C) 5 mM, (D) 10 mM, (E) 15 mM, and (F) 20 mM CdS quantum dot solutions. Binding increases with quantum dot concentration becoming noticeable at values of 10 mM and higher (D-F). Circular quantum dot aggregates form at the highest concentrations (E,F).

5.3.3.4 Film Stability

To ascertain the stability of both films in a biological environment, films were incubated in RNC cell culture medium for six days. Layers were sterilized using either UV light combined with sterile filtration (polylysine) or exposure to ethanol (siloxane). No bacterial or fungal growth was evidenced on either film. Samples from the same initial preparation were sacrificed on each day and rinsed with ddH_2O three times before viewing. Both films appeared to be stable over the test period (Figures 54-55).

Siloxane films demonstrated an increase in particle aggregation over time (Figure 54E-F); however, additional experiments are required to rule out sample to sample variation as a cause. Polylysine films displayed great variability in both fluorescent intensity and in the type of structures exhibited on film surfaces (Figure 55). This variation is typical from sample to sample, and is likely caused by the uncontrolled nature of polylysine and quantum dot adhesion. Fluorescence intensity for both films is slightly increased over that of films not cultured in medium (Figures 54,55 vs. 52D,53F; respectively), probably as a result of surface adsorption of fluorescent compounds in the medium. The stability of both films is sufficient for initial neuroelectronic interface development. Further improvements could be made through additional optimization.

Figure 54: Stability of Siloxane-Tethered Quantum Dot Films.

Fluorescence images of siloxane-quantum dot films exposed to RNC cell culture medium for (A) 0, (B) 1, (C) 2, (D) 4, (E) 5, and (F) 6 days. Films remained stable over the course of observation, although aggregation increased with time (D-E).

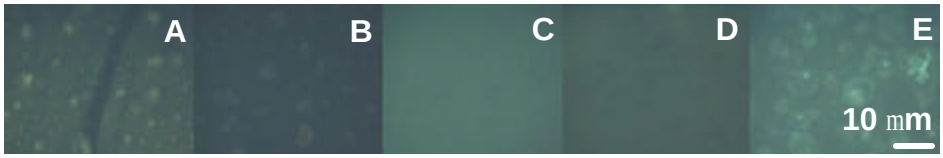

Figure 55: Stability of Polylysine-Tethered Quantum Dot Films.

Fluorescence images of polylysine-quantum dot films exposed to RNC cell culture medium for (A) 0, (B) 2, (C) 4, (D) 5, and (E) 6 days. Films remained stable for the test period. Sample to sample variation typical of polylysine films is evident.

5.3.3.5 Cell Culture on Tethered Films

To establish neuroelectronic interfaces, cells must adhere to film surfaces. Both poly-D-lysine and siloxane are commonly applied to slides to promote cell adhesion; however, the presence of the quantum dot layer may interfere with cell attachment. Additionally, cells excrete a variety of biological compounds (e.g., proteases [68], etc.) that could damage the quantum dot films. To examine the ability of the films to support cell culture, we plated RNCs on sterile, tethered quantum dot surfaces. Cells were harvested using standard procedures (Section 5.2.2.2), and medium was changed every 2 days.

Both siloxane- and polylysine-tethered films in culture exhibited significant differences from those exposed only to medium (Figures 56-57 vs. 54-55). Most notably, fluorescence was red-shifted and diminished. Decreased intensity could result from particle desorption; however, red-shifted fluorescence suggests that particles may be undergoing *in situ* Ostwald ripening (i.e., growth of larger particles at expense of smaller ones). Given that both films were stable for over six days in RNC culture medium, it is unlikely that medium catalyzed this process. However, cells are known to release several substances, one of which could have promoted oxidation. Smaller particles would

degrade, allowing the growth of larger ones. Alternatively, particles may have migrated within the tethered layers, allowing them to aggregate through collision events.

Lack of film stability in cell culture is a significant problem to implementation in a long-term neuroelectronic interface. However, longevity may be sufficient for proof-of-principle experiments establishing the ability of nanoparticles to interact with cellular receptors. Siloxane layers were stable for at least one day; polylysine layers for three days. The primary limitation for initial interface testing is the amount of time required for RNC cell adhesion. Insufficiently attached cells can be aspirated during whole-cell clamping experiments. Polylysine layers were stable for the longest time period; therefore, these films are most suitable for proof-of-principle experiments.

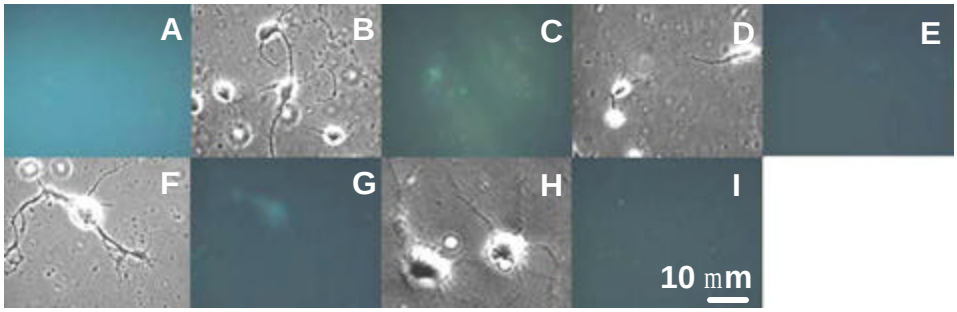

Figure 56: Cell Culture on Siloxane-Tethered Quantum Dot Films.

Fluorescence (A,C,E,G,I) and phase contrast (B,D,G,H) images of cell culture on siloxane-tethered quantum dot films at (A) 0, (B,C) 1, (D,E) 3, (F,G) 4, and (H,I) 5 days. The film remains intact at least one day, but fluorescence red-shifts and declines in intensity. Additionally, the film becomes less uniform with time and aggregates appear.

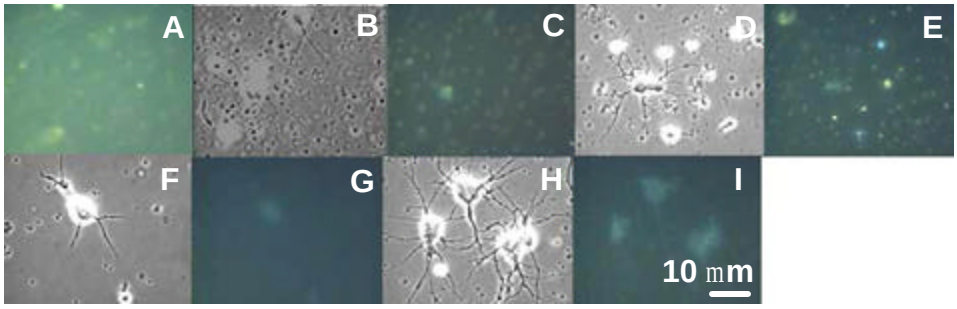

Figure 57: Cell Culture on Polylysine-Tethered Quantum Dot Films.

Fluorescence (A,C,E,G,I) and phase contrast (B,D,G,H) images of cell culture on polylysine-tethered films at (A) 0, (B,C) 1, (D,E) 3, (F,G) 4, and (H,I) 5 days. The film is stable for at least three days, but fluorescence is red-shifted and diminished after only one day. Aggregates remain fluorescent longer than the more homogenous background.

Several strategies could be pursued to improve the longevity of both layers. Increasing the original number of particles increases the persistence of fluorescence, although it does not prevent aggregation or red-shifted emission. This can be seen in the comparison between siloxane- and polylysine-tethered films (Figure 56 vs. 57). Polylysine films, which exhibit greater initial particle adhesion, are fluorescent for a longer period than siloxane films. Additionally, methods to improve particle surface coatings would improve stability to oxidation; however, these strategies must not diminish electrical signals produced by the particle.

5.4 Summary of Optimized Interface Formation Methods

We have presented three separate approaches for creating quantum dot–receptor interfaces between CdS and CdTe nanoparticles and primary neurons. Recognition-molecule directed binding, non-specific interactions, and tethered-nanoparticle films all produced quantum dot binding to cell surfaces. We examined the suitability of each of

these methods for neuroelectronic interface formation, and determined that recognition-directed binding and tethered films could be used to establish proof-of-principle. No method displayed the stability necessary for long-term neuroelectronic devices.

Biorecognition molecule interfacing was limited by particle uptake through endocytosis, constraining the application of this method to those receptors that are fixed or recycled at low rates. However, ion channels meet these conditions and quantum dot binding could be produced using this method. [40] Non-specific binding methods were also hindered by endocytosis, but more importantly by concerns over nanoparticle toxicity. Binding was most pronounced for particles presumably having a lower degree of ligand coverage on their surface, which has been linked to particle toxicity. [10] Tethered films exhibited low stability in cell culture, displaying decreased and red-shifted fluorescence after 1-3 days. This may result from cellular release of oxidizing agents. [68] If so, improved passivating agents could minimize these effects. [10, 20] However, film stability is sufficient for proof-of-principle experiments to demonstrate quantum-dot cell electrical interfacing. Our results demonstrate the complexity of developing interfaces that are both electrically active and biocompatible, and provide two potential means to establishing those interfaces.

In addition to interfacing techniques, we also examined the toxicity of quantum dots to primary cells. Previous reports of quantum dot–live cell interactions [11-16] did not report deleterious effects; however, most of these applications utilized immortalized cell lines. The one report investigating primary cell lines [10] found increased cell morbidity in the presence of oxidized quantum dot surfaces. Our findings corroborate the latter results. CdTe particles caused complete cell death in 48 hours, most likely because of oxidation of the particle core. [10, 50] These results emphasize the need for further

study of quantum dot toxicity using *primary* cells, which are more representative of the response of living organisms.

5.5 CONCLUSIONS

The development of interfacing technologies for *electrically active* quantum dot-receptor devices is more complicated than the creation of quantum dot fluorescent labels. Although quantum dots have been used in a variety of cultured cell lines [11-12, 14-15] and *in vivo* studies, [13, 16] these applications do not approximate the conditions required for a neuroelectronic interface. Neuroelectronic interfaces are designed to serve as laboratory models for neuroscience, computational devices, and prosthetics. [1] Thus, they require the use of plastic, primary cells capable of altering and forming new interconnections. A single study [10] has investigated the impact of quantum dots on a primary cell line (i.e., hepatocytes), and found toxicity to be significantly higher than that reported for cultured cell lines. Our results support this conclusion. CdTe particles produced complete cell death in 48 hours, most likely through oxidation of the particle core. [10, 50] This finding underscores the need for further testing of particle toxicity using *primary* cell lines, which are more indicative of *in vivo* conditions.

We adapted our previous model system (Chapter 4), using biorecognition-directed binding, for a primary neuronal cell line (i.e., rat neonatal cortical cells, RNCs). By altering the incubation methods and through careful selection of quantum dot material and synthesis conditions, we were able to create biocompatible interfaces with RNCs. The primary limitation of recognition-directed binding was the occurrence of endocytosis, cellular uptake of nanoparticles bound to the membrane surface. [33] Although endocytosis was shown to begin almost immediately after quantum dot

attachment, this procedure can be used to label receptors that are not recycled or recycled at a low rate. Therefore, ion channel labeling of primary cells is possible. [40]

Alternatively, we investigated non-specific binding as a method to form quantum dot-cell interfaces. We discovered that cell affinity is related to quantum dot synthesis conditions, particularly those circumstances leading to low ligand coverage on the particle surface. This could prove problematic for neuroelectronic interfacing as poor passivation has also been linked to quantum dot toxicity. [10] Additionally, endocytosis occurred, albeit at lower rates than for tagged receptors. Given these limitations, we chose to explore a third system using tethered nanoparticles to prevent cellular uptake.

Two methods of producing nanoparticle-tethered films on glass were explored. The first method, using thiol groups from mercaptosilanes to bind quantum dots, [46] produced uniform films with low levels of fluorescent intensity. Maximum intensity occurred at an intermediate siloxane concentration, indicating saturation of the glass surface, whereas fluorescence intensity increased with nanoparticle concentration for all values investigated. Films were stable for over six days in cell culture medium, but only 1-2 days with cells grown on their surface. The second method of film formation used poly-D-lysine, which binds negatively charged quantum dots through its positively charged surface. These films were not as uniform as the siloxane films, but demonstrated a greater degree of quantum dot binding. Affinity increased with increasing nanoparticle concentration. These layers were stable for over six days in medium, and 3 days with cells cultured on their surface.

For both siloxane and polylysine films, the loss of stability in cell culture appeared to occur through particle growth rather than desorption. This was indicated by a red-shift in particle fluorescence, and was most likely a result of Ostwald ripening. Oxidizing agents released by the cells may have accelerated this process. [68] In future

films, oxidation could be limited by improving the protective ligand layer of the particle. [10, 20] Nonetheless, film stability is sufficient to establish proof-of-principle for the neuroelectronic interface.

Thus, we explored a variety of interfacing technologies, utilizing both directed and non-specific binding. These systems were optimized for primary cells, which are more sensitive to environmental conditions than immortal, cultured cell lines. [2] Each system displayed limitations, most notably longevity of the interface and toxicity. The addition of a protective shell on the nanoparticle surface could address both of these concerns; [10] however, the requirement of electrical interfacing requires thin or conducting shells to preserve electrical properties. Our results demonstrate the difficulty of optimizing any interfacing method to maximize cell compatibility, interface longevity, and nanoparticle electrical properties. The systems presented here can be used to create viable neuroelectronic interfaces, and additional improvements will enable the development of long-term devices.

5.6 REFERENCES

1. W.L.C. Rutten. "Selective Electrical Interfaces with the Nervous System." Ann. Rev. Biomed. Eng. 4: 407, 2002.

2. R.I. Freshnay. Culture of Animal Cells, 3rd Ed., John Wiley and Sons, New York: 1994, p. 335.

3. R.I. Freshnay. Culture of Animal Cells. 3rd Ed., John Wiley and Sons, New York: 1994, p. 12.

4. N. Tokutomi, Y. Tokutomi, K. Fukunaga, E. Miyamoto, and K. Nishi. "Bradykinin-Evoked Non-Specific Cationic Current in Neuroblastoma Glioma Hybrid (NG108-15) Cells and its Down-Regulation Through Differentiation." Brain Res. 657: 202, 1994.

5. M. Fatehi, A.L. Harvey, and E.G. Rowan. "Characterization of the Effects of Depolarizing Toxins on Nerve Terminal Action Potentials: Apparent Block of Presynaptic Potassium Currents." Toxicon. 36(1): 115, 1998.

6. F.M. Benes, J.B. Taylor, and M.C. Cunningham. "Convergence and Plasticity of Monoaminergic Systems in the Medial Prefrontal Cortex During the Postnatal Period: Implications for the Development of Psychopathology." Cereb. Cortex. 10(10): 1014, 2000.

7. H.J. Luhmann, I. Hanganu, and W Kilb. "Cellular Physiology of the Neonatal Rat Cerebral Cortex." Brain Res. Bull. 60(4): 345, 2003.

8. M.E. Goldberger. "Mechanisms Contributing to Sparing of Function Following Neonatal Damage to Spinal Pathways." Neurochem Pathol. 5(3): 289, 1986.

9. C. Seydel. "Quantum Dots Get Wet." Science 300: 80, 2003.

10. A.M. Derfus, W.C.W. Chan, and S.N. Bhatia. "Probing the Cytotoxicity of Semiconductor Quantum Dots." Nano Lett. 4(1): 11, 2004.

11. B. Dubertret, P. Skourides, D.J. Norris, V. Noiureaux, A.H. Brivanlou, and A. Libchaber. "In Vivo Imaging of Quantum Dots Encapsulated in Phospholipid Micelles." Science 298: 1759, 2002.

12. W.J. Parak, R. Boudreau, M. Le Gros, D. Gerion, D. Zanchet, C.M. Micheel, S.C. Williams, A.P. Alivisatos, and C. Larabell. "Cell Motility and Metastatic Potential

Studies Based on Quantum Dot Imaging of Phagokinetic Tracks." Adv. Mats. 14(12): 882, 2002.

13. M.E. Åkerman, W.C.W. Chan, P. Laakkonen, S.N. Bhatia, and E. Ruoslahti. "Nanocrystal Targeting in vivo." Proc. Nat. Acad. Sci. 99(20): 12617, 2002.

14. J. K. Jaiswal, H. Mattoussi, J.M. Mauro, and S.M. Simon. "Long-term Multiple Color Imaging of Live cells Using Quantum Dot Bioconjugates." Nature Biotech. 21: 47, 2003.

15. X. Wu, H. Liu, J. Liu, K.N. Haley, J.A. Treadway, J.P. Larson, N. Ge, F. Peale, and M.P. Bruchez. "Immunofluorescent Labeling of Cancer Marker Her2 and Other Cellular Targets with Semiconductor Quantum Dots." Nature Biotech. 21: 41, 2003.

16. D.R. Larson, W.R. Zipfel, R.M. Williams, S.W. Clark, M.P. Bruchez, F.W. Wise, and W.W. Webb. "Water-soluble Quantum Dots for Multiphoton Fluorescence Imaging in Vivo." Science 300: 1434, 2003.

17. L. Patrick. "Toxic Metals and Antioxidants: Part II. The Role of Antioxidants in Arsenic and Cadmium Toxicity." Alt. Med. Rev. 8(2): 106, 2003.

18. C.-W. Lam, J.T. James, R. McCluskey, and R.L. Hunter. "Pulmonary Toxicity of Single-Wall Carbon Nanotubes in Mice 7 and 90 Days After Intratracheal Instillation." Toxic. Sci. 77: 126, 2004.

19. E. Oberdörster. "Manufactured Nanomaterials (Fullerenes, C60) Induce Oxidative Stress in the Brain of Juvenile Largemouth Bass." Env. Health Persp. 112(10): 1058, 2004.

20. V.L. Colvin. "The Potential Environmental Impact of Engineered Nanomaterials." Nature Biotech. 21(10): 1166, 2003.

21. A.C.P. Elder, R. Gelein, M. Azadniv, M. Frampton, J. Finkelstein, and G. Oberdörster. "Systematic Effects of Inhaled Ultrafine Particles in Two Compromised, Aged Rat Strains." Inhalation. Toxic. 16(6/7) 461, 2004.

22. G. Oberdörster, Z. Sharp, V. Atudorei, A. Elder, R. Gelein, W. Kreyling, and C. Cox. "Translocation of Inhaled Ultrafine Particles to the Brain." Inhalation Toxic. 16(6/7): 437, 2004.

23. M. Semmier, J. Seitz, F. Erbe, P. Mayer, J. Heyder, G. Oberdörster, and W.G. Kreyling. "Long-term Clearance Kinetics of Inhaled Ultrafine Insoluble Iridium Particles from the Rat Lung, Including Translocation into Secondary Organs." Inhalation Toxic. 16(6/7): 453, 2004.

24. M.P. Waalkes. “Cadmium Carcinogenesis.” Mut. Res. 533: 107, 2003.

25. A. Hartwig and T. Schwedtle. “Interactions by Carcinogenic Metal Compounds with DNA Repair Processes: Toxicological Implications.” Toxic. Lett. 127: 47, 2002.

26. L.E. Rikans and T. Yamano. “Mechanisms of Cadmium-Mediated Acute Hepatotoxicity.” J. Biochem. Mol. Toxicol. 14: 110, 2000.

27. J.B. Lansman, P. Hess, and R.W. Tsien. “Blockade of Current Through Single Calcium Channels by Cd^{2+}, Mg^{2+}, and Ca^{2+}. J. Gen. Physiol. 88: 321, 1986.

28. L. Spanhel, M. Haase, H. Weller, and A. Henglein. “Photochemistry of Colloidal Semiconductors. 20. Surface Modification and Stability of Strong Luminescing CdS Particles.” J. Am. Chem. Soc. 109: 5649, 1987.

29. J.E. Bowen Katari, V.L. Colvin, and A.P. Alivisatos. “X-ray Photoelectron Spectroscopy of CdSe Nanocrystals with Applications to Studies of the Nanocrystal Surface.” J. Phys. Chem. 98: 4109, 1994.

30. A.P. Alivisatos. “Perspectives on the Physical Chemistry of Semiconductor Nanocrystals.” J. Phys. Chem. 100: 13226, 1996.

31. B.O. Dabbousi, J. Rodrigeuz-Viejo, F.V. Mikulec, J.R. Heine, H. Mattoussi, R. Ober, K.F. Jensen, and M.G. Bawendi. “CdSe(ZnS) Core-Shell Quantum Dots: Synthesis and Characterization of a Size Series of Highly Luminescent Nanocrystallites.” J. Phys. Chem. B 101: 9463, 1997.

32. J. Aldana, Y.A. Wang, and X. Peng. “Photochemical Instability of CdSe Nanocrystals Coated with Hydrophilic Thiols.” J. Am. Chem. Soc. 123: 8844, 2001.

33. B. Alberts, A. Johnson, J. Lewis, M. Raff, K. Roberts, and P. Walter. Molecular Biology of the Cell, 4th Ed., Garland Science, New York: 2002, pp. 742-745.

34. W.C.W. Chan and S. Nie. “Quantum Dot Bioconjugates for Ultrasensitive Nonisotopic Detection.” Science 281: 2016, 1998.

35. F. Osaki, T. Kanamori, S. Sando, T. Sera, and T. Aoyama. “A Quantum Dot Conjugated Sugar Ball and Its Cellular Uptake. On the Size Effects of Endocytosis in the Subviral Region.” J. Am. Chem. Soc. 126: 6520, 2004.

36. I. Pastan and M.C. Willingham, Eds., Endocytosis. Plenum Press, New York: 1985.

37. E.R. Kandel, J.H. Schwartz, and T.M. Jessel. Principles of Neuroscience, 3rd Ed., Appleton and Lange, Norwalk, Connecticut: 1991, pp. 752-753.

38. A.K. Gupta and A.S.G. Curtis. “Lactoferrin and Ceruloplasmin Derivitized Superparamagnetic Iron Oxide Nanoparticles for Targeting Cell Surface Receptors.” Biomats. 25: 3029, 2004.

39. Personal communication from A. Derfus, University of California at San Diego, Biomedical Engineering Department, February 16, 2004.

40. E.R. Kandel, J.H. Schwartz, and T.M. Jessel. Principles of Neuroscience, 4th Ed., McGraw Hill, New York: 2000, pp. 937-939.

41. S.L. Hart, A.M. Knight, R.P. Harbottle, A. Mistry, H.-D. Hunger, D.F. Cutler, R. Williamson, and C. Coutelle. “Cell Binding and Internalization by Filamentous Phage Displaying Cyclic Arg-Gly-Asp Containing Peptide.” J. Bio. Chem. 269(17): 12466, 1994.

42. S. Castel, R. Pagan, F. Mitjans, J. Piulats, S. Goodman, A. Jonczyk, F. Huber, S. Vilaro, and M. Reina. “RGD Peptides and Monoclonal Antibodies, Antagonists of Alpha(v)-Integrin, Enter the Cells by Independent Endocytotic Pathways.” Lab Invest. 81(12): 1615, 2001.

43. Z.A. Peng and X. Peng. “Formation of High-Quality CdTe, CdSe, and CdS Nanocrystals Using CdO as Precursor.” J. Am. Chem. Soc. 123: 183, 2001.

44. S.F. Wuister, I. Swart, F. van Driel, S.G. Hickey, and C. de Mello Donegá. “Highly Luminescent Water-Soluble CdTe Quantum Dots.” Nano Lett. 3(4): 503, 2003.

45. T. Yoshihara, N. Esumi, M. J. Humphries, and S. Imashuku. “Unique Expression of Integrin Fibronectin Receptors in Human Neuroblastoma Cell Lines.” Int. J. Cancer 51: 620, 1992.

46. C. Abdelghani-Jacquin, A. Abdelghani, G. Chmel, M. Kantlehner, and E. Sackmann. “Decorated Surfaces by Biofunctionalized Gold Beads: Application to Cell Adhesion Studies.” Eur. Biophys. J. 31: 102, 2002.

47. A. Shahar, J. de Vellis, A. Vernadakis, B. Haber, Eds., A Dissection and Tissue Culture Manual of the Nervous System. John Wiley and Sons, New York: 1989, pp. 155, 184, 225.

48. Gibco Product Information Sheet, “Neurobasal and Neurobasal –A Medium.” Form 3946, March 2003.

49. R.I. Freshnay. Culture of Animal Cells., 3rd Ed., John Wiley and Sons, New York: 1994, pp. 153-154.

50. M.L. Steigerwald and L.E. Brus. “Synthesis, Stabilization, and Electronic-Structure of Quantum Semiconductor Nanoclusters.” Annu. Rev. Mater. Sci. 19: 471, 1989.

51. B. Alberts, A. Johnson, J. Lewis, M. Raff, K. Roberts, and P. Walter. Molecular Biology of the Cell, 4th Ed., Garland Science, New York: 2002, p. 762.

52. P. Bongrand. "Adhesion of Cells," in Handbook of Biological Physics, vol. 1, R. Lipowsky and E. Sackmann, Eds., Elsevier, Amsterdam: 1995, p. 767.

53. E.R. Kandel, J.H. Schwartz, and T.M. Jessel. Principles of Neuroscience, 4th Ed., Appleton and Lange, Norwalk, Connecticut: 2000, p. 112.

54. J.J. Kakkassery, J.-P. Abid, M. Carrara, and D.J. Fermín. "Electrochemical and Optical Properties of Two Dimensional Electrostatic Assembly of Au Nanocrystals." Faraday Discuss. 125: 157, 2004.

55. B. Alberts, D. Bray, J. Lewis, M. Raff, K. Roberts, and J.D. Watson. Molecular Biology of the Cell, 3rd Ed., Garland Publishing, New York: 1994, p. 502.

56. J.-F. Liu, L.-G. Zhang, N. Gu, J.-Y. Ren, Y.-P. Wu, Z.-H., Lu, P.-S. Mao, and D.-Y. Chen. "Fabrication of Colloidal Gold Micro-Patterns Using Photolithographically Self-Assembled Monolayers as Templates." Thin Solid Films. 327-329: 176, 1998.

57. T. Zhu, X. Fu, T. Mu, J. Wang, and Z. Liu. "pH Dependent Adsorption of Gold Nanoparticles on p-Aminothiophenol-Modified Gold Substrates" Langmuir. 15: 5197, 1999.

58. W. Li, L. Huo, D. Wang, G. Zeng, S. Xi, B. Zhao, J. Zhu, J. Wang, Y. Shen, and Z. Lu. "Self-Assembled Multilayers of Alternative Gold Nanoparticles and Dithiols: Approaching to Superlattice." Col. Surf. A 175: 217, 2000.

59. A. Gole, S.R. Sainkar, and M. Sastry. "Electrostatically Controlled Organization of Carboxylic Acid Derivatized Colloidal Silver Particles on Amine-Terminated Self-Assembled Monolayers." Chem. Mater. 12: 1234, 2000.

60. V.L. Colvin, A.N. Goldstein, and A.P. Alivisatos. "Semiconductor Nanocrystals Covalently Bound to Metal Surfaces with Self-Assembled Monolayers." J. Am. Chem. Soc. 114: 5221, 1992.

61. T. Nakanishi, B. Ohtani, and K. Uosaki. "Fabrication and Characterization of CdS-Nanoparticle Mono- and Multilayers on a Self-Assembled Monolayer of Alkanedithiols on Gold." J. Phys. Chem. B. 102: 1571, 1998.

62. T. Torimoto, N. Tsumura, M. Miyake, M. Nishizawa, T. Sakata, H. Mori, and H. Yoneyama. "Preparation and Photoelectrochemical Properties of Two-Dimensionally Organized CdS Nanoparticle Thin Films." Langmuir. 15: 1853, 1999.

63. M. Miyake, T. Torimoto, M. Nishizawa, T. Sakata, H. Mori, and H. Yoneyama. "Effects of Surface Charges and Surface States of Chemically Modified Cadmium Sulfide Nanoparticles Immobilized to Gold Electrode Substrates on Photoinduced Charge Transfers." Langmuir. 15: 2714, 1999.

64. M.N. Wybourne, J.E. Hutchison, L. Clarke, L.O. Brown, and J.L. Mooster. "Fabrication and Electrical Transport Characteristics of Low-Dimensional Nanoparticle Arrays Organized by Biomolecular Scaffolds." Microelec. Eng. 47: 55, 1999.

65. C.A. Berven, M.N. Wybourne, L. Clarke, J.E. Hutchison, L.O. Brown, J.L. Mooster, and M.E. Schmidt. "The Use of Biopolymer Templates to Fabricate Low-Dimensional Gold Particle Structures." Superlattices and Microstructures. 27(5/6): 489, 2000.

66. S.R. Emory, W.P. Ambrose, P.M. Goodwin, and R.A. Keller. "Observing Single Molecule Chemical Reactions on Metal Nanoparticles." Proceedings of SPIE-The Society for Optical Engineering. 4258: 63, 2001.

67. F. Patolsky, Y. Weizmann, O. Lioubashevski, and I. Willner. "Au-Nanoparticle Nanowires Based on DNA and Polylysine Templates." Angew. Chem. Int. Ed. 41(13): 2323, 2002.

68. B. Alberts, D. Bray, J. Lewis, M. Raff, K. Roberts, and J.D. Watson. Molecular Biology of the Cell, 3rd Ed., Garland Publishing, New York: 1994, p. 993-994.

Chapter 6: Integration of Receptor-Scale Interfaces into Micron-Scale Technology[5]

Technologies that monitor the nerve membrane potential will be required for establishing the ability of quantum dot-receptor connections to modulate neuron response. Here, we discuss two possible measurement systems to demonstrate interface functionality. Both of these strategies create whole-cell, micron-scale connections between cells and electrical components. Integration of our interface with these systems would demonstrate compatibility of our device with existing technologies.

The first of these techniques, whole-cell clamping, measures membrane potential changes as small as a few mV. [1-2] However, the method has many limitations that make integration with quantum dot-receptor interfaces difficult. We discuss the theory of this system, general operation, and our attempts to integrate this method with our interface.

The second strategy, the microelectrode array (MEA), has been used extensively to make connections with individual neurons and tissue. Devices are manufactured using photolithography techniques, [2] which limit feature size based on the wavelength of light used. While devices are suitable for demonstrating interface functionality, additional technologies are required to create smaller scale interfaces. We developed a method of patterning MEAs using electron beam lithography, which can produce features as small as 10 nm. [3] Here, we describe our efforts to develop MEAs and their potential integration with quantum dot-receptor interfaces.

---

[5] Portions of this material have been previously published in the following reference: J.O. Winter, C.E. Flynn, T.S. Liu, A.M. Belcher, B.A. Korgel, C.E. Schmidt. "Semiconductor–Neural Interfaces." Proceedings of the Second Joint EMBS/BMES Conference and the 24th Annual Conference and the Annual Fall Meeting of the Biomedical Engineering Society, 2:1704, 2002.

6.1 LIMITATIONS TO INTEGRATION WITH EXISTING MEASUREMENT TECHNOLOGIES

We have developed several interfacing techniques that create connections between quantum dots and the nerve cell membrane (Chapters 4, 5). To demonstrate electrical connectivity of these junctions, measurement technologies are required. The two most commonly used strategies to monitor nerve membrane potential are whole-cell clamping and microelectrode arrays (Chapter 1, Section 1.2). These methods require micron-scale interactions with the entire cell body, and may prove difficult to integrate with our interface. [2] Additionally, the development of long-term devices incorporating micron-scale and receptor-scale connections is limited by the stability of quantum dot–receptor and cell–device junctions. Thus, integration of our interfaces with existing technologies is challenging.

6.1.1 Whole-Cell Clamping

The whole-cell clamping technique, a variation of patch-clamp, was first demonstrated by Sakmann and Neher in 1976. [1] The technique uses electrolyte-containing micropipettes to form close interfaces with cell membrane surfaces. The membrane is then broken through the application of gentle suction, allowing contact with the intracellular fluid. This electrical continuity allows voltage or current changes in the cell to be monitored. A microscope and micropositioners are required to place electrodes on cell surfaces, whereas a pre-amplifier, oscilloscope, and computer are necessary to monitor cell signals. The method is extremely sensitive, displaying signal strengths up to two orders of magnitude higher than MEAs, [1-2] and is designed to measure electrical properties of single cells.

Whole-cell clamping offers many benefits for the monitoring of receptor-scale interfaces. The method is extremely sensitive, permitting measurement of the small voltage changes that might be produced at quantum dot-receptor junctions. [1-2] Additionally, it is compatible with both recognition-molecule directed and tethered-film interfaces. Whole-cell clamping measures the properties of single cells; and through the use of the patch-clamp variation of this technique, could even monitor individual receptors. [1] However, this technique could not be used to create electrical devices. Whole-cell clamping is an invasive technique. Cells are impaled with microelectrodes and survive at most a few hours. Thus, long-term devices could not be constructed. Additionally, the technique is difficult to master and requires equipment than can cost in excess of $100,000 for a single recording chamber.

6.1.2 Microelectrode Arrays

Microelectrode arrays (MEAs) have been employed since the 1970's as prosthetic devices, measurement systems, and computational components. [2] They typically consist of a series of planar electrodes manufactured on glass or silicon substrates. The first arrays were manufactured on glass using micropatterned gold electrodes to monitor neuronal signals. [4-5] However, modern devices are fabricated on silicon using photolithography, insulated with polyimide [6] or silicon nitride [7-9], and consist of titanium/gold [6], titanium/iridium [7], or titanium/platinum electrodes [8].

These arrays interact with cells through induction, and signal strength is dependant upon distance. [10] Cell placement on electrode surfaces occurs through random cell culture or direct placement using micropositioners. This produces substantial separation distances, up to a 100 nm, [11] limiting the sensitivity of MEA devices. These

large separation distances result from the presence of the glycocalix, a sugar coating on the membrane surface. [12] Because of this limitation, MEAs are most commonly used to monitor action potentials, and not subthreshold potentials (i.e., potentials below the 15 mV change required for an action potential to fire). To increase sensitivity and encourage proper cell placement, surfaces are sometimes modified with biomolecules, including laminin [13], polylysine [14], and axonin-1 [15]. Even with biomolecule modification, the smallest separation distances displayed are ~ 40 nm. [15] Additionally, the presence of biomolecules produced changes in cell morphology and neurite outgrowth patterns that may not be desirable. [13-15] Thus, these coatings cannot ensure intimate electrical contact between the device and the cell.

Microelectrode arrays have some advantages to their incorporation with quantum dot–receptor devices. MEAs produce non-invasive, long-term interfaces with neurons, and have produced functional devices with lifetimes as long as 75 days. [9] They are easy to fabricate, requiring access to micron-scale fabrication facilities, and can even be obtained commercially.

However, several challenges persist to integration with quantum dot–receptor interfaces. Because arrays are fixed structures, tethered quantum dot films may prove difficult to construct on their surfaces. Films deposition before electrode patterning is complicated because the UV wavelengths (i.e. < 350 nm) used to create MEAs can destroy film adhesion molecules [16] and promote photooxidation of quantum dots. [17] Film application after electrode patterning is also challenging because uniform films will cover the electrodes and may interfere with their function, whereas patterned films will require alignment with underlying electrode structures. Also, the use of biomolecules to promote MEA adhesion may interfere with film formation. Thus, of the interfacing

strategies that we explored (Chapter 5), MEAs are most compatible with recognition-molecule directed binding.

The main limitation in the use of MEAs is their lack of sensitivity. Devices cannot detect subthreshold signals, [2] and the signals produced by quantum dot-interfaces may fall in this range. Sensitivity could be improved by increasing the charge density of electrode materials; however, no suitable material has yet been identified. [18] The second route to increase sensitivity is to increase the contact surface area of the electrode. This demands large electrodes (i.e., order of 100 μm) that may interact with multiple cell bodies, a requirement that negates the benefits of receptor-scale interfaces.

6.1.3 Comparison of Measurement Technologies

Given the limitations of both whole-cell clamping and MEA technologies, the best option is to optimize quantum dot–receptor interfaces using more sensitive technologies (i.e., whole-cell clamping), and then to incorporate these improved interfaces into MEAs for long-term applications. Using this strategy, whole-cell clamping will be employed to establish the ability of quantum dots to modulate neuronal receptors. The technique can be applied to either biorecognition-mediated or tethered-film interfaces, allowing maximal application of our previously developed systems. Interfaces can then be optimized to obtain junctions capable of producing action potentials. We present our initial efforts to integrate quantum dot-receptor interfaces with whole-cell clamping measurement technologies.

Once optimized, quantum dot-receptor interfaces can be combined with MEAs to produce long-term devices. One of the major limitations in developing devices is the large feature size used in photolithography. [2] These sizes are suitable for demonstrating the ability of quantum dots to modulate the nerve membrane potential, but will ultimately

need to be decreased to take advantage of a receptor-scale interface. We demonstrate an alternative MEA patterning technique, electron beam lithography (EBL), which can produce feature sizes as small as 10 nm. [3] This technique could ultimately be used to produce subcellular contact with receptor-scale interfaces. This approach, combining whole-cell clamping for optimization of quantum dot-receptor interfaces and MEAs for long-term integration, offers an excellent strategy for development of a composite device.

6.2 MATERIALS AND METHODS

6.2.1 Whole-Cell Clamping

6.2.1.1 Cell Culture

Rat neonatal cortical cells (RNCs) were harvested and cultured as described previously (Chapter 5, Section 5.2.2.2). Cells were isolated from 1-2 day old rat pups, dissociated, and plated on laminin and poly-D-lysine-prepared substrates. The size of the whole-cell clamping recording chamber required substrates of 12 mm-diameter or less. Cells were cultured on 12 mm, No. 1, coverslips in supplemented neurobasal medium (Chapter 5, Table VII). Medium was changed 24 hours after harvest, and every 2 days thereafter.

6.2.1.2 Preparing for Whole-Cell Clamping

Capillary pipettes (TW150F-4, World Precision Instruments) were prepared as electrodes. Pipettes were fire-polished in a Bunsen burner and pulled to target resistances of 1-5 MΩ (see below) using a Sutter Flaming-Brown P-97 pipette puller. Meanwhile, aCSF (Chapter 5, Table VIII) was introduced into the recording chamber. The solution was continuously cycled using a perfusion pump for introduction and a vacuum aspirator

for removal. The aCSF solution was oxidized by bubbling with 5% CO_2 / 95% O_2 for 10-15 minutes before exposure to cells, and continuously thereafter.

Next, pipettes with electrode resistances in the target range (i.e., 1-5 mΩ) were identified. First, pipettes were filled with intracellular solution (Table IX) and mounted on the electrode holder, taking care not to damage the AgCl wire. Then, the electrode tip was slowly lowered into the aCSF solution, at which point the amplifier voltage declined. After re-zeroing, a 5 mV square wave was applied using the amplifier seal-test function, and the resulting change in current was determined using an oscilloscope. The electrode resistance was calculated using Ohm's law (i.e., V=IR, where V= 5 x 10^{-3} for the voltage step, I = the measured current, and R is the electrode resistance). Only electrodes with resistance values between 1-5 MΩs were used.

Table IX: Intracellular Solution

Component[1]	Concentration[2]
Potassium Methane Sulfonate	135 mM
NaCl	12 mM
EGTA	0.5 mM
HEPES	10 mM
Mg-ATP	2 mM
TRIS-GTP	0.3 mM

[1]Obtained from Sigma
[2]In distilled, deionized water

6.2.1.3 Monitoring Membrane Potential

An Olympus BX-50WI focusing head microscope with infrared differential interference optics (IR-DIC) and epifluorescence was employed to visualize cells, while electrical signals were monitored using Axon Instruments 200B patch clamp amplifier

and Digidata data acquisition system. First, 12-mm coverslips containing cells were placed in the microscope recording chamber and visualized with a 4X objective. Cells were centered in the viewing area with an S and D Instruments MC1000 course manipulator connected to the translational stage. An electrode was attached to the electrode holder and lowered into solution. Using the 4X objective and a programmable micromanipulator (Sutter Instruments, MP-285), the electrode was positioned next to a target cell. Then, switching to a 40X water immersion objective, the electrode was lowered onto the cell until a slight indentation in its surface was apparent.

Next, a 5 mV square wave was applied using the amplifier seal test function. Gentle suction to the cell surface was given by mouth, using tubing attached to the electrode holder. This produced a decline in the current, indicating the presence of a seal. When a seal was obtained, a holding voltage of -60 mV was applied, until current dropped to < 0.020 nA, indicating the formation of a strong (i.e., GΩ) seal. Capacitance was reduced using the amplifier capacitance adjustment knob, and 60-cycle line noise was diminished with a Humbug (Quest Scientific).

Then, additional suction was applied to break open the cell membrane, producing an increase in current. Control of the cell membrane potential was then transferred to the computer, and was modulated and monitored using ClampX software (Axon Instruments). Cells were exposed to negative voltage steps, to determine the access resistance (i.e., the resistance between the interior of the pipette and the cell cytoplasm). Access resistances were calculated in a similar manner to electrode resistance. A known voltage step was applied, the resulting current measured, and the resistance calculated using Ohm's law. Resistances less than 40 MΩ (e.g., average 10-20 MΩ) were used to ensure a good seal. Then, the cell was switched from voltage clamp (i.e., voltage

controlled by computer, monitoring cell current) to current clamp (i.e., current controlled by computer monitoring cell voltage) mode for monitoring the static membrane potential.

6.2.1.4 Optical Excitation

Optical excitation of the nanoparticles was supplied at the excitation wavelength of the nanoparticles (e.g., 362 nm for CdS pH 7 control particles (see Chapter 3)) using a computer controlled monochromator and delivered via liquid light guide (Cairn Instruments, London, UK). Cells placed in a BX-50WI microscope (Olympus, Tokyo, Japan) fitted with a Fura-2 fluorescence cube set (Omega Optical, Brattleboro, VT), which lacked an excitation filter. This allowed excitation wavelengths to be tuned, while providing visualization of fluorescence.

6.2.2 Microelectrode Array

6.2.2.1 Array Design

Arrays were manufactured on 1 cm square silicon chips cut from 4-6 inch wafers with thermally-grown 100 nm SiO_2 layers obtained from Wafer World. Arrays were composed of four 20 x 20 micron square electrodes attached to a triangular linker arm (Figure 58). This electrode size was chosen because the average cell body size for RNCs is ~20 μm, allowing single cell contact. The bond pads consisted of 2 x 2 mm squares attached to 2 x 1 mm linker arms that terminated in the linker-electrode structure. Both the triangular and rectangular linker structures were insulated with poly (methyl methacrylate) (PMMA), which also served as the EBL resist. Ultimately, the MEA structures will be incorporated into future quantum dot–receptor devices (Figure 59).

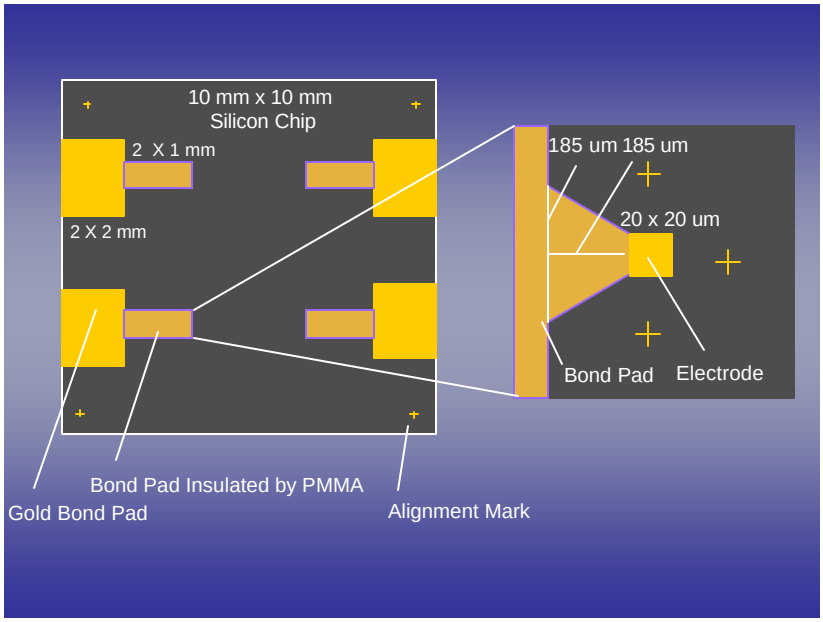

Figure 58: Microelectrode Array Design.

A four-electrode microelectrode array was created on a silicon substrate. Electrodes were 20 x 20 micron square and were connected to 2 x 2 mm bond pads.

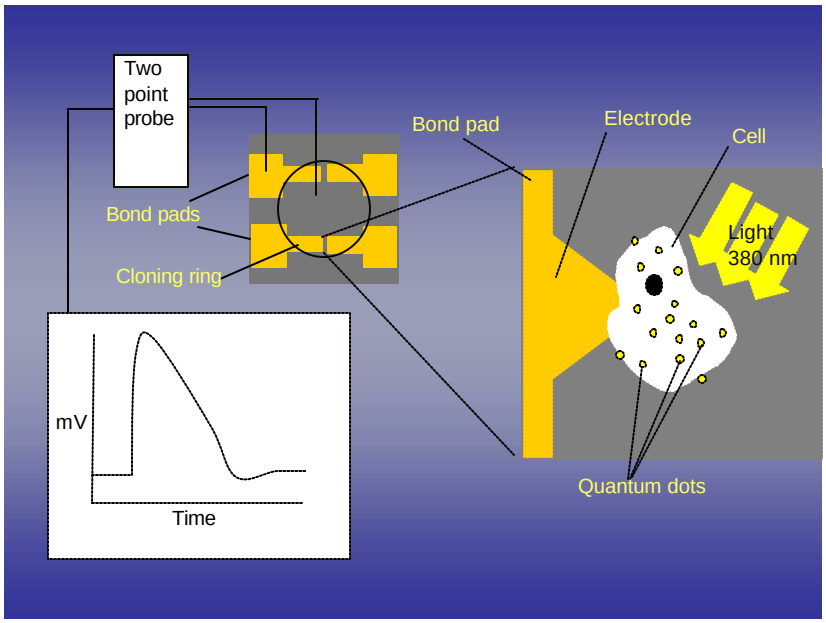

Figure 59: Microelectrode Array Device.

Ultimately, MEAs will be integrated with quantum dot–receptor interfaces through direct cell culture. Cloning rings glued on MEA surfaces isolate cells from bond pads, which are connected to a two-point probe for monitoring. Quantum dots are applied to cell surfaces using biorecognition molecule-directed binding, and are excited externally with either a laser or UV lamp.

Arrays were manufactured in a three-step process. First, bond pads were patterned using metal evaporation (Section 6.2.2.2). Gold was deposited onto silicon chips through a stainless steel mask fabricated using a drill bit. Then, electrodes were attached to the bond-pads using PMMA deposition (Section 6.2.2.3), EBL (Section 6.2.2.4), metal evaporation (Section 6.2.2.2), and PMMA-metal removal (Section 6.2.2.5). Finally, the electrodes were de-insulated using PMMA deposition (Section 6.2.2.3) and EBL (Section 6.2.2.4). Arrays were visualized using SEM (Section 6.2.2.7).

6.2.2.2 Metal Deposition

Evaporation was used to produce both bond pads and electrodes. Chips were placed in a Denton DV502 Vacuum Chamber Evaporator for gold deposition. Contact with a conductive surface was required to prevent overheating. The evaporator was placed under vacuum until pressures of at least 4 x 10^{-6} torr were achieved, typically 1.5 hours. Then, 10 nm of chromium was deposited (deposition current ~60 A) from a Cr-plated tungsten-rod source (RD Mathis Company), followed by 200 nm of gold deposited (deposition current ~100 A) from gold wire (Hauser and Miller). Thicknesses were determined using an XTM/2 deposition monitor with a quartz crystal transducer (Kurt J. Lesker, Co.).

6.2.2.3 PMMA Deposition

Silicon chips were prepared for PMMA deposition by sonicating for 10 minutes in successive solutions of acetone, ethanol, and distilled, deionized water (ddH_2O). Chips were blown dry with nitrogen or argon. Then, 100 µL of 4% or 6% 950,000 MW PMMA

in chlorobenzene (Microchem) was applied using a P-6204-A spin-coater (Specialty Coating Systems) at 3000 rpm, for 60 s. For electrodes, 4% PMMA was used, producing thicknesses of ~400 nm, as measured with an Alphastep 200 profilometer (KLA-Tencor). The thickness was optimized to be sufficiently large to permit lift-off, but small enough to minimize charging effects in the e-beam. For insulation, 6% PMMA was used, producing film a thickness of ~1 μm. Thick films were required to provide insulation between the gold wires and the conductive cell culture medium. Following spin coating, both PMMA layers were annealed at 170ºC for one hour.

6.2.2.4 Electron Beam Lithography (EBL)

Annealed samples were placed in the sample chamber of a Raith 50 EBL unit with LaB6 source. The chip was aligned using its edges (electrodes) or pre-existing alignment marks (insulation; Figure 58). The instrument was focused and stigmation adjusted until a round spot size of ~100 nm was obtained. Then, the pattern was written using a current of 100 pA, 20 kV accelerating voltage, 6 pixel step size, 220 $\mu A/cm^2$ dose (for PMMA resist), and a 45 s exposure time. Patterns were generated in 400 μm write-fields. Following e-beam exposure, current was reduced to 10 pA and a single image of one write field was obtained to confirm e-beam development of the PMMA resist.

Then, the chip was retrieved from the sample chamber and placed in a 1:3 methyl isobutyl ketone (MIBK):isopropanol (IPA) solution for 45 seconds to remove developed PMMA. Next, the chip was exposed to an absolute solution of IPA for at least 1 minute to quench the reaction. Chips were blown dry with compressed air, nitrogen, or argon. At this point, the chip was viewed using a scanning electron microscope (SEM, Section 6.2.2.7) or stereomicroscope to confirm the presence of the pattern.

6.2.2.5 PMMA-Metal Removal

Metallization (Section 6.2.2.2) produces a solid layer of chromium/gold on top of the mask. To remove the unnecessary gold and mask, the chips were sonicated in acetone for 5 minutes. Longer sonication times interfered with gold adhesion to the silicon. Removal of PMMA/gold was confirmed using SEM (Section 6.2.2.7). Incomplete removal typically resulted from an inadequate resist thickness, which allowed the formation of bridges between gold on the mask and gold within the patterned regions.

6.2.2.6 Cell Culture

To demonstrate device compatibility with cells, SK-N-SH cells were cultured on a PMMA test pattern (PMMA = 2%, 60 nm thickness) following the previously described protocol (Chapter 4, Section 4.3.3.6). To prepare chips for cell culture, they were first UV irradiated overnight. Then, freshly passaged SK-N-SH cells were plated on their surfaces at standard densities (~1 X 10^4 cells/cm^2). Cells were fed every two days with DMEM medium, supplemented with 10% FBS, and 1% penicillin-streptomycin. After four days, cells were observed using SEM (Section 6.2.2.7)

6.2.2.7 SEM

Images of MEAs were obtained with a LEO 1530 scanning electron microscope (SEM). Accelerating voltages of 2 kV and 10 kV were used to view cells and electrodes, respectively. Electrode samples did not require preparation and were viewed after electrode patterning and resist de-insulation to confirm MEA creation. However, cell-coated chips required additional processing for SEM visualization. Cells were fixed and dehydrated to provide compatibility with the SEM vacuum chamber. Cells cultured on

chip surfaces were rinsed twice with PBS and fixed through exposure to 3.7% formaldehyde solution (Table X) for 15 minutes. Then, cells were dehydrated using a series of increasing ethanolic solutions in water (Table XI). Remaining absolute ethanol was removed through overnight evaporation in a standard chemical hood. To increase electron density and allow for SEM viewing, cells were plated with chromium using a deposition chamber. Cells cultured on chips were then viewed using SEM to confirm adhesion and spreading on PMMA surfaces.

Table X: 3.7% Formaldehyde Solution

Component[1]	Amount
Paraformaldehyde	0.8 g
Sucrose	0.8 g
1 M NaOH	133 µL
PBS	10 mL

[1]Heat solution to 60 ºC to dissolve paraformaldehyde

Table XI: Cell Dehydration Protocol

Solution	Time
Water	30 minutes
Water	30 minutes
30% Ethanol	10 minutes
30% Ethanol	10 minutes
60% Ethanol	10 minutes
90% Ethanol	10 minutes
95% Ethanol	10 minutes
100% Ethanol	10 minutes
100% Ethanol	10 minutes

6.3 RESULTS AND DISCUSSION

6.3.1 Whole-Cell Clamping

Initially, we attempted to perform whole-cell clamping measurements using unlabeled SK-N-SH neuroblastoma cells. While we were able to generate action potentials through computerized voltage steps (Figure 60), cells died shortly after electrical stimulation. It is believed that this occurred because immortalized cell lines do not necessarily display the normal complement of ion channels. [19-21] Thus, the voltage steps required to produce action potential are excessive and damaging. Given these results, SK-N-SH cells are not a good model system for evaluating quantum dot-receptor interfaces, as they would require substantially more stimulation than normal to produce a response.

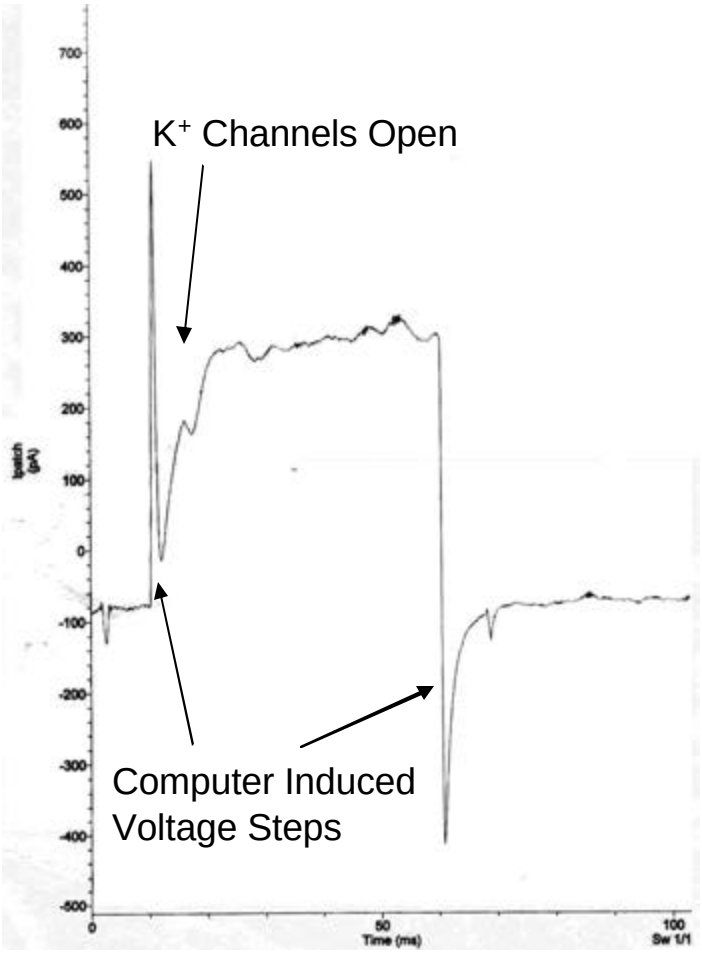

Figure 60: Whole-Cell Clamping Measurement of SK-N-SH Neuroblastoma Cell.

A positive voltage step was applied to an SK-N-SH neuroblastoma cell, producing an action potential. Initial spikes indicate capacitive charging of the membrane surface, followed by the opening of K^+ channels. The cell remains at this elevated voltage until the computer stimulation is removed. Then, the cell returns to resting potential.

To address these limitations, we selected a different cell type, rat neonatal cortical cells (RNCs). Our efforts to adapt quantum dot interfacing to this cell type were described in detail elsewhere (Chapter 5). The major limitations of integrating those interfaces with whole-cell clamping have been the sensitivity of the cells and the lack of interface longevity. RNC cells, as a primary cell line, are not as hardy or adhesive as immortal cells. [22] It can take several days for cells to extend neurites and as much as a week to form good contacts with the culture dish (or coverslip).

For recognition molecule directed binding this is not problematic. Cells may be cultured for several days on coverslips, and quantum dots can be applied just prior to

whole-cell clamping experiments. However, since endocytosis occurs within 30 minutes of labeling (Chapter 5, Section 5.3.1.5) and the formation of whole-cell clamping connections to a viable cell requires 20 minutes, the window for data collection is extremely short.

An obvious solution would be to attach quantum dots to ion channels directly, as these are recycled at a low rate. [23] There are many commercially available antibodies to ion channels; however, we have been unable to locate ones that bind the extracellular surface without activating or inactivating the channel. This is most likely because the extracellular surface of ion channels is highly glycosylated, [24] reducing the number of potential antibody binding sites. Additionally, we have been unable to identify a peptide that binds channels without producing activation or inactivation. This is not surprising as the majority of ion channel research is directed to pharmacology; most researchers are attempting to chemically modulate ion channel behavior and seek peptides for this purpose. [e.g., 25-28] One possibility would be to generate genetically engineered ion channels that display an adjacent binding site that could be targeted with an antibody (e.g. green fluorescent protein [29]). Alternatively, techniques like phage display [30] could be used to identify suitable binding peptides.

Tethered-films offer only a slight improvement to recognition molecule directed binding. The primary difficulty of tethered quantum dot films is their lack of stability in cell culture (Chapter 5, Section 5.3.3.5). Our films demonstrated good stability in medium, but were intact for only 1-3 days in culture. Because RNCs require 5-7 days to form good focal adhesions to the culture substrate, it is difficult to conduct whole-cell clamping experiments in this time window.

Improving film stability is critical for obtaining satisfactory measurements. Film stability could be increased through a variety of approaches. Particles that are more stable

to oxidative conditions encountered in culture could be employed (e.g., CdSe [31]). Ligand affinity to the quantum dot surface could be increased, or protective shells could be applied to quantum dot surfaces. [17] However, the use of shells is limited as they must not increase the separation distance between the particle core and the receptor, and they must not interfere with electrical signal conduction. Thus far, we have been unable to produce an interface with stability sufficient for whole-cell clamping measurements; however, optimization of either recognition molecule directed binding or tethered films should produce the desired longevity.

6.3.2 Microelectrode Array

6.3.2.1 Electrodes

As discussed previously (Section 6.1.3), MEAs are unlikely to measure low voltage potential changes that might be encountered during quantum dot–receptor interface optimization. However, they provide an excellent platform for long-term device development. To demonstrate the potential to integrate quantum dot–receptor interfaces with MEA technologies, we designed and fabricated four-electrode MEAs using electron beam lithography (EBL). EBL offers substantial advantages over photolithography. Most notably, substantially smaller feature sizes can be obtained (i.e., 10 nm for e-beam vs. 90 nm for best practice photolithography [3]). Thus, future devices could be manufactured with components that are capable of subcellular interfacing, unlike the micron-scale feature sizes currently used. Additionally, EBL offers ease of fabrication because the resist can be used as an insulator without the need of additional processing steps. [PMMA resists display a similar dielectric constant to polyimide, a typically used insulating

material [32].] Our electrode design consisted of a three-step process (6.2.2.1) that produced de-insulated gold electrode surfaces (Figure 61).

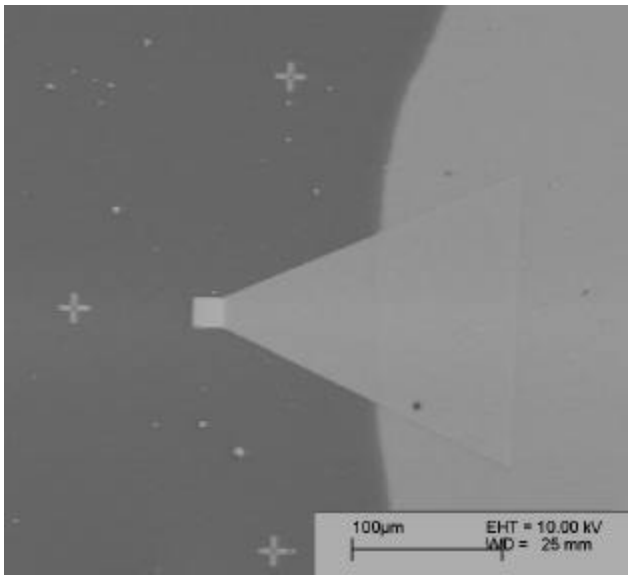

Figure 61: SEM Image of EBL Patterned MEA Electrode.

Gold electrodes were patterned using EBL and metal deposition. The electrode surface (square) appears brighter than surrounding structures because it is de-insulated. Remaining structures (i.e. triangular linker arm and bond pad (right)) are insulated with PMMA. Crosses surrounding the electrode are alignment marks, and are not electrically connected.

6.3.2.2 Cell Culture on MEAs

To demonstrate the ability of PMMA-insulated electrodes to support cell culture, we plated SK-N-SH cells on a test pattern consisting of boxes and lines. Cells were grown in culture for four days, fixed, dehydrated and observed (Section 6.2.2.6). Cells were able to adhere and spread on PMMA insulated surfaces (Figure 62). Additionally, cells demonstrated an affinity for the test pattern, extending neurites along the lines of exposed silicon. Cracking of the PMMA insulation resulted from both the thin layer used to test cell compatibility (i.e., 60 nm thicknesses) and the drying process used to prepare cells for SEM. Cracking was not demonstrated in patterns with the 1 µm thicknesses used for insulation. Thus, PMMA-insulated surfaces were found to support cell culture and present a suitable insulating material for wire and bond pad surfaces.

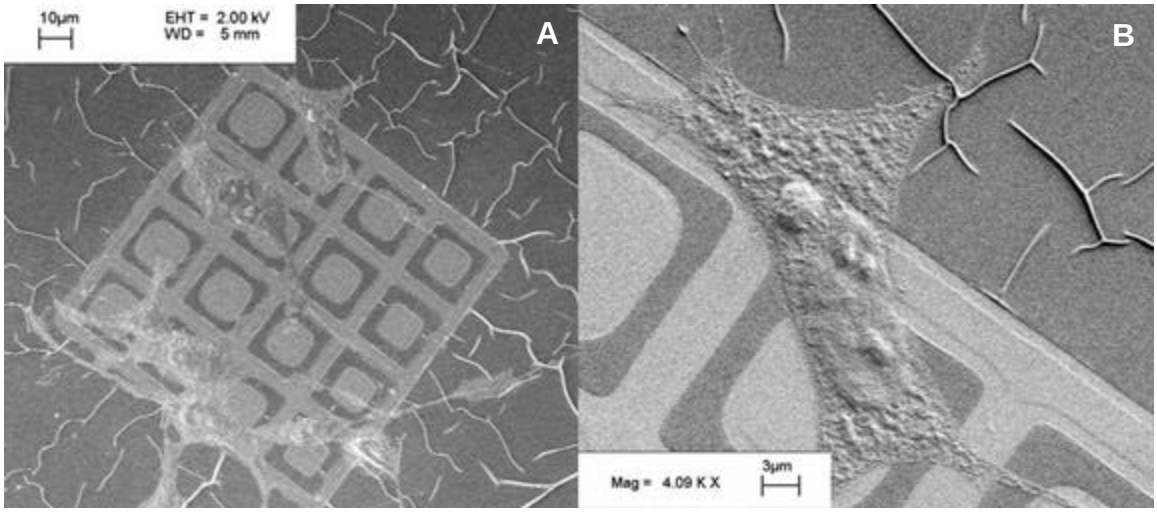

Figure 62: Cell Culture on MEAs.

(A,B) SEM images of SK-N-SH neuroblastoma cells grown on a test pattern of lines and squares. Dark regions are PMMA, light regions are underlying silicon. Cells adhere and spread on PMMA surfaces.

6.4 Summary of Integration Challenges

These results demonstrate the difficulty of incorporating quantum dot–receptor interfaces with micron-scale neuroelectronic devices. The most sensitive technique, whole-cell clamping, requires stable quantum dot-cell junctions that are challenging to obtain. Directly-labeled cells quickly internalize particles, while tethered-films do not remain intact long enough to support optimal cell adhesion. Optimization of interfacing technologies can address these limitations; however, whole-cell clamping is invasive [1] and cannot be used to create long-term neuroelectronic devices. On the other hand, MEAs, which can be used over months, [9] do not have the sensitivity to detect subthreshold signals. [2] Thus, they cannot be used for device optimization. Additionally, the creation of tethered films on MEA surfaces is difficult, as MEA patterning can interfere with film formation. [16-17] Further, MEAs do not currently display feature

sizes that take advantage of receptor-scale interfacing. [2] We have demonstrated an alternative patterning technique, electron beam lithography that could be used to produce cell-culture compatible MEAs with small feature sizes. However, development of tighter cell-electrode contacts or novel materials is required to increase the sensitivity of the system. Ultimately, these findings demonstrate that the creation of receptor-scale interfaces integrated with current micron-scale technologies is a challenging process.

6.5 CONCLUSIONS

Measurement systems are required to demonstrate the functionality of quantum dot–receptor interfaces. The two most commonly used technologies, whole-cell clamping and MEAs [1-2], depend upon micron-scale contacts with cell surfaces for measurement. Integration of both systems with our interface is difficult. Whole-cell clamping displays excellent sensitivity, but is invasive and requires a stable interface. [1] MEAs cannot detect subthreshold signals [2] and are not compatible with tethered film quantum dot interfaces. [16-17]

To measure electrical connectivity of quantum dot-receptor interfaces, we attempted to integrate recognition-molecule directed and tethered-film junctions with whole-cell clamping systems. Our initial efforts were unsuccessful, primarily because of poor quantum dot–cell interface stability. However, recognition molecule directed binding could be improved by conjugation to fixed receptors, while the stability of tethered-films can be increased through greater passivation of the quantum dot surface. [17] Thus, whole-cell clamping can ultimately be used to measure interface functionality.

Additionally, we developed a system to support the future integration of quantum dot–receptor interfaces into long-term devices. We fabricated four-electrode MEAs using electron beam lithography, which can produce feature sizes as small as 10 nm. [3] These

small sizes will allow for the development devices that can take full advantage of the receptor-scale interface. Thus, we have addressed some of the initial limitations to creating integrated receptor-scale neuroelectronic systems.

6.6 REFERENCES

1. E. Neher and B. Sakmann. “Single-Channel Currents Recorded from Membrane of Denervated Frog Muscle Fibres.” Nature. 260(5554):799, 1976.

2. W.L.C. Rutten. “Selective Electrical Interfaces with the Nervous System.” Annu. Rev. Biomed. Eng. 4: 407, 2002.

3. G.R. Brewer, Ed., Electron Beam Technology in Microelectronic Fabrication. Academic Press, New York: 1980.

4. C.A. Thomas, P.A. Springer, G.E. Loeb, Y. Berwald-Netter, and L.M. Okun. “A Miniature Microelectrode Array to Monitor the Bioelectric Activity of Cultured Cells.” Exp. Cell. Res. 74: 61, 1972.

5. G.W. Gross. “Simultaneous Single Unit Recording In Vitro with a Photoetched Laser Deinsulated Gold Multimicroelectrode Surface.” IEEE Trans. Biomed. Eng. 26: 273, 1979.

6. S.A. Boppart, B.C. Wheeler, and C.S. Wallace. “A Flexible Perforated Microelectrode Array for Extended Neural Recordings.” IEEE Trans. Biomed. Eng. 39(1): 37, 1992.

7. L.J. Breckenridge, R.J.A. Wilson, P. Connolly, A.S.G. Curtis, J.A.T. Dow, S.E. Blackshaw, and C.D.W. Wilkinson. “Advantages of Using Microfabricated Extracellular Electrodes for In Vitro Neuronal Recording.” J. Neurosci. Res. 42: 266, 1995.

8. G.T. Kovacs, C.W. Stroment, and J.M. Rosen. “Regeneration Microelectrode Array for Peripheral Nerve Recording and Stimulation.” IEEE Trans. Biomed. Eng. 39(9): 893, 1992.

9. T.D. Strong, H.C. Cantor, and R.B. Brown. “A Microelectrode Array for Real-Time Neurochemical and Neuroelectrical Recording in Vitro.” Sens. Actuators A. 91: 357, 2001.

10. P. Fromherz. “Neuroelectronic Interfacing: Semiconductor Chips with Ion Channels, Nerve Cells and Brain,” in Nanoelectronics and Information Technology, R.Waser, Ed., Wiley-VCH, Berlin: 2003, pp. 781-810.

11. P. Fromherz. “Electrical Interfacing of Nerve Cells and Semiconductor Chips.” Chem. Phys. Chem. 3: 276, 2002.

12. B. Alberts, D. Bray, J. Lewis, M. Raff, K. Roberts, and J.D. Watson. Molecular Biology of the Cell, 3rd Ed., Garland Publishing, New York: 1994, p. 502.

13. J.P. Ranieri, R. Bellamkonda, E.J. Bekos, A. Gardella, H.J. Mathieu, L. Ruiz, P. Aebischer. “Spatial Control of Neuronal Cell Attachment and Differentiation on Covalently Patterned Laminin Substrates.” Int. J. Dev. Neurosci. 12(8): 725, 1994.

14. C.D. James, R. Davis, M. Meyer, A. Turner, S. Turner, G. Withers, L. Kam, G. Banker, H. Craighead, M. Isaacson, J. Turner, and W. Shain. “Aligned Microcontact Printing of Micrometer-Scale Poly-L-Lysine Structures for Controlled Growth of Cultured Neurons on Planar Microelectrode Arrays.” IEEE Trans. Biomed. End. 47(1): 17, 2000.

15. H. Sorribas, D. Braun, L. Leder, P. Sonderegger, and L. Tiefenauer. “Adhesion Proteins for Tight Neuron-Electrode Contact.” J. Neurosci. Methods. 104: 133, 2001.

16. J.-F. Liu, L.-G. Zhang, N. Gu, J.-Y. Ren, Y.-P. Wu, Z.-H., Lu, P.-S. Mao, and D.-Y. Chen. “Fabrication of Colloidal Gold Micro-Patterns Using Photolithographically Self-Assembled Monolayers as Templates.” Thin Solid Films. 327-329: 176, 1998.

17. A.M. Derfus, W.C.W. Chan, and S.N. Bhatia. “Probing the Cytotoxicity of Semiconductor Quantum Dots.” Nano Lett. 4(1): 11, 2004.

18. D. Popovic, T. Gordon, V.F. Rafuse, and A. Prochazka. “Properties of Implanted Electrodes for Functional Electrical Stimulation.” Annals Biomed. Eng. 19(3): 303, 1991.

19. R.I. Freshnay. Culture of Animal Cells, 3rd Ed., John Wiley and Sons, New York: 1994, p. 12.

20. N. Tokutomi, Y. Tokutomi, K. Fukunaga, E. Miyamoto, and K. Nishi. “Bradykinin-Evoked Non-Specific Cationic Current in Neuroblastoma Glioma Hybrid (NG108-15) Cells and its Down-Regulation Through Differentiation.” Brain Res. 657: 202, 1994.

21. M. Fatehi, A.L. Harvey, and E.G. Rowan. “Characterization of the Effects of Depolarizing Toxins on Nerve Terminal Action Potentials: Apparent Block of Presynaptic Potassium Currents.” Toxicon. 36(1): 115, 1998.

22. R.I. Freshnay. Culture of Animal Cells, 3rd Ed., John Wiley and Sons, New York: 1994, p. 335.

23. E.R. Kandel, J.H. Schwartz, and T.M. Jessel. Principles of Neuroscience, 4th Ed. McGraw Hill, New York: 2000, pp. 937-939.

24. O. Sokolova. “Structure of Cation Channels, Revealed by Single Particle Electron Microscopy.” FEBS Lett. 564(3): 251, 2004.

25. W.A. Catterall. “Molecular Mechanisms of Gating and Drug Block of Sodium Channels.” Novartis Found Symp. 241: 206, 2002.

26. G.M. Nicholson, M.J. Little, and L.C. Birinyi-Strachan. “Structure and Function of Delta-Antracotoxins: Lethal Neurotoxins Targeting the Voltage-Gated Sodium Channel.” Toxicon. 43(5): 587, 2004.

27. G.I. Hatton and Z. Li. “Mechanisms of Neuroendocrine Cell Excitability.” Adv. Exp. Med. Biol. 449: 79, 1998.

28. H.R. Guy and S.R. Durell. “Structural Models of Na^+, Ca^{2+}, and K^+ Channels.” Soc. Gen. Physiol. Ser. 50: 1, 1995.

29. See for example: L.M. Diaz, R. Maiya, S.L. Boehm, H.A. Scott, S.E. Bergeson, R.D. Mayfield, and R.A. Morrisett. “Sindbis Viral Delivery of eGFP Labeled Dopamine D1 Receptors into Primary Cultured Neurons, Brain Slice Culture and in vivo.” Res. Soc. Alcoholism Abstr., 27: 93, 2003.

30. C.F. Barbas, D.R. Burton, J.K. Scott, and G.J. Silverman. Phage Display: A Laboratory Manual. Cold Spring Harbor Laboratory Press, Cold Spring Harbor, New York: 2001.

31. M.L. Steigerwald and L.E. Brus. “Synthesis, Stabilization, and Electronic-Structure of Quantum Semiconductor Nanoclusters.” Annu. Rev. Mater. Sci. 19: 471, 1989.

32. R. Bartnikas, R.M. Eichhorn, Ed., Electrical Properties of Solid Insulating Materials. American Society for Testing and Materials, Philadelphia: 1983, p. 172.

Chapter 7: Conclusions and Future Directions

7.1 Summary of Dissertation

Current neuroelectronic interfaces (e.g., microelectrode arrays and whole-cell clamping) have been used as methods to study neuron function and signaling, prosthetic devices, and computational systems. However, these micron-scale devices fail to take advantage of cell-signaling capabilities, which occur primarily through nanometer-sized proteins on the membrane surface. Present technologies cannot be manufactured in this size range, and alternative strategies are needed for receptor-scale interfacing.

We have presented one possible system, utilizing semiconductor quantum dots, to create these interfaces. Quantum dots are small crystalline solids with diameters less than the Bohr exciton length. They exhibit quantum confinement of the exciton, which produces interesting optical and electrical phenomena. Among these features, quantum dots can convert light into electrical signals through the formation of a dipole moment, electron transfer, and heat production. Additionally, quantum dots exhibit fluorescent emission with high quantum yields, narrow bandwidths, continuous excitation past the onset of absorption, and photostability. Because of these advantages, quantum dots have been used as components of both optoelectronic and biological systems. Our interface endeavors to combine these two applications to create a biological system with electrical capabilities. Although several modes of interaction between quantum dots and cells are possible, we believe that the electric field produced by the transition dipole moment is of suitable magnitude to modulate ion channels. Thus, utilizing optically excited quantum dots, it may be possible to modulate neuronal signaling.

To test our hypothesis, we created CdS quantum dots through arrested precipitation in aqueous media. We systematically varied our synthesis conditions to

identify particles with electrical properties optimal for the neuroelectronic interface (**Chapter 3**). Specifically, we examined the effect of increased reactant concentrations, altered reactant and ligand ratios, ligand length and charge, and pH on the resultant quantum dot absorbance and photoluminescence spectra. These optical spectra have been linked to the desired electrical properties for our interface. We found that reactant concentrations have little effect on the size and fluorescent emission wavelengths of the quantum dots produced, but particle stability in aqueous solution was reduced at higher concentrations. This is most likely a result of charge screening caused by increased salt concentrations, but could also occur because of increased solute concentrations in the fluid. On the other hand, reactant and ligand ratios, ligand length, and pH all produced changes in particle size and fluorescence. Larger particles were created at the smallest reactant ratios and ligand length, and at the highest ligand ratio and pH. Quantum yield was maximal at intermediate sizes, possibly indicating the formation of thermodynamically stable complexes that mediate controlled particle growth. Our results for ligand charge supported this theory. Quantum dot size trends for acid, base, and neutral ligands resembled published equilibrium data for aqueous CdS complexes. These equilibrium complexes may serve as intermediates to quantum dot formation. Based on our synthesis results, we determined that intermediate-sized particles with maximal quantum yields were most suitable for development of a neuroelectronic interface.

Next, we created close-range interactions between quantum dots and SK-N-SH neuroblastoma cells using biorecognition molecules (**Chapter 4**). Antibodies were coupled to quantum dot surfaces through the formation of amide bonds, and their presence was confirmed with UV-visible absorbance spectra. Antibody-quantum dot conjugates were exposed to cells, producing a fluorescent signal at their receptor targets. The conjugation chemistry for antibody linkage resulted in the formation of aggregates

and produced ~15 nm (per antibody used) separation distances between cells and the particles. To create more intimate contacts with cell surfaces, we utilized thiolated-peptides as quantum dot capping ligands. These peptides contained a recognition sequence capable of binding cell surface receptors. The presence of peptides was confirmed using UV-visible absorbance spectra, fluorescence anisotropy, and FTIR spectroscopy. Quantum dot-peptide conjugates exposed to cells produced much more discrete and intimate binding than the antibody system. Thus, we demonstrated two routes to forming nanoparticle interfaces with cell surfaces at close-proximity.

However, the interfaces were developed using an immortal cell line, which does not possess normal neuronal signaling patterns and also proliferates continuously. These features are not favorable for neuroelectronic device formation; therefore, we optimized our interface for use with a primary cell line: rat neonatal cortical cells (RNCs) (**Chapter 5**). These optimizations revealed the extreme sensitivity of primary cells to environmental conditions and potential toxicity of quantum dots that was not apparent in studies employing immortalized cell lines, which are more robust than primary cell lines. Additionally, we found that quantum dots bound to cell surface receptors are likely to undergo receptor-mediated endocytosis, which can begin in as little as 5 minutes. Thus, the use of recognition-molecule directed binding for quantum dot attachment is limited to those receptors that are not recycled or are recycled at extremely low rates. Although ion channels are in this category, we have had great difficulty in identifying a suitable molecule to produce external binding that does not also modulate channel behavior.

Therefore, we identified two alternative systems, using non-specific interactions, to form quantum dot–receptor interfaces (**Chapter 5**). The first of these employed non-specific affinities between quantum dots and cells to create delocalized binding of the membrane surface. This binding is believed to be the result of reduced ligand passivation

at the particle core. While binding was achieved, endocytosis occurred for these particles as well, limiting the application of this method in long-term neuroelectronic interface formation. Thus, we developed a third system using tethered quantum dot films to produce connections with cell surfaces. These films demonstrated good stability in cell culture medium, but exhibited diminished, red-shifted fluorescence when exposed to cells. This appears to be the result of Ostwald ripening, which may be accelerated by oxidizing agents released from cells. Additional nanoparticle passivation should produce more stable surfaces. Thus, two additional modes of nanocrystal-cell binding were created, one of which was suitable for neuroelectronic interface formation.

Finally, we attempted to confirm electrical continuity of our interfaces with two existing micron-scale measurement technologies (**Chapter 6**), whole-cell clamping and microelectrode arrays (MEAs). Measurement of our interfaces with the whole-cell clamping measurement technique proved difficult because it is an invasive, time-consuming process that requires stable interactions between quantum dots, cells, and the substrate. Our attempts to create stable interactions were limited at the quantum dot–cell interface and we suggested possible improvements. Additionally, we evidenced the potential to integrate our interface into a long-term device using the MEA platform. We created MEAs with electron beam lithography, which can produce substantially smaller feature sizes than the photolithography techniques currently used. These devices can ultimately display feature sizes that are compatible with receptor-scale interfacing. Whole-cell clamping and MEAs, combined with improvements in quantum dot–cell junction stability, will allow us to confirm interface electrical connectivity and to create new device classes.

7.2 CONCLUSIONS

Our results demonstrated three methods for forming quantum dot–cell interfaces with close-range proximity. Our primary interest was the establishment of electrical connectivity between quantum dots and individual cell receptors, but our techniques have far-reaching applications. Quantum dot-antibody binding is now used extensively for cell labeling [1], and quantum dot-peptide binding [2] has been employed to target specific structures *in vivo.* Additionally, the close interfaces formed by our methods are ideal for specialized fluorescence techniques, including FRET [3], which can be used in basic biological investigations [4] and in the development of biosensors [5]. Thus, our methods have already produced an impact in the field, and continue to display the potential for future application.

One of the most significant findings in our research was the extreme difficulty of optimizing quantum dots for both electrical and biological applications. In general, the highest quality Cd-based quantum dots produced are CdSe/ZnS core-shell particles, [6] and biological applications have employed these almost exclusively. [7] However, the presence of a ZnS shell may interfere with the formation of a dipole moment in the core, and almost certainly increases the separation distance between the dipole and the cell surface. Thus, these particles are not ideal for neuroelectronic interfaces. The alternatives, core-only particles, have been shown to be more susceptible to photooxidation, reducing nanoparticle stability and releasing toxic Cd^{2+} ions from their surfaces. [8] Particles can be protected by adding a biocompatible shell, but the most commonly used materials (e.g., SiO_2 [9], BSA [10], etc.) are insulating, and would reduce electrical signaling. Therefore, alternative passivation methods are needed.

Through careful optimization of quantum dots and their cellular interfaces, these challenges can be surmounted, allowing receptor-scale neuroelectronic devices to be

developed. These devices will provide new insights into cell signaling and propagation. Additionally, they can be incorporated with micron-scale technologies to create new kinds of prosthetic devices. For example, the current retinal implant devices utilize 16 pixels that interact with multiple cell bodies. [11] Quantum dot–receptor interfaces would allow subcellular contacts, providing unprecedented fine control. Further, new computational devices could be created that more closely approximate true neural networking. Ultimately, these devices display enormous potential to impact many fields and present a rich and challenging field of study.

7.3 FUTURE DIRECTIONS

7.3.1 Alternative Nanomaterials

Quantum dots exhibit strong dipole moments because of charge separation in the exciton, which results from trapping of the electron. However, round particles do not display an oriented moment, [12] meaning that the alignment of adjacent particles may produce destructive, as well as constructive electrical interference. Systems that promote particle alignment may create a greater collective dipole moment than individually-bound quantum dots. [13] This could be accomplished through controlled organization of quantum dots on self-assembled monolayers, using some of the tethering techniques that we developed. Additionally, the orientation of quantum dot dipole moments has been linked to the direction of particle growth. [14] Therefore, asymmetrical quantum dots [15] and nanowires [16] may offer a strategy to control dipole presentation to the cell. These additional organization techniques and nanomaterials should be explored as alternatives to individually-bound quantum dots.

7.3.2 Increasing Quantum Dot Resistance to Oxidation

The most significant limitation in the development of quantum dot–receptor interfaces is the competition between the desires for well-protected particles that are resistant to photo-oxidation and for uninsulated, electrically active particles that can conduct signals from their surfaces. Innovative passivation of nanocrystal surfaces is the key to overcoming this challenge. The passivation layer should be sufficiently dense to provide a barrier to oxygen diffusion, but must also allow for transmission of electric fields produced in the particle core.

Typically particles are passivated with monodentate thiols, [17] which contain one binding site for the particle core. During photooxidation, these thiols are converted to disulfides, with the nanocrystal acting as a catalyst. Depending upon their solubility, the disulfides may disassociate from the nanocrystal surface. Further, the particle core is also photooxidized, most likely at the group VI atomic sites. [18] These oxidation products break away from the nanocrystal surface, producing dangling Cd^{2+} sites. Eventually, the ligands detach, the particle degrades, and the quantum dots precipitate from solution. This results in several undesirable outcomes. Free Cd^{2+}, which is extremely toxic to cells, is released into solution. [8] The particle decay produces photobleaching and a loss of electrical properties. Thus, for stable nanoparticle-receptor interfaces, it is imperative to limit oxidation of the particle surface.

Several strategies could meet these needs. One possibility is to use multidentate ligands, which provide additional binding sites to the nanoparticle surface. This would further anchor the ligand, and also reduce the number of non-bonded core surface atoms available for photooxidation reactions. However, multidentate ligands must be chosen with care. There is some evidence that dithiols are not good choices because of their propensity to form disulfides, and their inefficient packing densities on the particle

surface. [17] A better approach might be to utilize ligands with different binding affinities. For example, adenosine triphosphate binds nanoparticle cores at nitrogen and phosphate groups. [19] This dual affinity may prove more resistant to oxidation than single thiols.

Alternatively, nanocrystals could be passivated with short-chain ligands that are cross-linked increasing the barrier to oxygen diffusion. [8] Cysteine-acrylamide has already been used for this purpose, producing nanoparticles that are stable for over a year. [20] Mercaptoacetic acid chains could be modified to contain methacrylate end-groups that could be cross-linked using UV irradiation, [21] or cysteamine-capped particles could be cross-linked using glutaraldehyde. [22] The primary limitation of this approach is the need for short monomers to promote intimate quantum dot–cell connections and minimize insulation of the electrical signal.

Finally, thick conducting shells could be used to provide oxidation barriers, although it is unclear how a conducting shell would affect particle electrical properties. Electrically conducting polymers, such as polypyrrole, offer one strategy to conductive nanoparticle passivation. [23] Alternatively, metal shells could be constructed directly on quantum dot surfaces. Conductive gold nanoshells have been grown on silica [24] and polystyrene [25] nanoparticles, and copper has been deposited on copper oxide [26]. Although metal shells have not been demonstrated on semiconductor quantum dots, there is no theoretical barrier to their creation. [26]

These strategies provide novel means to protect particles from oxidation, while promoting electrical interfacing. Additionally, these methods would impact other fields, as oxidation is a problem that extends beyond neuroelectronic interfacing. Oxidation limits the use of nanoparticles in biological systems and in aqueous media. [17, 27] The

reduction of particle oxidation could provide significant advances in nanocrystal biocompatibility and stability.

7.3.3 Improving Interfacing Techniques

The interface techniques that we developed have some limitations to integration into long-term neuroelectronic interfaces. Recognition molecule directed binding and non-specific binding to the cell surface are both subject to endocytotic uptake. To address this limitation it is necessary to use recognition molecules that target fixed receptors or receptors recycled at a low rate. Ion channels may provide a suitable target, but no strategy has been demonstrated for binding ion channels directly without activating or inactivating the channel. Commercially available proteins bind almost exclusively to the intracellular surface, which is inaccessible in living systems; and peptides that bind channels modulate channel behavior. However, viable peptides could be identified using phage display [28]. This technique scans libraries of peptides for affinity to a known surface, and would offer a strategy for relatively rapid identification of ion channel binding peptides. Alternatively, ion channels could be genetically mutated to express an additional protein in close proximity. For example, if a channel was engineered to be co-expressed with green fluorescent protein (GFP) [29], antibodies to GFP could be used to produce intimate binding to ion channels.

The most promising strategy for producing controlled interfaces that are not subject to endocytosis is the formation of tethered quantum dot films. We demonstrated some initial films, and with improvements in quantum dot resistance to photooxidation, these films offer significant advantages to direct labeling of the cell surface. Tethered-films allow for alignment of nanoparticle dipoles [13], and if combined with asymmetric materials, significant increases in electrical signaling could result. Functionalization with

biomolecules and patterning of the films could provide localized binding, similar to that of the biorecognition molecule approach. Together with improvements in quantum dot resistance to photooxidation, these strategies provide a straightforward means to developing long-term neuroelectronic interfaces.

7.3.4 A Look to the Future

Neuroelectronic interfaces with receptor-scale precision would offer significant advancement in the fields of neuroscience, medicine, and computation. These devices represent the first opportunity to probe neuronal signaling at the receptor level over the long-term. This capability provides a means to answer one of the most important questions in neuroscience: What is the nature of learning and memory? Additionally, new classes of prosthetic devices could be developed. While present devices target large deficits in neuronal function (i.e., loss of sight, hearing, sensation, motion), new devices could address more localized problems in neuronal signaling, including treatment of Parkinson's disease and epilepsy. Further, new kinds of computational systems could be developed to harness the computation power of a single cell and its receptors. Thus, receptor-scale neuroelectronic interfaces are poised to make a dramatic impact in the fields of biotechnology and medicine.

7.4 REFERENCES

1. C. Seydel. "Quantum Dots Get Wet." Science 300: 80, 2003.

2. M.E. Åkerman, W.C.W. Chan, P. Laakkonen, S.N. Bhatia, and E. Ruoslahti. "Nanocrystal Targeting In Vivo." Proc. Nat. Acad. Sci. 99(20): 12617, 2002.

3. S. Wang, N. Mamedova, N.A. Kotov, W. Chen, and J. Studer. "Antigen/Antibody Immunocomplex from CdTe Nanoparticle Bioconjugates." Nano Letts. 2(8): 817, 2002.

4. W. Berger, H. Prinz, J. Striessnig, H.-C. Kang, R. Haugland, and H. Glossmann. "Complex Molecular Mechanism for Dihydropyridine Binding to L-Type Ca2+-Channels As Revealed by Fluorescence Resonance Energy Transfer." Biochem. 33: 11875, 1994.

5. I.L. Mendintz, A.R. Clapp, H. Mattoussi, E.R. Goldman, B. Fisher, and J.M. Mauro. "Self-Assembled Nano-scale Biosensors Based on Quantum Dot FRET Donors." Nature Mats. 2: 630, 2003.

6. M.A. Hines and P. Guyot-Sionnest. "Synthesis and Characterization of Strongly Luminescing ZnS-Capped CdSe Nanocrystals." J. Phys. Chem. 100: 468, 1996.

7. W.J. Parak, D. Gerion, T. Pellegrino, D. Zanchet, C. Micheel, S.C. Williams, R. Boudreau, M.A. Le Gros, C.A. Larabell, and A.P. Alivisatos. "Biological Applications of Colloidal Nanocrystals." Nanotech. 14: R15, 2003.

8. A.M. Derfus, W.C.W. Chan, and S.N. Bhatia. "Probing the Cytotoxicity of Semiconductor Quantum Dots." Nano Lett. 4(1): 11, 2004.

9. D. Gerion, F. Pinnand, S.C. Williams, W.J. Parak, D. Zanchet, S. Weiss, and A.P. Alivisatos. "Synthesis and Properties of Biocompatible Water-Soluble Silica-Coated CdSe/ZnS Semiconductor Quantum Dots." J. Phys. Chem. B 105: 8861, 2001.

10. X. Gao, W.C.W. Chan, and S. Nie. "Quantum-Dot Nanocrystals for Ultrasensitive Biological Labeling and Multicolor Optical Encoding." J Biomed. Opt. 7: 532, 2002.

11. M.S. Humayun, J.D. Weiland, G.Y. Fujii, R. Greenberg, R. Williamson, J. Little, B. Mech, V. Cimmarusti, G. Van Boemel, G. Dagnelie, and E. de Juan. "Visual Perception in a Blind Subject with a Chronic Microelectronic Retinal Prosthesis." Vision Res. 43(24):2573, 2003.

12. Y. Masumoto, F. Naruse, and A. Kanno. “Photoinduced Electric Dipole in CuCl Quantum Dots.” J. Luminescence. 102-103: 629, 2003.

13. J.J. Kakkassery, J.-P. Abid, M. Carrara, and D.J. Fermín. “Electrochemical and Optical Properties of Two Dimensional Electrostatic Assembly of Au Nanocrystals.” Faraday Discuss. 125: 157, 2004.

14. K.L. Silverman, R.P. Mirin, S.T. Cundiff, and A.G. Norman. “Direct Measurement of Polarization Resolved Transition Dipole Moment in InGaAs/GaAs Quantum Dots.” App. Phys. Lett. 82(25): 4552, 2003.

15. E. C. Scher, L. Manna, and A. P. Alivisatos. “Shape Control and Applications of Nanocrystals.” Phil. Trans. Royal Soc. A 361(1803): 241, 2003.

16. Z. Tang, N.A. Kotov, and M. Giersig. “Spontaneous Organization of Single CdTe Nanoparticles into Luminescent Nanowires.” Science 297: 237, 2002.

17. J. Aldana, Y.A. Wang, and X. Peng. “Photochemical Instability of CdSe Nanocrystals Coated by Hydrophilic Thiols.” J. Am. Chem. Soc. 123: 8844, 2001.

18. A.P. Alivisatos. “Perspectives on the Physical Chemistry of Semiconductor Nanocrystals.” J. Phys. Chem. 100: 13226, 1996.

19. M. Green, R. Taylor, and G. Wakefield. “The Synthesis of Luminescent Adenosine Triphosphate Passivated Cadmium Sulfide Nanoparticles.” J. Mat. Chem. 13: 1859, 2003.

20. R.L. Sherman, Y. Chen, and W.T. Ford. “Cysteine Acrylamide Stabilized CdS and CdSe/CdS Nanoparticles in Aqueous Solutions.” Abstracts of Papers, 225th ACS National Meeting, New Orleans, LA, 2003.

21. See for example: J.B. Leach, K.A. Bivens, C.N. Collins, and C.E. Schmidt. “Development of Photocrosslinkable Hyaluronic Acid-Polyethylene Glycol-Peptide Composite Hydrogels for Soft Tissue Engineering. J. Biomed. Mat. Res. 70A(1): 74, 2004.

22. G.T. Hermanson. Bioconjugate Techniques. Academic Press, San Diego: 1996, pp. 218-220.

23. R.R. Bhattacharjee, M. Chakraborty, and T.K. Mandal. “Synthesis of Dendrimer-Stabilized Gold-Polypyrrole Core-Shell Nanoparticles.” J. Nanosci. Nanotechnol. 3(6): 487, 2003.

24. C. Loo, A. Lin, L. Hirsch, M.H. Lee, J. Barton, N. Halas, J. West, and R. Drezek. “Nanoshell-Enabled Photonics-Based Imaging and Therapy of Cancer.” Tech. Cancer Res. Treat. 3(1): 33, 2004.

25. G. Kaltenpoth, M. Himmelhaus, L. Slansky, F. Caruso, and M. Grunze. “Conductive Core-Shell Particles: An Approach to Self-Assembled Mesoscopic Wires.” Adv. Mats. 15(13): 1113, 2003.

26. K. Chatterjee, B. Satpati, P.V. Satyam, and D. Chakravorty. “Metal-to-Nonmetal Transition in Copper Nanoshells Grown on Copper Oxide Nanoparticles.” J. Appl. Phys. 96(1): 683, 2004.

27. W.G.J.H.M. van Sark, P.L.T.M. Frederix, A.A. Bol, H.C. Gerritsen, and A. Meijerink. “Blueing, Bleaching, and Blinking of Single CdSe/ZnS Quantum Dots.” Chem. Phys. Chem. 3: 871, 2002.

28. C.F. Barbas, D.R. Burton, J.K. Scott, and G.J. Silverman. Phage Display: A Laboratory Manual. Cold Spring Harbor Laboratory Press, Cold Spring Harbor, New York: 2001.

29. See for example: L.M. Diaz, R. Maiya, S.L. Boehm, H.A. Scott, S.E. Bergeson, R.D. Mayfield, and R.A. Morrisett. “Sindbis Viral Delivery of eGFP Labeled Dopamine D1 Receptors into Primary Cultured Neurons, Brain Slice Culture and in vivo.” Res. Soc. Alcoholism Abstr., 27: 93, 2003.

Glossary

Absorbance Onset- The wavelength at which absorbance of light begins.

Access Resistance- In whole-cell clamping, this describes the resistance between a capillary pipette and the cytoplasm.

Action Potential- A rapid change in cell membrane potential due to the influx of Na^+ ions. Action potentials occur when the resting potential of a cell rises 15 mV or more.

Alpha Helix- A secondary protein structure consisting of amino acids rotated into a helical formation.

Amino Acids-The smallest unit of a protein. Amino acids consist of the $H_2NCHRCOOH$ chemical structure, where R changes. There are 20 naturally occurring R groups.

Antibody- A molecule produced by the immune system to bind foreign elements in the body. Antibodies can be created with binding capability for any protein in a cell by injecting that protein into a foreign host. The antibodies are then isolated from the host, and used to bind the selected target.

Arrested Precipitation- A process by which normally insoluble compounds are suspended in a solvent. This occurs by binding of an external water-soluble component to the insoluble compound.

Artificial Cerebrospinal Fluid (aCSF)- A buffer used to approximate conditions in the cerebrospinal cavity.

Avidin- A protein present in egg white that forms strong connections to biotin, another biomolecule.

Axon- Extensions from neuron cell bodies that carry signals away from the cell. Axons can extend for up to 1 meter from the cell body before making contact with muscle targets.

Axon Hillock- A region near the cell body that integrates synaptic potentials. This region contains an abundance of voltage-gated ion channels. If the combined signal received is sufficient to open these channels, the cell will fire an action potential.

Band Gap- A region between the conduction and valence energy bands of a material. Because this region contains no potential energy states, electron occupation is forbidden. The band gap energy is the amount of energy required to transverse this band.

Bioconjugation- Chemical processes used to attach substances, such as fluorescent dyes, to biological molecules.

Bioelectronic Interfaces- Interfaces formed between biological entities and electrical components.

Biorecognition Molecule- Generic term for a molecule that demonstrates specific interactions with a cell component. Biorecognition molecules include peptides, antibodies, proteins, and DNA/RNA fragments. These molecules interact with a cellular component through hydrophobic/hydrophilic, electrostatic, hydrogen bonding, and van der Waals interactions. Interactions are usually very specific, with a single atom change capable of disrupting binding in many cases.

Biotin- A coenzyme in carbon dioxide transfer that binds strongly to avidin.

b-**Mercaptoethanol**- See Mercaptoethanol.

Bohr Exciton- The normal separation distance of an exciton (electron-hole pair) in a bulk material.

Bond Pad- The point of external electrical contact in a microelectrode array.

Bovine Serum Albumin (BSA)- A protein solution derived from a cow that is used to reduce non-specific binding to cells and tissue.

Carbodiimide - See EDC.

Carcinogen- A compound which has been shown to cause cancer in certain tests.

Cell Surface Receptor- Receptors for biorecognition molecules that are found on the cell surface. Typically, these receptors are engaged in cell motility, adhesion, and growth functions.

Central Nervous System (CNS)- The central nervous system includes the brain, spinal cord, and auditory, visual, and olfactory systems. The central nervous system also contains all neuron cell bodies.

Cochlear Implant- The cochlear implant interfaces nerve endings in the cochlea (inner ear) with a microelectrode array. A receiver worn externally interprets sound waves and converts them to electrical signals. These signals are then transmitted via radio waves to the microelectrode array. These signals are then sent to the brain via the nerve endings. The device is designed to bypass damaged mechanical components and cochlear hair cells in the inner ear.

Coherent Light- Light that possess the same wavelength and phase.

Colloids - A mixture of solvent and particulates that is in between a true solution and a suspension. Colloidal particles are usually less than 1 micron in diameter.

Conduction Band- A potential energy band containing the excited state energy values available for electron occupation.

Core-Shell Nanoparticles- Nanoparticles that are passivated by an inorganic shell. The shell material is usually a wider-band gap (i.e., more insulating material) than that used for the core.

Coulombic Attractions- Attraction of positive and negative charges to each other.

Cysteine- An amino acid (peptide component) with an SH functional group as the R group.

De Broglie Wavelength- The wavelength of a particle with momentum.

Debye Length- The length over which an electrical signal drops by a value of *e* from its initial value.

Debye Screening- Electrical interactions are screened in the presence of additional charges, reducing their strength. This reduction can be described by the Debye length.

Dendrite- Short neuronal extension that carries signals toward a nerve cell.

Dipole Moment- Charge separation in a molecule. Dipole moments may be permanent, created by defects in a material, or transient, occurring upon excitation.

DNA- A molecule composed of nucleotides which contains the blueprint for protein production.

EDC- 1-Ethyl-3-(3-Dimethylaminopropyl)-Carbodiimide Hydrochloride (see Figure 1A for structure). This chemical is commonly used to form amide (or peptide) bonds between carboxyl and amine groups.

Effective Mass- An approximation used to account for the effect of neighboring atoms and electrons in a crystal lattice in free electron equations.

Electrical Induction- A process where charge accumulation of one type attracts charges of the opposite type, usually across a membrane.

Electric Dipole Moment- A charge separation in a molecule that results in a magnetic or electric field between the poles of separation. Dipoles may be transient or permanent.

Electrode Resistance- The resistance of an electrode to current flow. In whole-cell clamping, this is directly related to the diameter of the capillary pipette employed.

Electron Beam Lithography (EBL)- A patterning technique that uses focused electron beams (provided by an SEM) to expose electron-sensitive resists.

Electron Decay- The decay of an excited electron from a state in the conduction band to a state in the valence band.

Electron-Hole Recombination- The combination of an excited electron in the conduction band and a hole in the valence band. This event usually produces an emitted photon with an energy value equivalent to the band gap.

Electron Transfer- A process by which an excited electron can be transferred from the lowest energy state in the conduction band of one material to a lower energy state in the conduction band of a second material.

Electrostatic Attractions- See Coulombic Attractions.

Endocytosis- A process by which the cell recycles its membrane and receptors. This process is used to engulf molecules on or near the particle surface.

Endocytosis, Receptor-Mediated- Endocytosis that is initiated by the binding to a ligand to a class of membrane-bound receptors.

Energy States- See Potential Energy States.

Energy Bands- Continuous bands of potential energy values that may be occupied by excited electrons. Bands are formed by overlapping potential energy states.

Exciton- An electron-hole pair coupled by Coulombic attractions.

Extracellular Matrix (ECM)- The protein matrix that surrounds cells. ECM is made of many proteins including fibronectin, laminin, elastin, and collagen.

Fab Fragment- The smallest portion of an antibody that maintains recognition capabilities. Fab fragments are comprised of the short arms of an antibody and average 5 nm in length.

Fibroblast- A cell type common in connective tissue. Fibroblasts are known for cell adhesion and a well-spread morphology.

Fluorescence Anisotropy- A spectral technique that evaluates polarization of emitted light. This technique is used to evaluate the bulk of fluorescent molecules. Heavier molecules display a greater degree of anisotropy in their fluorescence as a result of a low tumbling rate in solution.

Fluorescence Microscopy- Microscopy observing the output of fluorescent light rather than transmitted light. An excitation light source impacts the object in question, while the fluorescent output of the object is observed. Excitation wavelengths are filtered from the output so that only light related to the object is observed.

Fluorescence Resonance Energy Transfer (FRET)- The transfer of an excited electron from a donor material to an acceptor material. Fluorescence in the donor is quenched, and fluorescence in the acceptor may be produced.

Fluorescent Labels- Fluorescent molecules used to label components of cells.

Fluorophore- A fluorescent molecule.

Formaldehyde- A fixative used to cross-link cells and preserve their structure for later analysis.

Fourier Transform Infrared Spectroscopy (FTIR)- An analytical technique that examines the molecular absorption or transmittance of light in the infrared region of the electromagnetic spectrum (i.e., wavelengths > 800 nm wavelength).

Glia- Support cells in the nervous system. Examples of glia include oligodendrocytes, astrocytes, and Schwann cells.

Glycine- An amino acid (peptide component) with an H functional group as the R group.

Glycocalix- A protective sugar coating found on the outside of cells.

Green Fluorescent Protein (GFP)- A protein, produced by jellyfish, that produces a green fluorescent product when expressed. GFP is commonly used as a marker in genetically engineered species to confirm transfection.

Hepatocytes- Liver cells.

Hole- A positive charge in a crystal lattice resulting from the absence of an electron.

Immortal Cells- Cells that have divide continuously. These cells are either obtained from cancerous tumors or transformed using mutagenic agents. Immortal cells are often altered by the transformation process and do not behave entirely like their normal counterparts.

Immunoglobulin G- An antibody class that binds to foreign proteins.

Immunocytochemistry- A technique used to stain cellular components using antibodies. Antibodies known to bind the component in question are conjugated to reporter molecules (e.g., fluorescent dyes). If the antibody binds the cellular component in question the reporter molecule is activated.

Immunofluorescence- A form of immunocytochemistry employing fluorescent molecules.

in Situ- A process that occurs in place.

in Vitro- An experiment that takes place using cultured cells, external to an animal.

in Vivo- An experiment that occurs in an animal model.

Induction- An electrical response that occurs through indirect interactions produced by electrostatic attractions. An electrical signal can be transferred from a primary object to a second object without contact.

Integrin- A class of cell surface receptors that promote cell-ECM adhesion.

Ion Channel- A protein containing four repeated subunits with six transmembrane segments that regulates ion flow through nerve cells.

Ion Channel, Ligand-Gated- An ion channel that opens in response to ligand binding. Typically these channels open in response to neurotransmitters, allowing Ca^{2+} ions to enter the cell, producing synaptic potentials.

Ion Channel, Voltage-Gated- An ion channel that opens in response to a change in the cell membrane potential. Most voltage-gated channels pass Na^{2+} ions and open in response to synaptic potentials.

Laminin- One type of ECM protein. Laminin has been shown to play a role in neurite extension and cell adhesion. It is composed of an alpha and beta chain and promotes cell adhesion.

Laser- A device which produces coherent emitted light of a single wavelength. Lasers produces light through stimulated emission, emission created by excited electron adsorption of a photon at the same wavelength as would be emitted during electron-hole recombination.

Ligand- A molecule that binds to a particular binding site. In biological systems, typically refers to the component that binds a receptor with high affinity. For quantum dots, refers to the outer coating of the particle that binds the particle core.

Ligand Exchange- A process used to exchange nanocrystal passivating ligands. Particles are usually dried and resuspended in a gross excess of the target ligand, thus driving desorption of the existing surface ligand.

Light Emitting Diodes (LEDs)- Materials that emit light upon application of a voltage. This occurs when a positively charged and negatively charged material (p-n junction) are brought into contact with each other. The application of a voltage promotes recombination of the positive and negative charges producing emitted light.

Membrane Potential- The natural voltage potential that occurs across the cell membrane due to intracellular-extracellular charge separation. For mammalian cells, the resting potential is –70 mV. Increases of 15 mV or greater will cause the cell to fire an action potential.

Mercaptoacetic Acid (MAA)- Nanocrystal passivating ligand containing thiol and carboxyl end groups. [$HSCH_2COOH$]

Mercaptoethanol (MBE)- Nanocrystal passivating ligand containing thiol and alcohol end groups [$HS(CH_2)_2OH$]

Mercaptoethylamine (MEA, Cysteamine)- Nanocrystal passivating ligand containing thiol and amine end groups. [$HS(CH_2)_2NH_2$]

Mercaptopropionic Acid (MPA)- Nanocrystal passivating ligand containing thiol and carboxyl end groups. [$HS(CH_2)_2COOH$]

Microelectrode Arrays (MEAs)- Arrays of electrodes constructed on glass or silicon surfaces used to measure neuronal action potentials. The electrodes are usually from 10-100 microns in size. The most common type of array consists of platinized-gold contacts on glass substrates.

Monodentate Ligands- Ligands containing a single binding site for a nanoparticle surface.

Multidentate Ligands- Ligands containing multiple binding sites for the nanocrystal surface.

Nanocrystals- Crystalline particles smaller than 100 nm in diameter.

Nanoparticles- Particles smaller than 100 nm in diameter.

Neural Networks- Computational platforms that attempt to emulate neuronal signaling.

Neurite- Generic term for neuronal extension. Neurites can be either axons or dendrites.

Neuroelectronic Devices- Devices that integrate neurons with electrical technologies. Examples include prosthetic devices, microelectrode arrays, and biosensors.

Neurotransmitter- A ligand that is released at the synaptic terminal. Neurotransmitters bind ligand-gated ion channels initiating membrane potential changes at the post-synaptic neuron.

Neuron- The primary cell of the nervous system. Neurons are responsible for transmitting and interpreting electrical signals.

Nerve- Nerves consist of axon bundles extending from the central nervous system.

Non-Radiative Energy Loss- The loss of energy from an excited electron through mechanisms other than photon emission. For example, energy could be lost through crystal vibrations.

Nucleotide- The smallest components of DNA and RNA. Nucleotides include adenine, cytosine, guanine, thymine, and uracil.

Oligonucleotide- A molecule containing a small number of nucleotides.

Optoelectronic Devices- Devices which interconvert light and electricity. Examples include solar cells, LEDs, and lasers.

Ostwald Ripening- A process of nanoparticle growth where less thermodynamically stable small particles dissolve to promote the growth of large

particles. Ostwald ripening is characterized by an increase in the absorbance onset wavelength and a red-shift in particle fluorescent emission.

Papain- A molecule which promotes the break-up of antibodies into light and heavy chains. This molecule can be used to produce Fab fragments.

Passivation- Insulating layers that protect electrical materials from the external environment.

Patch-Clamping Technique- A technique that allows measurement of membrane potential changes. An electrolyte-filled micropipette is placed in contact with the cell surface. Then a portion of the cell membrane is ripped away from the cell surface. Voltage and current measurements may be collected from the removed portion of the membrane.

Peptide- A portion of a protein, composed of several amino acids.

Peripheral Nervous System (PNS)- Portion of the nervous system that includes all extensions from the central nervous system. The peripheral nervous system includes only axons, not cell bodies.

Phage Display- An approach for isolating peptides with specific binding affinities. Peptide libraries are screened against a surface. Peptides that do not bind the surface are washed away. Binding peptides are selectively removed from the surface using pH changes. Tests are repeated until the peptide with the strongest binding affinity is identified. That peptide is then sequenced and identified.

Phenotype- The shape and structure displayed by a given cell type.

Phosphate Buffered Saline (PBS)- A buffered solution used to approximate extracellular fluid.

Phosphate Buffered Saline, Dulbecco's (DPBS)- Phosphate buffered saline with Ca^{2+} and Mg^{2+} ions added to promote cell adhesion.

Photobleaching- The loss of fluorescence over time when exposed to excitation light. Occurs as a result of molecule-molecule and molecule-solvent interactions that result in chemical changes in the molecule.

Photoluminescence (PL)- Emission of light in response to photon absorption.

Photoluminescence Emission Bandwidth- The range of wavelengths over which fluorescent light is emitted in response to photon absorption. Photoluminescence emission wavelengths commonly display a Gaussian distribution.

Photoluminescence Excitation (PLE)- The range of absorbed wavelengths which produce a fluorescent emission response in a molecule.

Photooxidation- Oxidation of a material that occurs during exposure to light of a given wavelength.

Photovoltaic Devices- See Solar Cells.

Plasticity- The ability of neurons to alter and form new connections with neighboring cells.

Poly-D-lysine (polylysine)- A chemical consisting of multiple lysine amino acids. This chemical adheres to easily to glass and promotes cell adhesion, most likely through its abundant positively-charged amine groups.

Polyimide- A polymer coating used to insulate microelectrode arrays.

Poly(methyl methacrylate) (PMMA)- A polymeric resist used for electron beam lithography.

Potential Energy States- The energy values which an excited electron may assume. These values are dependant upon the composition of the material in question.

Precursor Decomposition- A quantum dot synthesis approach that utilizes reactants that decompose at high temperature. Reactants are heated and then combined to produce nanoparticles.

Primary Cells- Cells that are isolated directly from tissue. Primary cells usually do not divide and have a limited lifetime.

Probability Distribution Function- See Wavefunction.

Prosthetic Device- A device designed to replace lost function in the body.

Quantum Dots- Small clusters of atoms that have a size smaller than their exciton. This implies that the particle will behave as a wave, rather than a particle, and display quantum mechanical properties.

Quantum Confinement- Confinement of an electron, hole, or exciton wavefunction as a result of particle size. Quantum confinement produces quantum mechanical features in nanoparticle electrical and optical behavior.

Quantum Yield- The number of photons that are released as fluorescent output as a percentage of the number of photons absorbed.

Rat Neonatal Cortical Cells (RNCs)- A primary cell line harvested from the cortex of 1-3 day old rat pups.

Receptor- See Cell Surface Receptor.

Retinal Implant- The retinal implant interfaces nerve endings in the retina (eye) with a microelectrode array. A CCD camera worn by the user interprets light signals and recreates the pattern on the array using a laser. The array then transmits signal to nerve cells located in the retina.

RGDS- A peptide known to bind to integrins (i.e., cell surface receptors). The peptide is composed of the amino acids arginine-glycine-aspartic acid-serine.

Scanning Electron Microscopy (SEM)- A microscopy technique that uses scattered secondary electrons to form an image of electron dense samples.

Schrödinger Equation- An equation that describes the quantum mechanical behavior of molecules, particularly the probability of finding an electron in a given location at a given time.

Schlenk Line- A glass manifold that contains access to gas and vacuum lines, used to create an oxygen free environment.

Siloxanes- Molecules containing SiO groups. These molecules bind to glass (i.e., SiO_2) surfaces.

SK-N-SH Neuroblastoma Cells- A cancerous, immortal cell line isolated from neuroblastoma tumors of a 4-year old human patient. These cells approximate normal human brain cells, but do not display all the features of normal tissue.

Solar Cells- Devices which convert absorbed light into an electrical signal. This occurs by extraction of optically excited electrons from the conduction band.

Spontaneous Emission- See Photoluminescence.

Stimulated Emission- Photon emission that results from the excited electron adsorption of a photon possessing an energy value equivalent to that which would be emitted during electron-hole recombination.

Streptavidin- A biotin binding protein isolated from *Streptomyces avidinii*. See Avidin.

Synaptic Potential- A change in the neuronal membrane potential produced by opening of ligand-gated ion channels. Synaptic potentials do not propagate along dendrite lengths, instead traveling through diffusion. Potentials are integrated at the axon hillock.

Synaptic Terminal- The terminus of an axon that is in synaptic contact with a neighboring cell. Neurotransmitters are released from this terminal in response to an action potential.

Synapse- The region of connection between an axon and dendrite of neighboring neurons.

Trap Energy States- Energy states that are introduced into the forbidden band gap region by the presence of crystal defects or impurities.

Trapped Electron- An electron that occupies a forbidden energy level in the band gap. This occurs as a result of crystal defects or contaminants.

Valence Band- The potential energy band containing ground states for a material.

Wavefunction- A mathematical function, given by the Shrödinger equation, which describes the probability of finding an electron in a given location over time.

Whole-cell Clamping- A technique for measuring the cell membrane potential. An electrolyte-filled micropipette is placed in contact with the cell, and then the membrane is ruptured. The pipette is in direct contact with the intracellular fluid. Current and voltage changes can then be monitored.

X-Ray Photoelectron Spectroscopy (XPS)- A spectroscopic technique that can determine surface composition based on the energy of photons emitted as a result of the photoelectric effect.

YIGSR- A peptide component of laminin known to bind laminin integrins. It is composed of the amino acids tyrosine-isoleucine-glycine-serine-arginine.

Bibliography

Abdelghani-Jacquin C., A. Abdelghani, G. Chmel, M. Kantlehner, and E. Sackmann. "Decorated Surfaces by Biofunctionalized Gold Beads: Application to Cell Adhesion Studies." Eur. Biophys. J. 31: 102, 2002.

Åkerman M.E., W.C.W. Chan, P. Laakkonen, S.N. Bhatia, and E. Ruoslahti. "Nanocrystal Targeting In Vivo." Proc. Nat. Acad. Sci. 99(20): 12617, 2002.

Alberts B., A. Johnson, J. Lewis, M. Raff, K. Roberts, and P. Walter. Molecular Biology of the Cell, 4th Ed., Garland Science, New York: 2002.

Alberts B., D. Bray, J. Lewis, M. Raff, K. Roberts, and J.D. Watson. Molecular Biology of the Cell, 3rd Ed., Garland Publishing, New York: 1994.

Aldana J., Y Y.A. Wang, and X. Peng. "Photochemical Instability of CdSe Nanocrystals Coated by Hydrophilic Thiols." J. Am. Chem. Soc. 123: 8844, 2001.

Alivisatos A.P. "Perspectives on the Physical Chemistry of Semiconductor Nanocrystals." J. Phys. Chem. 100: 13226, 1996.

Atkins P. Physical Chemistry, 5th Ed., W.H. Freeman and Co., New York: 1994.

Atkins P.W. Physical Chemistry, 1st Ed., WH Freeman and Co., San Francisco: 1978.

Barbas C.F., D.R. Burton, J.K. Scott, and G.J. Silverman. Phage Display: A Laboratory Manual. Cold Spring Harbor Laboratory Press, Cold Spring Harbor, New York: 2001.

Barglik-Chory C., E. Dieman, A.F. Münster, H. Strohm, C. Remenyi, and G. Müller. "Influence of Synthesis Parameters on the growth of CdS Nanoparticles in Colloidal Solution and Determination of Growth Kinetics using Karhunen-Loeve Decomposition." Chem. Phys. Lett. 374: 319, 2003.

Bartnikas R., R.M. Eichhorn, Ed., Electrical Properties of Solid Insulating Materials. American Society for Testing and Materials, Philadelphia: 1983.

Battaglia D., and X. Peng, Nano. Lett. "Formation of High Quality InP and InAs Nanocrystals in a Noncoordinating Solvent." Nano Lett. 2: 1027, 2002.

Bavykin D.V., E.N. Savinov, and V.N. Parmon. "Specific Features of Luminescence of Q-CdS Colloids with Different Sizes." Russ. Chem. Bul. 47: 629, 1998.

Benes F.M., J.B. Taylor, and M.C. Cunningham. "Convergence and Plasticity of Monoaminergic Systems in the Medial Prefrontal Cortex During the Postnatal

Period: Implications for the Development of Psychopathology." Cereb. Cortex. 10(10): 1014, 2000.

Berger W., H. Prinz, J. Striessnig, H.-C. Kang, R. Haugland, and H. Glossmann. "Complex Molecular Mechanism for Dihydropyridine Binding to L-Type Ca^{2+}-Channels As Revealed by Fluorescence Resonance Energy Transfer." Biochem. 33: 11875, 1994.

Berven C.A., M.N. Wybourne, L. Clarke, J.E. Hutchison, L.O. Brown, J.L. Mooster, and M.E. Schmidt. "The Use of Biopolymer Templates to Fabricate Low-Dimensional Gold Particle Structures." Superlattices and Microstructures. 27(5/6): 489, 2000.

Bhattacharjee R.R., M. Chakraborty, and T.K. Mandal. "Synthesis of Dendrimer-Stabilized Gold-Polypyrrole Core-Shell Nanoparticles." J. Nanosci. Nanotechnol. 3(6): 487, 2003.

β-Mercaptoethanol MSDS Product Number M7522, version 1.12, 4/6/2004, from Sigma Aldrich.

Bongrand P. "Adhesion of Cells," in Handbook of Biological Physics, vol. 1, R. Lipowsky and E. Sackmann, Eds., Elsevier, Amsterdam: 1995.

Boppart S.A., B.C. Wheeler, and C.S. Wallace. "A Flexible Perforated Microelectrode Array for Extended Neural Recordings." IEEE Trans. Biomed. Eng. 39(1): 37, 1992.

Bowen Katari J.E., V.L. Colvin, and A.P. Alivisatos. "X-ray Photoelectron Spectroscopy of CdSe Nanocrystals with Applications to Studies of the Nanocrystal Surface." J. Phys. Chem. 98: 4109, 1994.

Bradburn G.R., T.J. Trentler, S.C. Goel, W.E. Buhro, and J.M. Jean. "Dependence of Quantum Yield from the Deep Trap States of CdS Nanoparticles on Particle-Size and Capping Group." 210th ACS National Meeting, PHYS-322 (Pt. 2): Chicago, 1995.

Breckenridge L.J., R.J.A. Wilson, P. Connolly, A.S.G. Curtis, J.A.T. Dow, S.E. Blackshaw, and C.D.W. Wilkinson. "Advantages of Using Microfabricated Extracellular Electrodes for In Vitro Neuronal Recording." J. Neurosci. Res. 42: 266, 1995.

Brewer G.R., Ed., Electron Beam Technology in Microelectronic Fabrication. Academic Press, New York: 1980.

Bruchez M., Jr., M. Moronne, P. Gin, S. Weiss, and A.P. Alivisatos. "Semiconductor Nanocrystals as Fluorescent Biological Labels." Science 281: 2013, 1998.

Brus L.E. "A Simple Model for the Ionization Potential, Electron Affinity, and Aqueous Redox Potentials of Small Semiconductor Crystallites." J. Chem. Phys. 80(9): 5566, 1983.

Brus L.E. "Electron-Electron and Electron-Hole Interactions in Small Semiconductor Crystallites: The Size Dependence of the Lowest Excited Electronic State." J. Phys. Chem. 80(9): 4403, 1984.

Bube R.H. Electrons in Solids, 2nd Ed., Academic Press, Boston: 1988.

Buhro W.E., and V.L. Colvin. "Semiconductor Nanocrystals: Shape Matters." Nat. Mats. 2: 138, 2003.

Bukowski T.J., and J.H. Simmons. "Quantum Dot Research: Current State and Future Prospects." Crit. Rev. Solid State Mat. Sci. 27(3): 119, 2002.

Bunk S. "Sensing Evil." The Scientist. 16(15): 13, 2002.

Bürgi H.-B. "Stereochemistry of Polynuclear Cadmium (II) Thioglycolates: Crystal Structure of Cadmium (II) Bisthioglycolate." Helv. Chim. Acta. 57: 515, 1974.

Byassee T.A., W.C.W. Chan, and S. Nie. "Probing Single Molecules in Single Living Cells." Anal. Chem. 72: 5606, 2000.

Callister W.D., Jr. Materials Science and Engineering: An Introduction. John Wiley and Sons, New York: 2000.

Campbell S.A. The Science and Engineering of Microelectronic Fabrication, 2nd Ed., Oxford University Press, New York: 2001.

Castel S., R. Pagan, F. Mitjans, J. Piulats, S. Goodman, A. Jonczyk, F. Huber, S. Vilaro, and M. Reina. "RGD Peptides and Monoclonal Antibodies, Antagonists of Alpha(v)-Integrin, Enter the Cells by Independent Endocytotic Pathways." Lab Invest. 81(12): 1615, 2001.

Catterall W.A. "Molecular Mechanisms of Gating and Drug Block of Sodium Channels." Novartis Found Symp. 241: 206, 2002.

Chan W.C.W., and S. Nie. "Quantum Dot Bioconjugates for Ultrasensitive Nonisotopic Detection." Science 281: 2016, 1998.

Chan W.C.W., D.J. Maxwell, X. Gao, R.E. Bailey, M. Han, and S. Nie. "Luminescent Quantum Dots for Multiplexed Biological Detection and Imaging." Curr. Opin. Biotech. 13: 40, 2002.

Chan W.C.W., T.L. Prendergast, M. Jain, and S. Nie. "One-Step Conjugation of Biomolecules to Luminescent Nanocrystals," in Molecular Imaging: Reporters, Dyes, Markers, and Instrumentation, Darryl J. Bornhop, Kai Licha, Eds., Proceedings of SPIE., vol. 3924, 2000, p. 2.

Chatterjee K., B. Satpati, P.V. Satyam, and D. Chakravorty. "Metal-to-Nonmetal Transition in Copper Nanoshells Grown on Copper Oxide Nanoparticles." J. Appl. Phys. 96(1): 683, 2004.

Chen H.M., X.F. Huang, L. Xu, J. Xu, K.J. Chen, and D. Feng. Superlattices and Microstructures. "Self-Assembly and Photoluminescence of CdS-Mercaptoacetic Clusters with Internal Structures." 27: 1, 2000.

Chiu D.T. "The Development of Autogenous Venous Nerve Conduit as a Clinical Entity," in P and S Medical Review vol. 3, issue 1. Columbia-Presbyterian Medical Center, Dec. 1995.

Coe-Sullivan S., W.-K. Keung, J.S. Steckel, M. Bawendi, and V. Bulovic. "Tuning the Performance of Hybrid Organic/Inorganic Quantum Dot Light-Emitting Devices." Org. Elec. Phy. Mats. Appl. 4(2-4): 123, 2000.

Colvin V.L. "The Potential Environmental Impact of Engineered Nanomaterials." Nature Biotech. 21(10): 1166, 2003.

Colvin V.L., A.N. Goldstein, and A.P. Alivisatos. "Semiconductor Nanocrystals Covalently Bound to Metal Surfaces with Self-Assembled Monolayers." J. Am. Chem. Soc. 114: 5221, 1992.

Colvin V.L., and A.P. Alivisatos. "CdSe Nanocrystals with a Dipole Moment in the First Excited State." J. Chem. Phys. 97(1): 730, 1992.

Connolly P., P. Clark, A.S.G. Curtis, J.A.T. Dow, and C.D.W. Wilkinson. "An Extracellular Microelectrode Array for Monitoring Electrogenic Cells in Culture." Biosens. Bioelec. 5: 223, 1990.

Creighton T. E. Proteins: Structures and Molecular Principles. W. H. Freeman and Co., New York: 1983.

Cui X., V.A. Lee, Y. Raphael, J.A. Wiler, J.F. Hetke, D.J. Anderson and D.C. Martin. "Surface Modification of Neural Recording Electrodes with Conducting Polymer Biomolecule Blends." J. Biomed. Mat. Res. 56(2): 261, 2001.

Dabbousi B.O., J. Rodriquez-Viejo, F.V. Mikulec, J.R. Heine, H. Mattoussi, R. Ober, K.F. Jensen, and M.G. Bawendi. "(CdSe)ZnS Core-Shell Quantum Dots: Synthesis and Characterization of a Size Series of Highly Luminescent Nanocrystallites." J. Phys. Chem. B 101: 9463, 1997.

Dahan M., S. L,vi, C. Luccardini, P Rostaing, B. Riveau, and A. Triller. "Diffusion Dynamics of Glycine Receptors Revealed by Single-Quantum Dot Tracking." Science 302: 442, 2003.

de Mello Donegá C., S.G. Hickey, S.F. Wuister, D. Vanmaekelbergh, and A. Meijerink. "Single-Step Synthesis to Control the Photoluminescence Quantum Yield and Size Dispersion of CdSe Nanocrystals." J. Phys. Chem. B. 107: 489, 2003.

Derfus A.M., W.C.W. Chan, and S.N. Bhatia. "Probing the Cytotoxicity of Semiconductor Quantum Dots." Nano Lett. 4(1): 11, 2004.

Diaz L.M., R.R. Maiya, S.L. Boehm, H.A. Scott, S.E. Bergeson, R.D. Mayfield, and R.A. Morrisett. "Sindbis Viral Delivery of eGFP Labeled Dopamine D1 Receptors into Primary Cultured Neurons, Brain Slice Culture and in vivo." Res. Soc. Alcoholism Abstr., 27: 93, 2003.

Ding S.-Y., M. Jones, M.P. Tucker, J.M. Nedeljkovic, J. Wall, M.N. Simon, G. Rumbles, and M.E. Himmel. "Quantum Dot Molecules Assembled with Genetically Engineering Proteins." Nano Lett. 3(11): 1581, 2003.

Douglas R., M. Mahowald, and C. Mead. "Neuromorphic Analogue VLSI." Ann. Rev. Neurosci. 18: 255, 1995.

Dubertret B., P. Skourides, D.J. Norris, V. Noireaux, A.H. Brivanlou, and A. Libchaber. "In Vivo Imaging of Quantum Dots Encapsulated in Phospholipid Micelles." Science 298: 1759, 2002.

Elder A.C.P., R. Gelein, M. Azadniv, M. Frampton, J. Finkelstein, and G. Oberdörster. "Systematic Effects of Inhaled Ultrafine Particles in Two Compromised, Aged Rat Strains." Inhalation. Toxic. 16(6/7) 461, 2004.

Emory S.R., W.P. Ambrose, P.M. Goodwin, and R.A. Keller. "Observing Single Molecule Chemical Reactions on Metal Nanoparticles." Proceedings of SPIE-The Society for Optical Engineering. 4258: 63, 2001.

Empedocles S.A., R. Neuhauser, K. Shimizu, and M.G. Bawendi. "Photoluminescence from Single Semiconductor Nanostructures." Adv. Mats. 11(15): 1243, 1999.

Eychmüller A., A. Hässelbarth, L. Katsikas, and H. Weller. "Fluorescence Mechanism of Highly Monodisperse Q-Sized CdS Colloids." J. Luminescence. 48-49: 745, 1991.

Fatehi M., A.L. Harvey, and E.G. Rowan. "Characterization of the Effects of Depolarizing Toxins on Nerve Terminal Action Potentials: Apparent Block of Presynaptic Potassium Currents." Toxicon. 36(1): 115, 1998.

Fojtik A., H. Weller, U. Koch, and A. Henglein. "Photo-Chemistry of Colloidal Metal Sulfides 8. Photo-Physics of Extremely Small CdS Particles: Q-State CdS and Magic Agglomeration Numbers." Ber. Bunsenges. Phys. Chem. 88: 969, 1984.

Freshnay R.I. Culture of Animal Cells, 3rd Ed., John Wiley and Sons, New York: 1994.

Fromherz P. "Electrical Interfacing of Nerve Cells and Semiconductor Chips." Chem. Phys. Chem. 3: 276, 2002.

Fromherz P. "Neuroelectronic Interfacing: Semiconductor Chips with Ion Channels, Nerve Cells and Brain," in Nanoelectronics and Information Technology, R.Waser, Ed., Wiley-VCH, Berlin: 2003, pp. 781-810.

Fromherz P., A. Offenhäusser, T. Vetter, and J. Weis. "A Neuron-Silicon Junction: A Retzius Cell of the Leech on an Insulated-Gate Field-Effect Transistor." Science 252: 1290, 1991.

Fromherz P., and A. Stett. "Silicon-Neuron Junction: Capacitive Stimulation of an Individual Neuron on a Silicon Chip." Phys. Rev. Lett. 75: 1670, 1995.

Fromherz P., V. Kiessling, K. Kottig, and G. Zeck. "Membrane Transistor with Giant Lipid Vesicle Touching a Silicon Chip." App. Phys. A 69: 571, 1999.

Gao X., and S. Nie. "Molecular Profiling of Single Cells and Tissue Specimens with Quantum Dots." Trends Biotech. 21(9): 371, 2003.

Gao X., W.C.W. Chan, and S. Nie. "Quantum-Dot Nanocrystals for Ultrasensitive Biological Labeling and Multicolor Optical Encoding." J Biomed. Opt. 7: 532, 2002.

Gerion D., F. Pinnand, S.C. Williams, W.J. Parak, D. Zanchet, S. Weiss, and A.P. Alivisatos. "Synthesis and Properties of Biocompatible Water-Soluble Silica-Coated CdSe/ZnS Semiconductor Quantum Dots." J. Phys. Chem. B 105: 8861, 2001.

Gibco Product Information Sheet, "Neurobasal and Neurobasal "A Medium." Form 3946, March 2003.

Goldberger M.E. "Mechanisms Contributing to Sparing of Function Following Neonatal Damage to Spinal Pathways." Neurochem Pathol. 5(3): 289, 1986.

Gole A., S.R. Sainkar, and M. Sastry. "Electrostatically Controlled Organization of Carboxylic Acid Derivatized Colloidal Silver Particles on Amine-Terminated Self-Assembled Monolayers." Chem. Mater. 12: 1234, 2000.

Goodman S.L., S.L. Cooper, and R.M. Albrecht. "Integrin Receptors and Platelet Adhesion to Synthetic Surfaces." J. Biomed. Mats. Res. 27: 683, 1993.

Graf J., R.C. Ogle, F.A. Robey, M. Sasaki, G.R. Martin, Y. Yamada, and H.K. Kleinman. "A Pentapeptide from the Laminin B1 Chain Mediates Cell Adhesion and Binds the 67,000 Laminin Receptor." Biochem. 26(22): 6896, 1987.

Green M., R. Taylor, and G. Wakefield. "The Synthesis of Luminescent Adenosine Triphosphate Passivated Cadmium Sulfide Nanoparticles." J. Mat. Chem. 13: 1859, 2003.

Gross G.W. "Simultaneous Single Unit Recording in vitro with a Photoetched Laser Deinsulated Gold Multimicroelectrode Surface." IEEE Trans. on Biomed. Eng. 26(5): 273, 1979.

Gupta A.K., and A.S.G. Curtis. "Lactoferrin and Ceruloplasmin Derivitized Superparamagnetic Iron Oxide Nanoparticles for Targeting Cell Surface Receptors." Biomats. 25: 3029, 2004.

Gurin V.S. "Large Clusters with Cadmium Sulfide Cores: Simulation of Thiolate Ligands on the Surface by ab initio MO LCAO Calculation." Surf. Rev. Lett. 7: 161, 2000.

Guy H.R., and S.R. Durell. "Structural Models of Na^+, Ca^{2+}, and K^+ Channels." Soc. Gen. Physiol. Ser. 50: 1, 1995.

Hamity M., and R.H. Lema. "The Effect of Methylviologen on the Photoluminescence Bands of Quantum-Sized CdS." J. Photochem. Photbio. A 99: 177, 1996.

Harlow E., and D. Lane. Antibodies: A Laboratory Manual. Cold Spring Harbor Press, Plainview, New York: 1988.

Hart S.L., A.M. Knight, R.P. Harbottle, A. Mistry, H.-D. Hunger, D.F. Cutler, R. Williamson, and C. Coutelle. "Cell Binding and Internalization by Filamentous Phage Displaying Cyclic Arg-Gly-Asp Containing Peptide." J. Bio. Chem. 269(17): 12466, 1994.

Hartwig A., and T. Schwedtle. "Interactions by Carcinogenic Metal Compounds with DNA Repair Processes: Toxicological Implications." Toxic. Lett. 127: 47, 2002.

Hässelbarth A., A. Eychmüller, and H. Weller. "Detection of Shallow Electron Traps in Quantum Sized CdS by Fluorescence Quenching Experiments." Chem. Phys. Lett. 203(2-3): 271, 1993.

Hatton G.I., and Z. Li. "Mechanisms of Neuroendocrine Cell Excitability." Adv. Exp. Med. Biol. 449: 79, 1998.

Hayes D., O.I. Micic, M.T. Nenadovic, V. Swayambunathan, and D. Meisel. "Radiolytic Production and Properties of Ultrasmall CdS Particles." J. Phys. Chem. 93: 4603, 1989.

Heiduschka P., and S. Thanos. "Implantable Bioelectronic Interfaces for Lost Nerve Functions." Prog. Neurobio. 55: 433, 1998.

Hemler M. "VLA Proteins in the Integrin Family: Structures, Functions, and Their Role on Leukocytes." Annu. Rev. Immunol. 8: 365, 1990.

Henglein A. "Photo-Degradation and Fluorescence of Colloidal Cadmium Sulfide in Aqueous Solution." Ber. Bunsenges. Phys. Chem. 86: 301, 1982.

Hermanson G.T. Bioconjugate Techniques. Academic Press, San Diego: 1996.

Herron N., Y. Wang, and H. Eckert. "Synthesis and Characterization of Surface-Capped, Size-Quantized CdS Clusters " Chemical Control of Cluster Size." J. Am. Chem. Soc. 112: 1322, 1990.

Hines M.A., and P. Guyot-Sionnest. "Synthesis and Characterization of Strongly Luminescing ZnS-Capped CdSe Nanocrystals." J. Phys. Chem. 100: 468, 1996.

Hitz C.B. Introduction to Lasing Technology. IEEE Press, Piscataway, NJ: 2001.

Hodgkin A. L., and A. F. Huxley. "A Quantitative Description of Membrane Current and its Application to Conduction and Excitation in Nerve." J. Physiol. 117: 500, 1952.

Hodgkin A.L., A.F. Huxley, and B. Katz. "Measurement of Current-Voltage Relations in the Membrane of the Giant Axon of *Loligo*." J. Physiol. 116: 424, 1952.

http://hyperphysics.phy-astr.gsu.edu/hbase/electric/dipole.html. Accessed July 2004.

Hu H., P.K. Nair. "Chemical Deposition of Photosensitive CdS Thin Films on Polyester Foils." J. Cryst. Growth 152: 150, 1995.

Huang J.M., and C.J. Murphy. Materials Research Society Luminescent Materials Symposium; San Francisco, 1999, pp. 33.

Humayun M.S., J.D. Weiland, G.Y. Fujii, R. Greenberg, R. Williamson, J. Little, B Mech, V. Cimmarusti, G. Van Boemel, G. Dagnelie, and E. de Juan. "Visual Perception in a Blind Subject with a Chronic Microelectronic Retinal Prosthesis." Vision Res. 43(24):2573, 2003.

Jaiswal J. K., H. Mattoussi, J.M. Mauro, and S.M. Simon. "Long-term Multiple Color Imaging of Live cells Using Quantum Dot Bioconjugates." Nature Biotech. 21: 47, 2003.

James C.D., R.R. Davis, M. Meyer, A. Turner, S. Turner, G. Withers, L. Kam, G. Banker, H. Craighead, M. Isaacson, J. Turner, and W. Shain. "Aligned Microcontact Printing of Micrometer-Scale Poly-L-Lysine Structures for Controlled Growth of Cultured Neurons on Planar Microelectrode Arrays." IEEE Trans. Biomed. End. 47(1): 17, 2000.

Kakkassery J.J., J.-P. Abid, M. Carrara, and D.J. Fermín. "Electrochemical and Optical Properties of Two Dimensional Electrostatic Assembly of Au Nanocrystals." Faraday Discuss. 125: 157, 2004.

Kaltenpoth G., M. Himmelhaus, L. Slansky, F. Caruso, and M. Grunze. "Conductive Core-Shell Particles: An Approach to Self-Assembled Mesoscopic Wires." Adv. Mats. 15(13): 1113, 2003.

Kalyanasundaram K., E. Borgarello, D. Duonghong, and M. Grätzel. "Cleavage of Water by Visible-Light Irradiation of Colloidal CdS Solutions: Inhibition of Photocorrosion by RuO_2" Angew. Chem. Int. Ed. Engl. 20(11): 987, 1981.

Kandel E.R., J.H. Schwartz, and T.M. Jessel. Principles of Neuroscience, 3rd Ed., Appleton and Lange, Norwalk, Connecticut: 1991.

Kandel E.R., J.H. Schwartz, and T.M. Jessel. Principles of Neuroscience, 4th Ed., McGraw Hill, New York: 2000.

Kaul R.A., N.I. Syed, and P. Fromherz. "Neuron-Semiconductor Chip with Chemical Synapse between Identified Neurons." Phys. Rev. Lett. 92: 038102, 2004.

Khosravi A.A., M. Kundu, B.A. Kuruvilla, G.S. Shekhawat, R.P. Gupta, A.K. Sharma, P.D. Vyas, and S.K. Kulkarni. "Manganese-Doped Zing-Sulfide Nanoparticles by Aqueous Method." Appl. Phys. Lett. 67: 2506, 1995.

Kimura S., W. Laosinchai, T. Itoh, X. Cui, and R.M. Brown, Jr. "Immunogold Labeling of Rosette Terminal Cellulose Synthesizing Complexes in a Vascular Plant (*Vigna angularis*)." Plant Cell 11(11): 2075, 1999.

Kleinfeld D., K.H. Kahler, and P.E. Hockberger. "Controlled Outgrowth of Dissociated Neurons on Patterned Substrates." J. Neurosci. 8: 4098, 1988.

Korgel B.A., and H.G. Monbouquette. "Quantum Confinement Effects Enable Photocatalyzed Nitrate Reduction at Neutral pH Using CdS Nanocrystals." J. Phys. Chem. B 101: 5010, 1997.

Korgel B.A., and H.G. Monbouquette. "Synthesis of Size-Monodisperse CdS Nanocrystals using Phosphatidylcholine Vesicles as True Reaction Compartments." J. Phys. Chem. 100: 346, 1996.

Kovacs G.T., C.W. Storment, and J.M. Rosen. "Regeneration Microelectrode Array for Peripheral Nerve Recording and Stimulation." IEEE Trans. Biomed. Eng. 39(9): 893, 1992.

Kricka L.J., Ligand-Binder Assays, Marcel Dekker, Inc., New York, 1985.

Kundu K., A.A. Khosravi, S.K. Kulkarni, and P. Singh. "Synthesis and Study of Organically Capped Ultra Small Clusters of Cadmium Sulphide." J. Mat. Sci. 32: 245, 1997.

Lam C.-W., J.T. James, R. McCluskey, and R.L. Hunter. "Pulmonary Toxicity of Single-Wall Carbon Nanotubes in Mice 7 and 90 Days After Intratracheal Instillation." Toxic. Sci. 77: 126, 2004.

Lansman J.B., P. Hess, and R.W. Tsien. "Blockade of Current Through Single Calcium Channels by Cd^{2+}, Mg^{2+}, and Ca^{2+}. J. Gen. Physiol. 88: 321, 1986.

Larson D.R., W.R. Zipfel, R.M. Williams, S.W. Clark, M.P. Bruchez, F.W. Wise, and W.W. Webb. "Water-Soluble Quantum Dots for Multiphoton Fluorescence Imaging In Vivo." Science 300: 1434, 2003.

Leach J.B., K.A. Bivens, C.N. Collins, and C.E. Schmidt. "Development of Photocrosslinkable Hyaluronic Acid-Polyethylene Glycol-Peptide Composite Hydrogels for Soft Tissue Engineering. J. Biomed. Mat. Res. 70A(1): 74, 2004.

Li W., L. Huo, D. Wang, G. Zeng, S. Xi, B. Zhao, J. Zhu, J. Wang, Y. Shen, and Z. Lu. "Self-Assembled Multilayers of Alternative Gold Nanoparticles and Dithiols: Approaching to Superlattice." Col. Surf. A 175: 217, 2000.

Liu J.-F., L.-G. Zhang, N. Gu, J.-Y. Ren, Y.-P. Wu, Z.-H., Lu, P.-S. Mao, and D.-Y. Chen. "Fabrication of Colloidal Gold Micro-Patterns Using Photolithographically Self-Assembled Monolayers as Templates." Thin Solid Films. 327-329: 176, 1998.

Lodish H., A. Berk, S.L. Zipursky, P. Matsudaira, D. Baltimore, and J.E. Darnell. Molecular Cell Biology, 4th ed., W. H. Freeman & Co, New York: 2000.

Loizou P.C. "Introduction to Cochlear Implants." IEEE Eng. Med. Bio. 18(1): 32, 1999.

Loo C., A. Lin, L. Hirsch, M.H. Lee, J. Barton, N. Halas, J. West, and R. Drezek. "Nanoshell-Enabled Photonics-Based Imaging and Therapy of Cancer." Tech. Cancer Res. Treat. 3(1): 33, 2004.

Luhmann H.J., I. Hanganu, and W Kilb. "Cellular Physiology of the Neonatal Rat Cerebral Cortex." Brain Res. Bull. 60(4): 345, 2003.

Maher M.P., J. Pine, J. Wright, and Y-C. Tai. "The Neurochip: A New Multielectrode Device for Stimulating and Recording from Cultured Neurons." J. Neurosci. Meth. 87: 45, 1999.

Makohliso S.A., P. Aebischer, L. Giovangrandi, H.J. Bühlmann, and M. Dutoit. "A Biomimetic Materials Approach Towards the Development of a Neural Cell-Based Biosensor." Proceedings of the 18th Annual International Conference of the IEEE Engineering in Medicine and Biology Society, Amsterdam, 1996, pp. 81-82.

Mann T.L., and U.J. Krull. "Fluorescence Polarization Spectroscopy in Protein Analysis." Analyst. 128: 313, 2003.

Masumoto Y., F. Naruse, and A. Kanno. "Photoinduced Electric Dipole in CuCl Quantum Dots." J. Luminescence. 102-103: 629, 2003.

Mattheakis L.C., J.M. Dias, Y.-J. Choi, J. Gong, M.P. Bruchez, J. Liu, and E. Wang. "Optical Coding of Mammalian Cells Using Semiconductor Quantum Dots." Anal. Chem. 327: 200, 2004.

Mattoussi H., J.M. Mauro, E.R. Goldman, G.P. Anderson, V.C. Sundar, F.V. Mikeluc, and M.G. Bawendi. "Self-Assembly of CdSe-ZnS Quantum Dot Bioconjugates Using an Engineered Recombinant Protein." J. Am. Chem. Soc. 122: 12142, 2000.

Maxwell D.J., J.R. Taylor, and S. Nie. "Self-Assembled Nanoparticle Probes for Recognition and Detection of Biomolecules." J. Am. Chem. Soc. 124: 9606, 2002.

McCammon J.A. "Theory of Biomolecular Recognition." Curr. Opin. Struct. Biol. 8(2): 245, 1998.

Mendintz I.L., A.R. Clapp, H. Mattoussi, E.R. Goldman, B. Fisher, and J.M. Mauro. "Self-Assembled Nano-scale Biosensors Based on Quantum Dot FRET Donors." Nature Mats. 2: 630, 2003.

Mirkin C.A. "Programming the Assembly of Two- and Three-Dimensional Architectures with DNA and Nano-scale Inorganic Building Blocks." Inorg. Chem. 39: 2258, 2000.

Miyake M., T. Torimoto, M. Nishizawa, T. Sakata, H. Mori, and H. Yoneyama. "Effects of Surface Charges and Surface States of Chemically Modified Cadmium Sulfide

Nanoparticles Immobilized to Gold Electrode Substrates on Photoinduced Charge Transfers." Langmuir. 15: 2714, 1999.

Molleman A. Patch Clamping: An Introductory Guide to Patch Clamp Electrophysiology. John Wiley and Sons, West Sussex, England: 2003.

Mortimer R.G. Physical Chemistry. Benjamin/Cummings Publishing Co., Redwood City, California: 1993.

Murphy C.J., and J.L. Coffer. "Quantum Dots: A Primer." App. Spect. 56(1): 16A, 2002.

Murray C.B., C.R. Kagan, and M.G. Bawendi. "Synthesis and Characterization of Monodisperse Nanocrystals and Close-Packed Nanocrystal Assemblies." Ann. Rev. Mat. Sci. 30: 545, 2000.

Murray C.B., D.J. Norris, and M.G. Bawendi. "Synthesis and Characterization of Nearly Monodisperse CdE (E = S, Se, Te) Semiconductor Nanocrystallites." J. Am. Chem. Soc. 115: 8706, 1993.

Nakanishi T., B. Ohtani, and K. Uosaki. "Fabrication and Characterization of CdS-Nanoparticle Mono- and Multilayers on a Self-Assembled Monolayer of Alkanedithiols on Gold." J. Phys. Chem. B. 102: 1571, 1998.

Neher E., and B. Sakmann. "Single-Channel Currents Recorded from Membrane of Denervated Frog Muscle Fibres." Nature. 260(5554): 799, 1976.

Nicholson G.M., M.J. Little, and L.C. Birinyi-Strachan. "Structure and Function of Delta-Antracotoxins: Lethal Neurotoxins Targeting the Voltage-Gated Sodium Channel." Toxicon. 43(5): 587, 2004.

Nosaka Y., and Y. Nakaoka. "Effect of the Amount of Reactant on the Photon-fluence Dependence in Laser-Induced Transient Formation at the Surface of Colloidal Semiconductor Particles." Langmuir 11(4): 1170, 1995.

Nosaka Y., H. Shigeno, and T. Ikeuchi. "Formation of Polynuclear Cadmium-Thiolate Complexes and CdS Clusters in Aqueous-Solution Studied by Means of Stopped-Flow and NMR Spectroscopies." J. Phys. Chem. 99: 8317, 1995.

Nosaka Y., H. Shigeno, and T. Ikeuchi. "Formation Steps of CdS Clusters in Aqueous Solution Containing 2-mercaptoethanol." Surf. Rev. Let. 3:1209, 1996.

Nosaka Y., K. Yamaguchi, H. Miyama, and H. Hayashi. "Preparation of Size-Controlled CdS Colloids in Water and Their Optical Properties." Chem. Lett. 4: 605, 1988.

Nosaka Y., N. Ohta, T. Fukuyama, and N. Fujii. "Size Control of Ultrasmall CdS Particles in Aqueous Solution by Using Various Thiols." J. Col. Interface Sci. 155: 23, 1993.

Novak J.L., and B.C. Wheeler. "Multisite Hippocampal Slice Recording and Stimulation Using a 32 Element Microelectrode Array." J. Neurosci. Meth. 23: 149, 1988.

Oberdörster E. "Manufactured Nanomaterials (Fullerenes, C60) Induce Oxidative Stress in the Brain of Juvenile Largemouth Bass." Env. Health Persp. 112(10): 1058, 2004.

Oberdörster G., Z. Sharp, V. Atudorei, A. Elder, R. Gelein, W. Kreyling, and C. Cox. "Translocation of Inhaled Ultrafine Particles to the Brain." Inhalation Toxic. 16(6/7): 437, 2004.

Osaki F., T. Kanamori, S. Sando, T. Sera, and T. Aoyama. "A Quantum Dot Conjugated Sugar Ball and Its Cellular Uptake. On the Size Effects of Endocytosis in the Subviral Region." J. Am. Chem. Soc. 126: 6520, 2004.

Parak W.J., D. Gerion, T. Pellegrino, D. Zanchet, C. Micheel, S.C. Williams, R. Boudreau, M.A. Le Gros, C.A. Larabell, and A.P. Alivisatos. "Biological Applications of Colloidal Nanocrystals." Nanotech. 14: R15, 2003.

Parak W.J., R. Boudreau, M. Le Gros, D. Gerion, D. Zanchet, C.M. Micheel, S.C. Williams, A.P. Alivisatos, and C. Larabell. "Cell Motility and Metastatic Potential Studies Based on Quantum Dot Imaging of Phagokinetic Tracks." Adv. Mats. 14(12): 882, 2002.

Pastan I., and M.C. Willingham, Eds., Endocytosis. Plenum Press, New York: 1985.

Patolsky F., Y. Weizmann, O. Lioubashevski, and I. Willner. "Au-Nanoparticle Nanowires Based on DNA and Polylysine Templates." Angew. Chem. Int. Ed. 41(13): 2323, 2002.

Patrick L. "Toxic Metals and Antioxidants: Part II. The Role of Antioxidants in Arsenic and Cadmium Toxicity." Alt. Med. Rev. 8(2): 106, 2003.

Peng Z.A., and X. Peng. "Formation of High-Quality CdTe, CdSe, and CdS Nanocrystals Using CdO as Precursor." J. Am. Chem. Soc. 123: 183, 2001.

Personal communication from A. Derfus, University of California at San Diego, Biomedical Engineering Department, February 16, 2004.

Personal Communication from Fred Mikeluc, Innovalight, Austin, Texas, June 29, 2004.

Pierschbacher M.D., and E. Ruoslahti. "Cell Attachment Activity of Fibronectin Can Be Duplicated by Small Synthetic Fragments of the Molecule." Nature 309: 30, 1984.

Pollak G., and H. Zakon. Vertebrate Physiology, Spring 2000 Ed., University Co-op Press, Austin, TX: 2000.

Popovic D., T. Gordon, V.F. Rafuse, and A. Prochazka. "Properties of Implanted Electrodes for Functional Electrical Stimulation." Annals Biomed. Eng. 19(3): 303, 1991.

Porter R.R. "The Hydrolysis of Rabbit "-globulin and Antibodies with Crystalline Papain." Biochem. J. 73: 119, 1959.

Qu L., and X. Peng. "Control of Photoluminescence Properties of CdSe Nanocrystals in Growth." J. Am. Chem. Soc. 124: 2049, 2002.

Ranieri J.P., R. Bellamkonda, E.J. Bekos, A. Gardella, H.J. Mathieu, L. Ruiz, P. Aebischer. "Spatial Control of Neuronal Cell Attachment and Differentiation on Covalently Patterned Laminin Substrates." Int. J. Dev. Neurosci. 12(8): 725, 1994.

Raptis S.G., M.G. Papdopolous, and A.J. Sadlej. "The Correlation, Relativistic, and Vibrational Contributions to the Dipole Moments, Polarizabilities, and First and Second Hyperpolarizabilities of ZnS, CdS, and HgS." J. Chem. Phys. 111(17): 7904, 1999.

Rikans L.E., and T. Yamano. "Mechanisms of Cadmium-Mediated Acute Hepatotoxicity." J. Biochem. Mol. Toxicol. 14: 110, 2000.

Rossetti R, S.M. Beck, and L.E. Brus. "Direct Observation of Charge-Transfer Reactions Across Semiconductor: Aqueous Solution Interfaces Using Transient Raman Spectroscopy." J. Am. Chem. Soc. 106: 980, 1984.

Rossetti R., J.L. Ellison, J.M. Gibson, and L.E. Brus. "Size Effects in the Excited Electronic States of Small Colloidal CdS Crystallites." J. Chem. Phys. 80(9): 4464, 1984.

Rossetti R., S.S. Nakahara, and L.E. Brus. "Quantum Size Effects in the Redox Potentials, Resonance Raman Spectra, and Electronic Spectra of CdS crystallites in aqueous solution." J. Chem. Phys. 79(2): 1086, 1983.

Rutten W.L.C. "Selective Electrical Interfaces with the Nervous System." Annu. Rev. Biomed. Eng. 4: 407, 2002.

Sarma V.R., E.W. Silverton, D.R. Davies, and W.D. Terry. "The Three-Dimensional Structure at 6 Å Resolution of a Human γG1 Immunoglobulin Molecule." J. Bio. Chem. 246(11): 3753, 1971.

Scher E. C., L. Manna, and A. P. Alivisatos. "Shape Control and Applications of Nanocrystals." Phil. Trans. Royal Soc. A 361(1803): 241, 2003.

Schneider J.A., B. Katz, and R.B. Melles. "Update on Nephropathic Cystinosis." Pediatr. Nephrol. 4(6): 645, 1990.

Sebastian P.J. "ZnCdS Films for Solar Cell and Photodetector Applications Deposited by in situ Chemical Doping of CdS with Zn." Adv. Mat. Opt. Elec. 5: 269, 1995.

Semmier M., J. Seitz, F. Erbe, P. Mayer, J. Heyder, G. Oberdörster, and W.G. Kreyling. "Long-term Clearance Kinetics of Inhaled Ultrafine Insoluble Iridium Particles from the Rat Lung, Including Translocation into Secondary Organs." Inhalation Toxic. 16(6/7): 453, 2004.

Seydel C. "Quantum Dots Get Wet." Science 300: 80, 2003.

Shah P., S. Husain, K.P. Johnston, and B.A. Korgel. "Role of Steric Stabilization on the Arrested Growth of Silver Nanocrystals in Supercritical Carbon Dioxide." J. Phys. Chem. B. 106: 12178, 2002.

Shahar A., J. de Vellis, A. Vernadakis, B. Haber, Eds., A Dissection and Tissue Culture Manual of the Nervous System. John Wiley and Sons, New York: 1989, pp. 155, 184, 225.

Sherman R.L., Y. Chen, and W.T. Ford. "Cysteine Acrylamide Stabilized CdS and CdSe/CdS Nanoparticles in Aqueous Solutions." Abstracts of Papers, 225th ACS National Meeting, New Orleans, LA, 2003.

Silverman K.L., R.P. Mirin, S.T. Cundiff, and A.G. Norman. "Direct Measurement of Polarization Resolved Transition Dipole Moment in InGaAs/GaAs Quantum Dots." App. Phys. Lett. 82(25): 4552, 2003.

Sokolova O. "Structure of Cation Channels, Revealed by Single Particle Electron Microscopy." FEBS Lett. 564(3): 251, 2004.

Sorribas H., D. Braun, L. Leder, P. Sonderegger, and L. Tiefenauer. "Adhesion Proteins for Tight Neuron-Electrode Contact." J. Neurosci. Methods. 104: 133, 2001.

Spanhel L., M. Haase, H. Weller, and A. Henglein. "Photochemistry of Colloidal Semiconductors. 20. Surface Modification and Stability of Strong Luminescing CdS Particles." J. Am. Chem. Soc. 109: 5649, 1987.

Steigerwald M.L., and L.E. Brus. "Synthesis, Stabilization, and Electronic-Structure of Quantum Semiconductor Nanoclusters." Annu. Rev. Mater. Sci. 19: 471, 1989.

Ste-Marie J., A.E. Torma, and A.O. Gübeli. "The Stability of Thiocomplexes and Solubility Products of Metal Sulphides." Can. J. Chem. 42: 662, 1964.

Stolik S., J.A. Delgado, A. Perez, and L. Anasagasti. "Measurement of Penetration Depths of Red and Near Infrared Light in Human "ex vivo" Tissues." J. Photochem. Photobiol. B 57: 90, 2000.

Strong T.D., H.C. Cantor, and R.B. Brown. "A Microelectrode Array for Real-Time Neurochemical and Neuroelectrical Recording in Vitro." Sens. Actuators A. 91: 357, 2001.

Stryer L., and R.P. Haugland. "Energy Transfer: A Spectroscopic Ruler." Proc. Natl. Acad. Sci. 58(2):719, 1967.

Swayambunathan V., D. Hayes, K.H. Schmidt, Y.X. Liao, and D. Meisel. "Thiol Surface Complexation of Growing CdS Clusters." J. Am. Chem. Soc. 112: 3831, 1990.

Talapin D.V., A.L. Rogach, E.V. Shevchenko, A. Kornowski, M. Haase, and H. Weller. "Dynamic Distribution of Growth Rates within the Ensembles of Colloidal II-VI and III-V Semiconductor Nanocrystals as a Factor Governing Their Photoluminescence Efficiency." J. Am. Chem. Soc. 124: 5782, 2002.

Tang Z., N.A. Kotov, and M. Giersig. "Spontaneous Organization of Single CdTe Nanoparticles into Luminescent Nanowires." Science 297: 237, 2002.

Taylor J., and S. Nie. "Probing Specific DNA Sequences with Luminescent Semiconductor Quantum Dots," in Nanoparticles and Nanostructured Surfaces: Novel Reporters with Biological Applications, C.J. Murphy, Ed.,, Proceedings of SPIE., vol. 4258, 2001, p. 16.

Thomas C.A., P.A. Springer, G.E. Loeb, Y. Berwald-Netter, and L.M. Okun. "A Miniature Microelectrode Array to Monitor the Bioelectric Activity of Cultured Cells." Exp. Cell. Res. 74: 61, 1972.

Tokutomi N., Y. Tokutomi, K. Fukunaga, E. Miyamoto, and K. Nishi. "Bradykinin-Evoked Non-Specific Cationic Current in Neuroblastoma Glioma Hybrid (NG108-15) Cells and its Down-Regulation Through Differentiation." Brain Res. 657: 202, 1994.

Torimoto T., N. Tsumura, M. Miyake, M. Nishizawa, T. Sakata, H. Mori, and H. Yoneyama. "Preparation and Photoelectrochemical Properties of Two-Dimensionally Organized CdS Nanoparticle Thin Films." Langmuir. 15: 1853, 1999.

Tri-octyl phosphine Oxide MSDS Product Number 223301, version 1.5, 6/28/2004, from Sigma Aldrich.

van Sark W.G.J.H.M., P.L.T.M. Frederix, A.A. Bol, H.C. Gerritsen, and A. Meijerink. "Blueing, Bleaching, and Blinking of Single CdSe/ZnS Quantum Dots." Chem. Phys. Chem. 3: 871, 2002.

Vassanelli S., and P. Fromherz. "Neurons from Rat Brain Coupled to Transistors." App. Phys. A 65: 85, 1997.

Venyaminov S.Y., and N.N. Kalnin. "Quantitative IR Spectrophotometry of Peptide Compounds in Water (H2O) Solutions. I. Spectral Parameters of Amino Acid Residue Absorption Bands." Biopolymers. 30(13-14): 1243, 1990.

Waalkes M.P. "Cadmium Carcinogenesis." Mut. Res. 533: 107, 2003.

Wang S., N. Mamedova, N.A. Kotov, W. Chen, and J. Studer. "Antigen/Antibody Immunocomplex from CdTe Nanoparticle Bioconjugates." Nano Letts. 2(8): 817, 2002.

Wang Y., and N. Herron. "Nanometer-Sized Semiconductor Clusters: Materials Synthesis, Quantum Size Effects, and Photophysical Properties." J. Phys. Chem. 95: 525, 1991.

Watson A. "Why Can't a Computer Be More Like a Brain"" Science 277: 1934, 1997.

Weast R.C., and M.J. Astle, Eds., CRC Handbook of Chemistry and Physics, 60th Ed. CRC Press, Boca Raton, Florida: 1979.

Weisbuch C., H. Benisty, and R. Houdré. "Overview of Fundamentals and Applications of Electrons, Excitons, and Photons in Confined Structures." J. Luminescence. 85: 271, 2000.

Weller H. "Colloidal Semiconductor Q-Particles " Chemistry in the Transition Region Between Solid-State and Molecules." Angew. Chem. Int. Ed. Engl. 32: 41, 1993.

Weller H., H.M. Schmidt, U. Koch, A. Fojtik, S. Baral, A. Henglein, W. Kunath, K. Weiss, and E. Dieman. "Photochemistry of Colloidal Semiconductors. Onset of Light Absorption as a Function of Size of Extremely Small CdS Particles." Chem. Phys. Lett. 124(6): 557, 1986.

Weller H., H.M. Schmidt, U. Koch, A. Fojtik, S. Baral, A. Henglein, W. Kunath, K. Weiss, and E. Dieman. "Photochemistry of Semiconductor Colloids. 14. Photochemistry of Colloidal Semiconductors-Onset of Light Absorption as a Function of Size of Extremely Small CdS Particles." Chem. Phys. Lett. 124: 557, 1986.

William Y.W., and X. Peng. "Formation of High-Quality CdS and Other II-VI Semiconductor Nanocrystals in Noncoordinating Solvents: Tunable Reactivity of Monomers." Angew. Chem. Int. Ed. 41: 2368, 2002.

Willingham M.C. An Atlas of Immunofluorescence in Cultured Cells, Academic Press, Orlando, 1985.

Willingham M.C., in Methods in Molecular Biology, Vol 115: Immunocytochemical Methods and Protocols, L.C. Javois, Ed., Humana Press Inc., Totowa, NJ: 1999.

Winter J.O., and C.E. Schmidt. "Biomimetic Strategies and Applications in the Nervous System," in Biomimetic Materials and Design, A.K. Dillow and A.M. Lowman, Eds., Marcel-Dekker, New York: 2002.

Winter J.O., T.Y. Liu, B.A. Korgel, and C.E. Schmidt. "Recognition Molecule Directed Interfacing Between Semiconductor Quantum Dots and Nerve Cells." Adv. Mat. 13: 1673, 2001.

Wu X., H. Liu, J. Liu, K.N. Haley, J.A. Treadway, J.P. Larson, N. Ge, F. Peale, and M.P. Bruchez. "Immunofluorescent Labeling of Cancer Marker Her2 and Other Cellular Targets with Semiconductor Quantum Dots." Nature Biotech. 21: 41, 2003.

Wuister S.F., I. Swart, F. van Driel, S.G. Hickey, and C. de Mello Donegá. "Highly Luminescent Water-Soluble CdTe Quantum Dots." Nano Lett. 3(4): 503, 2003.

Wybourne M.N, J.E. Hutchison, L. Clarke, L.O. Brown, and J.L. Mooster. "Fabrication and Electrical Transport Characteristics of Low-Dimensional Nanoparticle Arrays Organized by Biomolecular Scaffolds." Microelec. Eng. 47: 55, 1999.

Yoshihara T., N. Esumi, M. J. Humphries, and S. Imashuku. "Unique Expression of Integrin Fibronectin Receptors in Human Neuroblastoma Cell Lines." Int. J. Cancer 51: 620, 1992.

Zhu T., X. Fu, T. Mu, J. Wang, and Z. Liu. "pH Dependent Adsorption of Gold Nanoparticles on p-Aminothiophenol-Modified Gold Substrates" Langmuir. 15: 5197, 1999.

Vita

Jessica O. Winter was born to Joan and James Lutkenhaus July 17, 1975 in Dallas, Texas. She has one sister, Jodie Lutkenhaus, a chemical engineering graduate student at MIT. She received her high school education at Lawrence Dale Bell High School in Hurst, Texas; where she graduated with honors. From 1993-1997, she attended Northwestern University in Evanston, Illinois; obtaining a B.S. in Chemical Engineering, Cum Laude, with a sub-specialty in Biotechnology. While at Northwestern, she began her research career with Dr. Brian Hoffman, in inorganic biochemistry. Additionally, she gained industrial research experience through a four-semester co-operative education program with Allied Signal Research and Development in Des Plaines, Illinois. After graduation, she worked as an ion implant process engineer at Intel Corporation in Albuquerque, New Mexico. In Albuquerque, she married her college sweetheart, Adam Winter.

She returned to research in 1999, beginning her graduate studies at the University of Texas at Austin with Dr. Christine Schmidt as an advisor. She obtained her M.S. degree in Chemical Engineering in 2001, and also celebrated the birth of her first child, Ali Joan Winter. Her second child, Max Xerces Winter, was born the day after her defense. Jessica is the author of four first-author publications and proceedings. She has presented at four national meetings, and is the recipient of the Materials Research Society Graduate Student Gold Award and the Biomedical Engineering Society Graduate Student Award.

Permanent address: 2521 Stonegate Drive North, Bedford, Texas, 76021

This dissertation was typed by the author.